STUDIES ON ELECTROCHROMIC MATERIALS AND DEVICES

by

Philippe Ageorges

A thesis submitted in fulfilment of the requirements
for the degree of Doctor of Philosophy

STUDIES ON ELECTROCHROMIC MATERIALS AND DEVICES

by

Philippe Ageorges

A thesis submitted in fulfilment of the requirements
for the degree of Doctor of Philosophy

Solar Energy Materials Research Laboratory
School of Engineering
Oxford Brookes University
Gipsy Lane
Oxford OX3 0BP
United Kingdom

May 1996

Adsuefacte ad ea etiam, de quibus desperas.

Marci Antonini, imperatoris,

De seipsos et ad seipsum, Libri XII.

PREFACE

The objective of this thesis is devoted to technologies that can be used for advanced energy-efficient fenestration systems. A better understanding of energy impacts can make more efficient use of advanced fenestration technologies. Solar passive technologies, including low-e coatings, gas fills and insulating frames have helped to increase the overall thermal resistance of fenestration products. However, they do not consider natural season and daily variations. Switchable glazing technologies and electrochromism in particular are the focus of international research interests for both academic and industrial institutions.

A growing interest has been shown in studying new electrochromic materials and in understanding their fundamental mechanisms. International research activities are concentrated on the development and optimisation of the different materials and layers that may comprise future commercial electrochromic products. There is an increasing number of materials available, though their suitability in an ECD remains to be studied.

This work concentrates on the deposition and performance of two different types of complementary layers which may be used in the construction of electrochromic devices. These layers can act as active or as passive materials such as nickel oxide and titanium oxide doped with vanadium respectively. The films as well as the active tungsten oxide electrochromic layer were produced by R.F. magnetron sputtering techniques and their optical and electrochemical properties were optimised. Their electrochromism was studied under protonic and lithiated electrolytes. Prototype devices were assembled and tested under lithium ion insertion and extraction using an acrylate polymer. Finally, the different prototypes were characterised and compared to match the performance of an ideal EC device of interest for energy efficiency.

ACKNOWLEDGEMENTS

I would like to acknowledge and give thanks to all those who have helped with the development of this research. I would especially like to thank Prof M.G. Hutchins, my supervisor, for his support during all these years and his guidance throughout this thesis.

I wish to thank Dr Zorica Crnjak Orel (National Institute of Chemistry, Ljubljana, Slovenia) and Dr Alla Cordery for their continuous guidance and friendship during this work.

Special thanks to my colleague and friend Mrs Theresa-Jane Squire for all her work on the scanning electron microscope and her assistance with the spectroscopy measurements.

Thanks also to the members of the Solar Energy Materials Research Laboratory as well as all the academic and non-academic staff of the School of Engineering, Oxford Brookes University.

I am also extremely grateful to Dr Keith Refson (Department of Earth Sciences, Oxford University) for his explanations and assistance in writing Chapter 3 and Chapter 6 of this thesis, and to Dr Mark Burdis (Pilkington) for his help in Chapter 7 and Chapter 8.

Finally, I am very grateful to Mr Richard Holland for proofreading this thesis.

This work was funded in part by an award from the Commission of the European Communities, DG XII, Non-Nuclear Energies Programme, Joule I, in collaboration with Pilkington Technology Centre Ltd, Lathom, UK; the Department of Chemistry, University of Southampton, UK; and Danionics, Denmark.

ABSTRACT

This thesis investigates electrochromic thin films needed to construct a variable transmission electrochromic device. Such a device is made of 5 layers sandwiched between 2 pieces of glass: two electronic transparent conducting layers, an optically active electrochromic layer (WO_3), a ion-conducting polymer electrolyte and an ion-storage layer (NiO_x, TiO_x, VO_x, $V_zTi_yO_x$) .

Electrochromic NiO_x thin films were produced by R.F. magnetron sputtering and electrodeposition techniques and studied under proton intercalation. A visible transmittance modulation of 0.70 and 0.80 and a visible coloration efficiency of 35 and 100 $cm^2.C^{-1}$ for a thickness of 300 and 200 nm were obtained for sputtered and chemically-deposited NiO_x films respectively. Anodic films are extremely porous and soft. Under the mechanical stresses of ionic insertion/extraction they degrade more quickly than the compact nanostructure of physically deposited films. When studied under lithium intercalation, sputtered NiO_x films exhibit a nucleation loop observed in cyclic voltammetry indicating the growth of a new phase and are seen to degrade quickly. NiO_x films were not seen to be potential candidates for EC applications using Li^+ intercalation.

WO_3, TiO_x and VO_x thin films were deposited by R.F. magnetron sputtering and studied under Li^+ intercalation/deintercalation. Optimised WO_3 films exhibited good electrochromic properties: a visible transmittance modulation of 0.82 and a visible coloration efficiency of 49 $cm^2.C^{-1}$ for a thickness of 450 nm.

Electrochromic properties of TiO_x films were seen to not strongly depend on the sputtering process parameters whereas VO_x films showed a stronger dependence. TiO_x films are able to store a limited quantity of charge Q = 13 $mC.cm^{-2}$ for thicknesses greater than 13 nm. They are transparent in both charged and uncharged states $T_{v,u}$ and $T_{v,ch} > 0.80$, and are stable upon charge insertion/extraction. VO_x films can store a much larger quantity of charge Q = 35 $mC.cm^{-2}$ for a thickness of 70 nm. They are yellow in

the uncharged state and bluish in the charged state: $T_{v,u}$ and $T_{v,ch} > 0.70$, and the charge insertion/extraction process is seen to evolve during the initial cycles. Both TiO_x and VO_x films did not show all the required electrochromic properties for EC applications.

The main achievement of this work was the development of highly durable vanadium/titanium mixed oxide thin films. Work was carried out on different V/Ti ratios using specific deposition techniques developed for that purpose. Films with a vanadium to titanium ratio of about 50 % showed optimum performance characteristics for passive ion storage layer applications. Such layers deposited on ITO exhibited high visible transmittance: $T_{v,ch} > 0.62$, and a relatively low visible modulation (0.20), with high storage capacity $Q > 40$ mC.cm^{-2} for a thickness of 80 nm.

The laminated WO_3/PAAUA/$V_zTi_yO_x$ EC device was assembled and exhibited under specific switching conditions encouraging properties: a visible transmittance modulation > 0.50 over more than 10^5 cycles.

Table of Contents

PART A

FUNDAMENTAL CONCEPTS

Chapter 1

INTRODUCTION

1.1 Background

Over the past 25 years, a growing interest has been expressed by both research and industrial communities in the thermal performance and optical behaviour of glazings. More recently, in the face of energy implications and associated environmental problems, international organisations[1] and countries[2,3] have increased research and development activities in the field of energy efficient buildings. Today's commercial and residential architecture incorporates large areas of glass walls and fenestration for lighting and aesthetics. With such modern designs, traditional glazings with low thermal resistance would increase heating loads in winter, while in summer the transmission of solar radiation would increase the cooling loads. Space conditioning in developed countries represents 40 % to 60 % of the annual energy consumption used in heating, lighting and cooling[2].

Thermal losses through traditional single glazed windows account for some 10 % of the total heat loss of a building[2]. Energy efficient windows involve the control of the incoming radiation and of the heat gains or losses due to radiation, conduction and convection. Different climates require different approaches to regulate the throughput of radiant energy[4]. Windows should be designed such that the solar gains are greater than the energy losses. Among the different possibilities to reduce heat losses without blocking visible radiation, passive solar glazings offer an alternative technology to insulating shutters. Specific techniques have been developed over the past 20 years to achieve a static control of solar and heat gain, and they are already commercially available.

For residential and commercial buildings in cold climates, priority is given to heating energy insulation. Advanced window designs, such as multiple glazings, have been developed to reduce heat losses by a factor of two in *U-values*. By using low-emittance coatings or heat mirrors alone, it is possible to reduce the U-value significantly. In practice, combinations of techniques are used and for instance, the U-value can be further reduced with the use of a gas filling.

For cooling-dominated climates, solar gains through windows must be offset by cooling the building. Such a problem is again solved by the use of heat mirrors, that can filter solar gains. These advanced glazings selectively transmit visible light and reflect the near infrared component of the solar radiation.

The heating and cooling demands of buildings vary seasonally. The use of heat mirrors assists in reducing heat gains, by preventing the admission of solar radiation that may be present at certain times of the year. Thus a dynamic control of glazing properties seems to be an attractive alternative. Switchable systems can have their optical properties modulated in response to the demands of the building environment. Such materials are called *chromogenic*. There are 3 different chromogenic classes; *photochromic* materials which change their optical properties in response to the intensity of incident light; *thermochromic* materials which modulate their optical properties with temperature; and *electrochromic* materials which reversibly alter their optical properties as a function of an applied voltage. Promising results have been obtained for these materials which show a reversible change in the visible spectrum between dark and transparent states. Incorporated into a building, dynamic fenestration technologies could make a more positive contribution to energy saving throughout the year[2]. Such systems allow excessive solar gains to be rejected during periods of high solar radiation, while still allowing the window to admit as much solar radiation as possible during periods of lower daylight availability.

1.2 Optical properties of materials for solar energy conversion

The basic understanding of solar energy efficiency lies in the radiative properties of our natural surroundings. The radiation which prevails in our ambience is confined at specific and well-defined wavelengths. Figure 1.1(a) illustrates the solar spectral distribution[5,6] above the atmosphere (denoted Air Mass 0 or *AMO*) and at ground level (*AM2*) on the horizontal to the sun under clear weather conditions.

The terrestrial solar spectrum is seen to be confined in the range 0.3 - 3 μm. Figure 1.1(a) shows that about 45% of the sun's energy lies in the visible region, about 52% lies in the near infra-red and the remaining 3% is in the ultra-violet. The radiation that reaches the Earth has been attenuated and scattered by absorption in the atmosphere, and this is mainly due to the presence of carbon dioxide, water vapour and ozone. The integrated area under the solar spectrum (AM0) curve gives a solar intensity (or irradiance) constant of 1353 $W.m^{-2}$. After absorption in the atmosphere the maximum solar irradiance (AM2) is limited to less than 1000 $W.m^{-2}$.

Visible light is in the narrow range $0.4 < \lambda < 0.7$ μm, covering about half the energy of the solar radiation that reaches the Earth. Figure 1.1(c) shows the photopic response (V_λ) of the human eye.

All matter above absolute zero emits radiation. It is convenient to look at the ideal blackbody spectrum, called the Planck spectrum. Planck's law is a consequence of the quantum nature of electromagnetic radiation. Figure 1.1(b) also shows the spectral emissive distributions of four blackbodies (100°C, 50°C, 0°C and -50°C) derived from Planck's law which are of interest for most glazing applications. The spectra are confined in the range 2 - 100 μm. At room temperature the peak lies at about 10μm and will move towards shorter wavelengths as the temperature increases.

The blackbody spectral emissive power is equal to :

$$E_{b,\lambda} = \frac{2\pi h c^2}{\lambda^5 e^{hc/kT} - 1} \qquad [1.1]$$

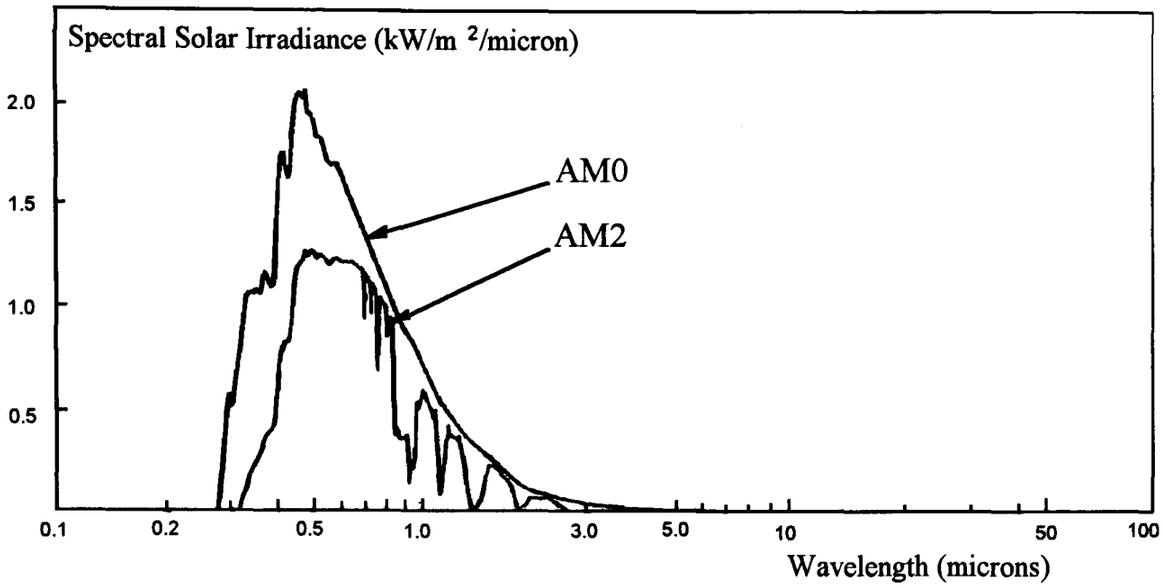

Figure 1.1(a) : Spectral distribution (G_λ) of solar spectrum for *AMO* and *AM2* at normal incidence.

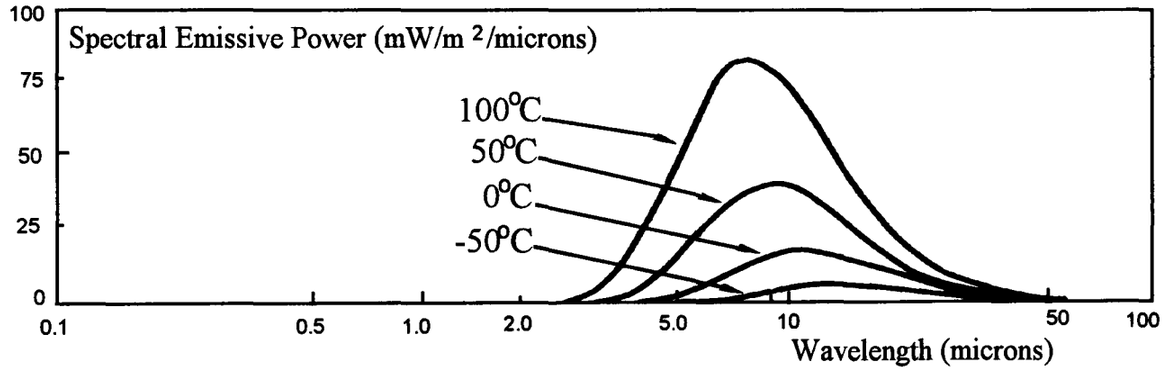

Figure 1.1(b) : Blackbody emissive power ($E_{b,\lambda}$) at different temperatures.

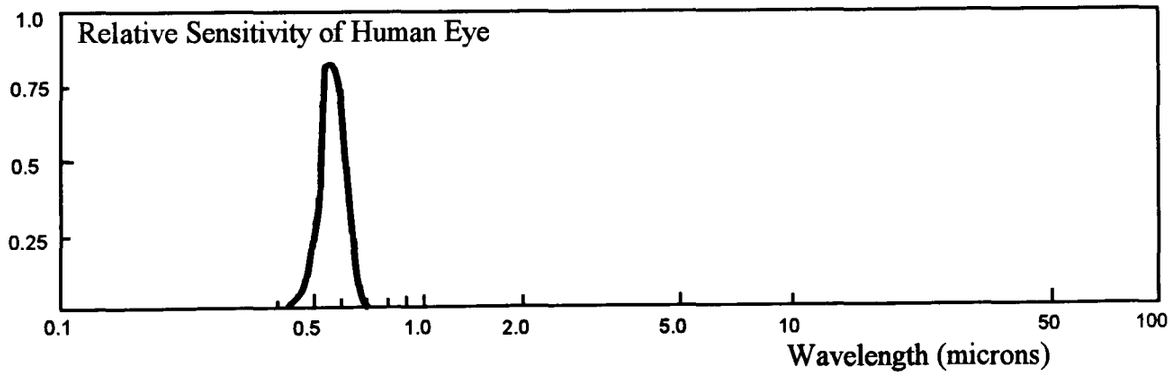

Figure 1.1(c) : Photopic response of the human eye (V_λ).

The wavelength of maximum emission λ_{max}, can be found from the above equation in equating its derivative to zero. The result is given by Wien's law :

$$\lambda_{max} \cdot T = 2897.8\ \mu m \qquad [1.2]$$

Thermal radiation for building and solar heating applications lies between 2.5 - 50 μm and in this range quantitative performance parameters are defined to describe the properties of energy efficient windows. Monochromatic radiation that is incident on a surface can either be absorbed, reflected or transmitted. From Kirchhoff's law and the law of conservation of energy this can be expressed as :

$$A_\lambda = \varepsilon_\lambda \qquad [1.3]$$

$$T_\lambda + R_\lambda + A_\lambda = 1 \qquad [1.4]$$

Where A_λ, R_λ, T_λ and ε_λ are respectively spectral absorptance, reflectance, transmittance and emittance coefficients.

To be able to describe the overall response of a surface to all relevant wavelengths in solar energy applications, it is necessary to define a set of optical properties integrated with respect to a defined spectral distribution (ϕ_λ) over a specific range of the spectrum (λ_1, λ_2). The integrated optical properties are angular dependent, and θ is the angle from the surface normal for the incident or emitted radiation.

The evaluation of the transmittance (T_s, T_v), reflectance (R_s, R_v) or absorptance (A_s, A_v, ε) of glazing materials requires a knowledge of the spectral distribution ϕ_λ. For calculation in the visible region of the spectrum ($\lambda_1 = 0.38\mu m$, $\lambda_2 = 0.78\mu m$), the distribution ϕ_λ is equal to the product of the relative spectral power distribution of an illuminant[7] and the photopic response of the human eye (V_λ).

For calculation in the solar range (λ_1= *0.3 μm*, λ_2= *2.5 μm*), the distribution ϕ_λ is equal to the solar irradiance G_λ for AM0 or AM2. For calculation in the thermal range of the spectrum (λ_1= *2.5 μm*, λ_2= *25 μm*), the function ϕ_λ is equal to the black body emissive power $E_{b,\lambda}$. The radiative properties ($X_{\lambda 1,\lambda 2}$ = T_s, T_v, R_s, R_v, A_s, A_v *or* ε) of films can be calculated from the general formula[7] :

$$X_{\lambda_1,\lambda_2}(\theta) = \frac{\int_{\lambda_1}^{\lambda_2} X_\lambda(\theta,\lambda)\phi_\lambda(\theta)d\lambda}{\int_{\lambda_1}^{\lambda_2} \phi_\lambda(\lambda)d\lambda} \qquad [1.5]$$

where X_λ can be T_λ, R_λ, A_λ, or ε_λ; and ϕ_λ represents the appropriate spectral distribution for the luminous, solar and thermal range.

Solar and thermal radiation are each confined in specific wavelength ranges. The key concept for energy efficiency is spectral selectivity which implies that the radiative properties of glazings differ in different wavelength ranges. It is, for instance, the possibility to combine the transmittance of visible radiation with the reflectance of thermal radiation. Figure 1.2 shows the spectral selectivity of a ZnO film[8] doped with aluminium over the solar spectrum.

1.3 Insulating glazings

Historically, fenestration products have always been a key part of any architectural design. The basic reason for an improved energy efficient glazing lies in the properties of the standard glass window itself.

Figure 1.3 shows the spectral transmittance and reflectance of a 6 mm thick glass. The spectrum shows a very high visible transmittance, which is a key property for advanced glazing development. Glass is also seen to be opaque in the thermal range. Some of the absorbed energy will increase the temperature of the glass, and the thermal emittance is high.

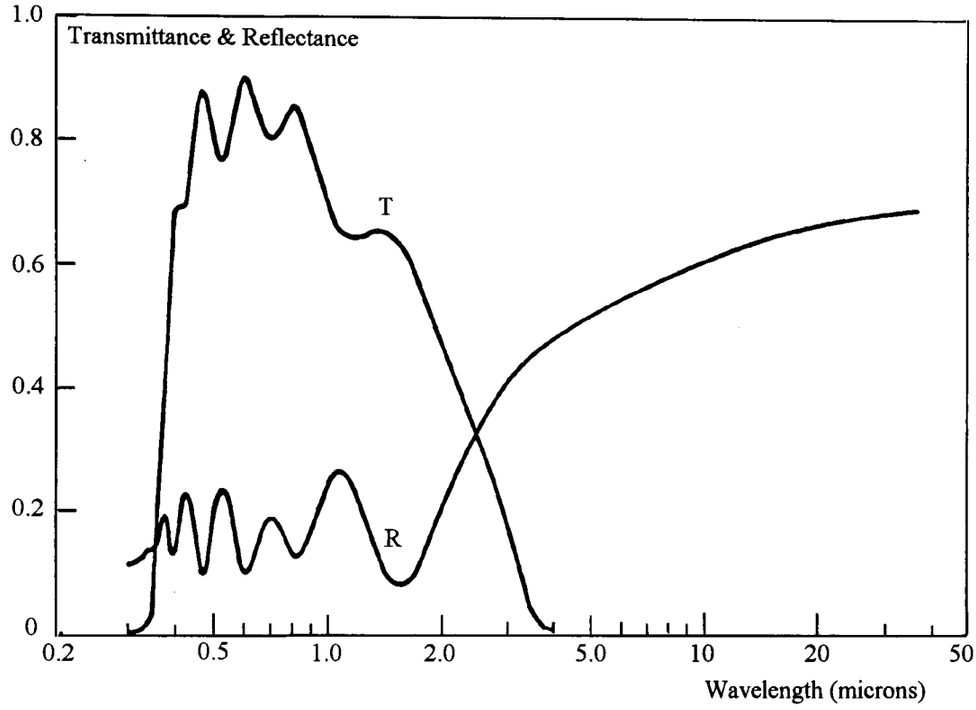

Figure 1.2 : Spectral transmittance and reflectance of a zinc oxide film doped with aluminium[8]: $T_v = 0.84$, $T_s = 0.70$, $R_s = 0.14$ and $\varepsilon_{300°K} = 0.30$.

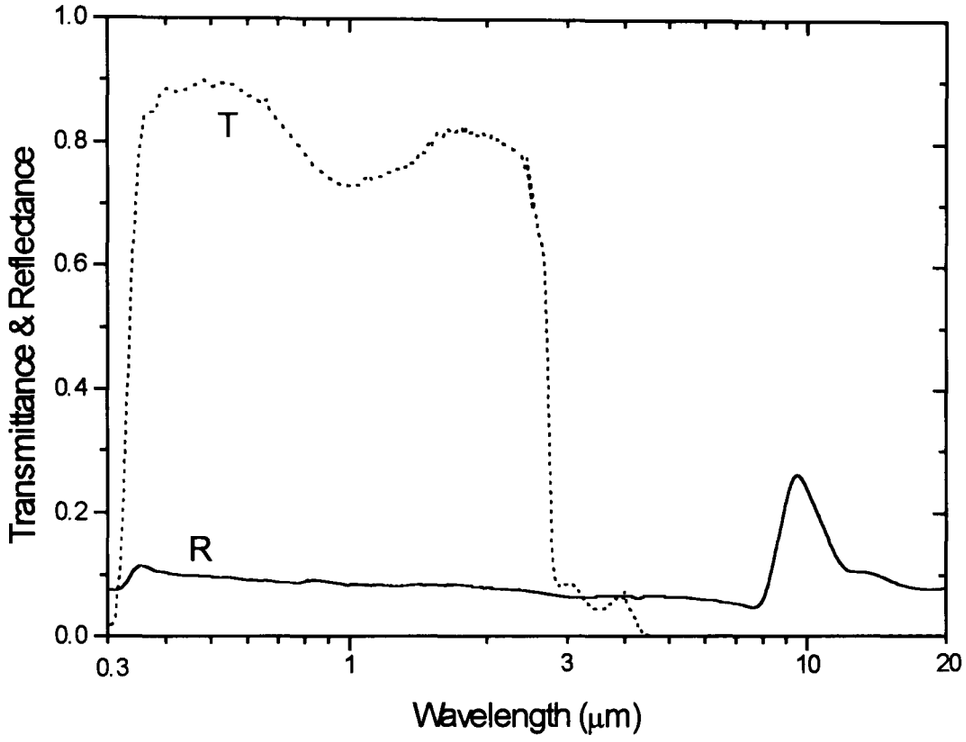

Figure 1.3 : Hemispherical transmittance and reflectance (0.3 - 20 μm) of a 6 mm thick float glass. $T_s = 0.79$, $T_v = 0.89$, $R_s = R_v = 0.07$, $E_{300°K} = 0.87$.

The method used to produce modern float glass was developed by Pilkington, where the glass solidifies on a bath of molten tin. The technique is very well developed and gives a very good uniformity and flatness of the pane. The design of high performance window products is based on understanding heat transfer and optics of window systems. In the past, total heat transfer was based on the glazed areas only. Recent research has demonstrated the importance of the frame and the edge on overall window thermal properties[9]. The total heat transfer coefficient (or *U-value*) of the total window system includes conductive, convective and radiative heat transfer. The solar heat gain coefficient (g_n *or SHGC*) of the total window system represents the solar heat gain through the window system relative to the incident solar radiation and is the sum of the solar transmittance and the longwave input of the solar radiation absorbed within the glazing that enters the building. Heat transfer through window systems can be separated into a heat transfer through the centre of glass areas and through the frame and edge areas. Also different environmental effects strongly influence window heat transfer such as : the solar spectrum, indoor and outdoor radiative temperatures, wind speed and direction and air flow inside the building.

For many years, northern European buildings have been using two sets of glass windows containing an air interlayer. This system could alter heat transfer by thermal radiation conduction or convection. After single glass windows, this glazing system was the first to combine high transmittance with a reduction in energy losses.

Technologically advanced windows are generally composed of more than one pane of transparent material (glass usually), and the radiative heat transfer is defined as an infrared radiation exchange from one layer to another. The radiative heat transfer across a gap is proportional to the effective emittance. Consequently, reducing the emittance of surfaces would reduce the radiative heat transfer through the whole system. Radiative properties of glazings can be altered by thin coatings called low-emissivity (or *low-e*) coatings[10] deposited on a glass surface.

1.3.1 Noble-metal coatings

If a metal is thin enough, it will be partially transparent to visible and solar radiation, but it will still show good infrared reflectance. Extremely thin layers of metal (0.03 μm) can

be used to reduce thermal loss[11]. These coatings are called noble-metal coatings or coinage metal films[12] due to the free electron and they are the simplest technique to increase long wavelength reflectance combined with a relatively good short wavelength transmittance. Heat mirrors are obtained with Cu, Ag and Au or with alternative materials such as TiN, ZrN and Al[12].

To be transparent such layers must be very thin. When deposited onto glass the coating goes through a series of different stages. Metallic materials will be formed at certain sites on the substrate surface like metal islands[12]. When deposition continues, more and more islands appear, then the growing coating forms a metallic network. The space between the metallic islands becomes smaller and smaller until a uniform layer is formed. Noble-metal films are reasonably uniform for thicknesses greater than 0.01 μm. The metallic conduction of such coatings is only possible when a sufficient thickness including a large network is obtained. The visible transmittance decreases with increasing thickness.

The interest of these coatings are : they can be produced at high deposition rate without control of the stoichiometry; they are good electronic conductors to be used in an electrochromic device. The disadvantages are : they are soft, porous, strongly oxidising, chemically reactive and their electrical resistance depends on their thickness to which the optical absorption will be directly proportional.

1.3.2 Dielectric/metal/dielectric coatings

The limited transmittance through reasonably uniform noble-metal layers is caused by reflection at the surfaces of the coating, and the transmittance can be improved by additional layers which stop the reflection of the metal[11,13]. Then dielectric/metal or dielectric/metal/dielectric multilayers are considered to overcome the problem. Dielectrics with high refractive indices such as Bi_2O_3, In_2O_3, TiO_2, SnO_2, ZnS and Al_2O_3 are the most widely used coatings. Fabrication of such coatings requires a precise control of the stoichoimetry and the deposition rate is usually low. In comparison to noble-metal films, these films are hard, compact, chemically resistant and anti-reflecting. Their thickness can be tuned to make coatings anti-reflecting and cause T_v to peak at different wavelength ranges. By selecting the appropriate thickness of a three layer system, it can be used to optimise the energy efficiency. For a warm climate, a maximum thermal

reflectance is a priority compared to the level of visible transmittance, and for a cold climate luminous transmittance has to be maximised as well as having a low emissivity. Figure 1.4 shows the hemispherical transmittance and reflectance of an Interpane Ipasol™ product which is a $BiO_2/Ag/BiO_2$ multilayer[14].

Another advantage of this multilayered system is the protection of the metallic film from chemical reactions and oxidation.

1.3.3 Doped oxide coatings

Alternative to the noble-metal based coatings are doped semiconductors. The semiconductor must possess a wide band-gap to allow high transmission in the luminous and solar ranges and the doping level must be high enough to allow the material to be metallic therefore conducting and infrared reflecting.

The unique transparent properties of heat mirrors are based on the existence of a forbidden energy gap in their band structure and the possibility to generate free electrons or holes by doping. The energy gap and the plasma wavelength (λ_p) define the transparency region of the heat mirror. λ_p is given by the concentration N of the dopant and will increase with an increasing N. In a metal, N is large enough to move λ_p to the UV/VIS region of the spectrum. In the case of semiconductors, N needs to be in the range (10^{19} - 10^{21} cm^{-3}) to bring λ_p to the near infrared[13].

Several materials based on Zn, Cd, In, and Sn have been used. The doping is achieved with the addition of a foreign element (extrinsic doping) or it can be achieved with a deficiency of oxygen (intrinsic doping). Like dielectric/metal/dielectric multilayers, these films are chemically resistant and mechanically durable and their resistivity is independent of thickness. Strict control of film stoichiometry during deposition is also necessary. They can be easily used on glass surfaces inside the glazing cavity.

Good results have been obtained with SnO_2 doped[15] with F, Sb and Mo; and ZnO[16,17] doped with In or Al. Another commonly used heat mirror is indium oxide doped with tin. Figure 1.5 shows the optical spectra of Pilkington K-Glass™ (SnO_2-F)[18]. The luminous transmittance is shown to be very high as well as the thermal reflectance. This type of coating is useful for energy efficient windows to be applied in a cold climate.

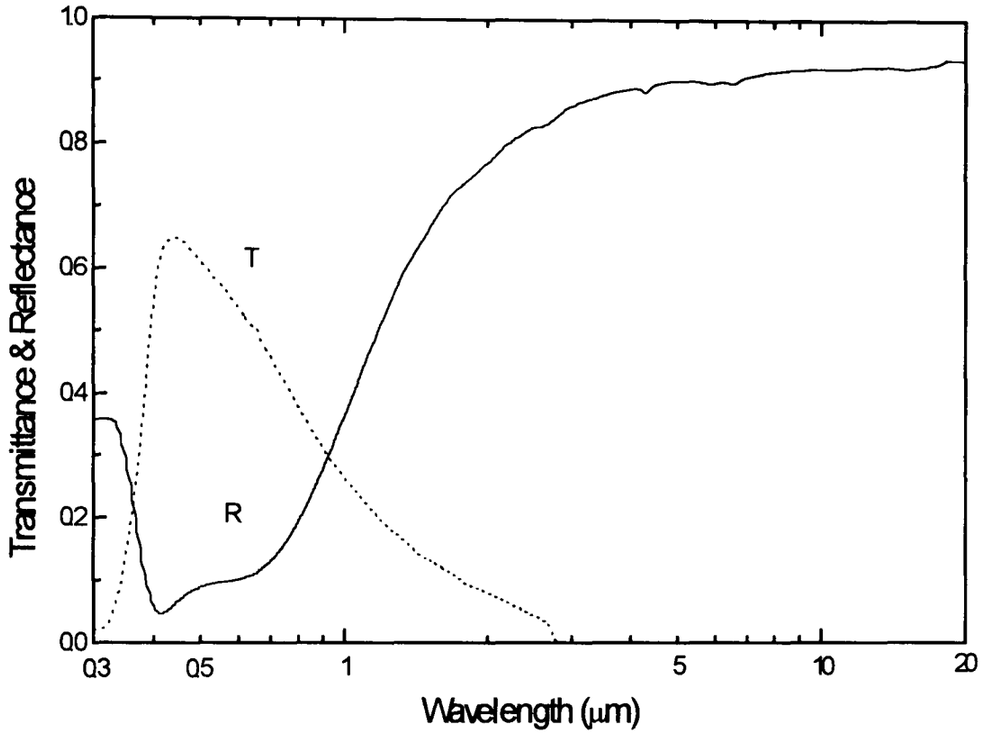

Figure 1.4 : Hemispherical transmittance and reflectance (0.3 - 20 μm) of an Interpane Ipasol™ (BiO_2/Ag/BiO_2) [14]. $T_s = 0.37$, $T_v = 0.57$, $R_s = 0.29$, $R_v = 0.10$, $E_{300°K} = 0.06$.

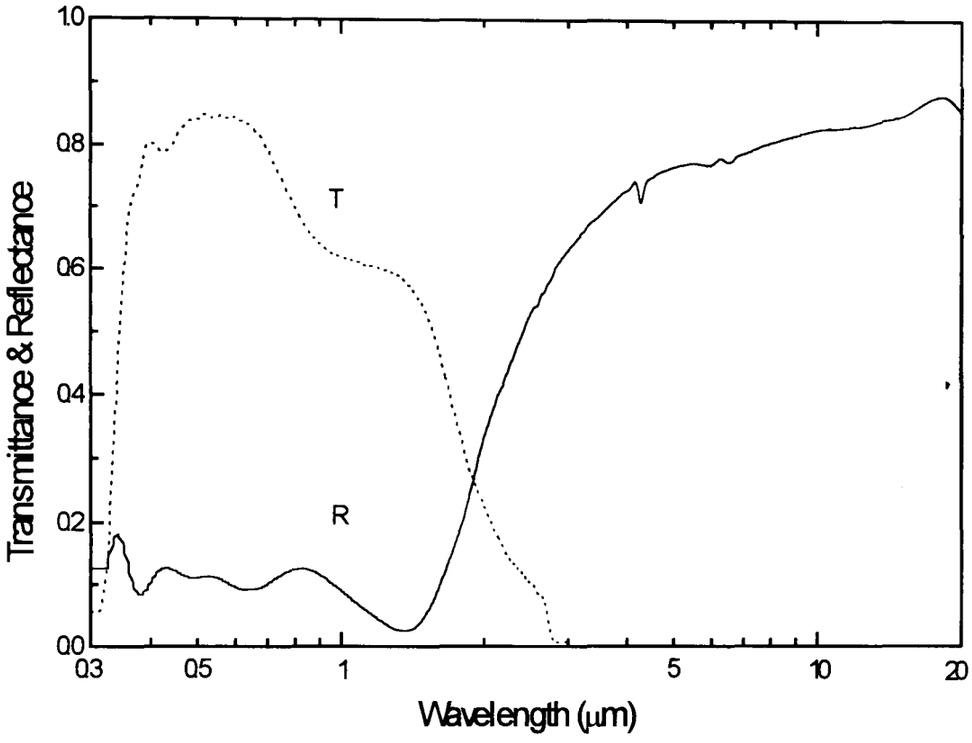

Figure 1.5 : Hemispherical transmittance and reflectance (0.3 - 20 μm) of a Pilkington K-Glass™(SnO_2-F)[18]. $T_s = 0.68$, $T_v = 0.84$, $R_s = R_v = 0.11$, $E_{300°K} = 0.16$.

It is also useful for electrochromic glazings because of their high electronic conductance combined with a high visible transmittance.

1.3.4 Solar gain control

Infrared reflecting thin films behave differently in respect of incident solar radiation. Heavily doped semiconductor materials where the plasma frequency (ω_p) is in the NIR transmit visible and near-infrared radiation. In contrast, noble-metal based coatings with high free electrons density transmit only the visible radiation. Semiconductor heat mirrors are used in cold climates where solar gain is required to be high. Noble-metal based solar gain control coatings have greater values of T_v coupled with lower values of T_s and low emissivity. As such they may have significant advantages in applications such as commercial buildings where solar gain is to be restricted to prevent overheating while providing high visible transmittance.

1.3.5 Gas filling

The use of low emissivity coatings can reduce heat transfer across a gap by a factor of two, which makes the conductive and convective heat transfer dominant. Heat transfer inside the gap is then due to conduction and natural convection. Air is a relatively good insulator, though conduction can be further reduced by filling the gap with lower conductivity inert (or noble) gases. Also, the use of a relatively high viscosity gas can limit convection. Suitable gases used in windows must also be non-toxic, inert, and the most commonly used[2] are listed in Table 1.1.

1.3.6 Edge seal and frames

High performance insulating glass units can be maximised with the use of a third low-e layer unit with two gas gaps. Significant improvements in centre of glass thermal performance make heat losses through the frame and the edge of a traditional window comparatively more important.

Gas	Thermal conductivity ($W.m^{-1}.°C^{-1}$)
Air	0.241
Argon	0.0162
CO_2	0.0146
Krypton	0.0086
Xenon	0.0049

Table 1.1 : Thermal conductivity of different gases[2].

The design of new energy efficient products raises the need to represent the performance of the whole window. Heat transfer through window frames is similar to heat transfer through windows e.g. convection, conduction and radiation effects. Modelling tools are used to examine temperatures and heat flows through different materials containing different air spaces. To reduce heat transfer, crucial improvements need to be focused on the thermal bridging effects of frame components. The solar heat gain through frame areas is a function of the solar absorptance and heat resistance of the material used but more significant is the infiltration through the window. The opening mechanism is usually the main reason for the infiltration and it should be adapted to climatic conditions (wind, rain, large temperature variations). The frame made of aluminium or vinyl should be designed for optimum thermal efficiency which incorporates different cavities filled either with air or with an insulating foam[2]. The window spacers should also be carefully chosen to limit bridging heat transfer. It includes foam or butyl spacers, U-shaped spacers or thermally broken metal[3].

All the above technologies are already widely commercially available. Computing tools are available to model and predict the energy performance and the optical characteristics of any type of glazing unit[19]. Table 1.2 gives an indication of typical performances for different combinations of glazing systems.

1.3.7 Alternative or complementary technologies

More recently, research efforts have also concentrated on future highly insulating and non-conventional window technologies. Evacuated windows are a possible alternative solution[21,22]. Another promising means to reduce conductive, convective and radiative heat transfer through window systems is to fill the space between the glass panes with transparent insulating media[23]. These materials can be flexible polymer foils, honeycomb materials, bubbles, foams, fibres and silica aerogels. They can be almost transparent to the eye (aerogels, polymers) or highly scattering (honeycomb, foams, bubbles, fibres). The characteristics of such media are to be almost transparent or translucent to the human eye, and to possess a structure in which air is trapped. However, optical properties are usually different from conventional insulating glass units, with transmitted light being often scattered.

Glazing type	Gas filling	Thickness of layers (mm)	T_v	g_n or SHGC	Total U-value ($W.m^{-2}.°K^{-1}$)
DGU with no coating	Air	5 - 16 - 5	0.81	0.76	2.9
DGU + hard heat mirror	Argon	5 - 14 - *5	0.75	0.72	1.9
DGU + soft heat mirror	Argon	5 - 14 - *5	0.74	0.61	1.3
DGU + soft heat mirror	Xenon	5 - 8 - *5	0.76	0.58	0.9
TGU + soft heat mirror	Krypton	4* - 8-4-8 - *4	0.63	0.55	0.7
TGU + soft heat mirror	Xenon	5* - 8-5-8 - *5	0.64	0.42	0.4

Table 1.2 : Typical key parameters for different glazing systems[20].
Legend : DGU: Double Glazed Unit; TGU : Triple Glazed Unit.

An energy efficient window is a device capable of providing sufficient natural lighting during the day[24] to minimise the use of artificial lighting and also thermal comfort during both day and night. Thermal comfort implies a control of overheating to minimise the use of a cooling system as well as limiting heat losses by radiation, conduction or convection to minimise the use of an heating or cooling load. The impact of solar gains will vary with building type and use, climate, season and the time of day. When minimising U-values are always better, this is different for solar heat gain coefficients. For some applications it needs to be maximised, and for others, it needs to be as low as possible.
For buildings in cooling-dominated climates, it may be important to minimise the solar radiation entering rooms through glazing units.

1.4 Variable solar gain control

Energy efficient windows can incorporate a system which enables a dynamic throughput of radiant energy. This solution is of particular interest in temperate and cooling-dominated climates when there is sometimes a need for preventing overheating during the hot season and when solar gain can reduce heating demands at other times of the year. This can be achieved by some form of reversible, variable transmittance window. Such an advanced system is called "chromogenic glazing" or "smart window". In addition to energy and thermal comfort benefits, the control of solar gain can enhance visual comfort by reducing glare.
For heating-dominated climates, window systems must be designed to limit the energy losses when solar gain has to be maximised. The use of multi-glazings will decrease losses due to conduction and convection. The use of "heat mirrors" or passive insulators can lower the heat transfer and provide maximum gain of solar radiation. Again, chromogenic glazings offer the opportunity to control the building's energy savings.
There are currently different types of switchable glazings, and three control mechanisms exist : they can be light sensitive or photochromic, heat sensitive or thermochromic and electrically activated or electrochromic.

Thermochromic, for instance, can respond well to thermal effects, but may not allow the proper transmittance of daylight, and might not distinguish both inside and outside temperatures or take into account the quantity of incident solar radiation. Photochromic glazings controls daylighting but are inappropriate to control solar heat gains. Electrochromic glazings offer the highest degree of control. Such windows can be integrated into building energy-management systems to permit a direct optimisation of lighting and cooling consumption.

Finally, the window should be integrated as one component of a building system to enable and control further energy savings. Such a window system integrated with the surrounding wall should allow the wall to have a better thermal performance and improve the performance of the window. This system uses solar shadings above the window and wall cavities with high infrared insulation. Cooling and heating systems, lighting and smart glazing systems could then be monitored by a computerised control system with the help of photo sensors, comfort sensors and thermostats. Because electrochromics can be controlled by a system which best suits each application, they are viewed by manufacturers as having greater potential for energy savings and user comfort than any other chromogenics.

Chapter 2

ELECTROCHROMIC MATERIALS AND ELECTROCHROMIC DEVICES

2.1 Introduction

The dynamic window described in Chapter 1 controls incoming radiation and regulation is climate-dependent. Among the different possibilities in chromogenics glazings, the most probable alternative uses of electrochromic thin films are to vary the amount of incoming radiant energy.

This Chapter presents a review of the electrochromism principle and materials known to exhibit electrochromic properties. Different electrochromic device designs are described with the aim of practical utilisation for energy control glazings. Among these, the five-layer laminated design presents particular advantages for future window applications. Most work in this thesis concerns materials of interest for the development of an all-solid state electrochromic window with good characteristics for energy efficiency. Ideal performance characteristics of such materials and devices are presented in this Chapter.

2.2 Electrochromism and electrochromic materials

Electrochromic materials have gradual and reversible optical properties at solar wavelengths achieved by the application of an external electric field. A clear statement of the electrochromic effect was published in 1961 by J.R. Platt[1] where the author reported: "*The absorption and emission spectra of certain dyes may be shifted by hundreds of Angstroms upon application of a strong electric field. The effect could be called 'electrochromism' in analogy to 'thermochromism' and 'photochromism'...*

It appears that [..] dyes and other organic and inorganic compounds might turn up phenomena of considerable interest and value. "

The electrochromic phenomenon was discovered in tungsten oxide films which have been the most studied material. There are two major categories of electrochromic materials: transition metal oxides including intercalated compounds, and organic compounds[2].

Table 2.1 presents some of the most common transition metal oxides which are coloured by oxidation or reduction, and Table 2.2 presents some of the most common organic materials that exhibit electrochromism.

All the well known transition metal oxide (*MeO*) materials which exhibit electrochromism possess similar features[3]. Particular crystal structures, composed of MeO_6 octahedra with corner-sharing and edge-sharing arrangements seem well suited for electrochromic behaviour. MeO_6 units can be arranged in cluster-type or columnar microstructures. Many electrochromic materials have defect perovskite, rutile or layered structures and the electronic bandstructure of these ionic arrangements explains the presence of cathodic or anodic electrochromism. Optical absorption can be due to intraband effects, interband transitions and polaron hopping (see Chapter 3).

These materials have their largest technological applications as ion insertion electrodes in solid-state batteries. Electrochromic metal oxides can be considered as intercalation compounds which change their optical properties.

A simplified representation of the reaction for a cathodic colouring material is :

$$MeO_x\,(transparent) + yM^+ + ye^- \rightleftharpoons M_yMeO_x\,(coloured) \qquad [2.1]$$

and for an anodic colouring material is :

$$M_yMeO_x\,(transparent)^- \rightleftharpoons MeO\,(coloured) + yM^+ + ye^- \qquad [2.2]$$

where M = Li^+,H^+,Na^+... and Me = *Transition Metal*.

Materials	Coloured state	Bleached state
Cathodic materials:		
Tungsten Oxide (WO_3)	*Blue*	*Colourless*
Molybdenum Oxide (MoO_3)	*Grey-Purple*	*Yellow*
Titanium Oxide(TiO_2)	*Blue*	*Colourless*
Niobium Oxide (Nb_2O_5)	*Bronze*	*Colourless*
Vanadium Oxide (V_2O_5)	*Blue, Grey, Black*	*Yellow*
Tantalum Oxide (Ta_2O_5)	*Neutral*	*Colourless*
Anodic materials:		
Nickel Oxide (NiO_x)	*Bronze*	*Colourless*
Iridium Oxide (IrO_2)	*Black*	*Colourless*
Rhodium Oxide(Rh_2O_3)	*Green, Brown, Purple*	*Yellow*
Cobalt Oxide (CoO_x)	*Purple, Grey, Black*	*Red*
Chromium Oxide (Cr_2O_3)	*Dark brown*	*Pale brown*
Manganese Oxide (MnO_2)	*Colourless*	*Colourless*
Iron Oxide (FeO_x)	*Red*	*Colourless*
Vanadium Oxide (VO_2)	*Blue, Grey*	*Yellow, brown*

Table 2.1 : List of cathodic and anodic inorganic electrochromic materials[4].

Materials	Coloured state	Bleached state
Viologens	*Blue, Violet, Red*	*Colourless*
Polyaniline	*Green, Blue, Purple*	*Colourless*
Polypyrrole	*Brown*	*Yellow*
Polythiophene	*Blue*	*Red*
Polysiothianaphene	*Black*	*Colourless*
Anthraquinones	*Blue, Green*	*Red*
Magnesium Phthalocyanines	*Green*	*Red, Violet, Blue*
Lutetium Diphthalocyanines	*Green*	*Red, Violet, Blue*
Tetrathiafulvalenes	*Yellow*	*Green, Purple*
Pyrazoline	*Yellow*	*Yellow, Blue*

Table 2.2 : List of some organic electrochromic materials[2,5,6,7,8,9,10].

More detailed consideration of the reaction is given in Chapter 3 and in chapters related to the transition metal oxide materials studied in this work.

With organic electrochromic compounds, coloration is achieved by an oxidation-reduction reaction, which may be coupled to a chemical reaction.

Detailed reviews of organic and inorganic electrochromic materials and more generally of chromogenic materials have been produced by the laboratory[11,12] and published by different authors[2,4,13].

2.3 Electrochromic devices for variable transmission control

To date the first large-scale commercialisation of electrochromic technology was for the car industry[14]. The earliest electrochromic patent, dating back to 1929, concerned an antidazzle and fog-penetrating device for car headlamps using aqueous electrochemichromic solutions[15]. In 1969, the first electrochromic display device was reported by Deb[16] using inorganic oxides such as amorphous WO_3 films as the colour centre. Technology evolved and electrochromic devices can now be constructed in several different ways. Various designs are possible including assemblies with 3 to 7 layers[14]. This Section presents some of the possible designs including a device with favourable commercial applications.

2.3.1 Smart window designs

The earliest electrochromic device for car application was designed with 3 layers. Figure 2.1(a) shows a simple three-layer configuration[14]. An electrochemichromic solution contains a redox couple responsible for a colour change when a potential is applied between the two transparent conducting layers. However, like liquid crystals, the system comes back to its original state when the potential is turned off.

A 4-layer configuration is shown in Figure 2.1(b). A liquid or polymeric electrolyte is sandwiched between a transparent conductor and an electrochromic WO_3 film coated on a second transparent conductor.

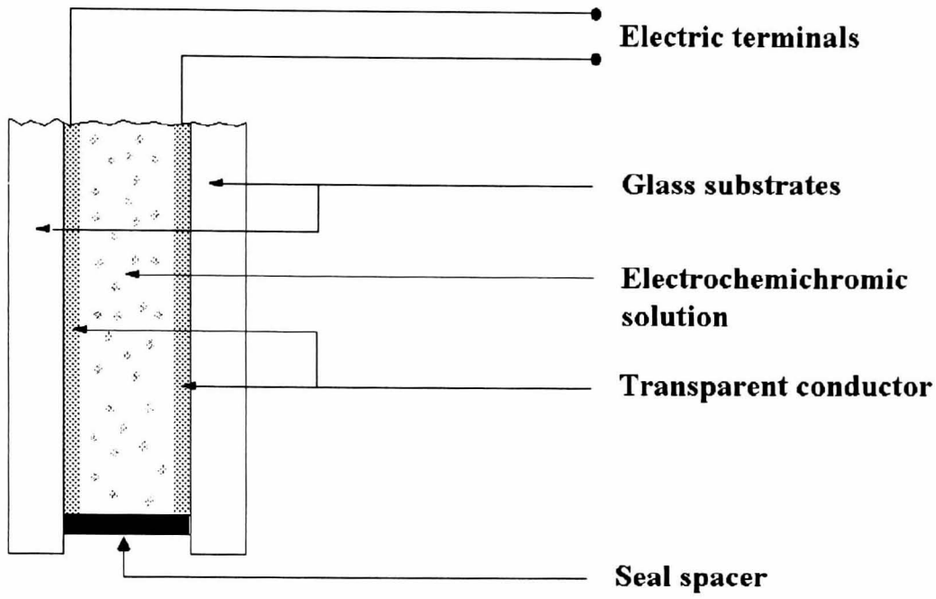

Figure 2.1 (a): A three-layer configuration of an electrochromic window device[14].

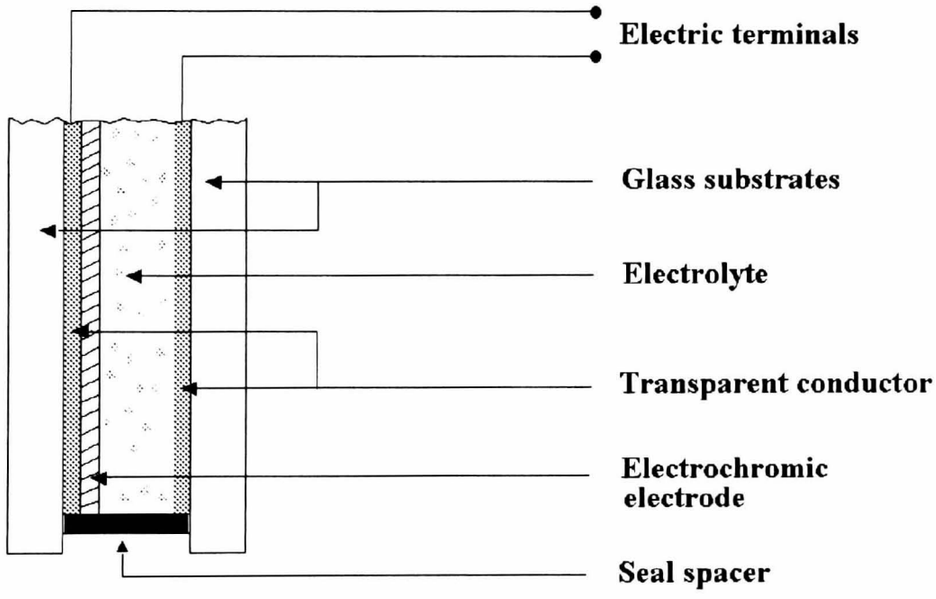

Figure 2.1 (b): A four-layer configuration of an electrochromic window device[14].

The ions responsible for the oxidation and the reduction of the WO_3 must have a redox reaction in the electrolyte or in the transparent conductor. A problem in this type of device is that a long lifetime may be hard to accomplish.

In his paper, Lyman[14] also reports a 7-layer reflective device. This system is symmetrically constructed using two 4-layer systems located on each side of a reflector layer. This configuration does not present any real advantage over the 4-layer design, and its manufacturing time and cost may be much higher.

Another possible electrochromic device system is the 5-layer configuration. This is shown in Figure 2.2, where a fifth ion-storing layer is added to the construction of the 4-layer device. As a consequence, a charge balanced process can take place. The different layers may be sandwiched between two glass panes and are therefore protected from the outside environment. The outermost layers are two transparent conducting films which drive the ions. These transparent conducting layers are usually highly doped semiconductors, such as In_2O_3 :Sn. The sheet resistivity of the layer is in the order of 1 - 30 Ω/□. This semiconductor is typically 0.1 to 0.3 μm thick. The second layer is the electrochromic layer. Usually this is 50 to 300 nm thick. Then follows a fast ion conductor or electrolyte which can be a transparent polymer such as a polymer based on polyethylene oxide or an all-solid state inorganic material. This layer exhibits ionic conduction but little or no electronic conduction. If a polymer is used, the device is laminated and the polymer layer is typically 5 to 50 μm thick. The fourth layer is the ion storage layer or counter electrode material which can be another electrochromic material. Its thickness is about that of the electrochromic layer. This layer can be optically passive and act purely as an ion storage layer or can serve as a complementary layer to the working electrode layer, e.g. one material is anodic and the other is cathodic. They work in such a way that they colour and bleach together. The 5-layer design is the most favoured system due to its similarity with solid-state batteries.

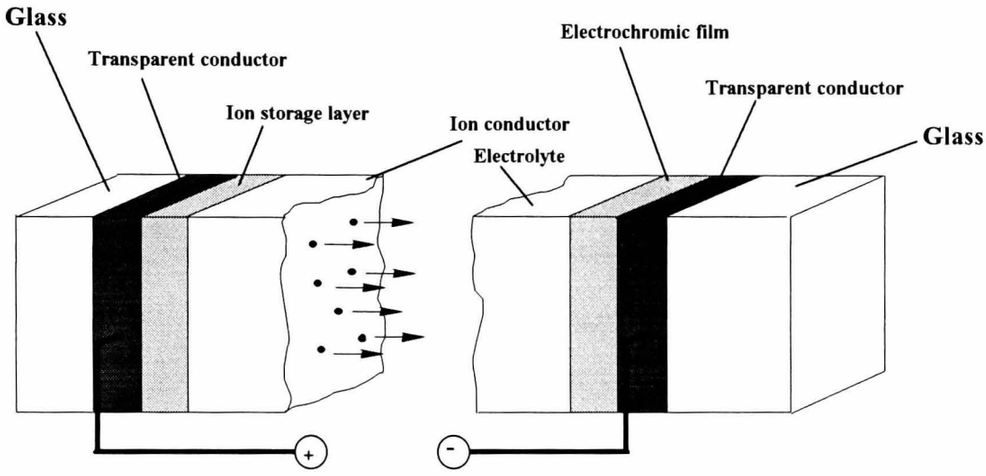

Figure 2.2 : Basic design of an electrochromic device (from Granqvist[2]).

2.3.2 Organic ion conductors

Over the past 30 years, conducting polymer technology has been rapidly developed mainly for battery applications. Polymers provide materials which are relatively light-weight; most of them are optically colourless or transparent; electrically insulating; and they possess a wide capacity for mechanical robustness and flexibility[17].

2.3.2.1 Ionic conduction in polymers

The useful properties of polymers are due to their long and repeating groups of atoms called monomers. Two types of chemical reaction can produce polymers[18]. The addition reaction will break a double or triple bond between two carbon atoms in the monomer to form new bonds that link the polymer chain. Such a method requires the generation of free radicals, which are molecules with free electrons. This can be achieved with the use of an initiator such as benzoyl peroxide. The use of radiation will enhance such a reaction. The condensation reaction will join two molecules together to make a larger one by removing some of the constituent atoms which themselves will create a stable molecule such as water.

The polymer chain is formed by atoms which are held together by strong chemical bonds involving the sharing or exchange of electrons[18]. Laterally they are weak. When polymer chains are formed from a solution, they fold back on themselves forming microscopic plate-like crystals. The random nature of the initiation and termination of the polymerisation produces molecules with a wide range of lengths. So the structure is a complex mixture of microscopic ordered and disordered elements. The folding of the polymer molecules masks the anisotropy of the individual molecules to produce a material with isotropic properties.

Polymers have saturated chemical structures. All the outer electrons are used in forming bonds between carbon atoms. Consequently, they are electrical insulators because there are no free electrons to carry charge through the material. The simplest polymer is poly(ethylene) which possesses a complete saturated chain and its backbone is shown in Figure 2.3 (a). To be conducting, some electrons must be less strongly localised in the chemical bonds. This is the case of poly(ethylene oxide)[19] shown in Figure 2.3 (b). The oxygen will be regarded as the donor sites for electrons.

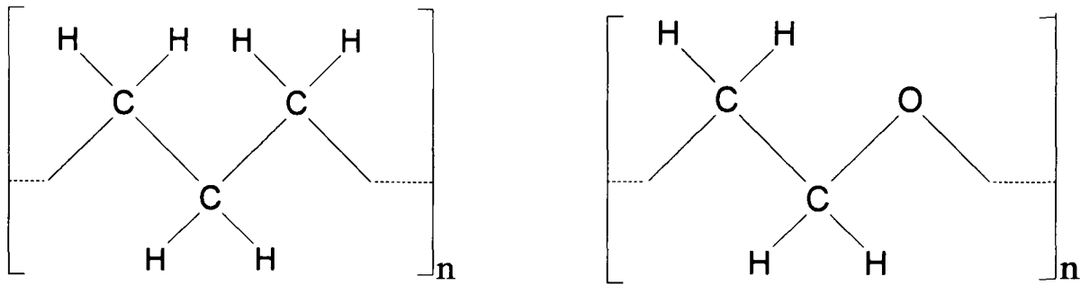

(a) **(b)**

Figure 2.3 : The backbone of poly(ethylene) (a) and of poly(ethylene oxide) (b)

To date, poly(ethylene oxide) (PEO) has been the most studied polymer primarily for batteries[20,21] and secondly for electrochromic displays[22,23] and sensors[24]. This macromolecule possesses groups of atoms with sufficient electron donor properties to form bonds with cations; the barrier to allow bond rotation is relatively low so that segments of the polymer can easily move. Finally they possess a suitable distance between "coordinating centres" to allow the formation of intra-polymer ion bonds.

The conductive performance of the polymer can be improved with the addition of a salt[25]. In this case the essential feature of the polymer is to act as a network to host a salt. The ionic motion takes place without long-range displacement of the solvent[16]. The ionic transport is created by the combination of ion motion coupled with the local motion of polymer segments and inter and intra-polymer transitions between ion sites. However the role of the polymer remains secondary as a conducting medium compared to the conduction of the salt.

The fabrication of the polymer electrolyte film involves the preparation of a solution with the salt. The quantity of salt added to the polymer is crucial for a good conductivity but too high a quantity can affect the polymerisation of the solution[27]. Usually a catalyst is added and then cured at high temperature or by the use of UV radiation to polymerise the material.

2.3.2.2 Ionic-conducting polymers for electrochromic devices

Complexes based on PEO-salt have been the most reported polymers but seem to show some limitations[28] for glazing applications. At temperatures below 65°C the polymer is shown to be crystalline and therefore a bad conductor. This is also shown at lower temperatures in polymers such as poly(propylene oxide) (PPO), poly(vinyl pyridine) (PVP)[29] and oligo(oxyethylene) methacrylate (MEO)[30] with lithium perchlorate as the salt.

A lot of efforts are being made to develop a solid polymer electrolyte with an amorphous structure at room temperature. This problem has been overcome by developing mixtures of different polymers. Several blends based on (PEO) have shown some promising results[31,32].

To obtain higher conductivity at room temperature, gel electrolytes have also been used as an alternative polymer-solvent-salt system. The polymer acts as a stiffener for the

solvent which dissolves the salt[33], for instance poly(methymethacrylate) (PMMA)[34]. Polyvinylidene fluoride (PVdF), polyacrylonitrile (PAN) and polyvinyl acetate (PVAc)[35] have been used to increase the viscosity of lithium perchlorate diluted in propylene carbonate.

Polymer electrolyte films have been produced in a very controlled manner in order to construct devices which take advantage of their unique properties. A large number of recent papers report the preparation and the characterisation of prototype devices composed of conductive polymer electrolytes. Although the lifetime of polymers can be irreversibly affected by environmental conditions[36] (temperature, UV radiation and humidity), intense progress is being made to overcome these problems, and many prototype smart windows have already been successfully fabricated[37,38].

2.3.3 Inorganic ion conductors

Solid state materials exhibiting ionic conduction are also known as superionic conductors. One of the first all-solid state electrochromic devices reported used sodium-β-alumina (Na^+ in β-Al_2O_3) as the solid electrolyte[39]. Initially reported by Yao and Kummer[40], this material has been extensively studied in the field of electrolytes for solid state batteries.

In Chapter 3, it is explained that in nearly-perfect crystals, ionic diffusion is always connected to the existence of lattice defects. Diffusion can take place through vacancies and through interstitial sites in ionic crystals. Such motion of ions is created under the influence of an external field. Ionic motion will increase in disordered structures where the existence of available sites is greater than the number of available ions.

A problem with β-alumina is the very slow diffusion of sodium ions into the electrochromic layer. Furthermore, it is a ceramic which makes the fabrication of large areas impractical[39], and it is an opaque material.

To date, inorganic ion conductors have been mainly studied in the field of solid-state batteries, fuel cells, electronic displays and memory devices. As a consequence, studies on these materials do not investigate the visible properties.

A detailed review of possible candidates was reported by Truong et al.[41] with some emphasis on smart window applications. Physically deposited inorganic ion conductors

are shown to conduct a wide range of cations such as Li^+, H^+, Na^+, K^+, Ag^+ and Cu^+. Only a few all-solid state devices have been reported where inorganic films such as $Ta_2O_5.xH_2O$[42,43], $LiNbO_3$[44] and Li_3N[45] have been incorporated as the ionic conducting layer.

More recently, alternative preparation methods such as electrochemical techniques or spraying processes have been used to deposit inorganic ion conductors. Devices based on electrochromic tungsten oxide films showed reversible EC characteristics with an electrodeposited[46] or spin-coated[47] $Ta_2O_5.xH_2O$ proton conductor. Electrophoretic deposition[48] has also been used to coat SnP (acetone used for the dispersion) as a solid electrolyte in an amorphous WO_3 device. Vacuum evaporation has also been employed in the deposition of AHP (Antimony Hydrogen Phosphate) thin films[49].

Although having an all solid-state electrochromic device that could be physically deposited with one technique presents a technological improvement, and some prototypes seem to have been successfully fabricated[42,43,44], important problems relating to device failures remain unsolved.

2.3.4 The laminated 5-layer design

2.3.4.1 Advantages of the 5-layer configuration

The advantage of the 5-layer configuration is the possibility of a charge-balanced operation, in which ions will intercalate/deintercalate a compound. The largest technological interest of intercalation compounds as ion-insertion electrodes is in solid-state batteries. The simple reaction implies a reversible intercalation using a highly electropositive alkali metal as the intercalated species, e.g. lithium. Owing to their crystal structure (see Chapter 3), transition metal oxides can intercalate ions, which is generally followed by a charge transfer in the host lattice. Consequently, their optical properties may change gradually upon ion insertion. This charge transfer is created by an applied potential and this gives the possibility to directly control the change in optical properties, and to leave the system at any state between a fully inserted state and a fully extracted one when reversing the applied potential, e.g. such system is said to have a memory.

2.3.4.2 Advantage of a laminated system

The problem associated with a liquid electrolyte in an EC device is based on the large area displays. If, for instance, there is a 0.5 mm gap between two glass panes of 2 x 2 square meters, 2 litres of electrolyte will be needed. A liquid electrolyte cannot only represent a potential safety hazard, but the pressure due to gravitational force on the glazing can deform the glass panes and the joints.

A solid-state inorganic electrolyte offers a promising alternative technology. Although several prototype windows have been successfully fabricated, important problems remain unsolved, which are : their very low optical response for glazing applications, their susceptibility to mechanical and thermal stresses, the problem of interfacial resistances and short circuits between the electrodes.

Polymer-based electrolytes offer the advantages of being flexible and robust at the same time and these properties can eliminate several problems associated with liquid or rigid solid ionic conductors. Films can easily be deposited on large surfaces and their mechanical robustness makes them well suited to large area fabrication.

2.3.4.3 Advantages of the electrochromic device based on WO_3 and lithium ions

Despite the interest in other transition metal oxides, which has resulted in hundreds of scientific and technical papers, tungsten oxide remains the most studied and the most understood electrochromic material. It may be used pure or doped with other metal oxides or even used in combination with another active electrochromic material. Therefore there is no doubt that this material promises to have a prominent role as the working electrode in commercial switchable windows.

Some early devices were reported using an aqueous electrolyte with electrochromic tungsten oxide[50]. However, quick degradation was observed mainly due to the dissolution of the tungsten oxide layer. The other main problem is the narrow potential range available above which oxygen and hydrogen evolution will occur in the system.

When using liquid electrolytes, improved durability was achieved with lithiated ion conductors[51]. The technology of solid-state batteries based on lithiated high ion conductors has been extensively developed and is well-understood[52]. Although lithiated systems are very moisture-sensitive, such technology represents today the most attractive solution for commercial applications.

2.4 Performance criteria of electrochromic materials and devices

In Chapter 1, it was indicated that electrochromic technology incorporated into an advanced glazing system can reduce energy loads (lighting, cooling and heating) as well as provide glare control and improve thermal comfort. In Section 2.3, the 5-layer laminated device was described to be the most promising device for large scale development, and consequently is the device of interest in this thesis.

The performance criteria of electrochromic windows are the key information to be defined for the development of commercial glazing. Electrochromic glazings are complex multilayers which can be incorporated into a solar-efficient window system. Only small potential differences, typically 1-5 V are required to alter a change in state. A continuous change between a bleached state to a coloured state is operated as long as charge is being transferred. This is of great interest in building energy management systems where glazings could be controlled for a particular environment and for the users comfort.

2.4.1 The optimum performance properties of electrochromic devices

The properties required for a good electrochromic window system are to be transparent in one state and coloured in the other state.

The lifetime of the device must be a minimum of 10 years of use, which means that it must tolerate 10^5-10^6 colour/bleach cycles without degradation. It must also be stable against solar radiation and temperature variations.

There are three types of ideal switchable electrochromics glazings[53]. Transmittance of the coating can be switched over the entire solar spectrum, only over the visible range or only over the infra-red spectrum. For any change in transmittance, a corresponding change in reflection and absorption will occur. An increase in reflection will reject solar heat, but might increase the effect of glare. The most probable effect of decreasing the transmittance will be the increase of heat absorption by the coating.

In hot countries where daylight carries heat energy, or in cold climates where heating loads have to be preserved, heat gains of the glazing will have to be minimised to achieve maximum energy saving. This can be achieved in a double glazing system where the

electrochromic is used in conjunction with heat mirrors. The effect of such coating would be to reflect both daylight heat and heat generated inside the buildings. The transmittance would be directly controlled by the electrochromic layer. The absorption should be broad over the visible region to give a neutral appearance of the glazing in its dark state and should be minimum in the near-infrared range. This is shown in figure 2.4.

In temperate climates, where solar heat gain could however mean extra energy consumption savings, reflectance over the infrared range can be modulated between 10-20% in the bleached state to 70% in the coloured state.

Durability is another important criterion for large-area chromogenic devices and UV radiation and temperature will be the two major stresses affecting electrochromic technology in a building. Table 2.3 and Figure 2.4 show the ideal performance characteristics of an electrochromic glazing which could have the highest impact in most parts of the world as an energy saving product. Nevertheless the problem should not be limited to the device optimisation but must also address the application of energy-saving systems combined with human comfort quality (see Chapter 1).

2.4.2 The optimum performance properties of the ECD individual layers

To obtain the ideal performance characteristics described in Section 2.4.1, ideal characteristics for every individual layer have to be defined. Each of the 5 layers plays a part in one or several of the overall characteristics of the device.

Most of the work in this thesis is about electrochromic materials to be used as active and passive electrodes. Table 2.4 presents the ideal properties of these materials.

Although they are not the object of this work, electronic and ionic transparent conductors have been developed by collaborative laboratories. The ideal characteristics of these layers are presented in Table 2.5.

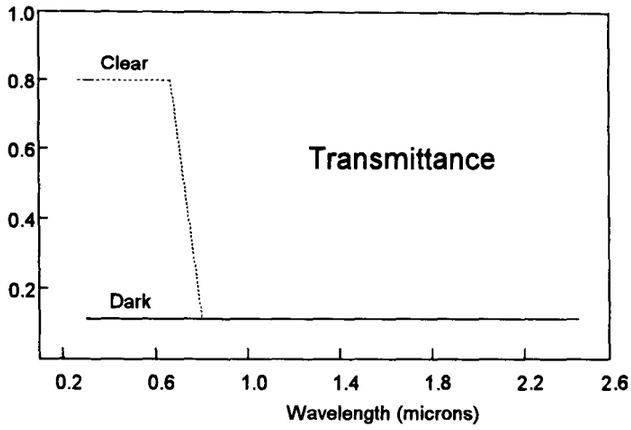

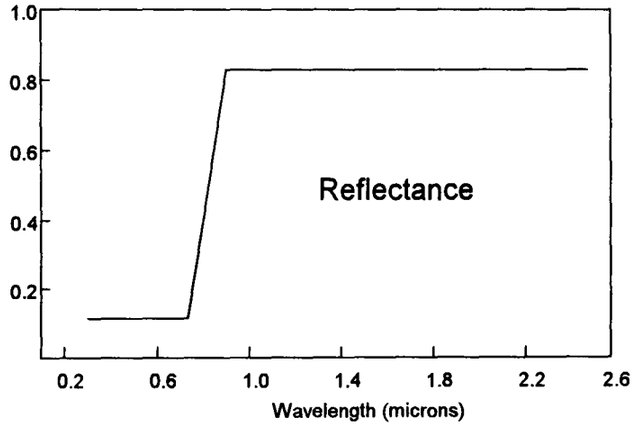

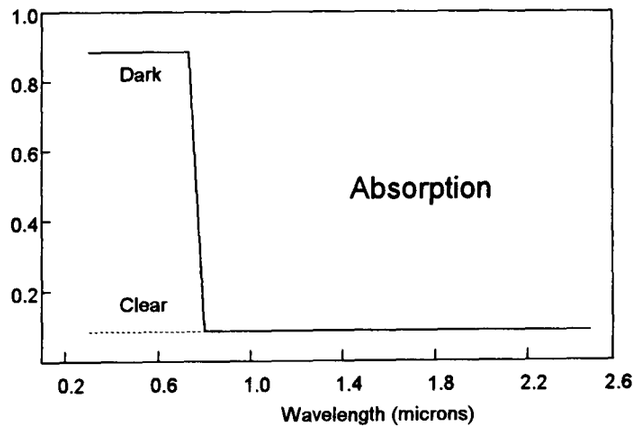

Figure 2.4 : Transmittance, reflectance and absorptance ideal spectra of a smart window system in the dark and clear states.

	Laminated 5-layer electrochromic device
Solar Transmittance	$T_{s,b} \geq 60 - 70\ \%$ $T_{s,c} \leq 10 - 20\ \%$
Visible Transmittance	$T_{v,b} \geq 70\ \%$ $T_{v,c} \leq 10\ \%$
Near IR Reflectance	$\geq 70\ \%$
Voltage Switching	- 5 V - + 5 V
Memory	> 12 hours
Switching Speed	1 - 5 mn
Lifetime	10 - 20 years
Cyclic Lifetime	$> 10^5$ cycles
Operating temperatures	- 30°C - +80°C

Table 2.3 : The optimum performance properties of an electrochromic smart window device[54].

	Active electrochromic layer	Passive ion storage layer
Solar Transmittance	$T_{s,b} \geq 60$ - 70 % $T_{s,c} \leq 10$ - 20 %	Uncharged/charged states > 70 %
Visible Transmittance	$T_{s,b} \geq 70$ % $T_{s,c} \leq 10$ %	Charge/uncharged states > 80 %
Near IR Absorptance	$A_{ir,c} < 10$ %	< 10 %
Voltage Switching	1 - 5 V	1 - 5 V
Switching Speed	1-5 mn	1-5 mn
Charge reversibility	> 95 %	> 95 %
Charge storage capacity	~ 30 mC/cm^2	> 30 mC/cm^2
Coloration efficiency	> 45 cm^2/C	< 10 cm^2/C
Cyclic Lifetime	> 10^5 cycles	> 10^5 cycles

Table 2.4 : The optimum performance properties of electrochromic materials.

	Electron conducting layer	Ion conducting layer
Visible Transmittance	> 90 % with a neutral appearance	> 90 % with a neutral appearance
Near IR Reflectance	> 90 %	> 90 %
Electronic resistivity **Sheet resistivity**	$< 10^{-4}$ Ω.cm < 10 Ω/□	infinite
Ionic conductivity	none	$\sim 10^{-4}$ S/cm
Voltage stability	- 5 V - + 5 V electrochemical stability with respect to the electrodes	- 5 V - + 5 V electrochemical stability with respect to the electrodes
Lifetime	> 20 years	10 - 20 years
Operating temperatures	- 30°C - +80°C	- 30°C - +80°C
Others		adhesiveness to hold two glass panes

Table 2.5 : The optimum performance properties of transparent electronic and ionic conductor materials.

Chapter 3

PROPERTIES OF ELECTROCHROMIC METAL OXIDES

3.1 Introduction

This Chapter presents a review of the chemical and physical properties of transition metal oxides in respect of their electrochromic behaviour. The electrochromism process is the insertion or extraction of ionic species into the lattice, followed simultaneously by the insertion or extraction of electrons into the electronic bands of a material. This Chapter concentrates on the most important factors which influence the electrochromic properties of inorganic transition metal oxides.

The first important factor of electrochromic transition metal oxides is that their crystal structures allow the ionic diffusion process to take place. This Chapter describes the main structural features of these oxides and shows how they are arranged to allow ionic intercalation.

As a consequence of their crystallographic structures, the second important factor is the electronic band structures of transition metal oxide materials. They are characterised by an incomplete filling of the band or bands and those where band overlap occurs. During the ionic intercalation, electrons are inserted into the bands to maintain the overall neutral charge. This Chapter describes how the variation of electronic density in the materials is the key concept for optical modulation of electrochromic materials.

3.2 The crystal structures of transition metal oxides

3.2.1 Static properties of crystals

All inorganic electrochromic materials found to date belong to the transition metal oxide group. They are intermediate crystals between the 3 main types which are described in this section.

At low temperatures, electrostatic forces between electrons and nuclei are responsible for the binding of atoms[1,2]. Attractive Coulomb forces between electrons and nuclei overcome the repulsive Coulomb forces between electrons to hold the structure together. Electrons move independently in well-defined orbits. The orbitals of higher energy which are filled last in accordance with the Pauli principle, are on the outside of the atoms and their energies can be easily modified by neighbouring atoms. The valence electrons are very important in holding solids together. If the atomic orbital of a particular type is completely filled up, more energy is required to break this closed shell. If electrons are extracted or added an ion is formed but the atoms are expected to be particularly stable. If two atoms can form ions by transferring electrons, then they can bind together by mutual Coulomb attraction (*ionic binding*). The second type of crystal is when two atoms share one or several electrons between them (*covalent bonding*). Finally the last type of bonding (*metallic bonding*) is when atoms do not possess a closed electronic shell configuration like the *Van der Waals* crystals. Electrons are weakly bound and tend to be shared by many atoms forming metallic bonds. The main characteristic of metals is their high electrical conductivity due to their large number of relatively free electrons. In the case of covalent crystals, valence electrons are used in bonding, therefore these materials are not good conductors. Nevertheless it is easier to find free electrons in covalent crystals than in Van der Waals or ionic crystals because many are semiconductors. In ionic crystals, binding forces are strong enough to make the materials bad conductors.

However, the ionic type of crystal structure is considered as the dominant type for electrochromic transition metal oxides. This structure is used for instance to model their electronic structures.

3.2.2 Structural features of some electrochromic materials

Transition metal oxides are mainly ionic in their structural features. The close interatomic distances between metal and oxygen provide their stability. This section describes the ways in which metal-oxygen units connect together in electrochromic materials used in this work. These connections have an important influence on electronic properties.

Electrochromic metal oxides and more generally transition metal oxides structures are octahedrally coordinated, although the symmetry is not perfect. Each octahedron can be represented with a metal atom in the centre and oxygen atoms at each of the six corners (MeO_6). The connections between octahedra can be characterised with share corners, edges or faces. These octahedra are arranged so that tunnels or channels with different types of cross section are available for the migration of cations. Most electrochromic metal oxide films are nonstoichiometric polycrystalline or amorphous materials.

The network of corner-sharing octahedra is characteristic of many transition metal oxide bronzes[3]. They are nonstoichiometric compounds in the coloured state formed by inserting atoms into the interstitial sites into the oxide lattice[4,5] and there is one interstitial site per metallic oxide molecule. The guest element (M) inserted into the lattice forms the oxide bronze, originally named by Wöhler[6] in 1823 after HWO_3 which was bronze in colour. Several transition metal oxides with formula M_yMeO_x exhibit similar electrochromic properties. The composition of a bronze can vary from y=0 to y=1. They consist of a $(MeO_x)_n$ covalent network into which yM^+ cations are inserted giving their outer electron to the transition metal array. Best known are the tungsten bronzes M_yWO_3 in which the donor cations occupy tunnels in the crystal structure within the metal oxide network of corner-shared octahedra. This structure is known as the defect *perovskite structure*[7,8] or *rhenium structure*.

Figure 3.1 (a) shows the unit cell for perovskite lattice of tungsten oxide. Figure 3.1 (b) shows an array of octahedra in the perovskite structure. Each octahedron must be imagined with a metal atom in the centre and oxygen atoms at each of the six corners.

The second important crystal structure is the *rutile form*[7,8]. The rutile structure is shown in Figure 3.2 (a). The rutile structure is built of hexagonally packed oxygen lattice with octahedrally coordinated metal ions with 'infinite' edge-sharing chains. The connection of metal-oxygen in the rutile structure is shown in Figure 3.2 (b).

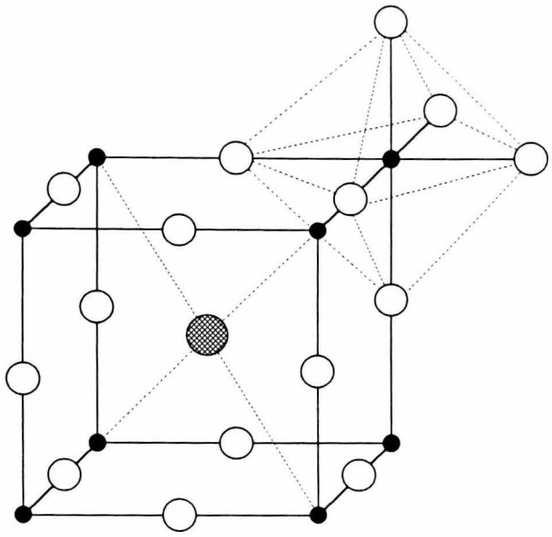

Figure 3.1 (a) : The unit cell for perovskite lattice of WO_3

Legend : ● tungsten, ○ oxygen, ◍ central cation

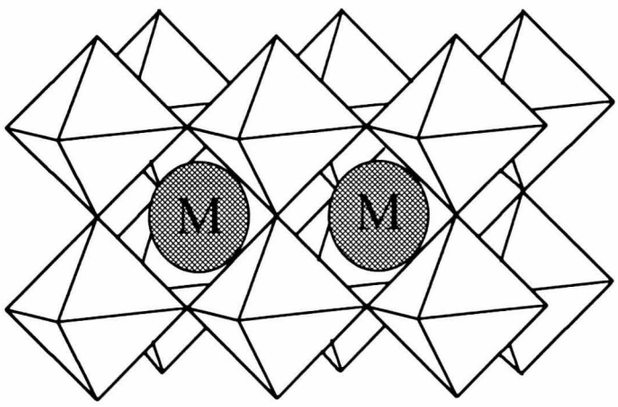

Figure 3.1 (b) : The perovskite structure of octahedra for a M_yMeO_x compound

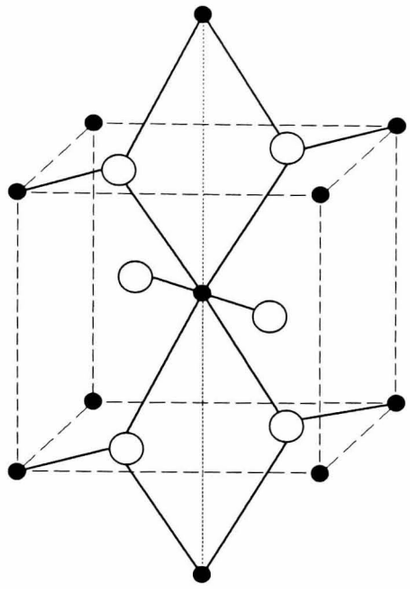

Figure 3.2 (a) : The unit cell for rutile lattice of TiO_2

Legend : ● titanium, ○ oxygen

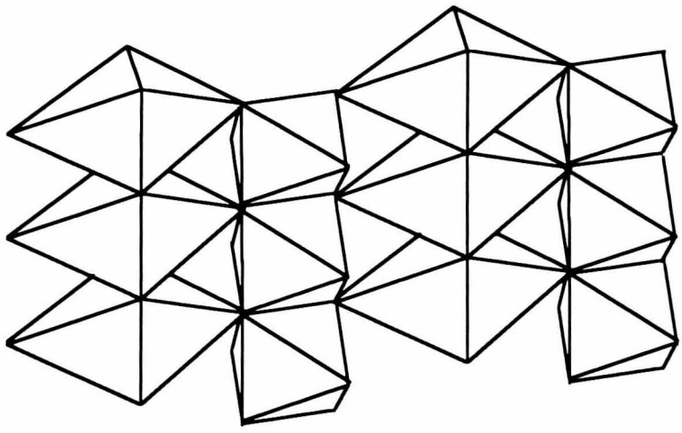

Figure 3.2 (b) : The connection of metal-oxygen octahedra in the rutile structure.

The chains are crosslinked forming vacant channels. Titanium oxide possesses different rutile-like crystal structures. The anatase phase has shown most interest for electrochromic titanium oxide. It consists of a tetragonal structure containing TiO_6 octahedra sharing 2 adjacent edges with two other octahedra forming planar double chains. These chains share corners with other similar chains creating zigzag rows of vacant sites to accommodate ions.

Vanadium dioxide is of tetragonal rutile type structure at temperatures above 68°C, and is of monoclinic configuration at lower temperatures and can still be considered as distorted VO_6 octahedra with a chain configuration characteristic for rutiles.

A number of electrochromic metal oxides present *layered and block structures*[7,8]. Sputtered electrochromic nickel oxide crystals in their as-deposited form are mainly amorphous and non-stoichiometric. Oxygen atoms being larger than nickel atoms, an excess of oxygen in NiO creates a large number of lattice vacancies. They usually present defect versions of the rocksalt structure. Figure 3.3 shows a defect-free rocksalt structure for NiO. Substitution of ions is therefore possible where an alkali metal replaces a missing nickel atom. Such structures, where half the transition metal atoms can be replaced by another atoms, can present alternate layers. Nickel oxide seems to be composed of weakly bound layers made of planes of NiO_6 octahedra sharing edges. The hydrated nickel oxide form has a brucite structure. Empty octahedral and tetrahedral sites contain protons.

3.2.3 Imperfections in crystals

The importance of non-stoichiometry in electrochromic transition metal oxides has been mentioned. The figures shown above describe perfect atomic arrangements that make an ideal crystal. However real crystals have defects and their concentration can be very large. This is of great importance for many physical properties.

At absolute zero temperature, crystals tend to have a perfectly ordered arrangement. When the temperature increases, the amount of thermal vibration of ions in their lattice sites increases as well as their chance to jump out of the lattice: this constitutes a point defect[8,9,10].

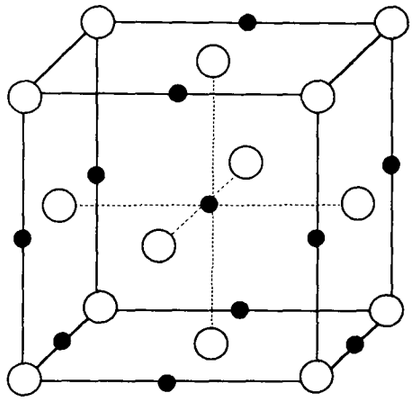

Figure 3.3 : The rocksalt structure of defect free NiO.

Legend : ● nickel, ○ oxygen

The simplest defect is when an atom is absent from a normal lattice site (*lattice defect*). Another is when an atom occupies an irregular site not normally occupied (*interstitial defect*). Ionic compounds can maintain their stoichoimetry in balancing such defects. When a single atom is removed from the lattice, electrical neutrality requires that the missing charge be balanced in some way. It can consist of a pair of "holes" where a missing cation will compensate a missing anion for no net charge. Alternatively the missing ion can be balanced by the presence of an impurity ion of higher charge (*Schottky defect*). Sometimes, electrical neutrality is achieved by not completely removing the ion but by simply moving it to a nearby interstitial site (*Frenkel defect*).

Defects can be eliminated by the formation of crystallographic shear phases. For instance, the alignment of oxygen vacancies in a plane can be shared in such way with another plane that the vacancies are eliminated.

3.2.4 Ionic diffusion in solids

We know that the electrochromic behaviour of transition metal oxides is due to the electronic insertion into its band structure. This intercalation is a consequence of the diffusion of ionic species into the material lattice in order to maintain an overall charge neutrality. Both ionic and electronic conductions are independent, the first being related to the crystal structure and the latter being determined by the electronic bandgap which depends on the individual properties of the constituent ions. A perfectly well ordered crystalline ionic transition metal oxide would in theory not allow any ionic diffusion, therefore electrochromism would not exist. This section presents the main features for ionic diffusion in transition metal oxide materials.

Ionic diffusion is connected to the existence of lattice defects[11] and the most common types of diffusion in crystals are through *vacancies*, through *interstitial sites* and through a combination of both called *interstitialcy mechanism*. In ionic crystals, such motion of ions is created under the influence of an external field.

In a vacancy diffusion[11], ions will move to vacant lattice positions. This is shown in Figure 3.4 (a). The ionic conductivity is high if the number of vacancies is large enough so that an effective number of ions responsible for the diffusion can be present.

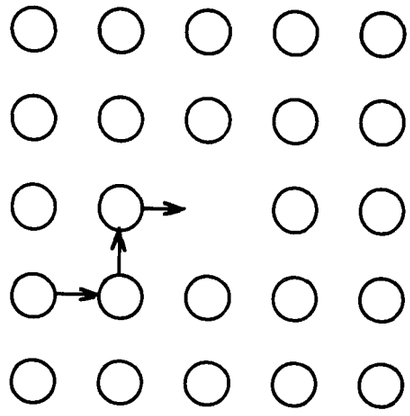

Figure 3.4 (a) : Vacancy diffusion in solids

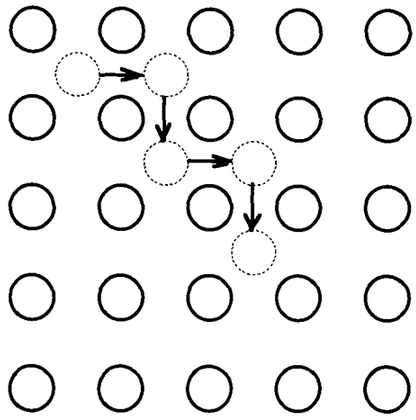

Figure 3.4 (b) : Interstitial diffusion in solids

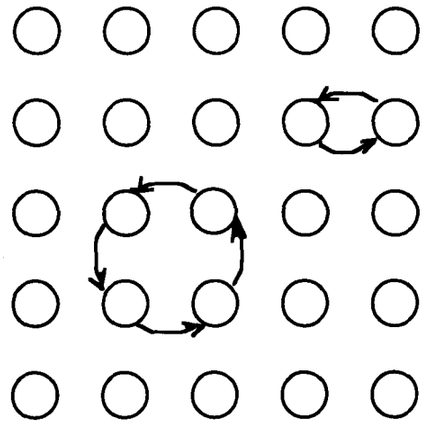

Figure 3.4 (c) : Direct interchange diffusion in solids

If the number of available sites is greater than the number of diffusing ions so that the ions can distribute over all the available sites, a high conductivity can be expected. The characteristics of fast ionic conduction can usually be increased with larger temperatures introducing excitations and structural changes in the lattice. The effect will be the disordering of ions which are constituent units of crystals.

Ionic conduction can also occur in the form of interstitial diffusion[11] where ions will move to normally unoccupied positions like a tetrahedral hole in an octahedral lattice. This is shown in Figure 3.4 (b).

Finally the combination of interstitial and vacancy mechanisms will be the motion of ions into interstitial sites when others will move into the vacancy created. This is shown in Figure 3.4 (c).

In nearly-perfect crystals, the ion diffusion takes place in the form of hopping, and can be described by the random walk theory[11].

However the activation energy is usually very low and it takes a long time to move an ion from one site to another. The probable path which ions would follow between the 2 sites in crystallographic channels and their probable energy will depend on their size. For a favourable size the activation energy of an ion can be low. The ionic motion is also connected to the polarizability of the lattice. An ion will either attract or repel its neighbours from the equilibrium positions. This will create a local polarisation cloud around the central ion, which will be carried with it. The ion motion and the lattice motion are connected.

However, the hopping theory in nearly ordered lattices will only contribute to a very low ionic conduction. Another model based on a vacancy mechanism, where a row of ions moves cooperatively by one interstitial site so that an ion will force an adjacent ion to move out into another adjacent interstitial site.

A disordered lattice where extra interstitial sites are available and where activation energy can be reduced will favour cooperative motions of ions. The major feature of this lattice is that the number of available sites is greater than the number of conduction ions. In disordered systems no clear distinction can be made between the vacancy mechanism and the interstitial or interstitialcy mechanism. Also, preferential sites among available sites as well as the repulsive interactions among ions will contribute positively or negatively to the activation of the diffusion process.

The corner-sharing framework of electrochromic metal oxides can be varied and gives rise to interstices with different sizes. Some of the most common of these structures are based on those of the tungsten bronzes. Depending on the size and concentration, different M cations can be accommodated in the tungsten oxide crystal structure configuration. The cubic structure configuration can accommodate small ions[12] (H^+, Li^+, Na^+), the tetragonal can accommodate ions up to the size of K^+ with the hexagonal configuration for larger ions. The hexagonal tunnel phase of the tungsten bronze is shown in Figure 3.5. The diffusion of cations is most rapid in hexagonal structure[13] where the size of the diffusion channel better matches the size of the mobile ion. Additionally, it is important for the metal oxide to be firstly a single crystal host, secondly to be a small grained polycrystalline thin film (less than 0.5 μm) and finally an amorphous film[5].

The layered and block structures show high ionic diffusion at ambient temperatures. By analogy with the layered β-aluminas, we can assume other layered materials to show high ionic mobility[14].

Finally, the existence of non-stoichiometric compounds makes transition metal oxides more sensitive to preparation conditions.

3.3 The electronic structure of electrochromic transition metal oxides

In the previous section, some basic structural features of transition metal oxides were described. The variation of corner-sharing frameworks, and the presence of defects create channels which can accommodate different cations. As a consequence, the ionic insertion combined with a simultaneous electronic insertion to maintain a charge neutrality inside the crystal is responsible for the alteration of the electronic properties. These properties are essential for transition metal oxide materials to exhibit an electrochromic behaviour. These solids, under normal temperature and pressure, possess a wide range of properties associated with the filling of the *d* orbitals. A particular characteristic of transition metal oxides is their wide range of electronic properties because of the multiplicity of oxidation states.

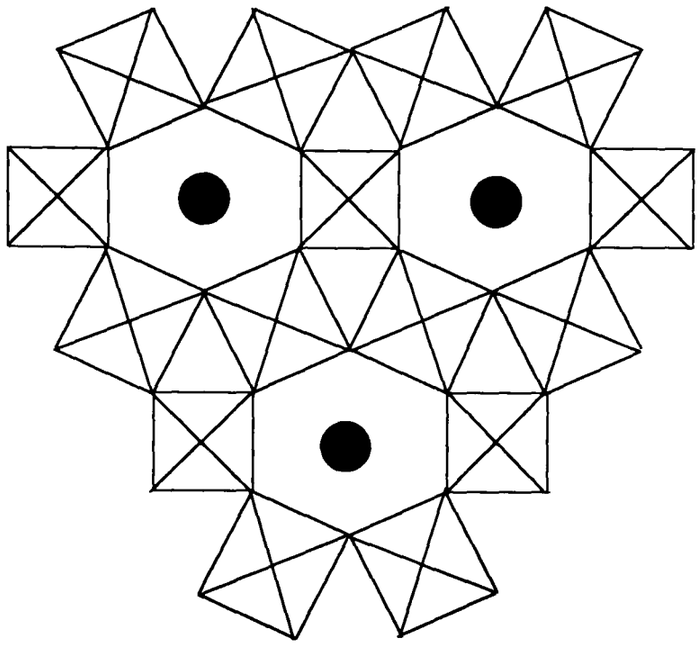

Figure 3.5 : Structure projections of the hexagonal phase of the tungsten bronze M_yWO_3.

In most cases, the crystal structure of electrochromic transition metal oxides is considered based on the ionic type of structure. This can be used to model their electronic structures. Electronic studies are based on quantum mechanical calculation of the total energy. The *ab initio* calculations and *Hartree-Fock* approximations are used to model the electronic structure of well-ordered materials[15,16]. However, defects in materials are much more difficult to treat and require the use of alternative methods[17].
This section presents the electronic band structure of the transitions metal oxides studied in this thesis.

3.3.1 Dynamic properties of crystals

The electron motion is divided into approximately two basic models. In the case of Van der Waals and ionic crystals, electrons are not allowed to move from one constituent to another. The electron orbits are slightly perturbed by the electrical forces of other constituents, but electrons are expected to move in their atomic orbits. In the case of covalent and metallic crystals, the above model is true for the inner electrons, while the outer valence electrons are shared between atoms. Excitations of the crystal occur when electrons are promoted from one state to a higher energy state.
The other type of excitation will be the motion of nuclei which is called vibrational excitation. This excitation has a wave form and is quantised.

3.3.2 The electronic structure of electrochromic materials

It is the energy states of the valence electrons which must be considered in explaining the optical spectra of materials. When atoms are brought together to form a solid, valence electrons start to interact with each other[18]. The electronic levels start to split and at some specific interatomic spacing the system tends to a minimum energy state corresponding to the equilibrium. The discreet energy levels spread into a range of sub-levels called energy bands. The band into which the ground state splits is called the valence band. The lower bands corresponding to inner-lying electronic levels are usually omitted since they have little effect on the main properties of solids. The band just above the valence band is called the conduction band. The energy bands of finite width in a

solid are filled up with electrons according to the Pauli Principle. The Fermi level is the boundary below which all states are filled and above which all states are empty at absolute zero. The basis of optical properties lies in the nature of the electronic energy of bands.

With transition metals, the atomic d orbitals assume crucial importance, due to the different bonding properties associated with these orbitals[18,19]. These complexities include the existence of variable oxidation states. The energy difference between a cation d^n configuration and d^{n+1} or d^{n-1} is rather small, and many transition elements can have several stable oxidation states. This does not exclude phases of intermediate composition, where oxidation states have mixed, or have fractional values. This is associated with the presence of shear planes or Magneli phases and the existence of non-stoichiometry creating a larger number of defects.

The essential concept in understanding the electronic properties of transition metal oxides is the d-symmetry of the principal valence atomic orbitals. The bonding interactions transform the O2p and the metal d orbitals into bonding and anti-bonding orbitals of mixed atomic character. Figure 3.6 shows an energy level diagram of the defect free perovskite lattice of WO_3. On the left side of Figure 3.6 (a) are shown the atomic levels of the metal (W). On right side of Figure 3.6 (e) are shown the O2s and O2p states. These are the valence shells accessible to electrons of the isolated atom. The cation is surrounded by 6 anions, whereas each anion is linearly surrounded by 2 cations (see Figure 3.1). As a result of this arrangement, the 5d levels split up as shown in Figure 3.6 (b). Similarly, the O2p orbitals split into 2 sub-groups as shown in Figure 3.6 (d). Figure 3.6 (c) shows 5 π- and σ-type bonding bands. These are due to the overlaps and interactions in varying degrees of the anions and cations states when they are brought together to form the metal oxide crystal.

The d-electron configuration represents the number of electrons remaining when all the metal oxygen bonding levels are filled. An ionic band structure has a filled valence band composed of combinations of O2p and metal oxide 2s orbitals, while the conduction band is formed from the metal d orbitals. The common geometry in transition metal oxides is octahedral. The d orbitals of transition metals can have five types of degeneracy which give rise to different bonding interactions with nearby atoms: the two e_g orbitals and the three t_{2g} orbitals.

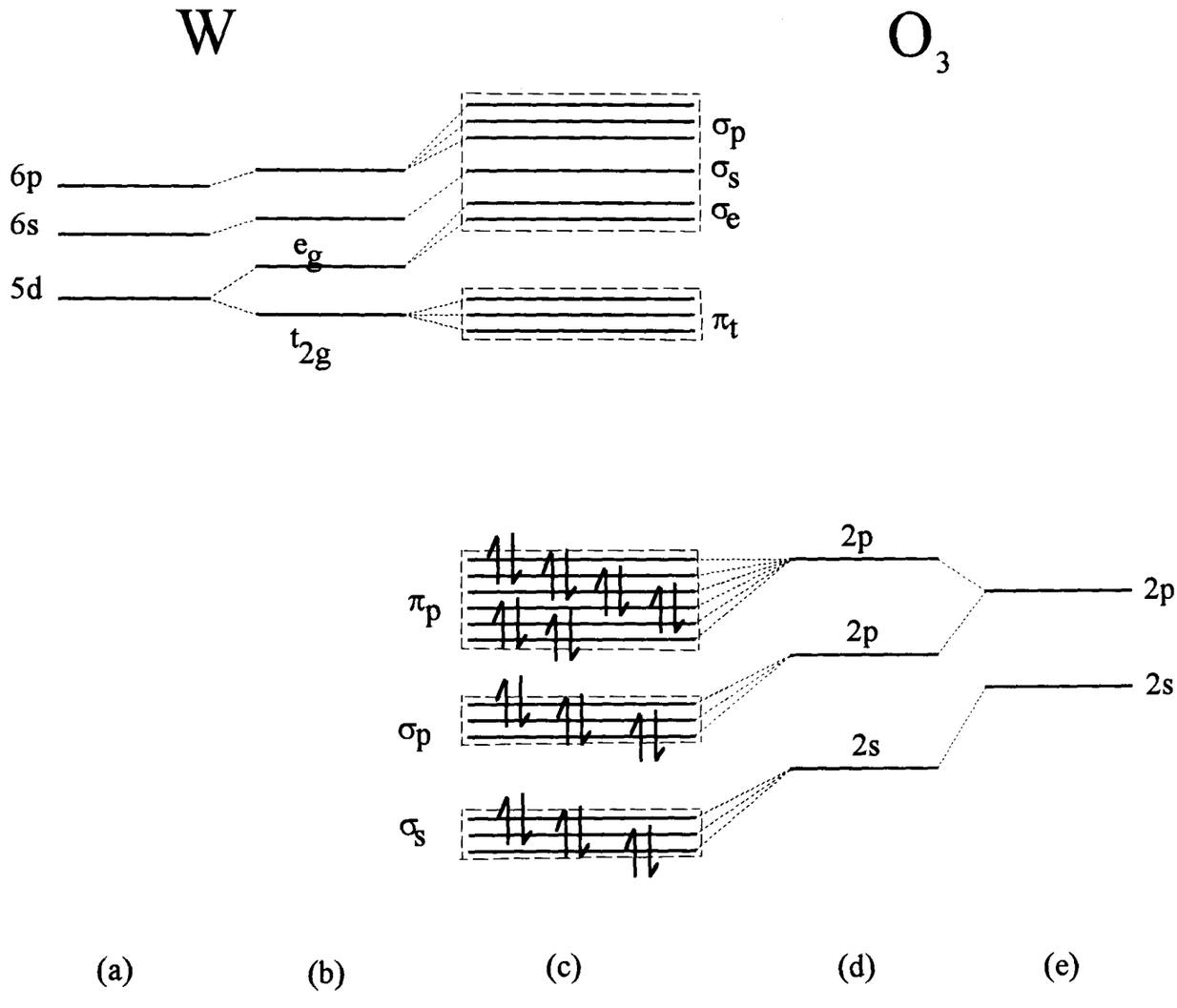

Figure 3.6 : Energy level diagram for the defect-free perovskite lattice of WO_3 [20].

The e_g orbitals point directly at the electronegative oxygen, when the t_{2g} orbitals point away from the nearest ions into empty space. Similarly the O2p orbitals are also split into orbitals pointing to the nearby electropositive Me ion, when others point away into empty space. The optical gap is usually defined as the transition between the highest valence band state into the first maximum of the conduction band state of the band structure. However, defects in materials create one or several intermediate bands inside the band gap. They can allow preferential transitions from the valence band, consequently creating a possible absorption.

In the case of tungsten oxide the conduction band is empty, and the Fermi energy level lies in the gap. The material is an insulator and typical bandgaps are in the range 3-4 eV which render the material transparent. When alkali elements are inserted into the material, electrons are inserted into the lowest part of the t_{2g} band. In fact, the nature of the electronic structure is not a rigid band model. For crystalline or well-ordered tungsten oxide[21], the increase of impurity concentration leads to the formation of an impurity band, split off from the conduction band into the gap. The effect will be the narrowing of the bandgap, making the material less blue and more golden-bronze in appearance. It is after this series that the general class of oxide bronzes was named. At a specific doping level, the impurity band broadens sufficiently that it merges with the conduction band into a single conduction band. The critical concentration for many doped transition metal oxides is found to be at about $x>0.3$ with M_xMeO_3. Finally at high doping levels, the band widens sufficiently that the Fermi level gets extended into the conduction band, and metallic behaviour is reached. The excess electrons in the conduction band can therefore hop from one available site to another by absorbing a photon. The energy required is low, consequently the material appears darker. This is called polaron absorption. Due to the metallic behaviour, materials also exhibit strong reflection below the plasma edge.

For a disordered tungsten oxide, the mean free path for electrons is reduced and becomes more localised. The metallic behaviour disappears as well as the infrared reflectivity. Figure 3.7 shows the bandstructure of defect tungsten oxide materials in the doped and undoped states. When undoped the optical gap Δ is wide, and the material is transparent. The disorder moves the Fermi energy close to the valence band.

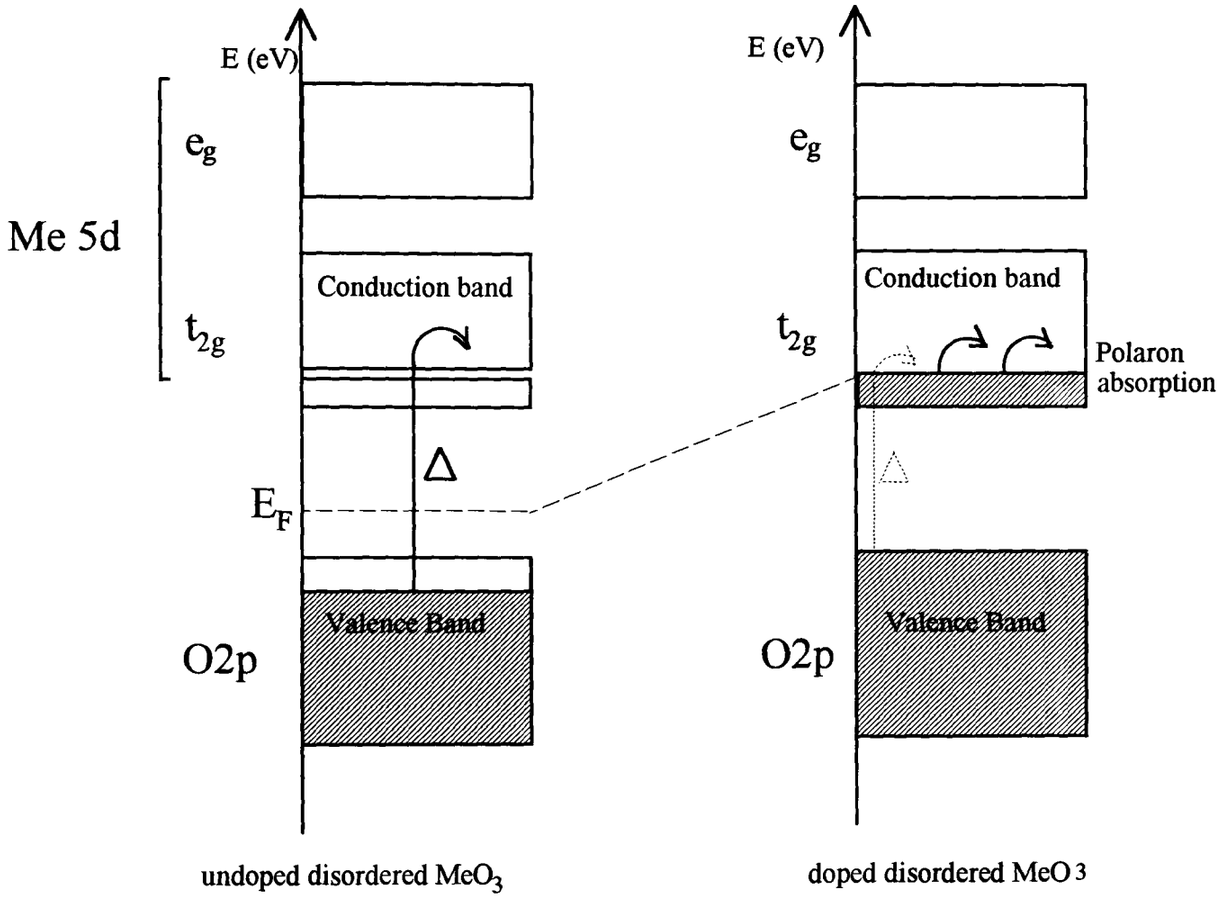

Figure 3.7 : Schematic bandstructure of highly disordered metal oxide in doped and undoped states. This structure is for a perovskite lattice.

When the material is doped the Fermi level moves towards the conduction band, the split-off band is created from the conduction band. The optical gap is smaller, therefore the material becomes blue. When the material is highly doped the split-off band merges with the conduction band and polaron absorption appears.

The metallic behaviour of tungsten oxide does not occur in all transition metal oxides[22] such as $M_xV_2O_5$, even at the highest attainable doping. The optical gap of disordered V_2O_5 is of the order of 2.2 eV. As in ordered tungsten oxide, the electronic structure is not rigid. There is a split-off conduction band when the material is doped, and because transitions between the two 2 bands are not allowed, a widening of the optical gap[23] is created. The material appears bluish. At high doping concentrations, one can expect polaron absorption.

Titanium oxide presents an electronic structure similar to tungsten oxide. Well-ordered TiO_2 would not allow any ionic insertion due to its high compactness, therefore only disordered oxide is considered. If a rigid band model is assumed, the creation of defects into TiO_2 will move the Fermi level away from the valence band so that it eventually comes close to the conduction band. When materials are doped with an alkali element, electrons occupy defect states corresponding to the originally empty conduction band states. The material goes from a non-absorbing state to a darker state due to polaron absorption.

The electronic structure of nickel oxide has gained considerable interest in high temperature superconductors[24] and in electrochromism in particular because in both systems, materials are derived by appropriate doping. Therefore the mechanism of the doping has attracted considerable attention[25]. The creation of nickel defects in NiO produces a charge compensation state of Ni^{3+} centres. The large number of nickel defects introduces states inside the gap and a shift of the Fermi level. Nickel oxide belongs to a group of magnetic insulators. NiO compound is commonly called *Mott* insulator[26] due to the fact that the bandgap excitation is based on electron transfer between 3d orbitals on different ions.

Owing to the band structure of NiO, it is expected to exhibit intraband absorption. However recent work[27] shows that the bandgap excitation for nickel oxide is a transition of charge between oxygen 2p to metal 3d. NiO compounds are then called charge-

transfer insulators. Nevertheless, the presence of the intraband transition is still crucial in nickel oxide and will only be considered in the present case.

Figure 3.8 shows the bandstructure of defect nickel oxide in the undoped and doped states. The onset of strong optical absorption in pure crystalline NiO occurs at 3.5 eV and can be identified as a transition from the top of the valence band to the conduction band minimum[28]. The optical gap of strong absorption occurs at 4.3 eV. In an almost defect-free state, the material is transparent. Non-stoichiometric NiO creates a defect of electrons, therefore decreasing the density of states in the t_{2g} orbital. These nickel defect states seem to behave as colour centres and lead to states just above and below the Fermi energy. This is as if the Fermi level has moved down to the top of the valence band. These states have the particularity to have been produced not near the conduction band but in the middle of the gap instead. Transitions can therefore occur between the maximum of the valence band into the intermediate gap above the Fermi level creating strong absorption of small energy. This makes the as-deposited and non-stoichiometric NiO dark in appearance. When additional electrons are inserted during intercalation, the Fermi level moves away from the valence band, and the optical gap widens. The material becomes transparent.

3.4 Adsorption on transition metal oxides

The interaction[29,30] between metal oxide surfaces and atoms and molecules in the surroundings cannot be ignored. The interaction increases on a macroscopic disordered material, and non-stoichiometric surfaces are usually more active than stoichiometric ones. When defects or vacancies are present on surfaces, the partially occupied d-orbital offers an active site for adsorption of species. These effects could enhance the coloration mechanism of electrochromic materials as well as being responsible for the failure of electrochromic devices. Owing to the fact that transition metal oxides possess different valence states, a wide range of adsorption behaviour can exist. In air, most of the interaction involves CO_2, CO, H_2, O_2 and H_2O principally.

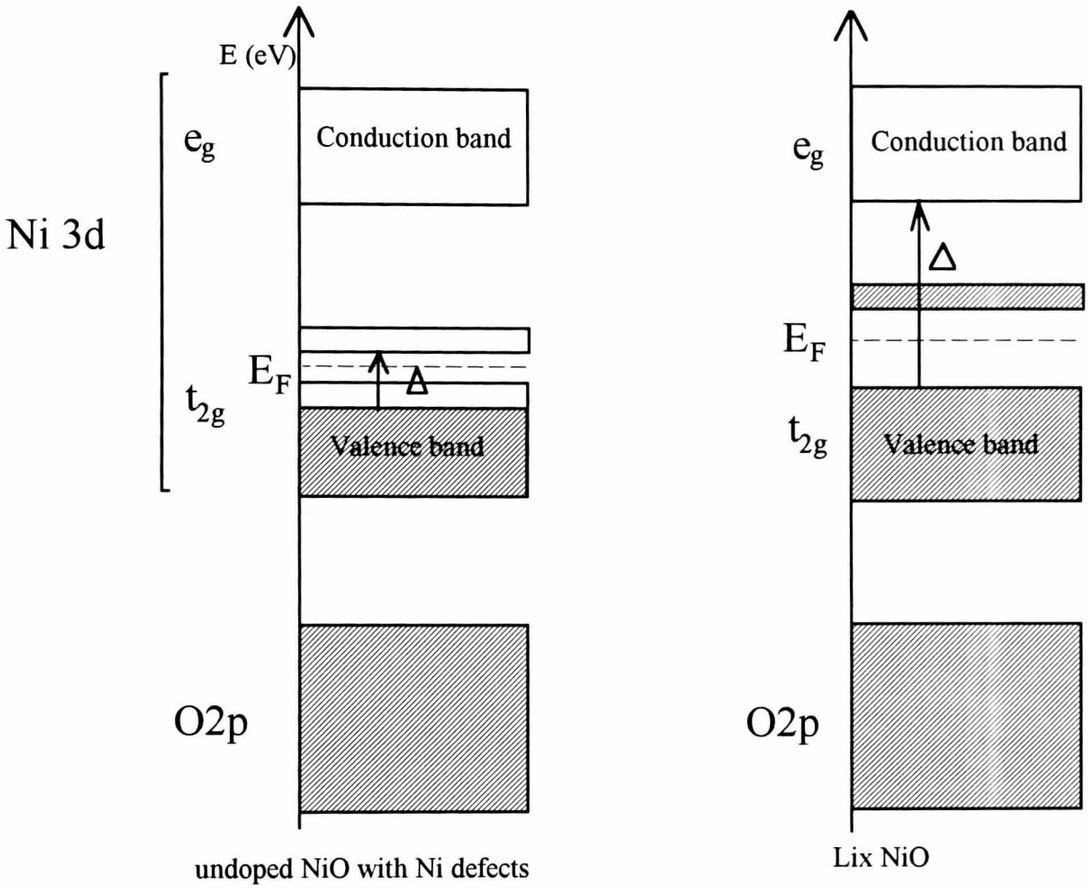

Figure 3.8 : Schematic bandstructure of defect NiO films in a doped and undoped state.

Adsorption can occur in different ways, either during the deposition process, where, for instance, moisture present in the deposition chamber is incorporated into the film, or it could also occur during the handling of the films in air throughout the manufacturing processes of a smart window device.

Chemisorption processes occurring on ionic oxide surfaces are due to donor/acceptor interactions. Electrostatic attraction of sites on materials can interact with molecules or ions and their orbital overlap.

Materials like titanium oxide films possess sufficient compactness to limit chemisorption with species of the surroundings. On the other hand, the different possible oxidation states of vanadium oxide offer different active sites for absorption. However adsorption in this last material has not been studied in great detail. Temperature, non-stoichiometry or disorder enhance the adsorption of water molecules. The most common reaction is the deprotonation of an adsorbate producing hydroxyl groups in polycrystalline oxides like tungsten oxide. Studies[31] showed that water molecules bond to W sites, and can be seen from the presence of W-H_2O stretch modes on sodium-doped tungsten oxide surfaces. Such a result is of importance for the handling and storage of deposited tungsten oxide films.

In the case of transition metal oxides like nickel oxide, which have partially filled d orbitals, d electrons can be easily removed. The oxidation of such materials is similar to defect metal oxide mentioned above and can enhance a wide range of adsorption reactions. Non-stoichiometric NiO containing Ni defects can interact[32] strongly with O, O_2 and H. The presence of adsorbed O will initiate adsorption of H_2O. Water molecules are not adsorbed as such but are dissociated by adsorbed O. Studies[31] have shown the presence of OH^- species in the lattice. However, without adsorbed O, NiO even with defects seems to show little adsorption of water.

Chapter 4

EXPERIMENTAL METHODS AND TECHNIQUES

4.1 Introduction

This chapter describes the main experimental techniques used in the preparation and characterisation of electrochromic thin films and devices in this study. Thin films described in this thesis were mainly prepared by reactive R.F. and/or D.C. magnetron sputtering.

Electrochromic thin films properties have been electrochemically and optically characterised. Spectrophotometers have been used to measure the spectral transmittance and reflectance of the films in the ultraviolet (*UV*), visible (*VIS*), near infrared (*NIR*) and infrared (*IR*) ranges. Instruments used and optical properties calculations are described in this chapter.

Electrochemical properties were simultaneously measured with optical transmittance using a spectro-electrochemical cell purposely designed for in-situ characterisation. This last technique is reviewed together with the electrophysical characterisation techniques used in this work.

4.2 Sputtering deposition techniques

4.2.1 The process

Spray pyrolysis and sputter deposition are the two principal techniques used in industry for preparing thin films on the scale of square metres. A brief description of sputtering technology, and the operating principles used in this work are given in this chapter.

The properties of thin film coating are directly related to its chemical and physical nature and are then dependent on the preparation technique employed.

Electrochromic films are directly dependent on the degree of crystallinity, crystal structure and level of impurities in the film. The main advantage of sputtering over other thin film deposition techniques is the good adhesion of the coating. A good control of the film stoichiometry and of the deposition rate can be achieved. Sputtering is also notable for its versatility and the possibilities of process control, but on the other hand is a costly investment.

The sputtering process is the bombardment of a target material by the ions of a glow discharge. The discharge is created by applying an electric field across a low-pressure gas. Figure 4.1 shows the basis of a sputtering system cross-section[1]. The process takes place in a chamber where unwanted impurities are removed by pumping down to a high vacuum (5×10^{-6} Torr). Then an inert gas such as argon is introduced into the chamber. A negative voltage is applied to the target so causing it to attract positive ions (argon ions) present in the plasma. The argon ions collide with the target surface and the target material is knocked out by a process of momentum transfer and condenses onto the substrate material. Secondary electrons emitted from the target surface generate more ionisation.

More than one ion is required to release most materials in a given area. As more power is applied, the bombarded area increases until the whole target area is covered. When the number of electrons produced is sufficient to give ions that can create the same number of electrons, the discharge is called[2] "normal discharge" and the gas starts to glow. If the power is increased further, both voltage and current density are increased in the discharge. This mode[2] is known as the "abnormal glow" and is the condition under which most sputtering is carried out. The atoms leaving the target are able to travel to the substrate when the number of gas molecules is suitably low. At high pressures, when the chamber contains a lot of gas molecules, most of the atoms will collide with the molecules and return to the target and the sputtering rate drops. The bombardment of the target causes the production of secondary electrons as well as other particles (desorbed gases) and radiations (photons and X-rays). These affect the properties of the growing film.

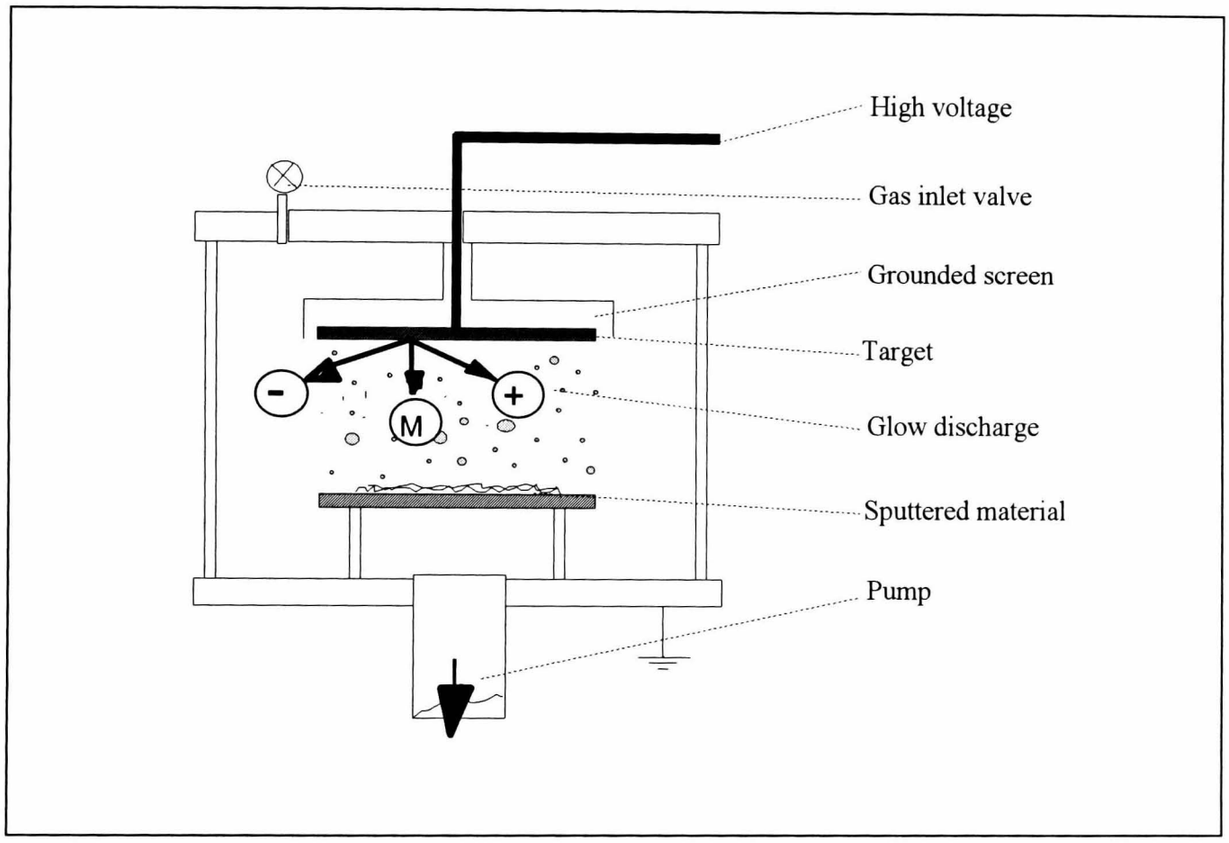

Figure 4.1 : Cross-section of a simplified sputtering system.

Many other factors can affect the sputtering process such as substrate temperature, target to substrate spacing, sputter gas purity, working pressure, target voltage, and whether the substrate is electrically grounded or biased.

Non-conductive materials can also be sputtered by the use of a Radio Frequency (R.F.) power supply. In this case, the target surface is coupled to the power supply through a resistance-capacitance (RC) network. In order not to cause a complete (D.C.) discharge on each half of the cycle, the frequencies used are greater than 50 kHz. Both cathode and anode would be sputtered otherwise.

The electrons oscillate in the glow space, and can gain sufficient energy to create more ionisation. The discharge is less dependent on the secondary electron emission. The discharge in both D.C. and R.F. sputtering processes can be supported by a magnetic field. Magnets placed behind the target create a flux which gives rise to a magnetic field almost parallel to the target surface. The combined effect of the electric and magnetic field lines causes the electrons in the plasma to follow helical paths perpendicular to both electric and magnetic fields. As electrons are confined close to the target region, ionising collisions are increased. Then the rate of ion bombardment at the target will increase as well as the deposition rate. Figure 4.2 illustrates how the magnetic field lines are arranged. The electrons move continuously in a closed loop which is called "the racetrack". This high ionisation region causes an erosion pattern on the target and gives a non-uniform thickness of the deposited film.

4.2.2 The Nordiko R.F./D.C. magnetron sputtering system

A Nordiko NS-3750 series magnetron sputtering system was used to prepare electrochromic films. A 1.25 kW R.F. generator and a 6 kW D.C. generator supply two water cooled 4" x 12" vertical electrodes. A rotary substrate carrier mounted inside the chamber can be indexed from the control rack of the instrument[3] to permit static or co-sputtering deposition. A power splitter allows the substrate to be R.F. sputter etch-cleaned and also R.F. bias sputtering to be carried out. The pumping system includes a two-stage high capacity rotary pump (640 l/mn) coupled with a 3500 l/s water-cooled diffusion pump. A liquid nitrogen cold trap is used for the removal of condensables. The pumping system is automatically controlled from the control rack of the machine.

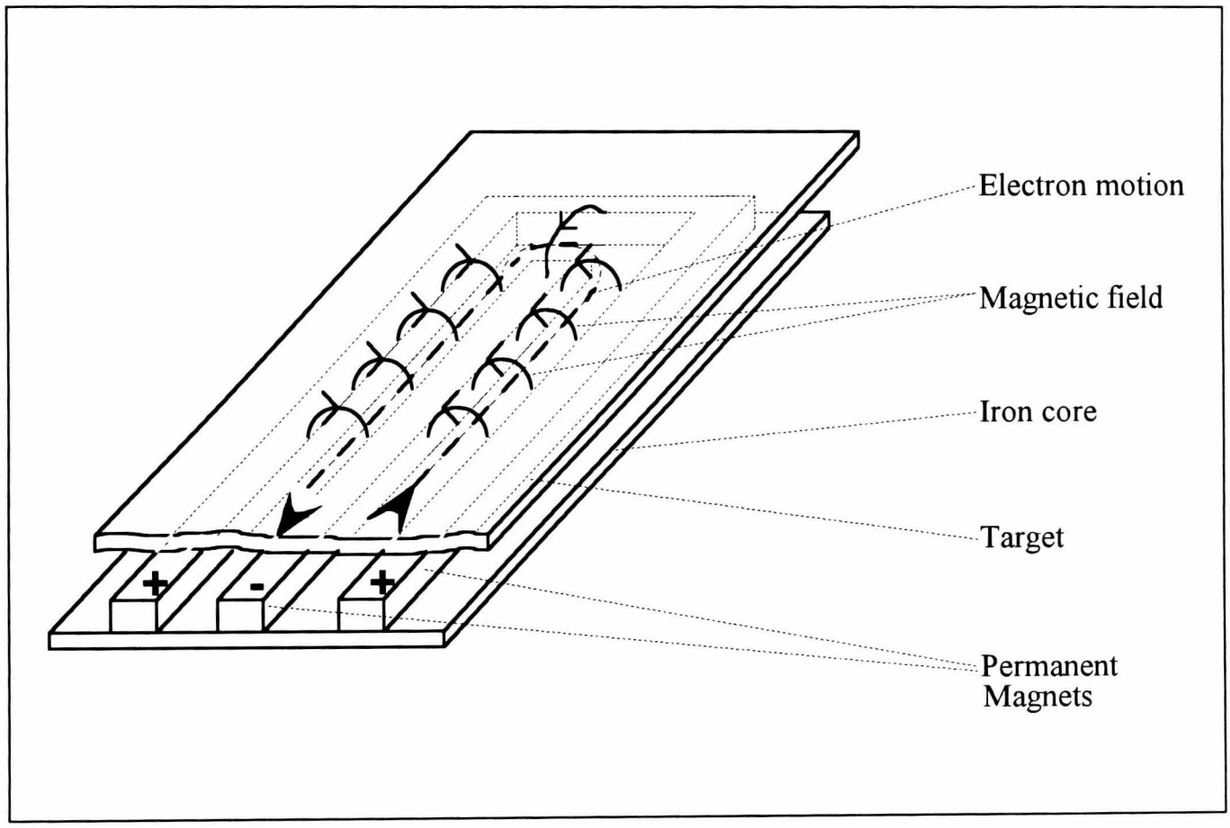

Figure 4.2 : Schematic of the magnetic field configuration onto the electrode.

A manually-driven shutter is provided to permit sputter cleaning of the targets. Control of three process gases is provided using a 3 channel mass flow control system.

Figures 4.3 and 4.4 present a schematic diagram and a photograph respectively of the Nordiko sputter coater.

A typical sequence for normal operation of the CVC LCS-100 magnetron sputter coater is as follows.

Glass and ITO substrates were held vertically on a carousel positioned at 10 cm from the target. The carousel holds 3 different sets of substrates, and each of them can be indexed to the appropriate target. Substrates were held in place with heat-resistant tape. The chamber was sealed and an automatic pump-down started. The chamber pressure was first reduced to 0.1 Torr with a rotary pump. This usually took 3 minutes from atmospheric pressure. The roughing valve was then closed and the foreline valve opened. The diffusion pump valve was opened ensuring that the foreline pressure did not exceed 0.1 Torr. This prevented the diffusion pump from stalling. After a further period of 30 minutes, the pressure of the chamber reached a vacuum below 5×10^{-6} Torr. A shutter was indexed between the target and the carousel to carry out presputtering. The required flow rates were set on a controller unit. Presputtering was performed to reach steady-state conditions before the actual film was deposited. After a required time, the shutter was removed and deposition onto the substrate initiated. When the deposition was completed, the generators were switched off, and the gas flows turned off. Samples were then left for 20 minutes to cool down before venting the chamber with nitrogen gas. This prevented water condensation build-up on the inside of the chamber walls which could increase the next pump-down time. New substrates were fitted onto the cooled platform, and the pump-down cycle recommenced.

4.2.3 The CVC R.F. / D.C. magnetron sputtering system

The LCS-100 CVC is a 4 cathode (6" diameter) upward-sputtering magnetron system. Three electrodes are supplied by a 1 kW R.F. generator power. An adjustable R.F. power splitter allows the substrates to be sputter-etched and also bias sputtering to be carried out. A R.F. matching unit is provided and can be adjusted with controls on the control panel. The fourth electrode is powered by a 4.5 kW D.C. power supply.

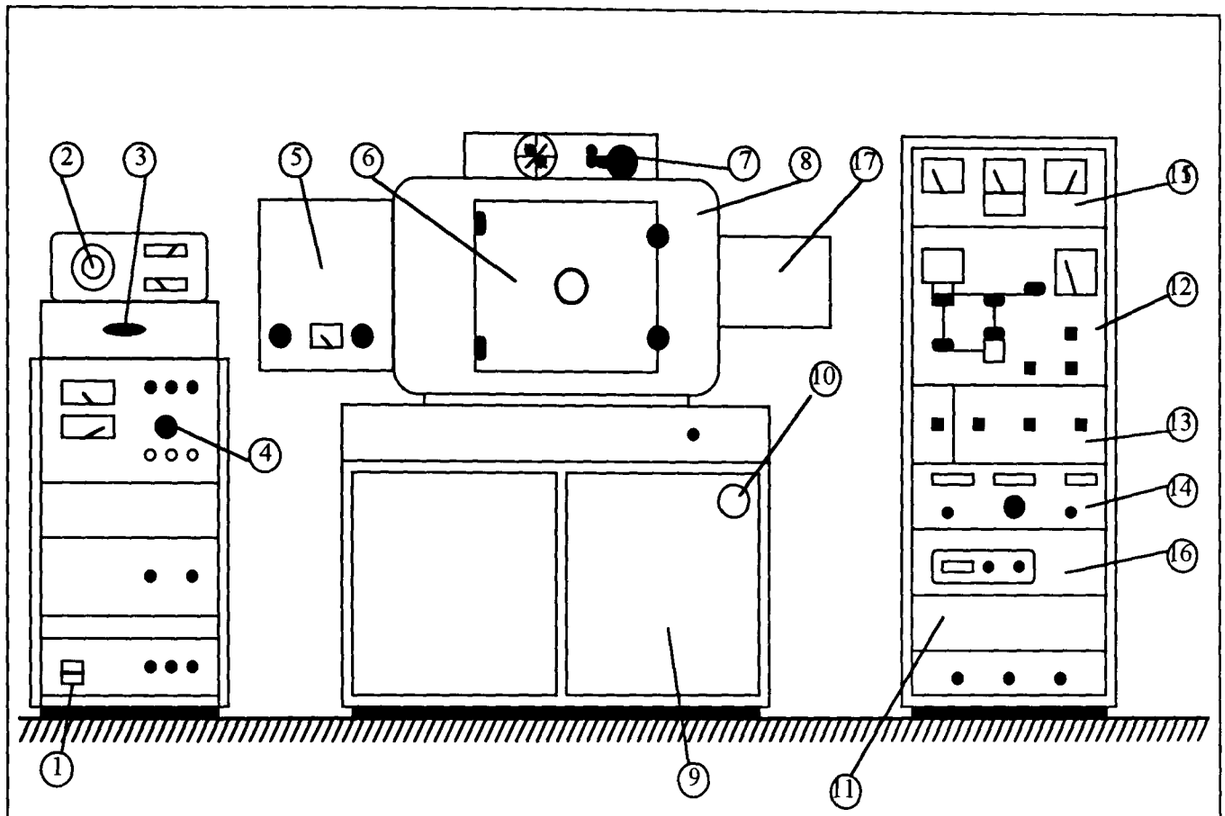

Legend

1	R.F. Generator /Power supply	10	Liquid nitrogen filler
2	Power splitter	11	Main control rack
3	R.F. mode switch	12	Pumping system
4	R.F. power supply control	13	Gas inlet system
5	R.F. electrode matching unit	14	D.C. generator/power supply
6	Front opening door of chamber	15	Gauges control unit
7	Manual shutter drive	16	Gas inlet control unit chamber
8	Non-magnetic stainless steel vacuum	17	D.C. electrode unit
9	Pumping station		

Figure 4.3 : Schematic of the Nordiko NS-3750 sputter coater.

Figure 4.4 : The Nordiko NS-3750 sputter coater.

A 1.5 kW quartz halogen heater assembly is mounted in the chamber lid to provide a heat source during the deposition process. A titanium shutter is provided to enable substrate-etching and target-presputtering. Three different gases are controlled directly from the front panel. The chamber is pumped by a CTI cryopump coupled with a rotary pump.

A schematic diagram and a photograph of the instrument are shown in Figure 4.5 and Figure 4.6 respectively.

A typical sequence for normal operation of the CVC LCS-100 magnetron sputter coater is as follows.

An horizontal rotating platform with different windows was positioned at 6 cm above the target. Glass and ITO substrates were held at the top of these windows. The platform holds 4 different sets of substrates, and each of them can be indexed to the appropriate target. The chamber was closed and an automatic pump-down started. The chamber pressure was first reduced to 0.5 Torr with a rotary pump. This usually took 3 minutes from atmospheric pressure. Then the cryopump valve was opened to increase the vacuum above 5 x 10^{-6} Torr. When the chamber was cleaned, this second stage took 15 minutes. A rotating titanium shutter was indexed between the target and the substrate platform to carry out presputtering. The required flow rates were set on a controller unit. Presputtering was performed to reach steady-state conditions before the actual film was deposited. After a required time, the shutter was opened and deposition onto the substrate initiated. When the deposition was completed, generators were switched off, and the gas flow turned off. Samples were then left for 20 minutes to cool down before venting the chamber with nitrogen gas. This prevented water condensation build up on the inside of the chamber walls which could increase the next pump-down time. New substrates were fitted onto the cooled platform, and the pump-down cycle recommenced.

4.2.4 Substrate preparation

Different substrate sizes were cut to fit the sample holders of instruments. The standard sizes were : 2" x 2", 3" x 3" and 4" x 4".

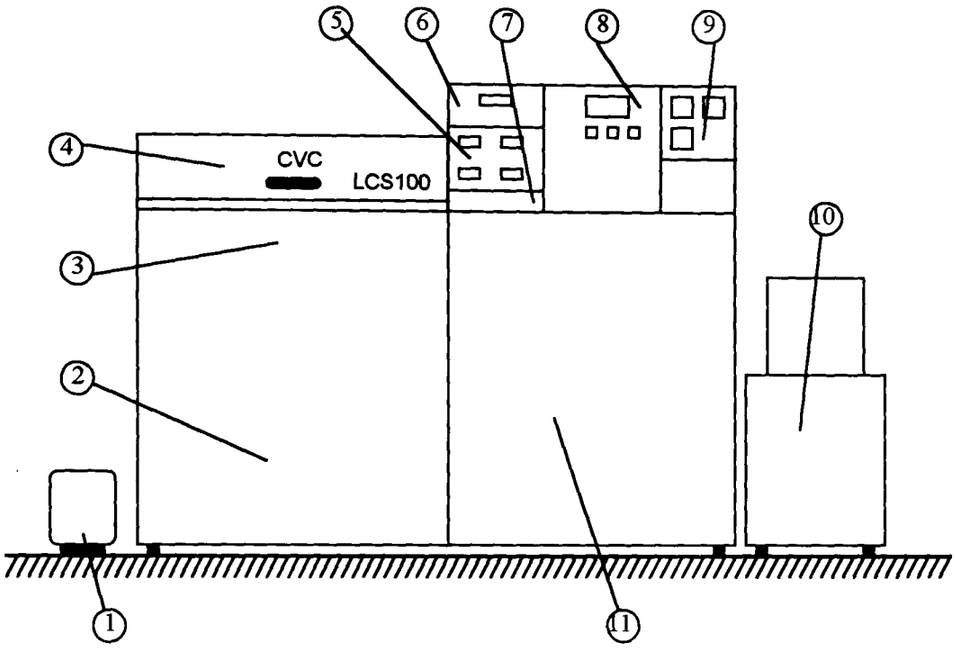

Legend

1	Rotary pump	7	R.F. electrodes power supply control
2	Magnetron electrodes units	8	Pumping system control
3	Titanium chamber	9	Gas inlet system
4	Top opening door of chamber	10	Cryopump
5	Matching unit	11	D.C. / R.F. power supply
6	DC electrode power supply control		

Figure 4.5 : Schematic of the CVC LCS-100 sputter coater.

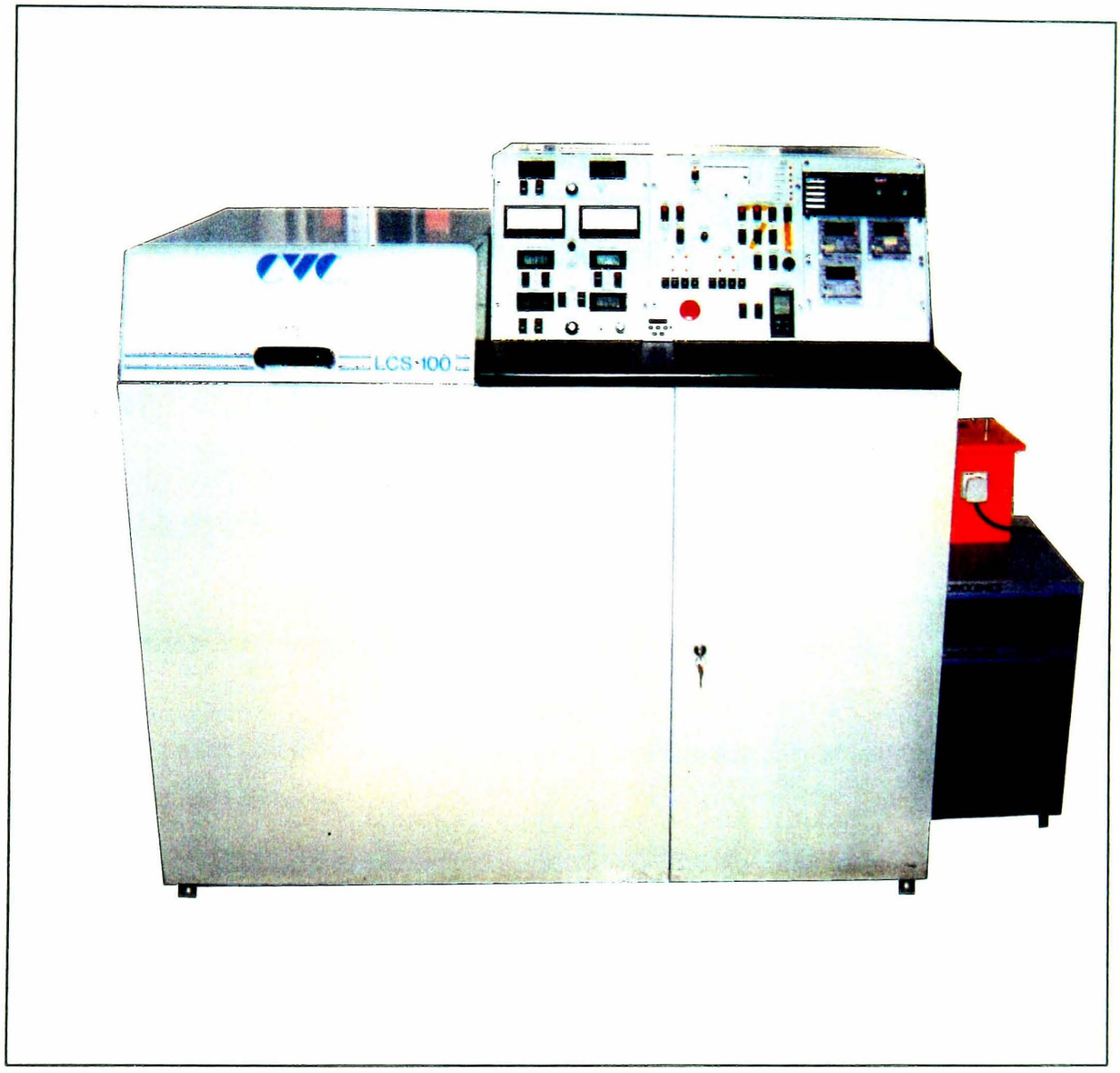

Figure 4.6 : The CVC LCS-100 sputter coater.

Substrates were ultrasonically cleaned in a 4 % diluted solution of Decon 90, then thoroughly rinsed with distilled water. The substrates were finally rinsed with propanol-2 then dried with a nitrogen gun. The substrates were vertically stored in polypropylene racks which were themselves enclosed in air-tight polypropylene boxes. All samples were handled with protective gloves. To permit film thickness measurements as well as electrochemical investigations, all ITO substrates were masked with a heat- and chemically-resistant Kapton™ tape[4]. This polyimide tape is backed with a thermosetting adhesive silicone which does not carbonise at temperatures below 280° C. A substrate surface area of 1 x 5 cm^2 was masked with tape. It was removed after deposition, leaving an uncoated area of ITO for electrical contacts as well as a step for film-thickness measurements.

4.3 Optical characterisation techniques

4.3.1 Optical properties measurements with an integrating sphere

Radiation transmitted and reflected by most materials is a combination of both specular and scattered components.

Spectrophotometers used in this thesis were equipped with integrating spheres to carry out near-normal total hemispherical reflectance and transmittance optical measurements. The ideal integrating sphere[5,6] wall has 100% reflecting and totally diffusing properties. The ideal integrating sphere shape is obviously a perfect sphere. Also the sphere should not have any ports, but light has to enter the sphere and has to be detected. When the light enters the sphere through the entrance port, it strikes the sphere wall on the opposite side, and is then reflected and totally diffused if the sphere wall is a perfect Lambertian surface (100% reflected and totally diffused). The light is then evenly distributed throughout the sphere i.e. the intensity is uniform over the sphere wall. A fraction of this light escapes through the exit port, and the rest is again reflected. The light intensity at the sphere wall is directly proportional to the diffused light, which is a function of the reflections and transmissions it has undergone.

4.3.1.1 Measurement method in transmittance

The transmittance of a sample T_{sample} is measured with an integrating sphere at near-normal incidence with reflectance R_{wall}. The transmittance has to be separated into its specular and diffuse components. The transmitted light is then the sum of both direct or specular component and scattered or diffused component. Most of the solar energy materials prepared in this thesis are mainly specular, therefore the diffuse component is almost equal to zero. The signal S which is displayed on the instrument describes the optical properties by the following simplified equations.

The sample signal is given by :

$$S_{sample} = C.I_i.R_{wall}.T_{sample}.R_{Al} \qquad [4.1]$$

with C the instrument amplification, I_i the incident beam intensity, and R_{Al} the reflectance of the aluminium reference standard.

Figure 4.7 (a) shows a transmittance measurement at near-normal incidence using an integrating sphere.

The reference signal is :

$$S_{reference} = C.I_i.R_{Al}.R_{wall} \qquad [4.2]$$

This is illustrated in Figure 4.7 (c).

The ratio is

$$S_{sample}/S_{reference} = T_{sample} \qquad [4.3]$$

The ratio given by the instrument in transmittance mode shows that it is an absolute measurement.

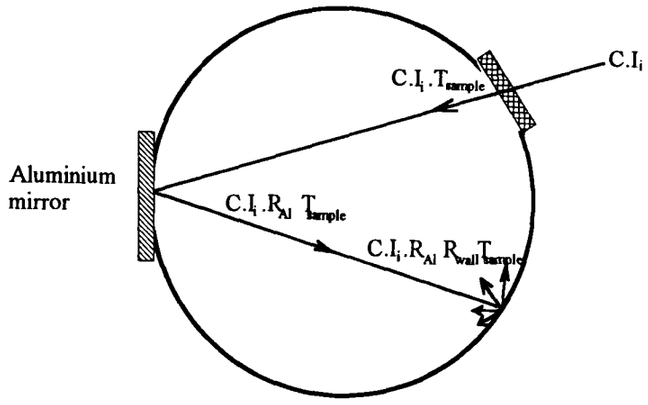

Figure 4.7 (a) : Integrating sphere in the transmittance measurement mode.

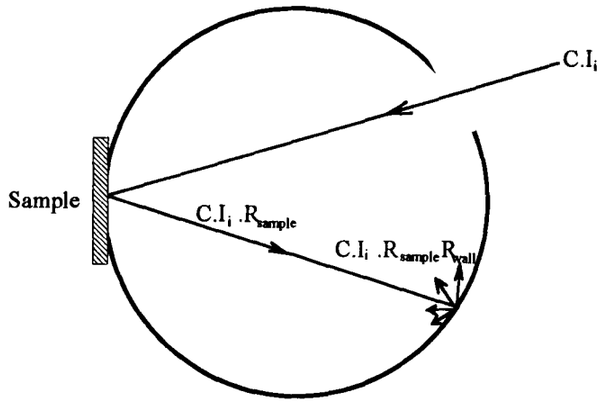

Figure 4.7 (b) : Integrating sphere in the reflectance measurement mode.

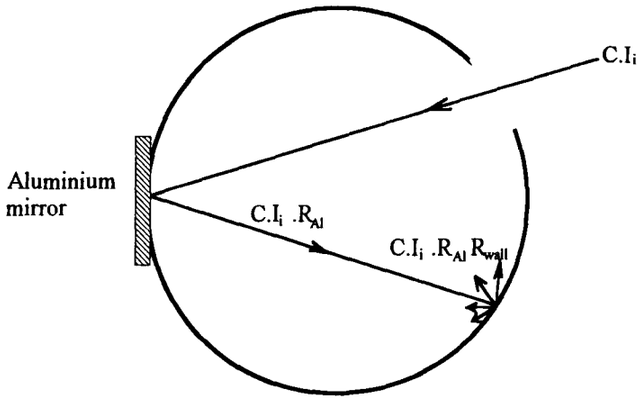

Figure 4.7 (c) : Integrating sphere in the reference measurement mode.

4.3.1.2 Measurement method in reflectance

The reflectance can be separated into its specular and diffuse components. Again, the diffuse component is equal to zero for all the films produced in this work.

The signal S which is displayed on the instrument describes the optical properties by the simplified equations which follow.

The sample signal is

$$S_{sample} = C.I_i.R_{sample}.R_{wall} \qquad [4.4]$$

and the reference signal is

$$S_{reference} = C.I_i.R_{wall}.R_{Al} \qquad [4.5]$$

The ratio is

$$S_{sample}/S_{reference} = R_{sample}/R_{Al} \qquad [4.6]$$

Equation *[4.6]* shows that the reflectance measurement is relative to a reference standard. The ratio given by the instrument has to be multiplied by the absolute reflectance of the calibrated mirror to give the absolute reflectance of the sample.

Figure 4.7 (b) shows the reflectance diagram at near-normal incidence.

At near-normal incidence, the specular component for both transmittance and reflectance mode can be directed out and only then the diffuse component is measured. This was the way to check that the reflected and transmitted diffuse components were almost equal to zero.

4.3.1.3 Oblique incidence optical measurements

The determination of the angular properties of architectural glazings, in particular thin-film coated products, is of increasing importance for complete product performance description. Angular dependent data are required to improve window description in

design applications and full simulation building energy analysis tools[7,8] and performance rating and energy labelling fenestration components[9].

Three major problems occur for transmittance measurements at different angles of incidence: (i) the angular position of the sample, (ii) the polarisation of the spectrophotometer's beam which is generally unknown and (iii) the refraction of the beam in a sample which results in a lateral shift of the beam transmitted.

Unlike transmittance measurements, all reflectance measurements require calibration against a known reference reflectance standard. In all cases, the instrument is calibrated by substituting the test sample for the reference mirror. This measurement is performed twice: first with the reference reflectance standard and then with the unknown sample. In addition to the problems which occur for angular transmittance measurements is the absence of an international reflectance standard. There is no standard method for the calibration of angular dependent reflectance of specularly reflecting samples. In absence of an international reference, an aluminium mirror calibrated at near-normal incidence is used. A review of these problems has been published[10,11] and is summarised in Appendix.

4.3.2 The Beckman 5240 spectrophotometer

Optical properties measurements in the solar range (0.3 - 2.5 μm) were carried out using a *Beckman 5240* spectrophotometer fitted with a 6" diameter barium sulphate ($BaSO_4$) coated integrating sphere. A calibrated aluminium standard was used as the reference[12]. Figures 4.8 and 4.9 present a schematic diagram and a photograph respectively of the Beckman spectrophotometer.

The spectrophotometer is a dual-beam instrument. Total or diffuse near-normal hemispherical reflectance and transmittance can be carried out. The instrument operates in 2 ranges : the near infrared spectral range from 2.5 to 0.7 μm and the visible and ultra-violet spectral range from 0.8 μm to 0.3 μm. A tungsten lamp is used to cover the whole solar range. The monochromator is a rotating grid. Two detectors are used on the sphere, (i) a lead sulphide detector for near infrared and (ii) a photomultiplier for visible and ultraviolet measurements.

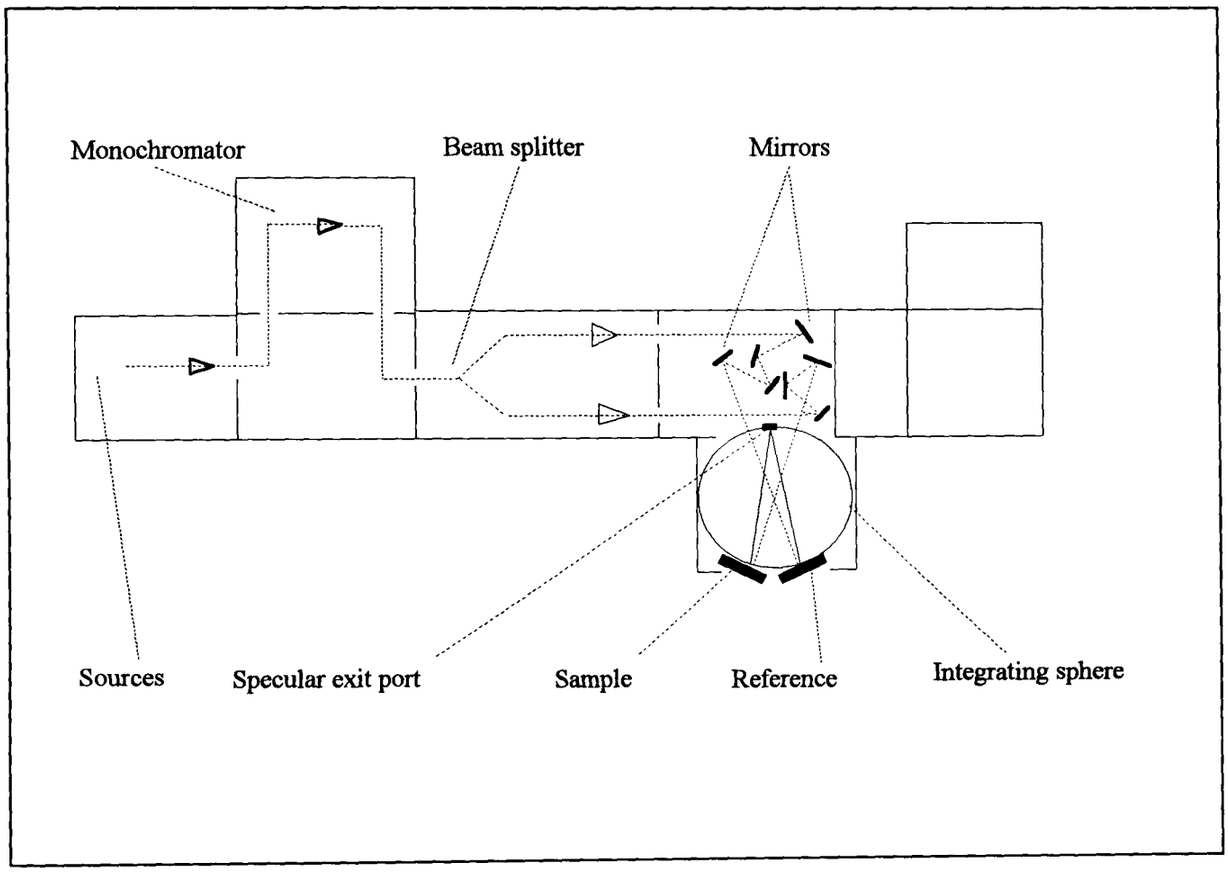

Figure 4.8 : Schematic of the Beckman 5240 UV/VIS/NIR spectrophotometer.

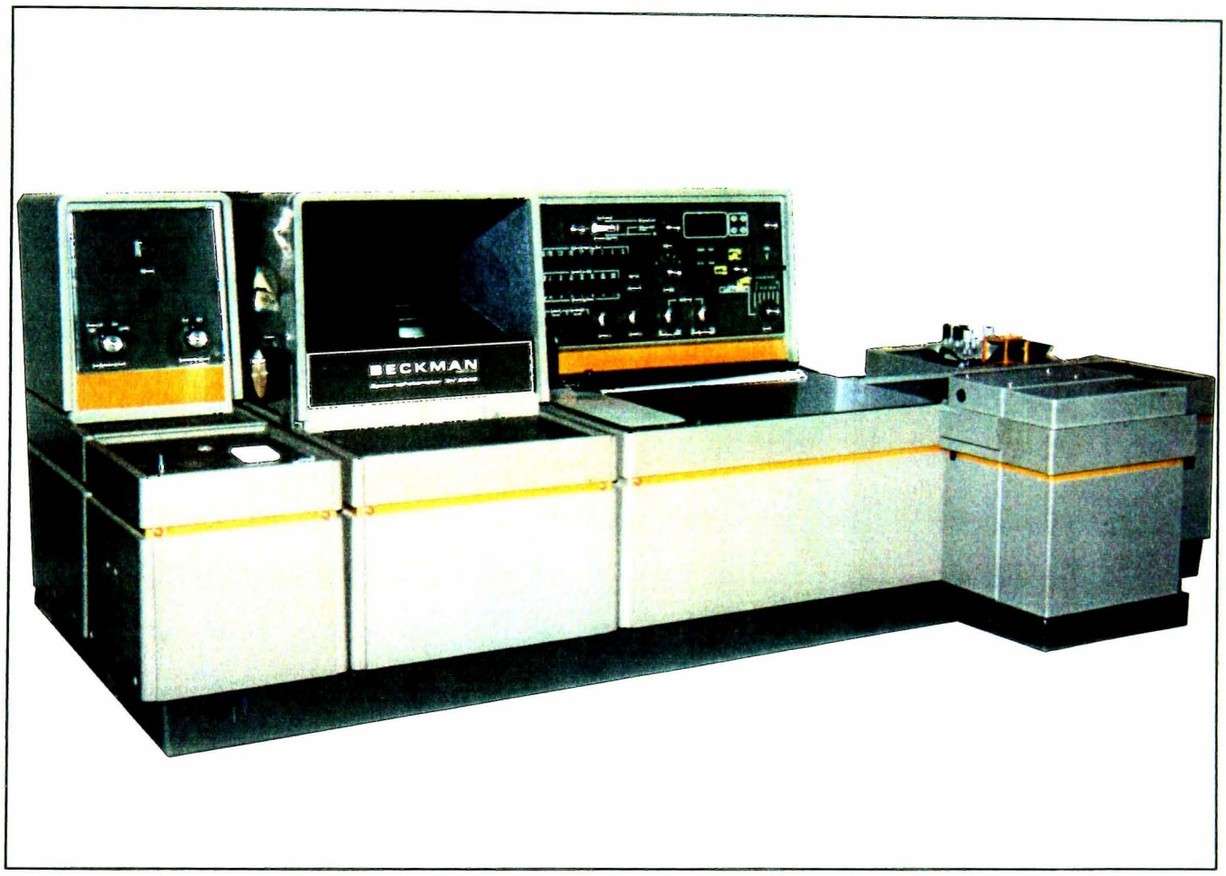

Figure 4.9 : The Beckman 5240 UV/VIS/NIR spectrophotometer.

The data are transferred to a computer in order to plot out the spectral curves and calculate relevant solar optical properties. The standard instrument error of the Beckman spectrophotometer is ± 0.01.

4.3.3 The Fourier Transform UV/VIS/NIR/IR Bruker IFS-66

The *Bruker IFS66* is a single beam ratio recording and Fourier Transform spectrophotometer. Figures 4.10 and 4.11 present a schematic diagram and a photograph respectively of the instrument.

The radiation can be directed to the sample compartment where specular transmittance or specular reflectance can be measured. An attachment can be fixed in the sample compartment to carry out specular measurements at normal and non-normal incidence. A silicon diode and DTGS detectors are available for the *UV/VIS/NIR* range and the *NIR/IR/FIR* range respectively. The spectrophotometer is equipped with two 8" diameter spheres.

Total near-normal hemispherical spectral reflectance and transmittance in the *UV/VIS/NIR* is measured with a barium sulphate coated sphere and the *NIR/IR/MIR* range is measured with a diffuse gold coated Labsphere. Diffuse gold and barium sulphate standards are available as reference samples. An EG&G Jadson, liquid nitrogen cooled, cadmium mercury telluride (MCT) infrared detector is mounted onto the gold sphere. A silicon detector for the *UV/VIS* range and a germanium detector for the *VIS/NIR* range are mounted onto the barium sulphate sphere. Two types of sources are available to cover all spectral ranges, and these are given in Table 4.1. The sample compartment is continuously purged with carbon dioxide.

The whole instrument is controlled by computer. Run under OS2, OPUS/IR software controls all the set up of the measurement process, and collects and saves data. A certain number of macros have been written to perform different types of calculation or correction. It includes calculations in the solar and visible and infra-red ranges[13].

The standard instrument error of the Bruker spectrophotometer is ± 0.005.

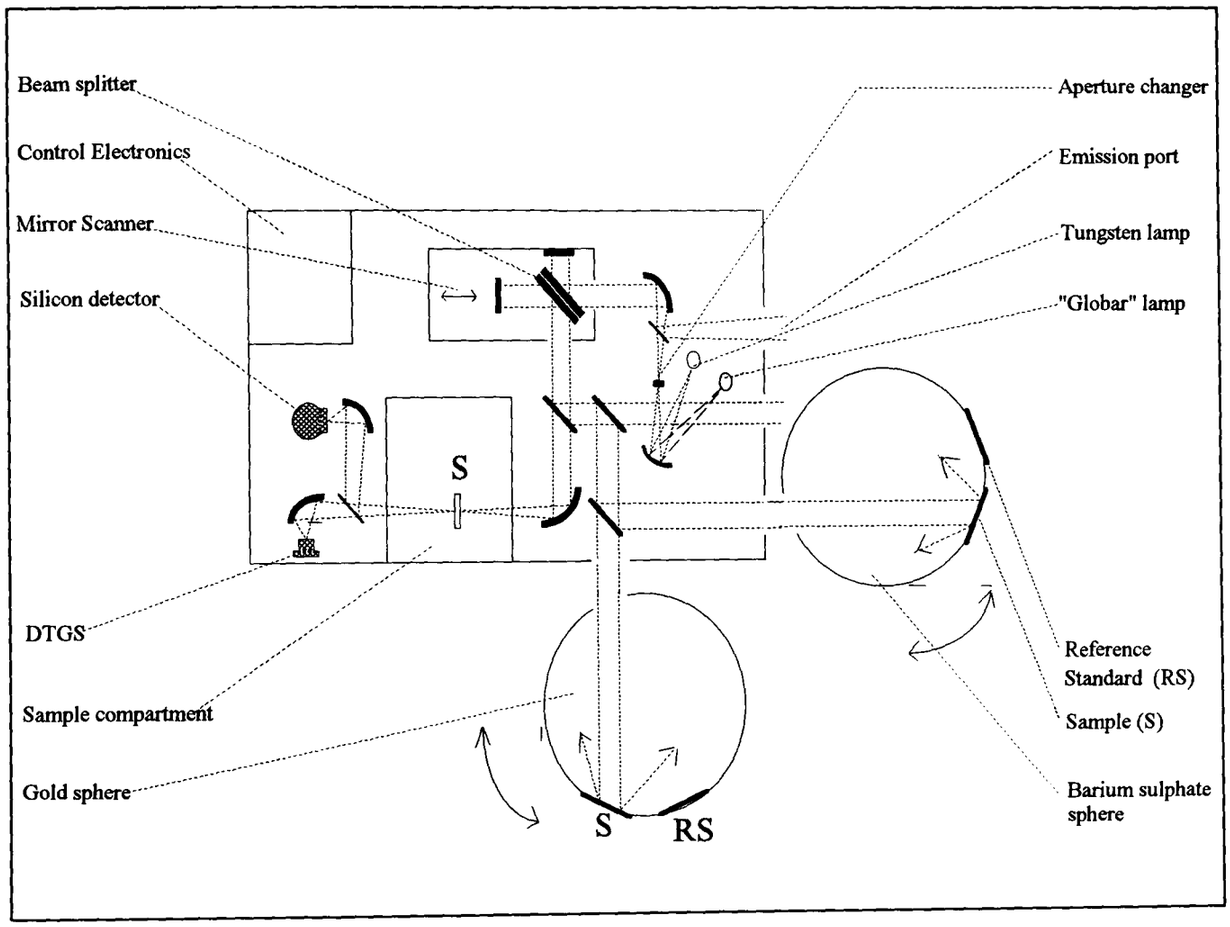

Figure 4.10 : Schematic of the Bruker IFS-66 FTIR spectrophotometer.

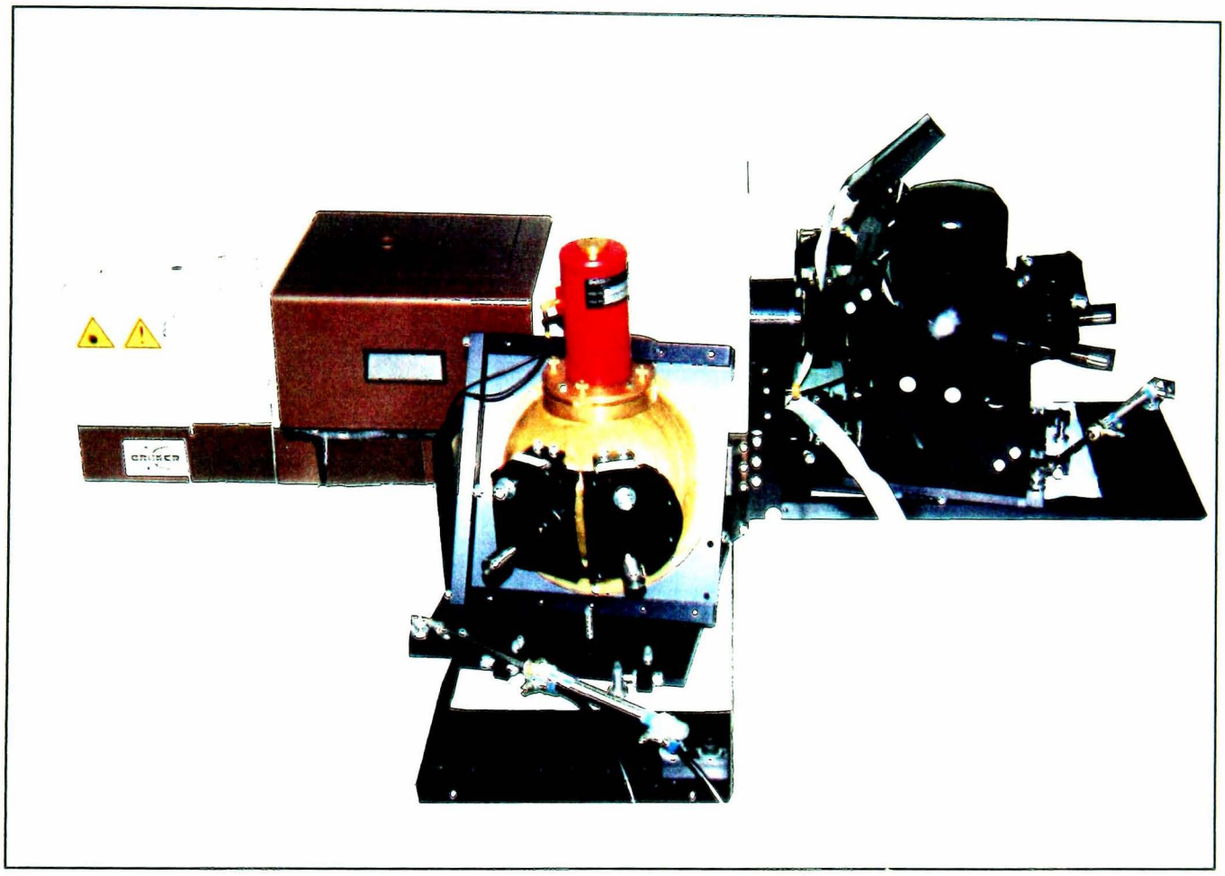

Figure 4.11 : The Bruker IFS-66 FTIR spectrophotometer.

Spectral ranges (μm)	Sources	Windows of the beam splitter
0.33 - 1.1	Tungsten	Quartz
1.0 - 2.5	Tungsten / Globar	Quartz / KBr
1.0 - 25	Globar	KBr

Table 4.1 : List of sources and windows available in the Bruker FTIR 66.

4.3.4 Optical properties calculations

The solar transmittance (T_s) or reflectance (R_s) was calculated by convoluting the measured spectral profile with a spectral distribution for (AM2) (see Chapter 1). The absorptance is calculated using Kirchoff's law.

If the solar spectral distribution is divided into twenty bands of equal energy, then the selected ordinates[14] method can be used and the equation [1.5] rewritten as follows:

$$X_{\lambda_1,\lambda_2} = \frac{\sum_{i=1}^{20} X_{\lambda_i}}{20} \qquad [4.7]$$

with $X_{\lambda 1,\lambda 2}$ equal to T_s or R_s and $X_{\lambda i}$ the values of spectral transmittance or reflectance at the wavelength in each band which divides the total band energy into 20 parts.

The visible transmittance (T_v) or reflectance (R_v) was calculated using the relative spectral power distribution D_λ of illuminant[15] D_{65} multiplied by the sensitivity of the human eye V_λ(see Chapter 1) and the spectral bandwidth $\Delta\lambda$ in the following formula:

$$X_{\lambda_1,\lambda_2} = \frac{\sum_{0.38\mu m}^{0.78\mu m} D_\lambda X_\lambda V_\lambda \Delta\lambda}{\sum_{0.38\mu m}^{0.78\mu m} D_\lambda V_\lambda \Delta\lambda} \qquad [4.8]$$

with $X_{\lambda 1,\lambda 2}$ equals to $T_V$or R_V.

The values for ($D_\lambda.V_\lambda.\Delta\lambda$) are given for intervals of 10 nm and in such way that $\Sigma D_\lambda.V_\lambda.\Delta\lambda$ is equal to 100. This calculation is made according to the ISO 9050 standard[16]. The trichromatic coefficients specify any given colour in terms of the three primary colours required to produce that colour. The colour specifications are given in terms of average daylight illumination[15].

They are the constant number of units of certain primary colours that a unit amount of radiant energy at any specific wavelength in the visible region is composed of. The tristimulus values of the red, green and blue primaries are designated by X, Y and Z respectively. They are calculated using a 30 selected ordinates method[17]. The measured transmittance or reflectance of X, Y and Z are added at specific wavelengths and multiplied by specified factors to give the tristimulus values. These values are normalised to give the trichromatic coefficients.

4.3.5 Optical bandgap calculation

The optical gap (E_g) of an absorbing semiconductor can be written[18] as:

$$\hbar\omega\alpha_\lambda \sim \left(\hbar\omega - E_g\right)^n \qquad [4.9]$$

where $\hbar$ is the Planck constant divided by 2π, ω the angular frequency, α_λ the absorption and n the type of optical transitions that dominate.

In the spectral region of fundamental absorption we have as an approximation[18]:

$$\alpha_\lambda = d^{-1}.ln\frac{1-R_\lambda}{T_\lambda} \qquad [4.10]$$

where d is the thickness.

For crystalline semiconductors, n is equal to (0.5), (1.5), 2 and 3, when transitions are direct allowed, direct forbidden, indirect allowed and indirect forbidden respectively[19]. In the case of ITO, n is equal to 0.5[18]. Equation [4.11] is calculated and plotted as a function of the photon energy. This is shown in Figure 4.12.

$$F\left(R_\lambda, T_\lambda\right) = \left\{E_\lambda.ln\left[\left(1-R_\lambda\right)/T_\lambda\right]\right\}^2 \qquad [4.11]$$

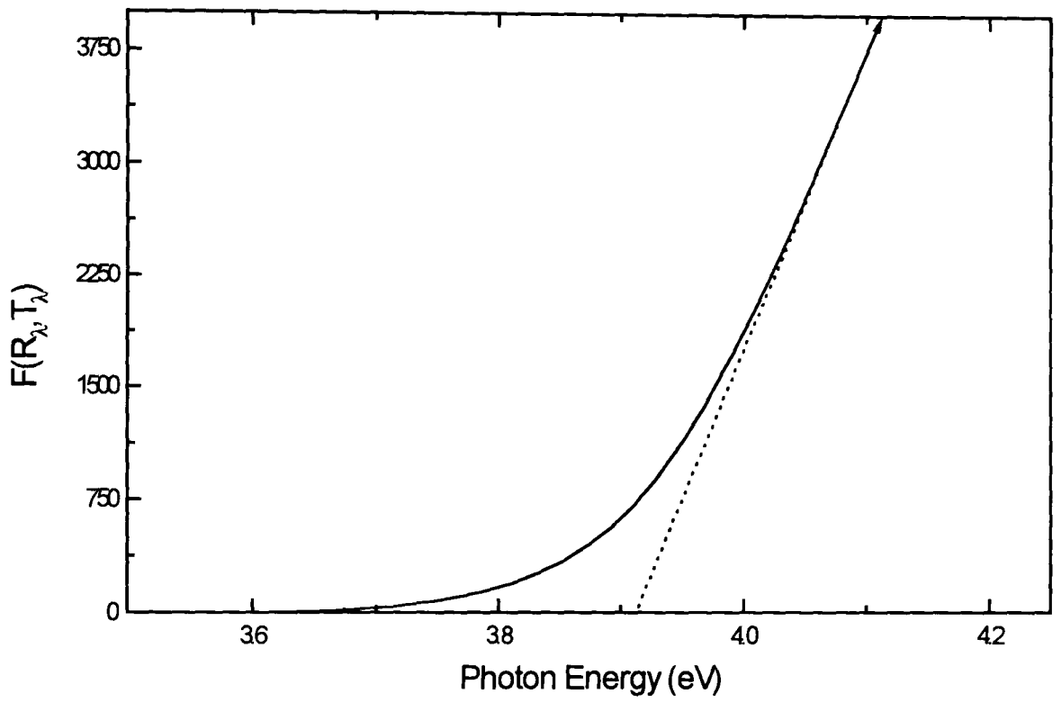

Figure 4.12 : F(R,T) as a function of the photon energy for evaluation of the optical bandgap of ITO.

The optical bandgap energy is evaluated by extrapolating the function to zero. The result obtained for ITO is $E_g = 3.85$ eV.

In the case of amorphous semiconductors[20,21] such as tungsten oxide, n is equal to 2 and equation [4.12] is used.

$$F(R_\lambda, T_\lambda) = \left\{E_\lambda . ln\left[(1 - R_\lambda) / T_\lambda\right]\right\}^{1/2} \qquad [4.12]$$

The optical bandgap energy is evaluated in the same way as for ITO.

4.4 Electrophysical characterisation techniques

The electrochemical techniques are used to investigate a number of important characteristics giving a background to subsequent performance assessment of the electrochromic film studied. Therefore the use of a standard electrochemical cell with a liquid electrolyte will be the first practical test for ionic intercalation and deintercalation.

4.4.1 Basics of electrochemistry

An electrochemical process is a heterogeneous chemical process involving the transfer of electrons to a surface[22]. The electrode reaction can be either anodic or cathodic.

In an anodic process, species are oxidised by the loss of electrons to the electrode. Conversely in a cathodic reaction, species are reduced by the gain of electrons from the electrode.

The cathodic reaction, in which a metal oxide (MeO_x) is reduced when a negative voltage is applied, can be represented by the following chemical process:

$$MeO_x + yM^+ + ye^- \rightarrow M_yMeO_x \qquad [4.13]$$

The counterpart reaction to [4.13] will be an anodic reaction [4.14], in which a positive potential applied to the working electrode will oxidise a species (M_yMeO_x).

$$M_yMeO_x \rightarrow MeO_x + yM^+ + ye^- \qquad [4.14]$$

Electrochemical reaction is only possible in a cell with both anode and cathode to maintain an overall balance of the amount of charge reduced and oxidised. In addition to electron transfer at the anode and cathode surfaces, ions must pass through the solution between the electrodes and electrons pass through external wires connected to the electrodes. Then the current through the external circuit is :

$$i = AI \qquad [4.15]$$

where A is the electrode area and I the current density (or charge transfer which is a positive quantity for an anodic process and negative for a cathodic one).

The reaction depends on the kinetics of the two electrode reactions. It is essential to have an overpotential, δ, to increase the rate at which an electrode reaction occurs. Also to move ions through the electrolyte in the cell, energy must be supplied. Hence the total cell voltage V is given by

$$V = E^c_e - E^a_e - |\delta_a| - |\delta_c| - iR \qquad [4.16]$$

where $(E^c_e - E^a_e)$ is the potential difference of the cathode and anode in the cell, (δ_a) is the anodic overpotential, (δ_c) is the cathodic overpotential, and R the resistance of the electrolyte. In this equation, the overpotentials and the iR terms represent energy inefficiencies which need to be minimised.

A third electrode is used in the cell in order to investigate the I-V response of the process at only one of the electrodes. This is the reference electrode which is positioned very close to the working electrode surface to minimise the iR drop.

The 3-electrode cell arrangement is presented in Figure 4.13. The working electrode *(WE)* is, for instance, the electrochromic tungsten oxide sample to be studied.

The counter electrode *(CE)* has to be larger than the *(WE)* and the reference electrode *(RE)* has to be close to the *(WE)*. The potential E is the potential between *(WE)* and *(RE)* and I the current between *(WE)* and *(CE)*.

A potentiostat circuit is used to control these electrodes. Figure 4.14 shows the principle of a potentiostat. The operational amplifier is the key component of the potentiostat. The feedback circuit drives the current between the working and secondary electrodes while ensuring that none passes through the reference electrode. The working electrode should be smaller than the counter electrode so that no serious polarisation can occur, and therefore the characteristics of the counter electrode reaction must not contribute to the response of the cell. Electrochemical process is undertaken with solutions containing a large excess of base electrolyte.

In an unstirred solution, diffusion is the only form of mass transport for the species considered. If the counter and working electrodes are two perfectly flat and parallel surfaces of infinite dimensions, concentration variations can only occur perpendicular to the electrode surface. Hence the diffusion process can be described by Fick's law[22]:

$$Flux = -D_i dC_i / dx \qquad [4.17]$$

where D_i is the diffusion coefficient and C_i the species concentration in the electrolyte.

4.4.2 Liquid electrolytes

Liquid electrolytes allow us to investigate the electrochromic properties of the deposited films. Initial development has been reported with protonic insertion using aqueous electrolytes such as H_2SO_4 with tungsten oxide films or KOH with nickel oxide films. Electrolytes of $LiClO_4$ (lithium perchlorate) or CF_3SO_3Li (lithium trifluoromethanesulfonate or lithium triflate) in (propylene carbonate) PC have been used extensively. Work has to be carried out in a moisture-free environment usually inside a glove-box, owing to the highly hygroscopic nature of lithium. When using lithium perchlorate, one must be aware of its potentially explosive nature. The electrolyte has to be purged from water by heating it to 90°C in a vacuum (~10 mT).

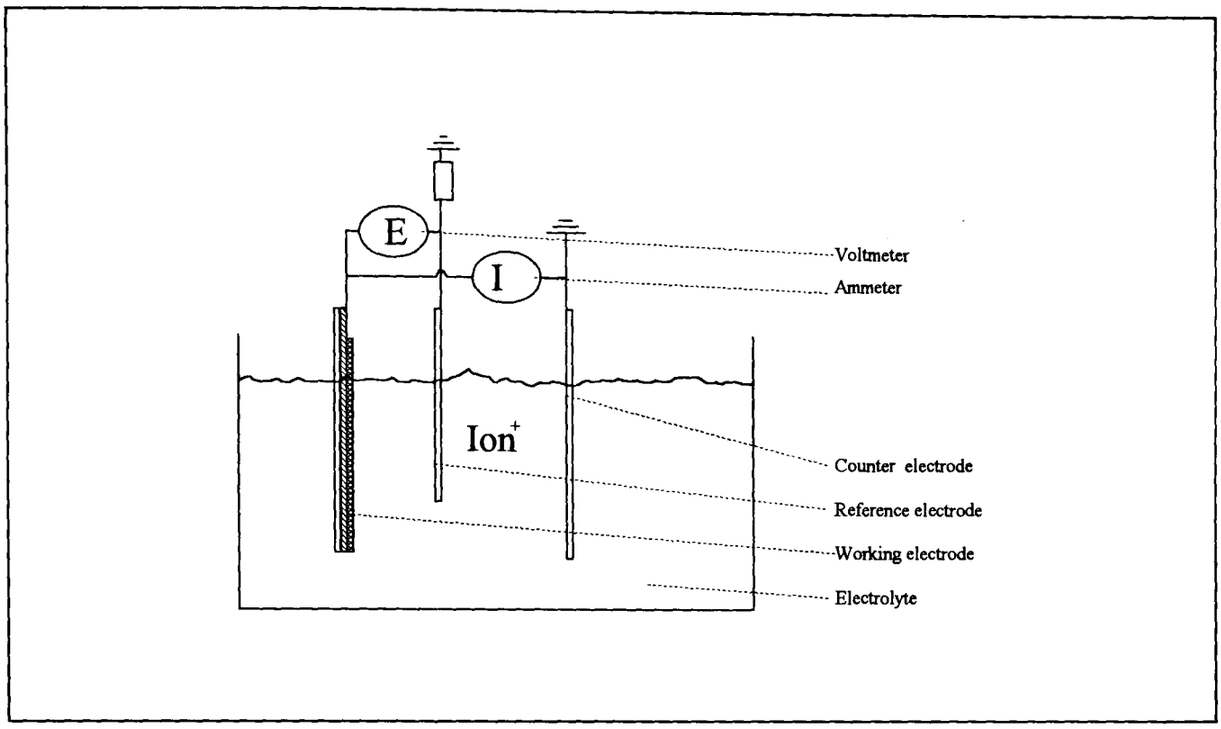

Figure 4.13 : The electrochemical cell.

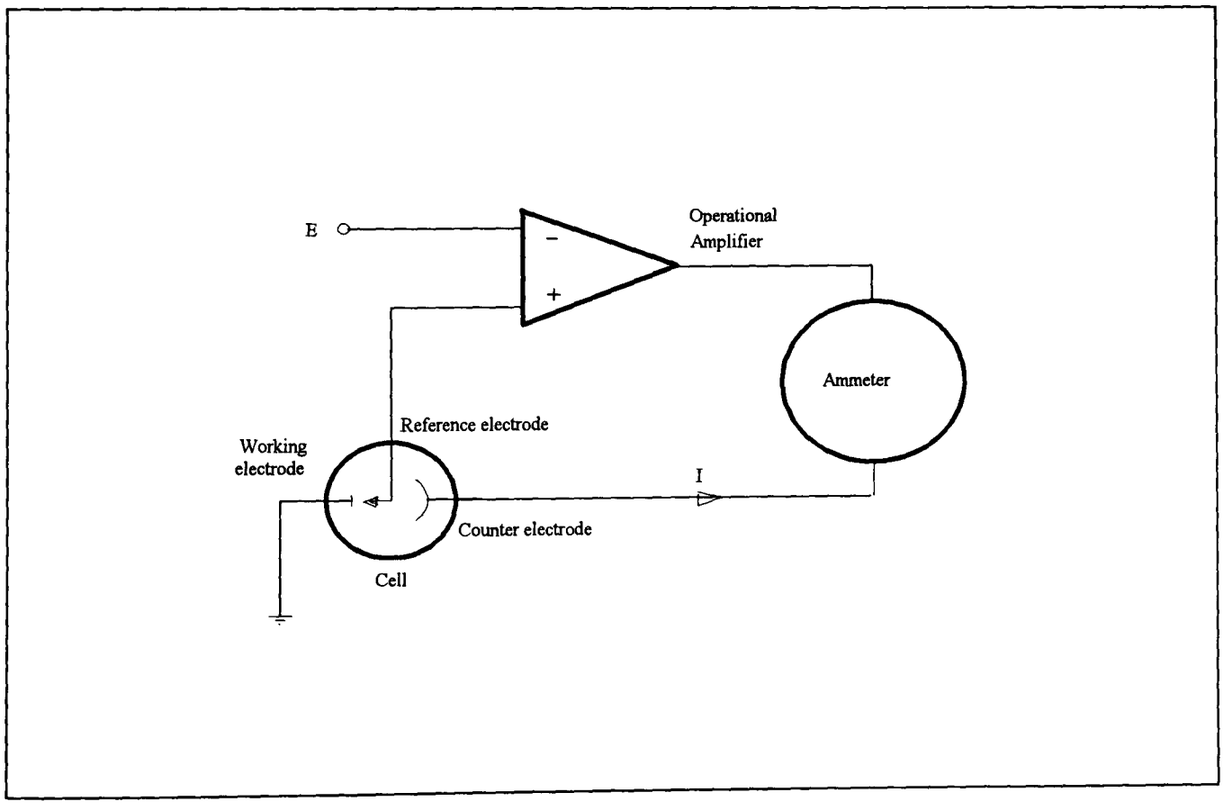

Figure 4.14 : The principle of a potentiostat.

This was left to purge for 24 hours. This process dehydrates the lithium hydroxide present in the solution. For this reason the electrochemical cell is airtight and assembled in the glove-box.

4.4.3 The electrochemical instrumentation

An EG&G scanning potentiostat model 362 was used to apply a constant DC voltage ramp to the electrochemical cell. EG&G Condecon 310 cyclic voltammetry software was used to record current, potential and time.

For electrochemical experiments in an aqueous electrolyte, the reference electrode used was a saturated calomel (SCE) electrode and the counter electrode was a 5 x 5 cm^2 platinum-coated titanium wire mesh (1 mm diameter wire).

For electrochemical experiments in a lithiated electrolyte, the reference electrode used was a 99.9 % purity lithium ribbon and the counter electrode was a 5 cm platinum wire (1 mm in diameter).

4.4.4 Cyclic voltammetry

The electrochemical spectrum contains valuable information indicating potentials at which processes occur. In cyclic voltammetry, the potential at the working electrode, controlled by the reference electrode, is continuously swept back and forth between the potential limits (V_1 *and* V_2) at a fixed sweep rate. Figure 4.15 shows the triangular potential sweep rate applied between the *WE* and the *RE* .

Cyclic voltammetry is a very important technique to use when studying an electrochromic system for the first time. A cyclic voltammogram will show several peaks and by observing how these appear and disappear as the potential limits and sweep rate are varied, it is possible to determine the possible reversibility of the reaction process. The current response is recorded in an I function of V plot. Figure 4.16 shows the I-V curve of vanadium doped with titanium oxide film in a 1M lithium perchlorate in a propylene carbonate solution. The potential limit in the positive direction is the oxygen gas evolution potential; in the negative direction, it is the hydrogen gas evolution potential.

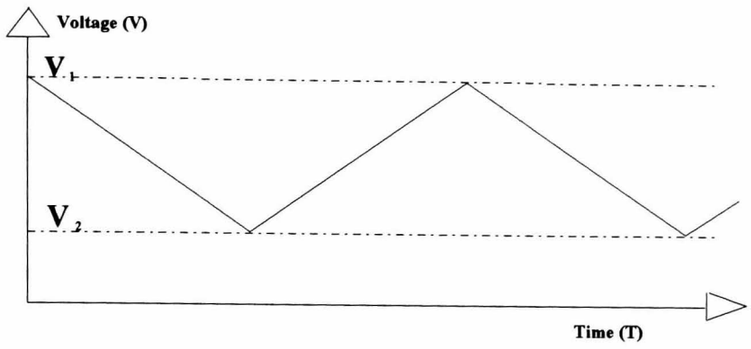

Figure 4.15 : Triangular potential applied between the working and the reference electrodes for cyclic voltammetric measurements.

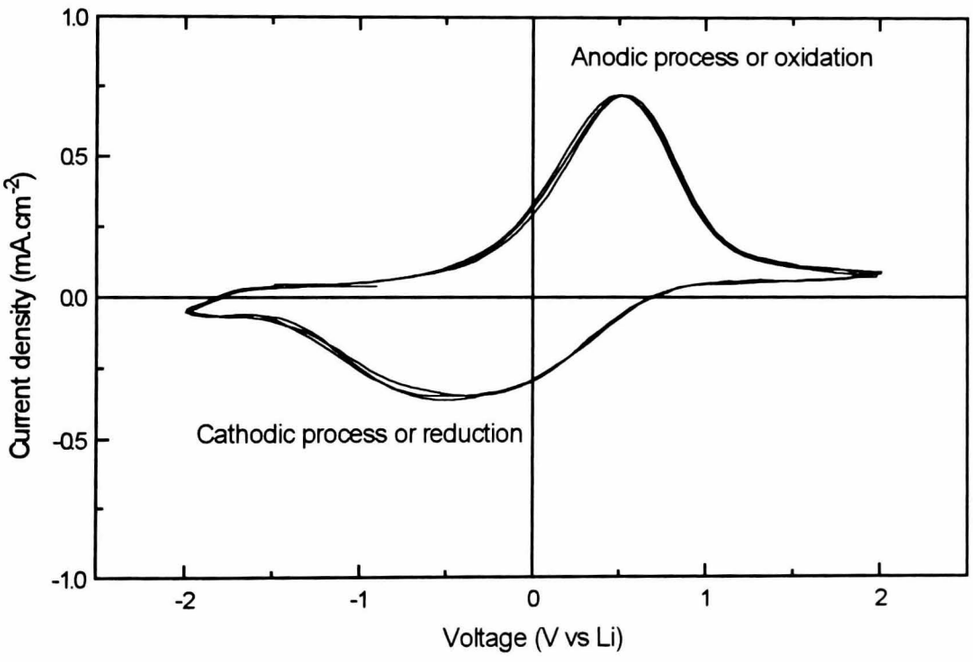

Figure 4.16 : Cyclic voltammogram of a vanadium/titanium oxide film in a 1M lithium perchlorate in PC solution at 20 mV/s scan rate.

Cyclic voltammetry can be used for both quantitative and qualitative experiments. In a qualitative experiment, kinetic parameters can be studied, and in a quantitative study it is useful to record voltammograms over a wide range of sweep rates and for different potential limits. The potential stability can then be determined and reactions with different time constants can be separated. It is possible to relate the processes represented by peaks with the potential limits and sweep rate variations.

Figure 4.16 shows perfect reversibility; both anodic and cathodic peaks mirror each other and both anodic and cathodic peaks have similar shapes, therefore the chemical reaction process is reversible. These are good cyclic voltammograms for electrochromic materials. Reversibility of a reaction process can also be checked when sweep rates are modified: currents should always peak at the same anodic and cathodic potentials.

The current and voltage were measured against a Fluke calibrated multimeter[23]. The instrument standard error for the current is ± 0.02 and for the voltage ± 0.005.

4.4.5 The spectro-electrochemical cell

A dedicated cyclic voltammetry system comprising a 362 scanning potentiostat, a Condecon 310 and a CV and CA EG&G software were used.

A prototype electrochemical cell was designed and installed for use in the Bruker IFS-66 Fourier transform spectrophotometer. A mounting assembly was built to enable the operation of this cell in the spectrophotometer. This cell is fitted with a 3-electrode arrangement and 2 quartz windows. It was specially designed[24] for optical measurements to be performed in the visible range of the spectrum. Figure 4.17 (a) and Figure 4.18 show a schematic and a photograph respectively of the spectro-electrochemical cell.

This facility enables in situ investigation of the dynamic response of optical properties of electrochromic materials in aqueous or anhydrous electrolyte to be performed whilst simultaneously observing the electrochemical behaviour. Figure 4.17 (b) presents a schematic diagram of the experimental set-up .

In the case of non-aqueous electrolytes, the cell is assembled inside an atmosphere controlled glove-box. When removed from the glove-box, the cell is purged with dry argon for 5 minutes to eliminate air which could contain water.

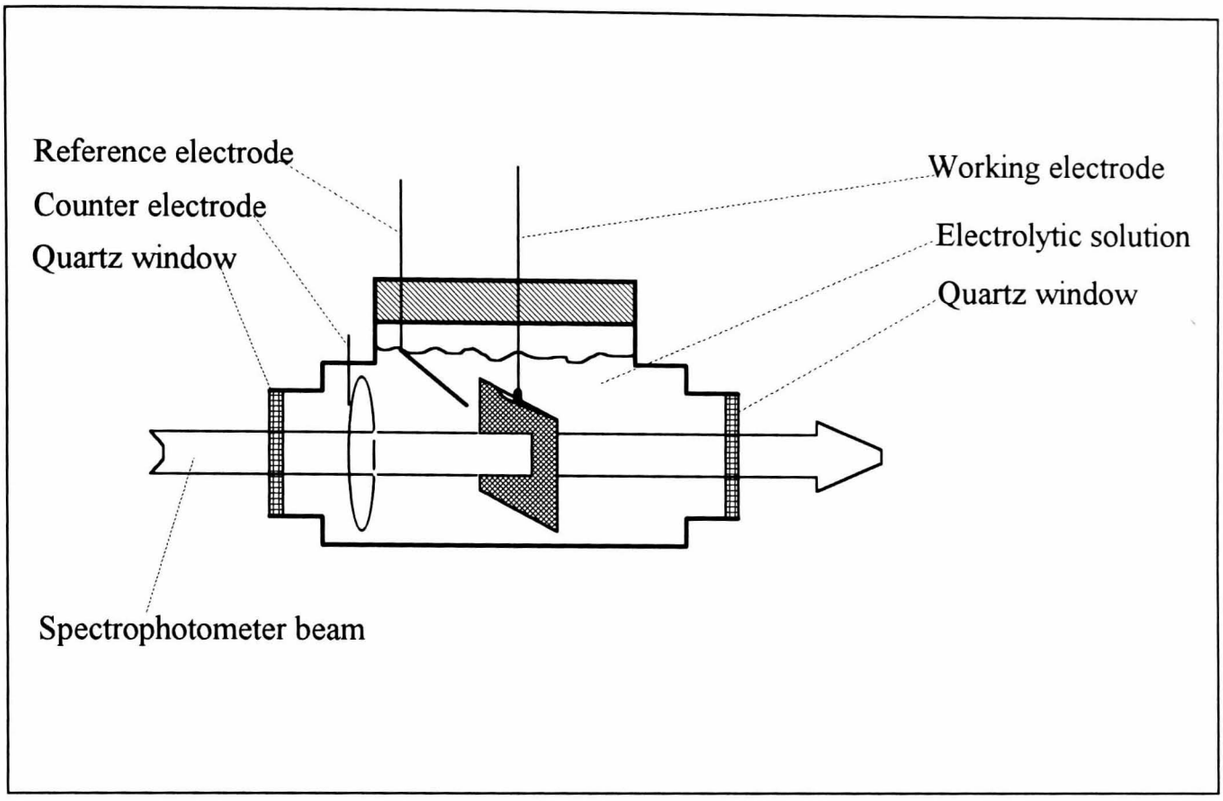

Figure 4.17(a) : Schematic of the spectro-electrochemical cell.

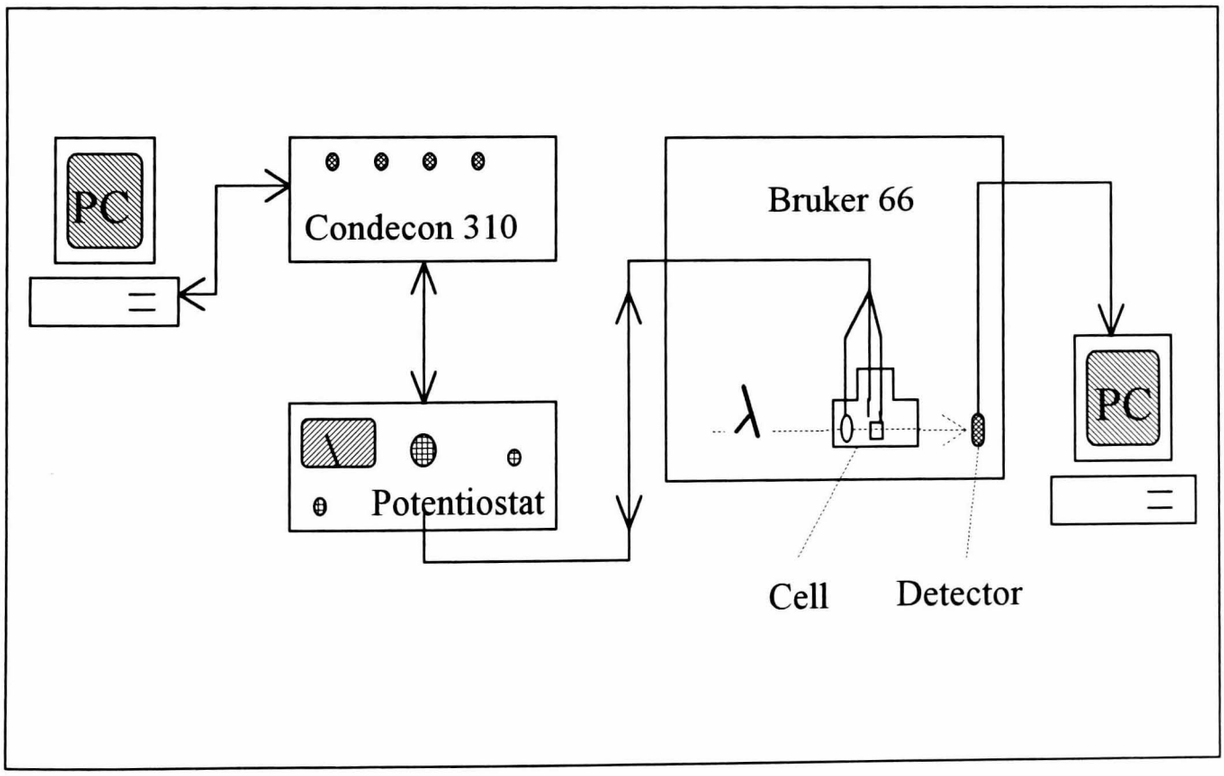

Figure 4.17 (b) : Schematic of the spectro-electrochemical experiment set-up.

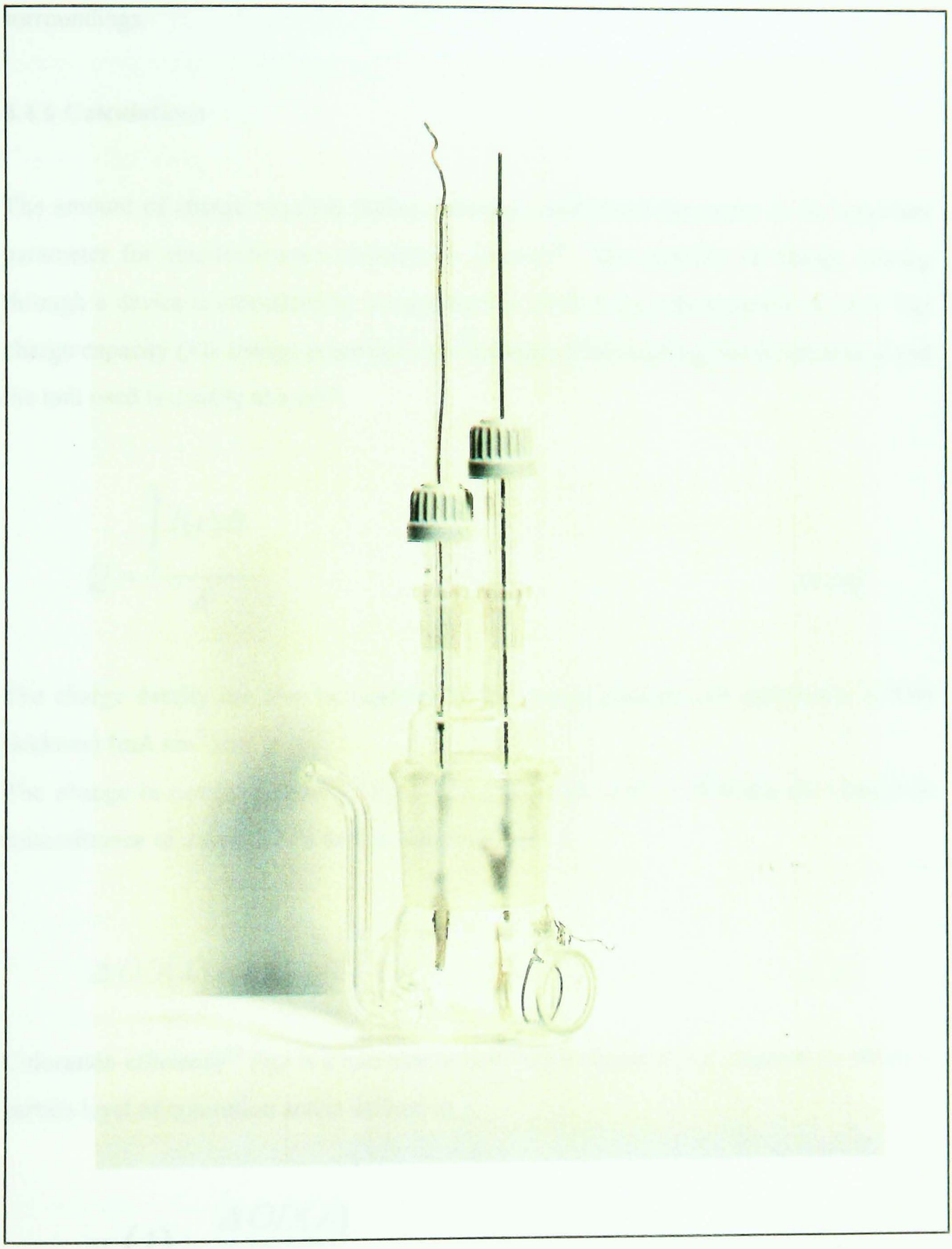

Figure 4.18 : The spectro-electrochemical cell.

The advantage of this cell is that it is airtight and therefore, electrochemical experiments can be performed in the cell without major moisture contamination from the surroundings.

4.4.6 Calculations

The amount of charge required during coloration and bleaching cycles is an important parameter for electrochromic materials or devices[25]. The quantity of charge passing through a device is calculated by integrating the current *I(t)* over a period of time. The charge capacity Q is always presented as a function of the working electrode area A and the unit used is usually $mA.cm^{-2}$.

$$Q = \frac{\int_{t_1}^{t_2} I(t)dt}{A} \qquad [4.18]$$

The charge density can also be reported as the charge capacity per nanometer of film thickness ($mA.cm^{-2}.\mu m^{-1}$).

The change in optical density[25] *(ΔOD)* is a parameter used to describe the change in transmittance of a device or a sample and is defined as :

$$\Delta OD(\lambda) = log\left(\frac{T_{\lambda b}}{T_{\lambda,c}}\right) \qquad [4.19]$$

Coloration efficiency[25] (η_c) is a measure of how much charge *(Q)* is required to obtain a certain level of coloration and is defined as :

$$\eta_c(\lambda) = \frac{\Delta OD(\lambda)}{Q} \qquad [4.20]$$

Both coloration efficiency and optical density can be integrated over the solar or visible spectrum. Therefore the solar and/or visible transmittance in the bleached and coloured states are directly used in equations [4.19] and [4.20].

In the visible range of the spectrum, a typical value of η_c for electrochromic materials is in the order of 40 $cm^2.C^{-1}$.

The standard error for the charge capacity is estimated to be equal to ± 8 %, and for the coloration efficiency to be equal to ± 10 %.

4.5 Other physical characterisation techniques

4.5.1 The Scanning electron microscope

A Jeol JSM 840 scanning electron microscope (SEM) was used to study film topography and microstructure by the secondary emission of electrons detected using an Everhart-Thornley detector. Non-conducting samples were coated with a thin layer of gold (about 5 nm) using a Polaron SEM sputter coater system. This prevents any charging effects on the sample as well as giving better resolution. However this layer can alter the surface morphology of the sample. The SEM has a magnification of up to 300,000 times.

A Link energy dispersive spectroscopy (EDS) attachment was also available on the microscope. Quantitative compositional analysis can be performed with this system. High energy electrons bombard a sample and the X-rays emitted from the elements of the film are analysed[26]. For accurate measurements, thick films (4 μm) are required.

4.5.2 Electrical measurement of sheet resistivity

An important parameter for the transparent electronic conductor coatings is the sheet resistivity ρ_s. This is measured in ohms per square (Ω/□) where the square refers to a unit area of the film.

The sheet resistivity is related to the film thickness d:

$$\rho_s = \frac{\rho}{d} \qquad [4.21]$$

where ρ is the D.C. electrical resistivity.

Measurement technique of the sheet resistance was described by Smiths[27]. A probe consisting of four small area tips is brought into contact with the surface of the film as shown in figure 4.19.

A D.C. current I is passed through the 2 outer probe tips and the voltage dropped across the 2 inner tips. If the film is assumed to be homogeneous in thickness and electrical resistivity then ρ_s is calculated from

$$\rho_s = \frac{V.\pi}{I.ln(2)} \qquad [4.22]$$

The film resistivity can be found from equation [4.21] if the film thickness is known. The Kulicke and Soffa 4-point probe used consists of osmium alloy tips of 0.08 mm diameter and 1 mm spacing. Osmium alloy is a relatively soft material and therefore will not break through the film. Small springs support the tips in order to give a constant pressure onto the film surface.

The standard error of the instrument set up was calibrated against the Fluke calibrated multimeter, and is equal to ± 5%.

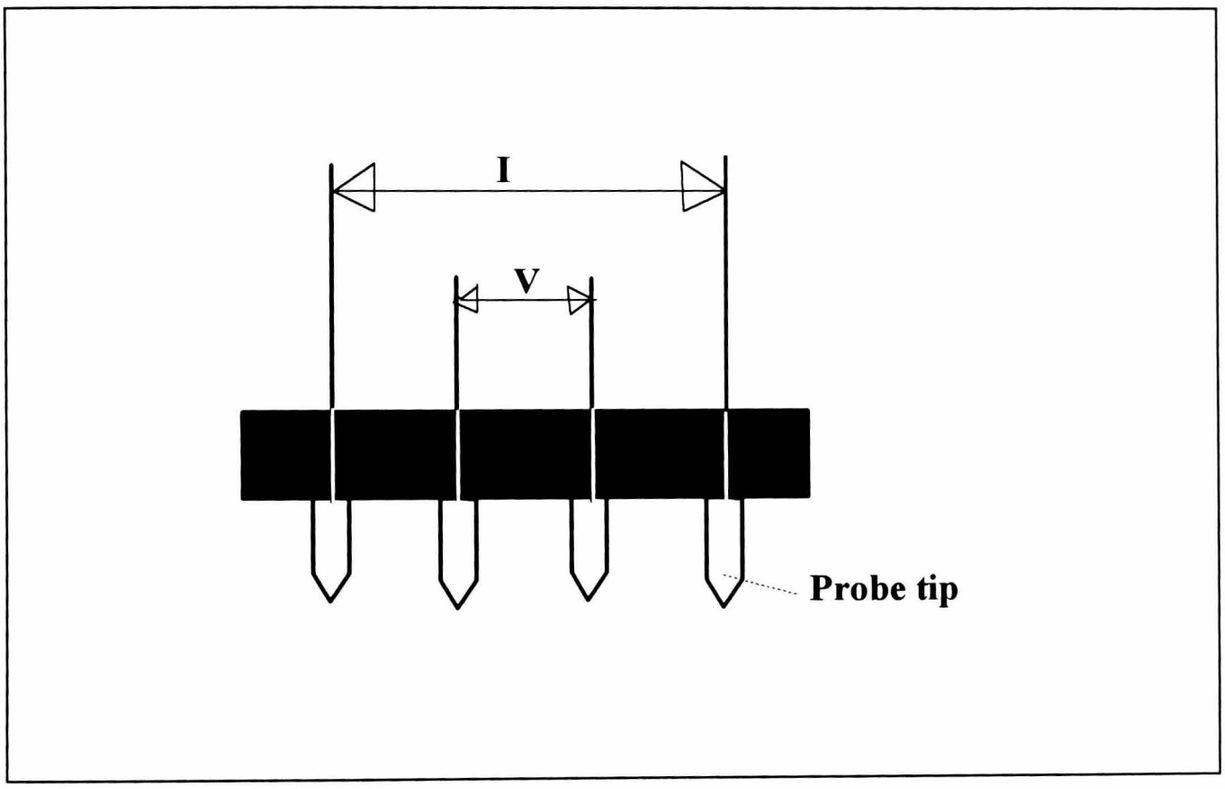

Figure 4.19 : Schematic of the 4 point probe.

4.5.3 Film thickness measurement

A Dektak IIa surface profilometer has been used to determine film thickness. A stylus can be moved from an uncoated area of the sample to the step and onto the top surface of the film. The stylus movement is amplified and recorded on a chart from which the film thickness can be measured. The measurement range is from 10 nm to 65.5 μm.
This method requires the film to be sufficiently hard so that the stylus does not break through. Substrates were masked during deposition so that a step is present to carry out film thickness investigation.
The resolution of the instrument is equal to 5 nm. The standard error is ± 10 nm.

4.5.4 Remarks

This chapter presented the principal techniques used for this thesis. Other techniques not available on site were used during the different stages of this work, such as atomic absorption spectroscopy (Pilkington), TEM and X-Ray spectroscopy (University of Southampton).

PART B

THE ELECTROCHROMIC PROPERTIES OF TRANSITION METAL OXIDE MATERIALS

Chapter 5

DEPOSITION AND CHARACTERISATION OF WORKING ELECTRODE FILMS OF TUNGSTEN OXIDE

5.1 Introduction

Tungsten oxide films have been studied in much more detail than any other inorganic material. Many investigations of the physical and electrochromic properties of tungsten oxide films have been carried out and several deposition methods have been used to prepare the films. The principal methods are : sputtering[1], evaporation[2], electrodeposition[3], spray pyrolysis[4], sol-gel technique[5], e-beam technique[6] and chemical vapour deposition[7]. Due to the good electrochromic properties of the film, WO_3 is considered as one of the most promising electrochromic materials to be used in display applications and smart windows[8], even if its appearance is not entirely architecturally favourable.

Electrochromic coloration is exhibited in both amorphous and crystalline forms and occurs by the injection of ionic species in conjunction with electrons. WO_3 films are transparent but, due to their microscopic structure, will allow the intercalation of ions to form a tungsten bronze. It has been shown in Chapter 3 that physical and structural properties of WO_3 films are strongly linked to its electrochromism. The microstructure of the materials is directly related to the preparation conditions. As a consequence, the optical properties modulation depends critically on the film preparation. Absorptance is associated with non-stoichiometry and is modulated upon ion insertion. This quantity is important for evaluating the physical absorption mechanism of the thin layer. Transmittance modulation is seen in both ordered and disordered tungsten oxide films,

whereas reflectance modulation is principally seen in the crystalline material (see Chapter 3).

Research work on electrochromic WO_3 within the Solar Energy Materials Research Laboratory commenced in 1987 and concentrated on R.F. diode sputtering[9] and on D.C. magnetron sputtering[10] of films from a metallic target. They were studied under protonic intercalation/deintercalation and their optimum electrochromic properties are summarised in Table 5.1.

This chapter presents the electrochromic properties of R.F. magnetron sputtered tungsten oxide films to be used as the active electrochromic layer in a smart window device. The electrochromic device will be discussed in Chapter 8. The aim of this chapter was first to study sputtered WO_3 thin film under lithium intercalation and to optimise the deposition parameters of tungsten oxide thin films prepared from a metal target. The second objective was to obtain electrochromic WO_3 films with better electrochromic properties than films produced in previous studies in the laboratory and to compare them with the electrochromic properties of films supplied by a collaborative laboratory.

5.2 Optimisation of sputtering deposition parameters for tungsten oxide films

5.2.1 Experimental

In this investigation, WO_3 films were prepared in a mixed Ar-O_2 atmosphere from a metallic tungsten target using an R.F. magnetron sputtering technique. The instrument used was the CVC LCS-100 sputter coater (see Chapter 4). Table 5.2 shows the different sputtering parameters used for the deposition of WO_3 films. The substrates were Pilkington ITO coated glass. The thickness of the ITO film was about 200 nm and the sheet resistance was in the range 14-16 Ω/□.

The substrate was ultra-sonically cleaned (see Chapter 4) and the ionic intercalation/deintercalation of deposited films was studied using the electrochemical cell inside the Bruker 66 spectrophotometer (see Chapter 4). Cyclic voltammetry was used to study the current flowing in and out of the WO_3 films.

	R.F. diode sputtered WO_3 film Bleached/coloured	D.C. magnetron sputtered WO_3 film Bleached/coloured
Solar Transmittance	0.51 / 0.08	0.63 / 0.02
Visible Transmittance	~0.75 / ~0.24	0.80 / 0.04
Charge capacity ($mC.cm^{-2}$)	15	28
Film thickness (nm)	406	
Coloration efficiency		
Solar range	54	52
Visible range	~33	46
($cm^2. C^{-1}$)		
Switching time	< 180 s	< 150 s
Deposition conditions		
Pressure (mT)	15	10 - 17
Power (W/cm^2)	3.7	1.35 - 1.65
Oxygen content (%)	10	10 - 15
Thickness (nm)	300 - 350	350 - 400

Table 5.1 : Summary table of electrochromic properties and deposition conditions parameters of R.F. diode and D.C. magnetron sputtered tungsten oxide film on ITO prepared by Christie[9] and Hutchins et al.[10] and studied under protonic intercalation.

Target material	W (99.9% pure)
Target size (cm^2 diameter)	15.2
Power densities (W/cm^2) standard error : ± 10 %	0.55, 1.10, 1.65, 2.20, 2.75 (13.56 MHz)
Sputtering pressures (mT) standard error : ± 10 %	5, 7, 10, 20
Oxygen concentration (%) standard error : ± 15 % of concentration value	2, 4, 7, 10, 15, 20, 25
Substrate temperatures (°C) standard error : ± 10°C	200, 170, 150
Duration (mn) standard error : ± 1 mn	15, 30, 60, 90, 120

Table 5.2 : List of sputtering conditions used to investigate the influence of deposition process parameters on the electrochromic properties of R.F. magnetron deposited tungsten oxide films.

This technique, described in Chapter 4, is of particular interest to give an indication of the electrochemical processes involved in the reaction. In the case of electrochromic materials, the reversibility of the reaction is crucial as well as the stability of the reaction over many switching cycles. From these measurements, the charge involved in the reaction process was also calculated. WO_3 films were cycled in 1M lithium perchlorate in PC. Safe potential limits versus a lithium ribbon were defined between + 1 V and + 4.5 V. A typical cyclic voltammogram is shown in Section 5.3.

5.2.2 The growth-rate of sputtered WO_3 films

Most of the samples were transparent and colourless in the as-deposited state. When the oxygen concentration in the mixed gas atmosphere was low, as-deposited films were blue or metallic in appearance. Due to the insufficient oxygen content in the chamber, the coloured films in the as-deposited state could not be bleached to a transparent state. Deneuville et al.[11] have shown that as-deposited WO_x films are transparent for $x > 2.6$, blue in the range $2.5 < x < 2.6$ and metallic in appearance for $x < 2.5$.

The oxygen content in the chamber has a direct effect on the sputtering rate for the deposition of tungsten oxide films. Figure 5.1 shows an abrupt decrease in deposition rate for O_2 concentrations above 4 %. This is due to the oxidation of the target, creating an insulating layer. At higher oxygen concentrations the deposition rate decreases slowly to a value below 0.13 nm/s. A similar effect is seen with the electrical properties of the deposited films. At oxygen contents below 2%, the films produced have metallic properties and are conductors. Then above 3 %, films are transparent and have dielectric properties.

The deposition rate of WO_3 films depends not only on the oxygen content of the mixed gas but also on the total pressure and power density. Higher sputtering rate can be achieved by increasing the power applied onto the target. As a consequence, stress can be built up in the films as well as increasing the temperature of the substrate, making films more crystalline. The sputtering rate can also be optimised at a specific pressure. Figure 5.2 shows the dependence of the deposition rate on the total pressure of the mixed gas. Below 5 mT, the films are metallic in appearance, and above 5 mT, oxide film thickness is slowly decreasing down and below 13 nm/s.

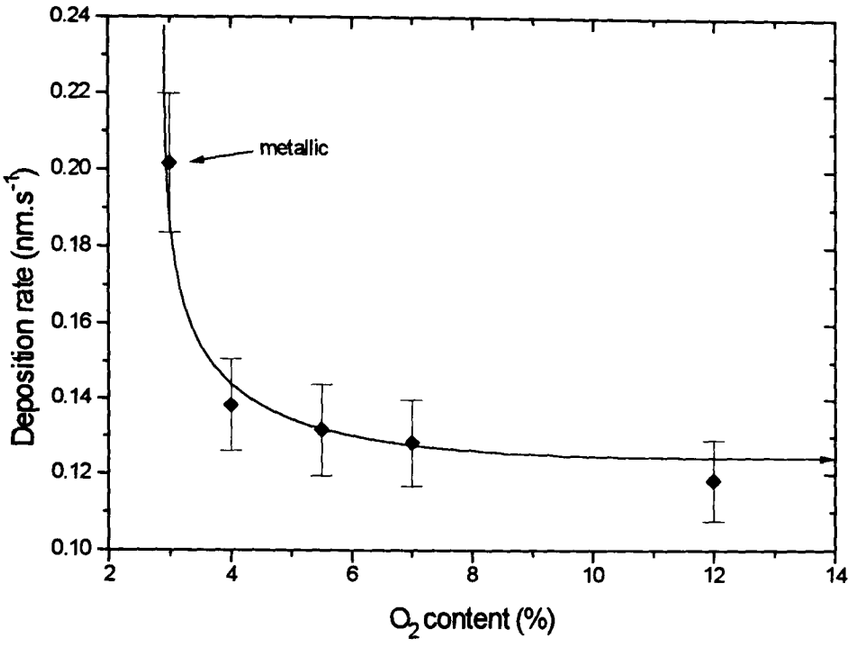

Figure 5.1 : Deposition rate of tungsten oxide films as a function of oxygen content in the mixed gas at a pressure of 10 mT and a working power of 1.65 W/cm^2. Standard error on oxygen content : ± 15 % of content value.

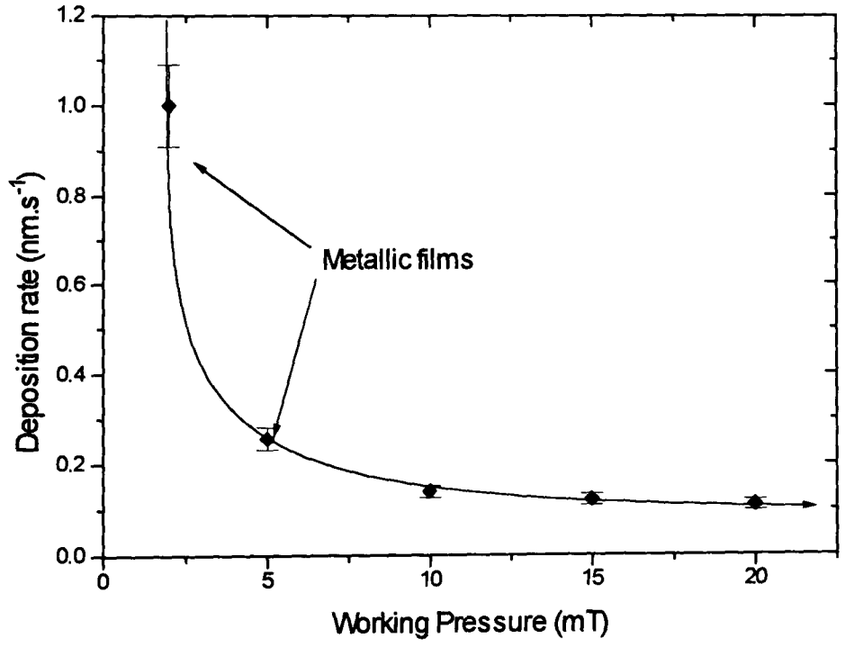

Figure 5.2 : Deposition rate of tungsten oxide films as a function of working pressure during the process at an O_2 content of 7 % and a working power of 1.65 W/cm^2.
Standard error on working pressure : ± 10 %.

5.2.3 WO_3 films prepared at different substrate temperatures

Substrate temperature during the deposition process affects the coloration efficiency and the reversibility of films. Cooling the substrate was controlled by the input R.F. power and by placing heat sink plates at the back of the substrates. Good thermal contact with the cold backing plate had to be ensured in order to keep the substrate as cool as possible. Films made at powers in the range 0.55 - 1.65 W/cm^2 with a substrate temperature lower than 180°C exhibited better electrochromic properties. Figure 5.3 shows the variation of coloration efficiency in the visible range of the spectrum as a function of temperature. The principal reason for the variation in η_c is the amorphous or polycrystalline structure of films. High process temperatures will increase the degree of crystallinity of materials and reduce the possibility of ionic intercalation and the coloration efficiency. All future depositions were carried out with cooled plates placed at the back of the substrates. The power density was chosen to be 1.65 W/cm^2.

5.2.4 Coloration efficiency of WO_3 films prepared at different sputtering conditions

To carry out the optimisation of sputtering conditions, electrochromic efficiency of deposited WO_3 films was studied as a function of the different parameters.

Figure 5.4 shows the visible coloration efficiency of tungsten oxide films as a function of the working pressure. A maximum is obtained at total pressures of 10 - 12 mT. Figure 5.5 shows the η_c as a function of the oxygen concentration. η_c increases with increasing oxygen content for ratios below 10%, where a maximum is reached and then remains constant. At oxygen contents greater than 4%, the surface of the target is assumed to be completely oxidised. One could therefore consider that the electrochromic performance of films are similar when deposited with oxygen concentration greater than 7% as indicated in Figure 6.5. At this point, it was noticed that almost 93 % of the intercalated charge was deintercalated for films produced at low oxygen contents (7 - 10 %), whereas for films produced at higher oxygen ratios more charge remains irreversibly inserted after each cycle.

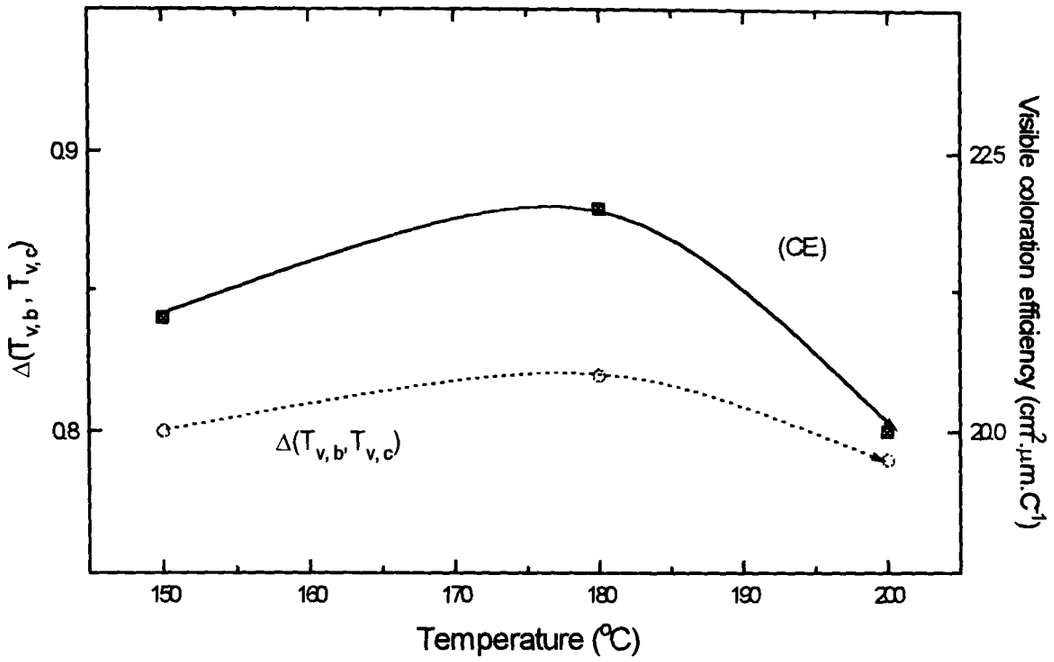

Figure 5.3 : Coloration efficiency as a function of process temperature of tungsten films prepared at a working pressure of 10 mT, at an O_2 content of 7 % and at a working power of 1.65 W/cm^2.
Standard error on temperature : ± 10°C, and on η_c : ± 10 %.

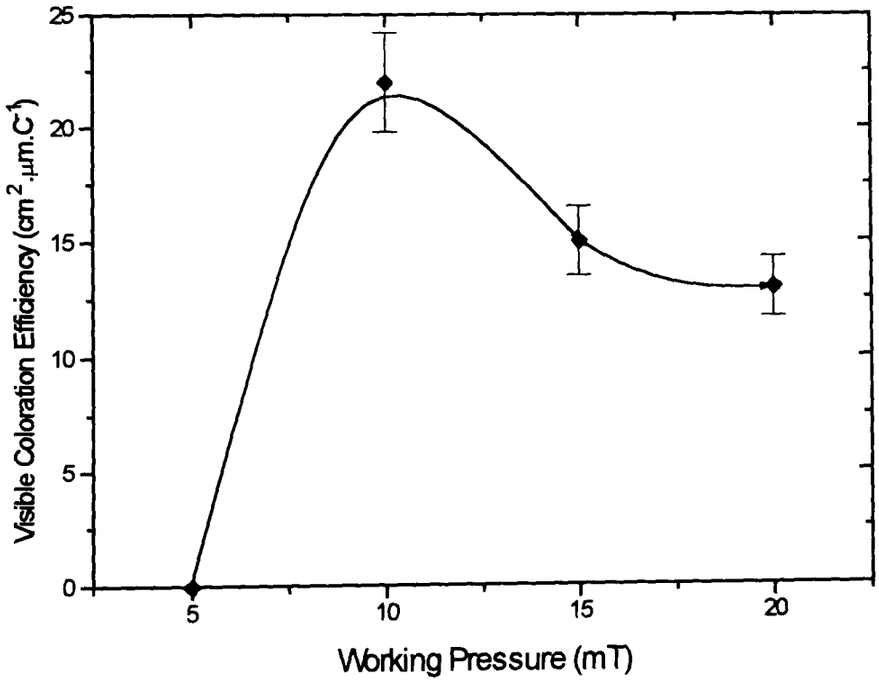

Figure 5.4 : Coloration efficiency of tungsten oxide films as a function of working pressure, at a working power of 1.65 W/cm^2, at an O_2 content of 7 % and for a duration of 1 hour.
Standard error on working pressure : ± 10 %.

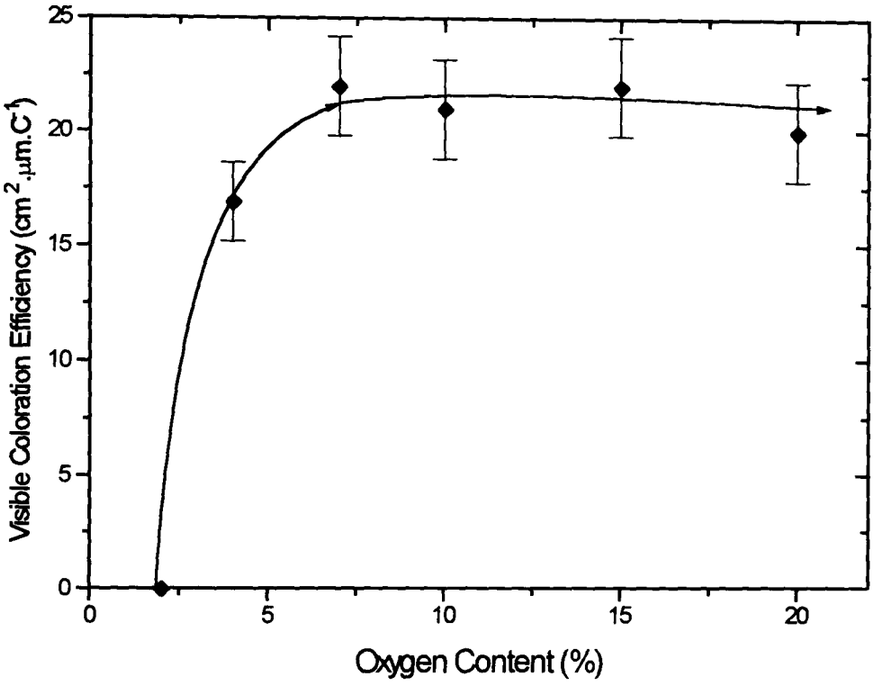

Figure 5.5 : Coloration efficiency of tungsten oxide films as a function of O_2 content, at a working pressure of 10 mT, at a working power of 1.65 W/cm^2 and for 1 hour.

Standard error on oxygen content : ± 15 % of content value.

Figure 5.6 shows the coloration efficiency as a function of the film thickness. Maximum is obtained for thickness in the range 400-500 nm. At higher thicknesses films can store a large amount of charge and remain dark in the bleached state. There is also a large quantity of charge irreversibly inserted into the layer. On the contrary, thinner films have a lower quantity of charge that can be inserted/extracted and have a coloured state which cannot reach a dark appearance.

5.3 Comparison of the properties of R.F. magnetron sputtered WO_3 films and other sputtered WO_3 films

As part of the IEA Task 18 collaboration, sputter-deposited WO_3 films were provided by OCLI, Santa Rosa, USA[12] in order to investigate their physical, optical and electrochemical properties. The aim of this section is to study the properties of optimised films produced in this work and to compare them with the electrochromic properties of optimised WO_3 films produced with a similar technique but in a different laboratory.

5.3.1 Film composition and microstructure

The surface microstructure of tungsten oxide was observed using the SEM, X-ray microanalysis and XRD equipment.

Figure 5.7 shows the SEM micrographs of an optimised tungsten oxide film produced in this work. The surface is very homogeneous. At similar magnification, the microstructure of tungsten oxide films seems to be very similar to the structure of OCLI's films[13]. Figure 5.8 shows an AFM picture of an OCLI film and at very high magnification, the film seems to be made of nanocrystalline grains in the order of 20 to 30 nm.

Figure 5.9 shows the XRD patterns of the as-deposited WO_3 film, where the peaks for the ITO films can be observed. This would suggest that WO_3 produced in this work is essentially amorphous with the possibility of being nanocrystalline. Similar results were observed with OCLI films[14].

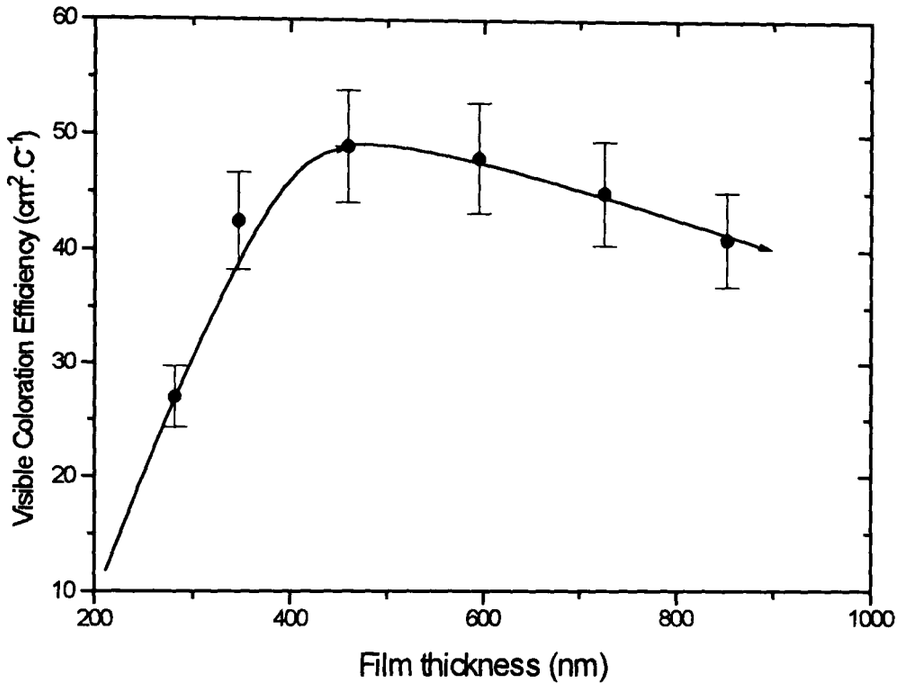

Figure 5.6 : Coloration efficiency of tungsten oxide films as a function of film thickness, at an O_2 content of 4%, a working pressure of 10 mT and at a working power of 1.65 W/cm^2.
Standard error on thickness : ± 10 nm.

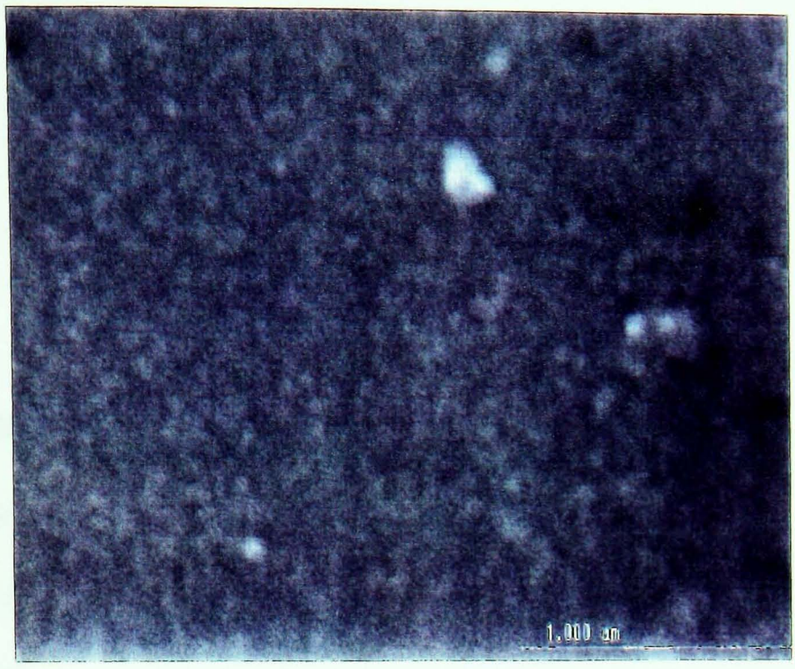

Figure 5.7 : SEM photograph of R.F. magnetron sputtered WO_3 film produced in this work (x 20000).

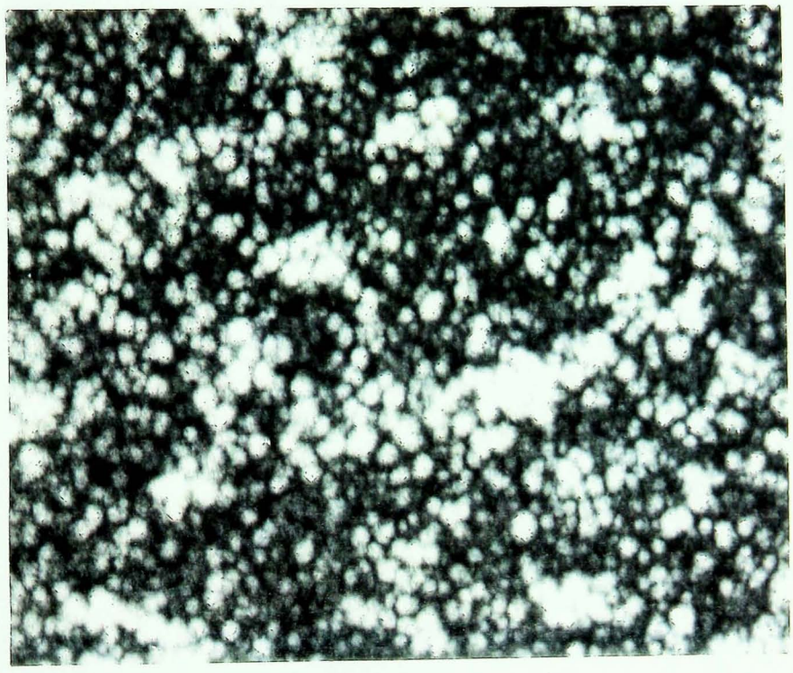

Figure 5.8 : AFM photograph[13] of a sputtered WO_3 film supplied by OCLI, Santa Rosa, USA (image size 2 x 2 µm).

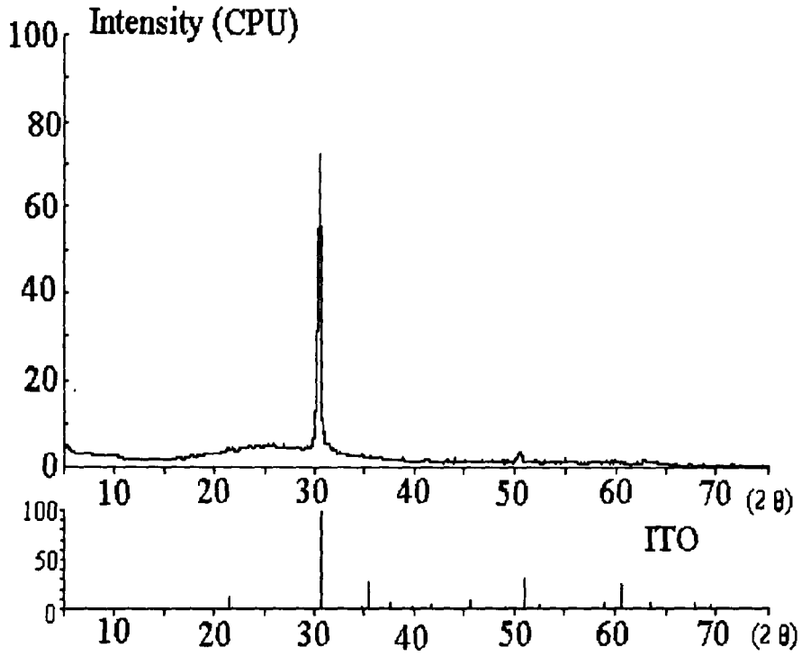

Figure 5.9 : XRD patterns of the optimised R.F. magnetron sputtered WO_3 film.

The X-ray microanalysis gives an approximate chemical composition of the WO_3 film, and the tungsten to oxygen ratio in our films was estimated to be greater than 2.9. Analysis of the best OCLI films gave a W/O ratio of equal to 3.27[13].

Near grazing incidence FTIR reflectance spectroscopy of WO_3 film using p-polarised light was used to study the resonant frequency of bands characteristic of longitudinal optical modes of the crystal. This is shown in Figure 5.10. A certain number of peaks can be seen and can be assigned to different vibration modes. The adsorption of water described in Chapter 3 can be seen in this spectrum with an O-H bending vibration[15] at 3350 cm^{-1}, and an O-H stretch vibration of H_2O molecule[15] at 1620 cm^{-1}. Otherwise, stretching modes of terminal W=O bond[15] are seen at 940 cm^{-1}, and stretching mode[16] of O-W-O at 630 cm^{-1}. Similar results are also observed with OCLI WO_3 films[17].

5.3.2 Electrochemical properties

Figure 5.11 shows the cyclic voltammograms 21 to 25 of the optimised tungsten oxide film. The graph is smooth, indicating no well-defined phase changes taking place. A similar result has been observed with OCLI's films[18] and sputtered WO_3 films[19] in general. This behaviour can be seen over more than 3000 switching cycles, indicating that the reaction process remains the same. The size of peaks on both anodic and cathodic sides are fairly similar, indicating good reversibility of the electrochemical reaction occurring during ionic intercalation and deintercalation processes.

A common characteristic of amorphous materials is the permanent incorporation of ionic species into the film lattice over the first switching cycles[20]. This is shown in Figure 5.12 for the optimised WO_3 film. Over the first 2 switching cycles, 10 % of the inserted charge is left inside the layer. For the next switching cycles the charge inserted remains almost constant, of the order of 46 mC/cm^2. In subsequent scans almost 95% of the inserted charge is then extracted. This shows that the process is stable over switching cycles. The small charge imbalance is probably due to ionic species being trapped in the highly disordered material, but might also be due to some side reaction on the film surface. The charge imbalance effect was reported in Section 5.2 to depend on the oxygen content used during deposition.

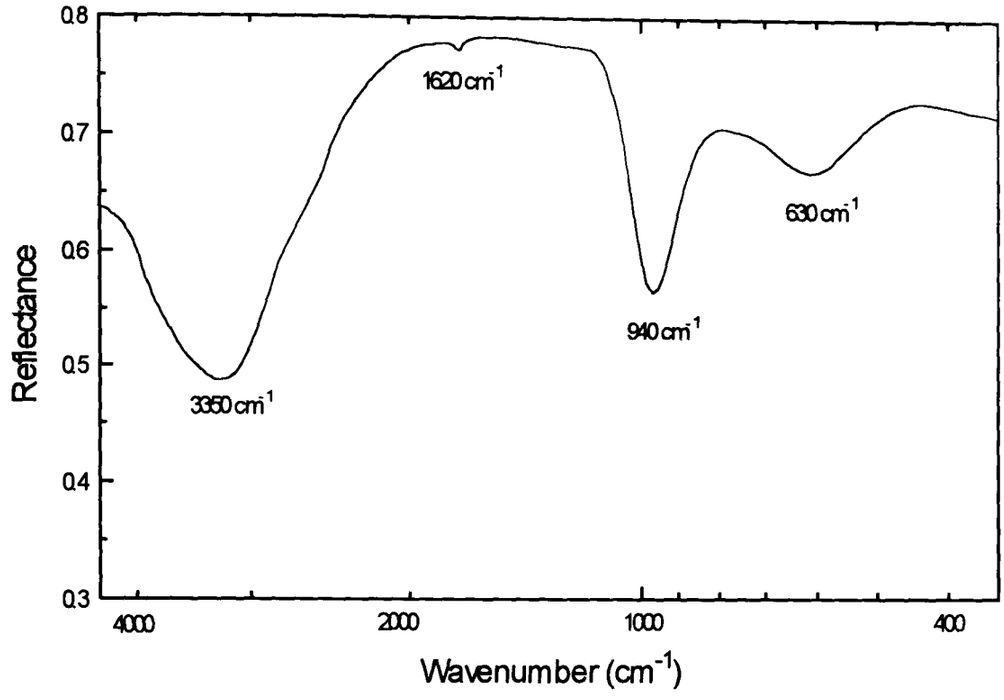

Figure 5.10 : IR spectrum at near grazing incidence of the optimised WO_3 film.

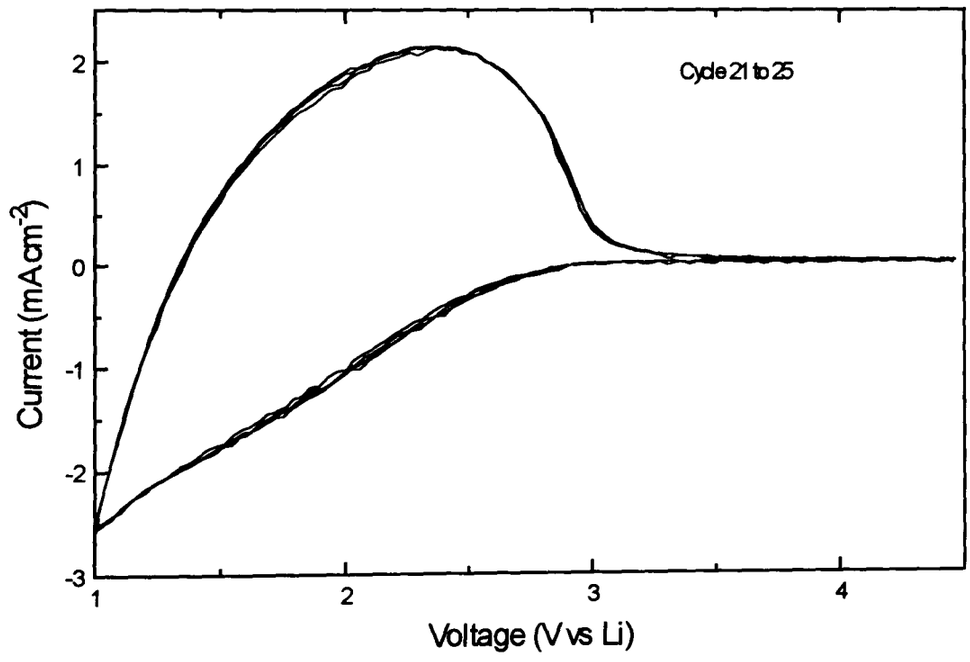

Figure 5.11 : Cyclic voltammogram 21 to 25 of WO_3 in 1M $LiClO_4$ in PC, driven at a 20 mV/s scan rate.

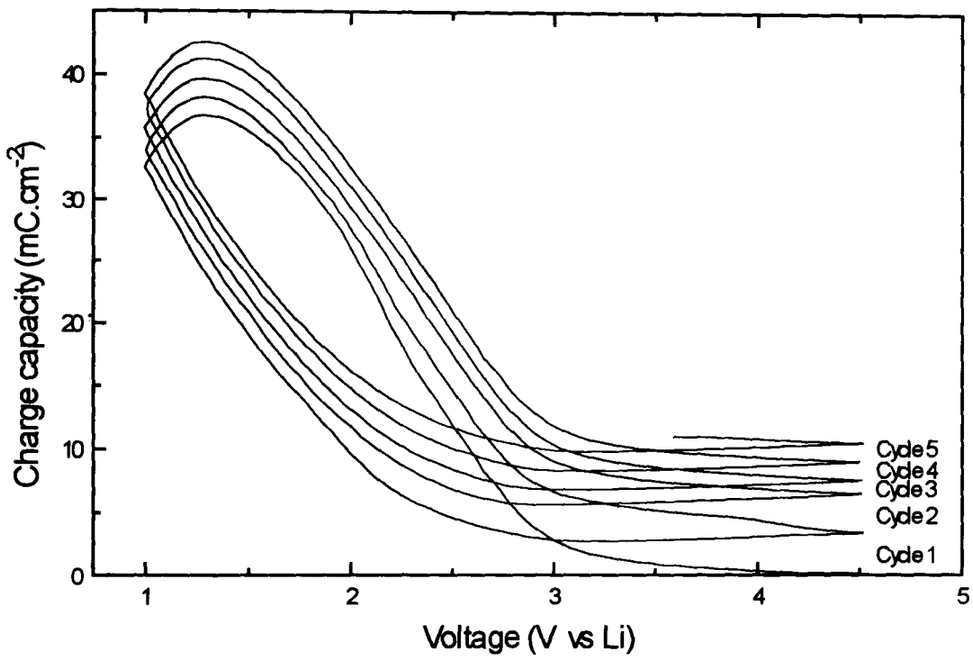

Figure 5.12 : Charge passing through WO_3 film in 1M $LiClO_4$ in PC, driven at 20 mV/s scan rate.

At oxygen concentrations higher than 7 %, the percentage of charge left inside the layer after each switching cycle was measured to be higher than 10 %. At lower oxygen concentrations the charge left after each cycle remains in the range 5 to 7 %. F. Michalak[21] suggested that a possible reason might be the formation of LiO_2 at the surface and inside the film. This would explain the high irreversibility of the intercalation/deintercalation process during the first scan. The formation of LiO_2 would decrease with the limited number of free oxygen molecules available in the film and after the third scan would reach a minimum. Finally, another possible reaction is the irreversible formation of lithium tungstate (Li_2WO_4)[22,23]. That might explain the increasing charge imbalance over cycling when films contain higher proportions of oxygen as well as the continuous charge imbalance during the cycling. However, further investigation is required to investigate the reasons for the irreversibility.

OCLI WO_3 films exhibited lower charge capacity[24,25] in the range 25 to 28 mC/cm^2 when studied in lithium-based electrolyte. The charge imbalance was also noticed and estimated to be almost equal to 10 %[17]. However, the charge imbalance was measured to be lower for OCLI films studied in a protonated electrolyte[18]. The proportion was $\leq$ 5 %. This latter result might suggest that species formation in a lithiated electrolyte such as LiO_2 and Li_2WO_4 could be responsible for the irreversible charge intercalation whereas the material disorder trapping both H^+ and Li^+ is always present, and might be responsible for a large proportion of charge imbalance. One can expect the WO_3 film to saturate with trapped lithium ions after a large number of scans, creating an irreversible coloration.

The sputtered WO_3 films colour and bleach extremely rapidly even with a relatively low potential. The current versus time response is shown in Figure 5.13. It takes no more than 2 minutes to fully bleach or colour the WO_3 films. However it was noticed that the coloration process was slower than the bleaching process.

5.3.3 Transmittance properties of WO_3 films

Optical measurements include the transmittance and reflectance of the ITO on glass substrate. The optical properties of the ITO substrate can be seen in Chapter 8.

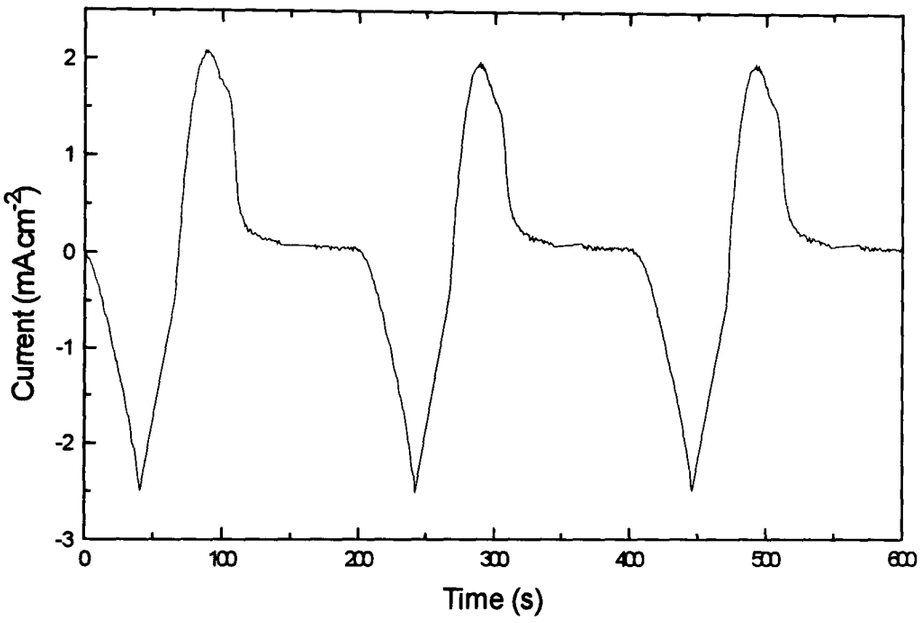

Figure 5.13 : Current time response of WO_3 film in 1M $LiClO_4$ in PC, driven at a 20 mV/s scan rate.

Figure 5.14 shows the spectral transmittance of a WO_3 film in the solar range after being cycled in lithium perchlorate more than 20 times.

The near-infrared cut-off is strongly influenced by the properties of the ITO coated glass. At visible wavelengths, the oscillations are due to optical interference of the ITO layer. The overall solar transmittance of the layer is modulated from $T_{s,b} = 0.59$ to $T_{s,c} = 0.01$ and in the visible range of the spectrum the modulation is from $T_{v,b} = 0.83$ to $T_{v,c} = 0.04$. The bleached state is very transparent and almost colourless. On the other hand, the coloured state is very dark and looks blue in appearance. These optical properties remain unchanged over more than 1000 switching cycles.

OCLI films exhibit very similar transmittance properties. However, the coloured state appeared clearer. The overall solar transmittance of the film is modulated from $T_{s,b} = 0.59$ to $T_{s,c} = 0.04$ and in the visible range of the spectrum the modulation is from $T_{v,b} = 0.78$ to $T_{v,c} = 0.05$.

Figure 5.15 shows the modulation of absorption coefficient of the optimised WO_3 as a function of the incident energy. The optical bandgap is modulated between 3.3 eV for the bleached state to 3.5 eV for the coloured state at maximum Li^+ content. A similar result is observed for the OCLI film and this is shown on Figure 5.15.

5.3.4 Reflectance and absorptance properties of WO_3 films

To carry out reflectance properties measurements, samples had to be taken out of the electrochemical cell and placed directly in front of the sphere port of the spectrophotometer. Owing to the fact that lithium perchlorate is highly hygroscopic, a protonated electrolyte (0.1 M H_2SO_4) was used in order to carry out experiments in a non-dry environment.

Figure 5.16 shows the reflectance modulation of an OCLI film as a function of the quantity of proton inserted into the layer. This result shows a reflectance modulation in the near infrared part of the spectrum. This is essentially due to the transparency modulation of WO_3 revealing the reflective properties of the ITO substrate. This is shown in Figure 5.17. Doping WO_3 films increases the solar absorption of the film.

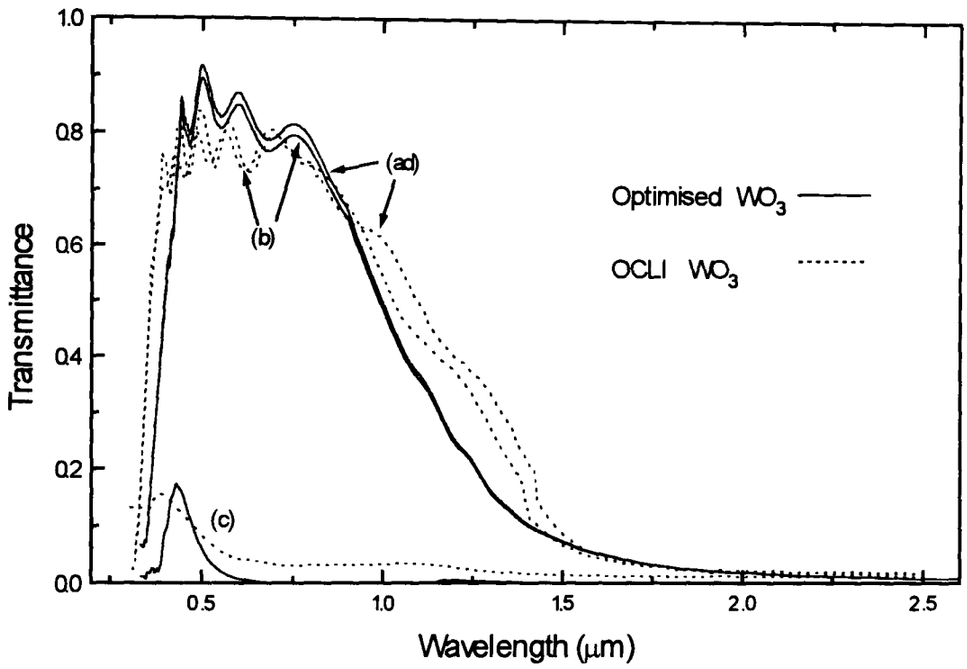

Figure 5.14 : Transmittance modulation of an optimised R.F. magnetron sputtered WO_3 and of an OCLI films in the as-deposited (ad), coloured (c) and bleached (b) states respectively.

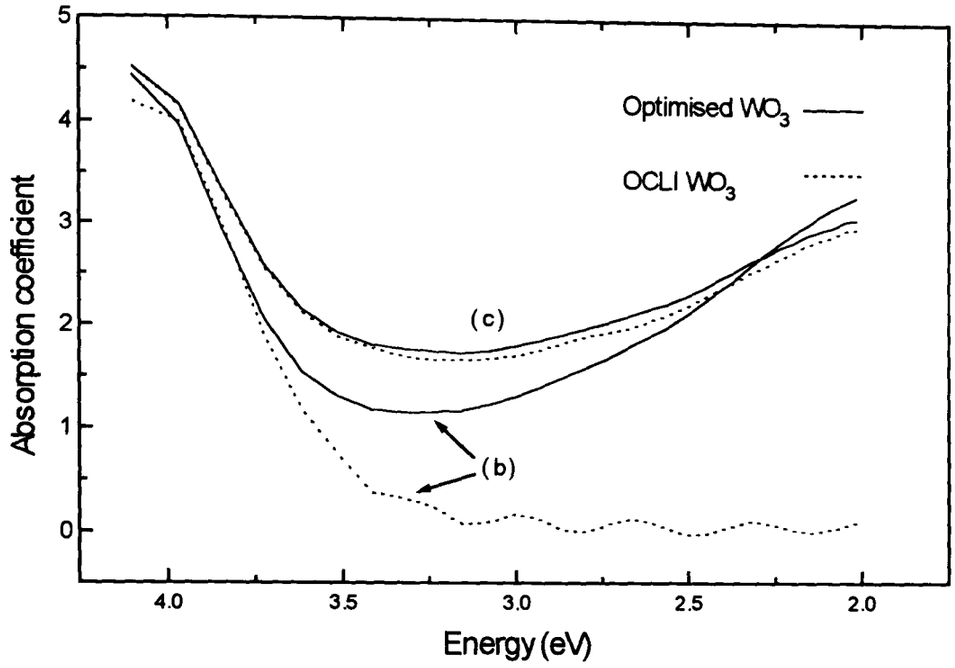

Figure 5.15 : Absorption coefficient of an optimised WO_3 and of an OCLI WO_3 film as a function of the incident energy in the bleached (b) and coloured (c) states respectively.

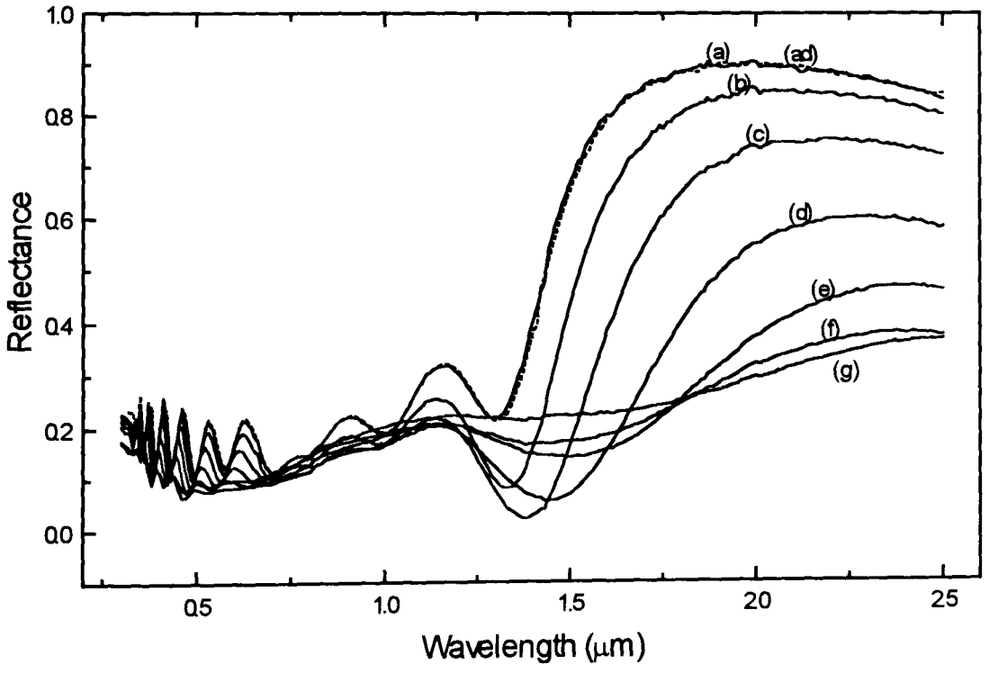

Figure 5.16 : Reflectance modulation of OCLI WO_3 film under proton insertion; (ad) as-deposited, (a) 0, (b) 0.5, (c) 1.5, (d) 3.2, (e) 7.0, (f) 17.2, (g) 43 mC/cm^2.

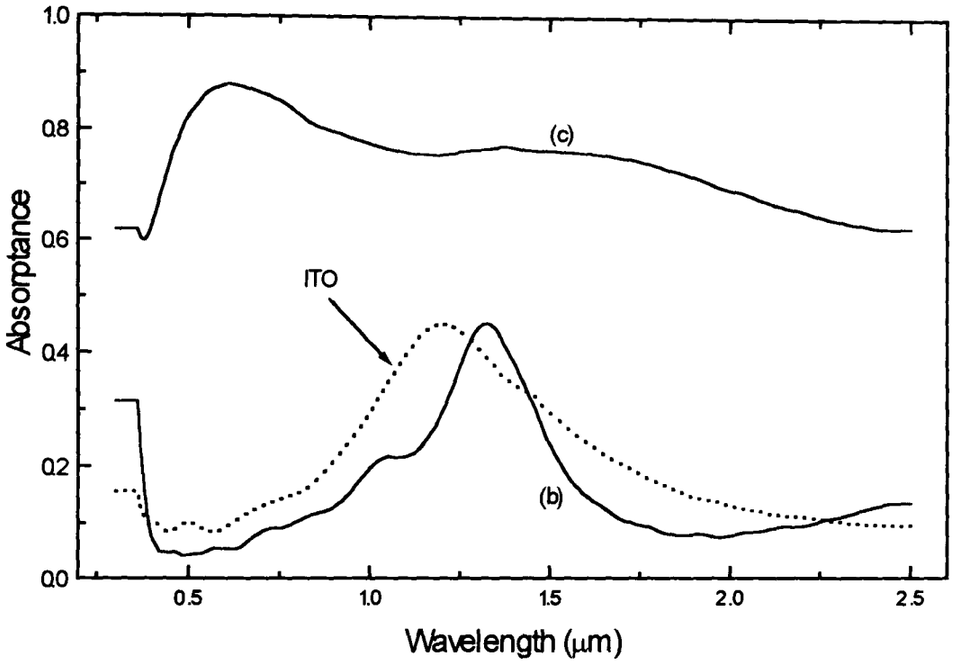

Figure 5.17 : Spectral absorptance of an of an OCLI WO_3 film under proton insertion in the bleached (b) and coloured (c) states respectively and spectral absorptance of an ITO substrate.

With the ITO substrate as a background the solar absorptance of the WO_3 film is modulated from $A_{s,b} = 0.12$ to $A_{s,c} = 0.80$, therefore almost 70 % of the incident solar energy will be absorbed by the film.

5.4 Summary and Conclusion

WO_3 films produced in this chapter by reactive R.F. magnetron sputtering from a metallic target exhibit good electrochromic properties. Table 5.3 summarises all the properties and deposition parameters of sputtered tungsten oxide films under lithium intercalation/deintercalation. The optimised R.F magnetron sputtering parameters obtained in this work are similar to the R.F. diode and D.C. magnetron sputtering parameters previously obtained by the laboratory (see Table 5.1). The R.F. magnetron sputtered WO_3 films with the highest electrochromic efficiency was found to be for low oxygen ratio inside the sputtering chamber of the order of 4-6 %, for an optimum gas mixture pressure of about 10-15 mT. Tungsten oxide films show better coloration efficiency when sputtered on a cooled substrate, meaning that electrochromic behaviour is improved when films are amorphous or polycrystalline. To limit the increase of temperature on the substrate, sputtering deposition has to be performed at low power density (≤ 1.65 W/cm^2). An optimum thickness seems to be of the order of 500 nm. These optimum deposition parameters of WO_3 films from a metallic target seem to be in reasonably good agreement with published results[26] and results obtained previously by D.C. magnetron sputtering[10].

In parallel with this work, the testing of sputter deposited OCLI WO_3 films showed many structural, optical and electrochemical similarities with the WO_3 produced in this work. Table 5.4 presents a summary of the electrochromic properties of OCLI films studied under H^+ and Li^+ insertion/extraction. These results seem to show favourable electrochromic properties with Li^+ insertion/extraction and seem to be closed to the properties of WO_3 films produced in this work. It is comforting to see that these latter films are very comparable with optimised films produced by a similar technique in a different laboratory.

This chapter shows that relatively good electrochromic WO_3 films are easy to deposit by sputtering techniques. Their optical properties do not vary drastically with the deposition process parameters as well as with the sputtering deposition technique used. Whereas the electrochemical properties of WO_3 films depend mainly on the conditions process parameters used during deposition. A high degree of visible transmittance modulation and good stability over long run switching cycles is obtained, combined with a relatively high η_c. Sputtered tungsten oxide layer is a promising candidate as a working electrode in an all solid state electrochromic device.

However, the high absorption of the coloured film in the near infrared range of the spectrum is not ideal for all future applications. This could mean an overheating of the electrochromic device when left in the fully coloured state. Applicability of such film may have to be combined with infrared reflecting layers placed between the environment and the layer itself.

In the following chapter, oxide films are sputter deposited and studied as possible counter electrode in an all-solid state device. These layers do not only required to have high T_v and to be durable, but also, they now have to match the charge capacity of the WO_3 layer, e.g. their own charge capacity has to be higher than 33 $mC.cm^{-2}$.

	Optimised WO_3 film with Li^+ as-deposited/bleached /coloured
T_s	0.61 / 0.59 / 0.02
T_v	0.85 / 0.83 / 0.04
Optical bandgap (eV)	3.3 / 3.3 / 3.5

Q ($mC.cm^{-2}$)	33 ± 3
Film thickness (nm)	460 ± 10
η_c ($cm^2.C^{-1}$)	
Solar range	44 ± 4
Visible range	40 ± 4
Switching potentials	+ 1 V / + 4.5 V vs Li
Switching time (s)	< 120
Lifetime (cycles)	> 1000

	Optimised R.F. magnetron sputtering parameters
Target material	W (99.9 % purity)
Target size	15.2 cm diameter
Power density	~ 1.6 W/cm^2
Sputter pressure	10 - 15 mT
Oxygen content	7 - 10 %
Temperature	< 200 °C
Thickness	~ 500 nm

Table 5.3 : Summary of the electrochromic properties and of optimised deposition process parameters of R.F. magnetron sputtered tungsten oxide films under lithium intercalation/deintercalation.

	OCLI WO_3 film with H^+ (Li^+) as-deposited/bleached /coloured
T_s	0.60 / 0.59 / 0.04 (H^+)[18] N/A / 0.71 / 0.09 (Li^+)[24,25]
T_v	0.81 / 0.78 / 0.05 (H^+)[18] N/A / 0.81 / 0.10 (Li^+)[24,25]
Optical bandgap (eV)	3.3 / 3.3 / 3.5 (H^+)[18]

Q ($mC.cm^{-2}$) **Film thickness** (nm)	43 ± 4 (H^+)[18] 28 ± 3 (Li^+)[24,25] 360 [13]
η_c ($cm^2.C^{-1}$) **Solar range** **Visible range**	 27 ± 3 (H^+)[18] 32 ± 3 (Li^+)[24,25] 28 ± 3 (H^+)[18] 32 ± 3 (Li^+)[24,25]
Switching potentials	- 0.8 V / + 0.8 V vs SCE
Switching time (s)	< 120
Lifetime (cycles)	NA

Table 5.4 : Summary of the electrochromic properties of the best sputtered OCLI WO_3 film under proton intercalation/deintercalation. Electrochemical results with lithium have been taken from references 22 and 24.

Chapter 6

DEPOSITION AND CHARACTERISATION OF COUNTER ELECTRODE FILMS OF NICKEL OXIDE

6.1 Introduction

The focus of attention in the present chapter is the use of nickel oxide as a potential counter electrode in a "smart window". Its relevance to electrochromic device design is that nickel oxide exhibits an anodic bronze coloration and could obviously be used in conjunction with tungsten oxide films.

In aqueous environments, nickel oxide exhibits a very reversible electrochromism below the oxygen and hydrogen evolution potentials, a long open circuit memory as well as a good durability. It can be deposited using a variety of techniques other than sputter and electrochemical depositions presented in this chapter[1,2,3].

A large part of this chapter deals with protonic insertion and extraction into microcrystalline nickel oxide films produced by the R.F. magnetron sputtering technique. Their electrochromic behaviour was tested in aqueous potassium hydroxide. However, more recent work has been started on the intercalation of lithium ions in an aprotic environment. Different ions were also used in an attempt to demonstrate the electrochromic mechanism of nickel oxide material. Finally, this chapter concludes on the applicability of nickel oxide films as a counter electrode in smart window designs.

6.2 Background

In 1967, Miller and Thomas[4] reported a detailed survey of the nickel oxide electrode. At the time, the complexity of the electrode process had been noticed and most of the studies concerned applications in batteries[5]. With the advance of potentiostatic and linear sweep techniques, investigations of electrochemical behaviours of the nickel oxide electrode took place. The charge cycle of the electrode in a strongly alkaline solution will be the anodic formation of a thin oxide film of nickel[6,7,8]. Since the nickel hydroxide electrode in the electrolyte solutions lies above the reversible oxygen potential, the oxide surface can provide a path for oxygen evolution[9]. The application of linear potential sweeps to nickel hydroxide electrodes usually produces a single peak in both anodic and cathodic directions.

Some more complex anodic peaks are mentioned by Sattar and Conway[7], and others[10] attributed these to the change from α-$Ni(OH)_2$ to β-$Ni(OH)_2$ with an α structure highly disordered and more hydrated. This was described in a general way by Oliva et al.[11] with two corresponding oxidised states (coloured state): β-NiOOH and γ-NiOOH phases, the latter oxyhydroxide type (γ) being the more hydrated. Hydrated nickel oxide can have a layered structure (see Chapter 3). Both nickel hydroxides and oxyhydroxides possess a brucite structure with weakly-bound layers of edge-sharing NiO_6 octahedra[12]. Empty octahedral sites are found between the layers where water can intercalate. A schematic of the nickel hydroxide unit cell is show in Figure 6.1, and a graphical representation of the layered brucite structure of the β-$Ni(OH)_2$ phase is given in Figure 6.2.

Studies[11] have been directed to the solid-phase processes occurring during the oxidation of $Ni(OH)_2$ to NiOOH. The system has been kinetically controlled during this stage either by a diffusion process, or by a charge transfer reaction at a growing oxidation boundary. The two forms of $Ni(OH)_2$, differing in their lattice water content, have considerable interest in the nature of the H_2O content and its function in the electrode process. IR spectroscopy studies have helped in the distinction between free OH^- and H_2O and in the detection of hydrogen bonding. The assignment of absorption frequencies is agreed : free OH^- stretching at 3647-3650 cm^{-1} and there are broad bands at 3500, 1620 and 540 cm^{-1} to represent lattice water modes[13].

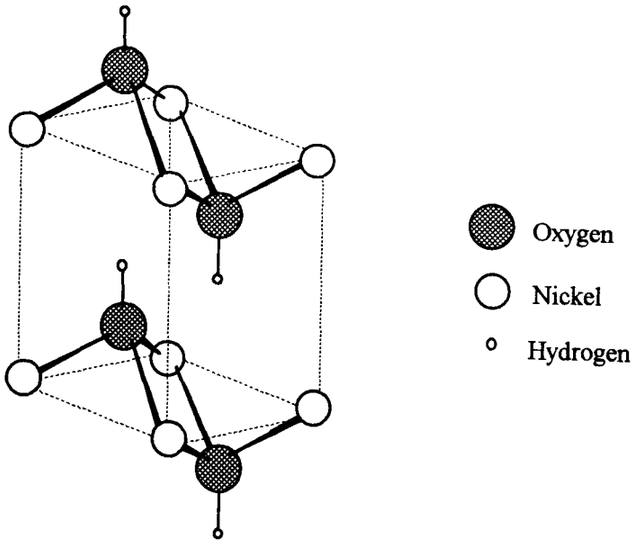

Figure 6.1 : Nickel hydroxide $Ni(OH)_2$ unit cell[13].

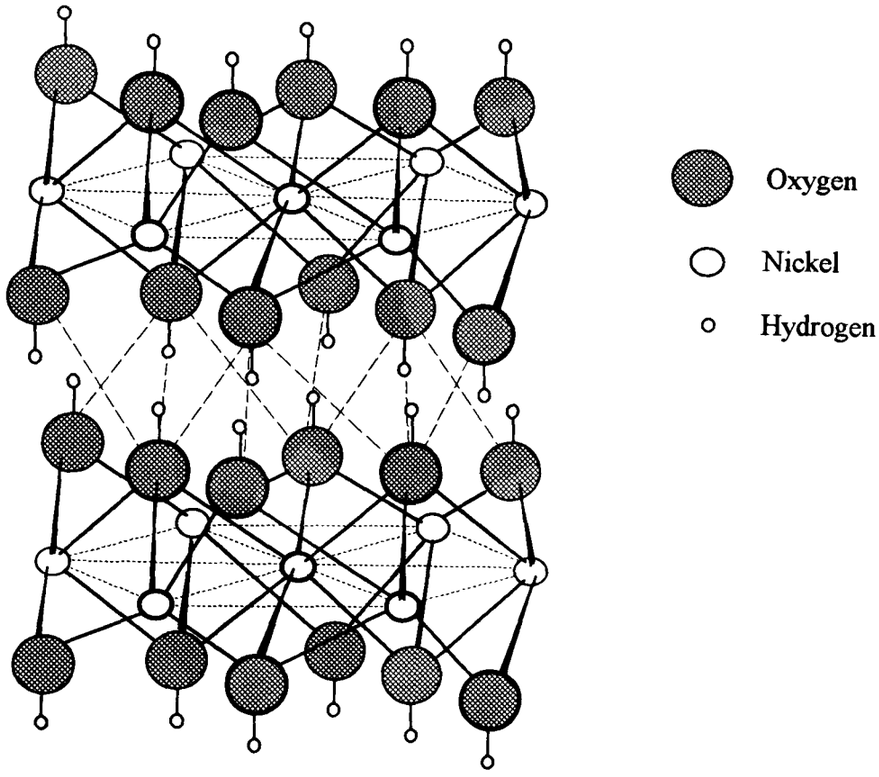

Figure 6.2 : The layered geometry of the brucite structure of β-$Ni(OH)_2$. It is an hexagonal arrangement of Ni^{2+} ions with an octahedral coordination of oxygen[14].

The change in absorption[15,16,17] from a sharp peak at 3647 cm^{-1} to a broad peak at 3400 cm^{-1} when charging $Ni(OH)_2$, shows that there was no free OH^- in the NiOOH phases. The narrow free OH^- peak on the reduction phase appears to show no frequency shift or asymmetry in profile.

Research on electrochromic nickel oxide within the Solar Energy Materials Research Laboratory commenced in 1988 and concentrated on diode sputtering of films from a metallic nickel target[18]. Results showed that the electrochromic properties were strongly influenced by the deposition process conditions. Controversy[19] has existed over the nature of the nickel oxide coloration mechanism. Different reactions have been proposed and concern has been expressed over the role of water and particularly the relative importance of H^+ and OH^- ions as the principal agents responsible for the electrochromic properties. By producing electrodeposited nickel hydroxide films[17], it was possible to investigate and compare electrochromic with those of sputtered films. Figure 6.3 and Figure 6.4 show the transmittance properties of a nickel oxide film produced by diode sputtering and of a nickel hydroxide film produced by electrodeposition respectively. Physically deposited films, which essentially contain no water, were then compared[20] with electrochemically deposited films which contain bound H_2O. It was therefore possible to determine the relative importance of each ion, and it was found that the mechanism was not the same[21]. In sputtered films the coloration mechanism is dominated by cationic ions and in electrochemical films which contain water, the coloration mechanism is dominated by OH^- ions.

Therefore the mechanism for electrochemically deposited films can be described as:

$$Ni(OH)_2 \text{ (bleached)} + OH^- \rightleftharpoons NiOOH \text{ (coloured)} + H_2O + e^- \qquad [6.1]$$

In the case of sputtered films, the proposed mechanism can be written as an initial irreversible intercalation that activates the electrodes:

$$Ni_{1-x}O \text{ (as-deposited)} + yM^+ + ye^- \rightleftharpoons M_y Ni_{1-x}O \text{ (bleached)} \qquad [6.2]$$

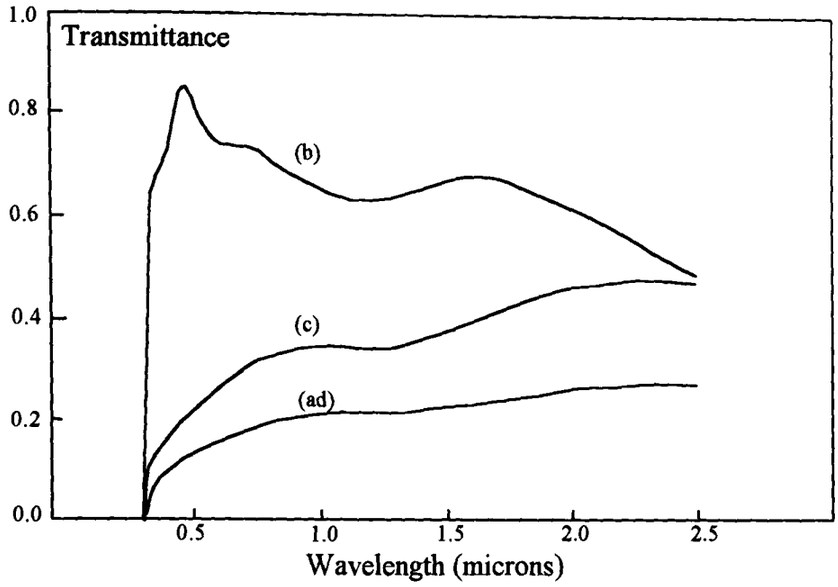

Figure 6.3 : Total near-normal hemispherical spectral transmittance of an R.F. sputtered nickel oxide film on ITO prepared by Hutchins et al.[18] at a power of 10.2 W/cm^2, a pressure of 6.4 x 10^{-2} mbar, an oxygen to argon ratio of 6 % and a deposition time of 2 hours. Solar transmittance in the as-deposited state (ad) $T_s = 0.17$, in the coloured state (c) $T_s = 0.30$ and bleached state (b) $T_s = 0.70$.

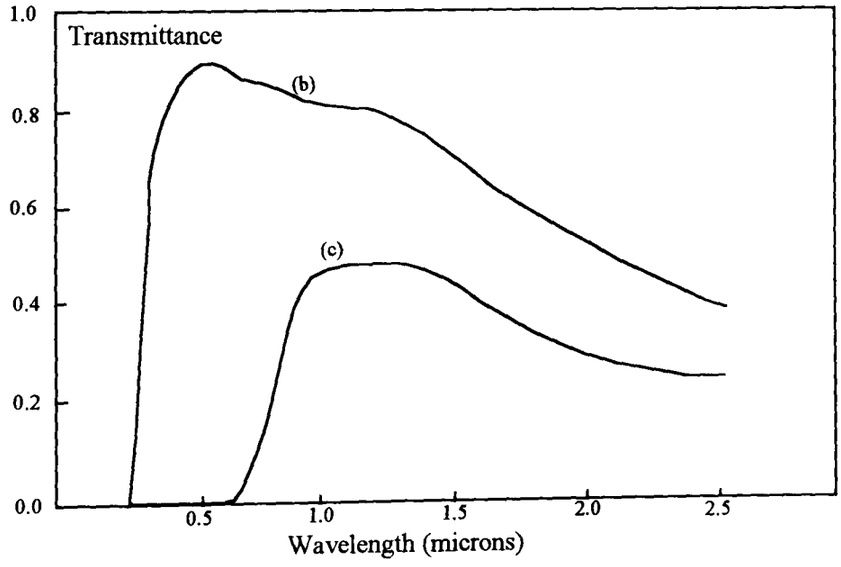

Figure 6.4 : Total near-normal hemispherical spectral transmittance of an optimised nickel hydroxide film on ITO prepared by Hutchins et al.[17]. Solar transmittance in the coloured state (c) $T_s = 0.22$ and bleached state (b) $T_s = 0.75$.

followed by a reversible reaction on further insertion of ions:

$$M_y Ni_{1-x}O \text{ (bleached)} \rightleftharpoons M_{y-z} Ni_{1-x}O \text{ (coloured)} + zM^+ + ze^- \qquad [6.3]$$

The work presented in this Chapter is an extension and an improvement of previous work of the laboratory. Deposition process conditions of nickel oxide films by reactive sputtering and electrodeposition are optimised under protonic intercalation, and a comparison of their physical, electrochemical and optical performance characteristics are detailed in this Chapter. Sputtered nickel oxide layers are also studied as a potential counter electrode in a lithium-based electrochromic device. Finally, the applicability of both films in a prototype window is shown in this chapter.

6.3 Film preparation

Nickel oxide and nickel hydroxide films were prepared by R.F. magnetron sputtering and electrodeposition techniques respectively. For these films, deposition parameters were optimised and only optimised results are presented. A systematic investigation of physical, optical and electrochemical properties of films produced under different deposition parameters was carried out. A systematic examination of all deposition process parameters was carried out.

Thickness, solar transmittance and reflectance were measured for all as-deposited films. Solar transmittance and charge inserted and extracted were then measured after switching the film between its coloured and bleached states several times. The coloration efficiency was then calculated and was defined as one of the key experimental results for the optimisation of the deposition process parameters.

6.3.1 Sputter deposition

The substrates were 5.1 x 5.1 cm^2 (2" x 2") pieces of glass coated with ITO on one side. The sheet resistivity of the conductive layer was 14 Ω/□. Substrates were cleaned in a 3% diluted solution of Decon 90, then thoroughly rinsed with distilled water. The

substrates were finally rinsed with propanol-2 and dried with a nitrogen gun. The samples were stored vertically in polypropylene racks which were themselves enclosed in an air-tight container.

Electrochromic nickel oxide thin films were prepared using the Nordiko NS 3750 sputtering system (see Chapter 4). Oxide films were prepared by reactive R.F. magnetron sputtering from a nickel target in an oxygen atmosphere. Sputtering was performed at different powers, pressures, oxygen concentrations and durations. Unless stated, films were deposited at a sputtering power of 1.77 W/cm^2, a working pressure of 15 mT, a deposition time of one hour, an oxygen to argon ratio of 9% and at the sputtering process temperature (~ 200°C). The ITO substrates were masked to expose an area of 5.1 x 4.3 cm^2 and mounted on the substrate carrier. Details about sputtering conditions used for nickel oxide films are summarised in Table 6.1. Estimated errors for each parameter are given in the table. Instrument standard errors given by manufacturers, and reading errors have been used for these values.

Figure 6.5 shows the deposition rate of nickel oxide films as a function of pressure. A maximum is seen at a pressure of about 15 mT for all sputtering powers used. Figure 6.6 shows the deposition rate as a function of the oxygen content. The rate peaks at about 4 % oxygen content. Below this concentration, the film is a mixture of nickel metal and nickel oxide and shows electronic conductivity. For oxygen concentrations above 4%, oxygen starts to contaminate the metallic target. The oxide layer formed at the target will slow down the deposition rate. At that point, deposited films exhibit a very high electronic resistivity.

The uniformity of film thickness was found to be of the order of 94%. The estimated error on the deposition rate is equal to 9%. The reproducibility of the deposition process on the film thickness was of the order of 90%.

6.3.2 Electrodeposition

The deposition of electrochromic films by electrochemical methods has been studied by different groups[23,24,25]. Electrochemically-deposited nickel hydroxide can be prepared in different ways.

Target material	Ni (99.9% pure)
Target size (cm^2)	10.2 x 30.5 (4"x12")
Power densities (W/cm^2) standard error : ± 10 %	0.65, 0.97, 1.61, 1.77, 1.94, 2.26, 2.91 (13.56 MHz)
Sputtering pressures (mT) standard error : ± 10 %	05, 10, 14, 16, 18, 20, 25, 35
Oxygen concentrations (%) standard error : ± 15 % of concentration value	1, 2, 4, 5, 6, 6.5, 7, 7.5, 8, 8.5, 9, 9.5, 10, 12, 15, 20, 30, 50
Substrate temperatures standard error ± 10 °C	~ 200°C, ~ 150°C
Durations (mn) standard error ± 1mn	30, 45, 60, 75, 90, 120

Table 6.1 : List of sputtering conditions used to investigate the influence of deposition process parameters on the electrochromic properties of R. F. magnetron deposited nickel oxide.

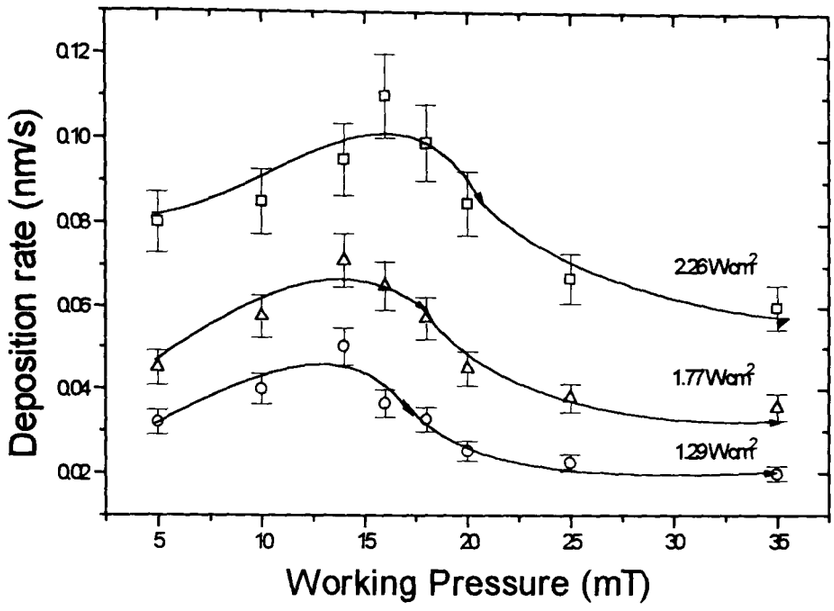

Figure 6.5 : Deposition rate of nickel oxide films as a function of the sputtering pressure at different working powers, and at an oxygen content of 9 %. Standard error on working pressure : ± 10 %.

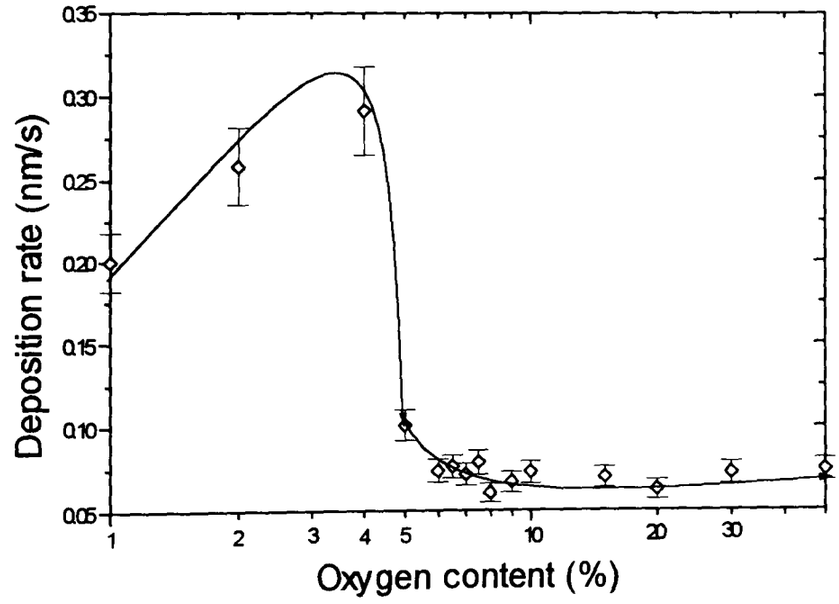

Figure 6.6 : Deposition rate of nickel oxide films as a function of the oxygen content in the sputtering chamber at 1.77 W/cm² and a total working pressure of 15 mT.
Standard error on oxygen content : ± 15 % of content value.

It can either be obtained through the electrodissolution of nickel in an alkaline electrolyte which is closely related to corrosion mechanisms or through the cathodization of a conducting substrate. A third procedure consists of the chemical precipitation of the hydroxide on the surface of any inert conductive material. The precipitation of $Ni(OH)_2$ offers an interesting way of obtaining the reversible $Ni(OH)_2$/NiOOH electrode when the system is properly polarised. Previous work[20] showed that nickel oxide anodically deposited was very sensitive to the solution concentration, deposition time and sample cleanness. The optimum electroplating solution contained 6.3 ml of ammonium hydroxide (1.43 M), 1.642 g of nickel sulphate and 100 ml of stabilising agent (polyoxyethylene sorbitan monorolaurate) in 133.7 ml of distilled water. Prior to deposition, samples were ultrasonically washed in 7 % diluted Decon 90 then rinsed in distilled water. Platinum and saturated calomel electrodes were used as the counter and reference electrodes respectively. Deposition potentials were -250 mV to +1100 mV at a scan rate of 20 mV/s. Anodically-deposited films are about 200 nm thick for 1 hour deposition time. A scanning potentiostat EG&G was used to control deposition of anodic coatings.

Thin films of nickel hydroxide were also deposited in this thesis using the electrodeposition technique developed in previous work. The deposition process was repeated and films plated onto ITO with different sheet resistivities (14, 35 or 90 Ω/□). Due to the high conductivity of the ITO coated glass used in the present work (14 Ω/□) compared to the ITO substrate used in previous work (90 Ω/□), electrochemical potentials had to be studied and optimised in order to improve the deposition and limit the degradation of films produced.

6.4 Optimisation of sputtered and anodic nickel oxide for protonic intercalation/deintercalation

6.4.1 Sputtered films

After deposition, each film was cycled in an electrochemical cell using the equipment described in Chapter 4. The nickel oxide film or working electrode was placed opposite

the counter electrode which consisted of a 5 x 5 cm^2 grid of titanium wires coated with platinum. A saturated calomel reference electrode was placed close to the working electrode. The films were cycled 20 times between (- 0.6 V/ + 0.6 V), at a scan rate of 20 mV/s, and in a 1M KOH solution at room temperature. The films were rinsed and dried with a nitrogen gun and then optically measured. Films were coloured and bleached for 2 minutes at + 0.6 V and - 0.6 V respectively.

6.4.1.1 Nickel oxide films prepared at different power densities and sputtering pressures

The colour of the as-deposited films is dark-brown/grey. After 20 colouring and bleaching cycles, films were coloured and bleached reversibly. For each set of data (in the two following figures) a best regression polynomial was fitted to guide the eye, and to make the graphs clearer (actual data points are not shown).

Figure 6.7 gives the difference of solar transmittance in the bleached and coloured states as a function of power density at different working pressures and for a constant oxygen content and a constant duration. All samples were black in appearance in the coloured state and transparent/grey in the bleached state. Films deposited at power densities higher than 2.0 W/cm^2 would not bleach easily but would become totally dark in the extracted state. On the contrary, films deposited at power densities lower than 1.5 W/cm^2 would not colour easily but would bleach almost totally.

Figure 6.7 also shows that films deposited at pressures lower than 14 mT and films deposited at pressures higher than 16 mT would not reach a good bleached and/or coloured state. A maximum difference is obtained between $T_{s,b}$ and $T_{s,c}$ for films sputtered at 1.77 W/cm^2 power and at 14/16 mT working pressures. The visible transmittance of such film was 0.71 in the bleached state and 0.04 in the coloured. Optical spectra can be seen in section 6.5.3.

Figure 6.8 shows the coloration efficiency of the nickel oxide films over the solar range as a function of the working pressure. Maximum η_c decreases for pressures higher than 18 mT and for pressures lower than 14 mT as well as for power higher and lower than 1.77 W/cm^2. A maximum of 0.036 cm^2/mC is obtained for 200 μm thick nickel oxide film sputtered at 1.77 W/cm^2 power and at 16 mT working pressure. About 20 mC/cm^2 of protonic charge can be reversibly inserted from these films.

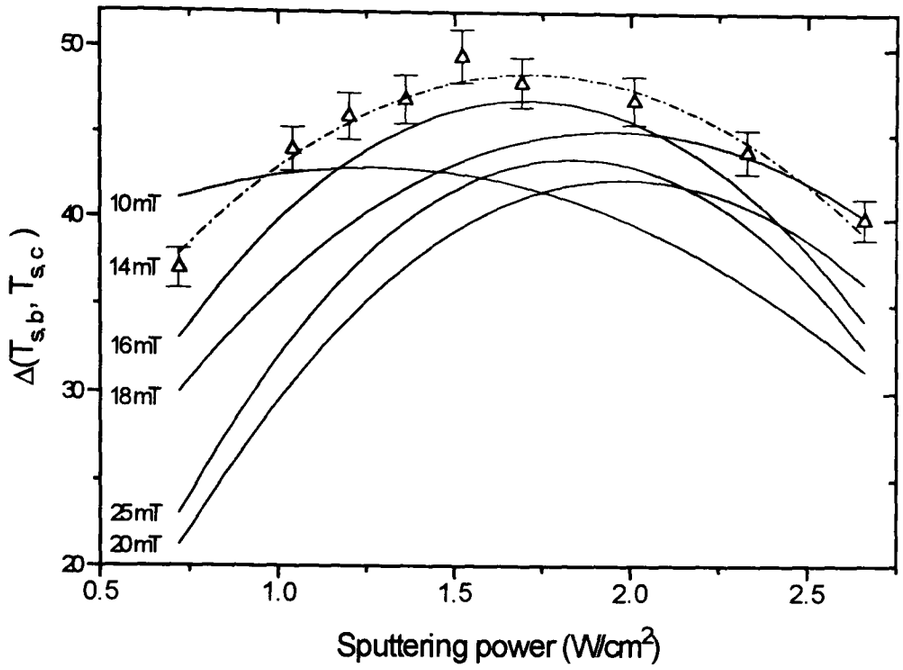

Figure 6.7 : The difference of solar transmittance in the bleached ($T_{s.b}$)and coloured($T_{s,c}$) states as a function of sputtering power at different working pressures, 9 % oxygen content, and 60 mn duration.
Standard error on sputtering power : ± 10 %.

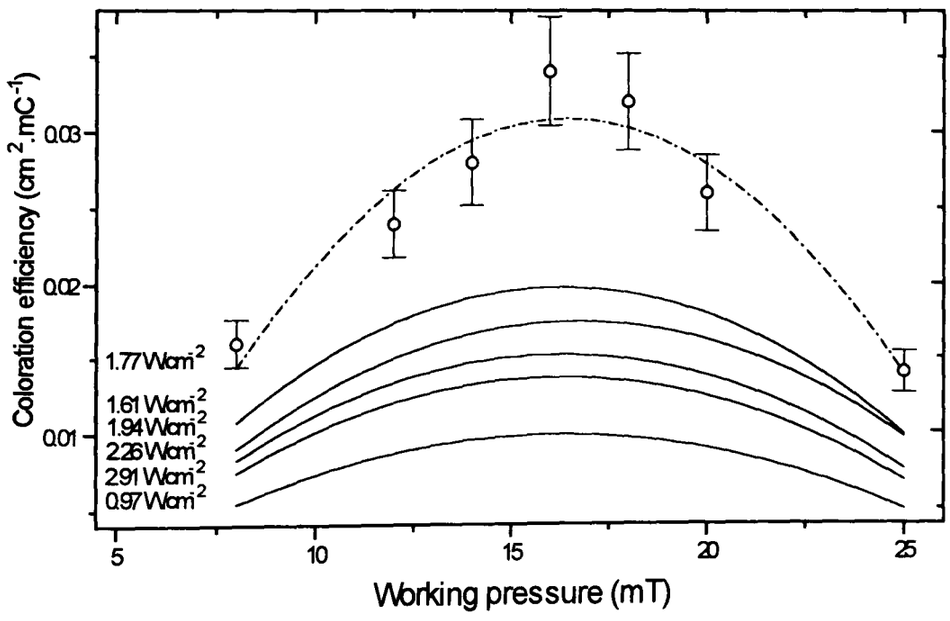

Figure 6.8 : Coloration efficiency over the solar range of nickel oxide films as a function of working pressure at different sputtering powers, 9 % oxygen content, and 60 mn duration.
Standard error on working pressure : ± 10 %.

These figures show that optimum η_c and highest difference between $T_{s,b}$ and $T_{s,c}$ are obtained at a sputtering power of about 1.77 W/cm^2 and a working pressure of about 16 mT.

6.4.1.2 Nickel oxide films prepared at different oxygen contents and temperatures

The oxygen content has been investigated for two different conditions : first when the sample carrier is cooled down to less than 10°C prior to deposition, and when it is left at the temperature of the instrument which is about 17°C. The sample carrier is a very heavy metallic carousel which acts as a heat sink during deposition. When the carrier was cooled down, the substrate temperature was about 150 °C, instead of 200 °C.

Figure 6.9 shows the variation of the coloration efficiency of nickel oxide films over the solar range as a function of the oxygen content in the chamber. These results show that the bleaching and colouring response of films improves when films are sputtered on a cooled substrate. η_c is increased by about 40 % when films are deposited onto a cooler substrate.

Nickel oxide films formed on a cooler substrate would have a more amorphous structure compared to films deposited onto a warmer substrate which would exhibit a more crystalline or polycrystalline structure. XRD patterns do not show any noticeable difference in structure and films seem to be amorphous. Furthermore, SEM pictures show that nickel oxide films possess a nanocrystalline structure (see section 6.5.1). The effect of substrate heating has been reported by Tolstikhina[26] with films made by CVD. They noticed that nickel oxide density increased with substrate temperature, creating a strong absorption across the luminous region.

Figure 6.9 also shows a peak in coloration efficiency for films deposited at oxygen content of about 7 - 8 %. At percentages higher than 12 %, η_c remains unaffected by the quantity of oxygen introduced into the chamber. The optimum result obtained gives a $T_{v,b}$ of 0.71 and a $T_{v,c}$ 0.04 for a total quantity of charge of 14 mC/cm^2. The visible η_c is equal to about 0.09 cm^2/mC which is higher than in previously published papers on R.F. magnetron sputtered nickel oxide films[27,28].

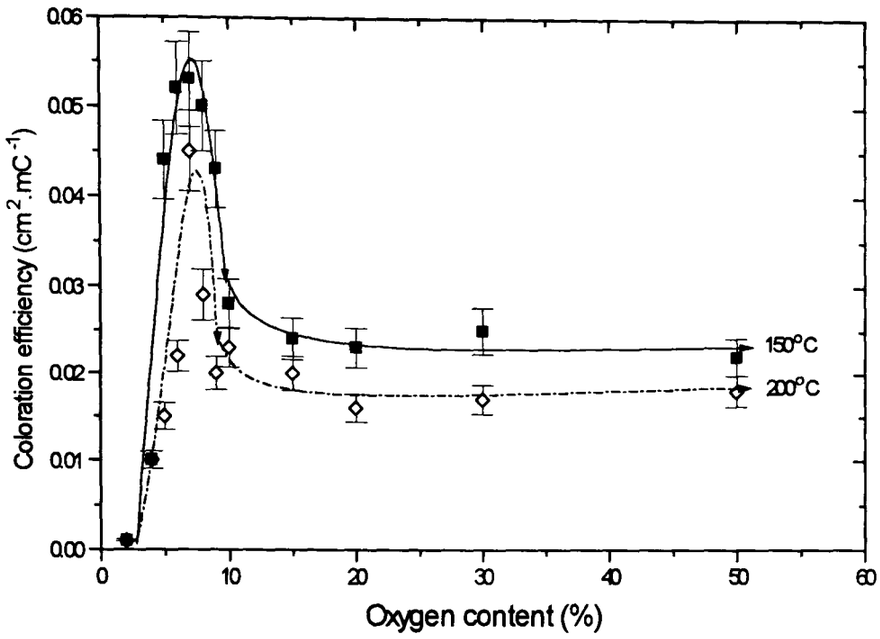

Figure 6.9 : Coloration efficiency of nickel oxide films as a function of oxygen content at different substrate temperatures, at 1.77 W/cm² power, 16 mT pressure and 60 mn duration. Standard error on oxygen content : ± 15 % of content value.

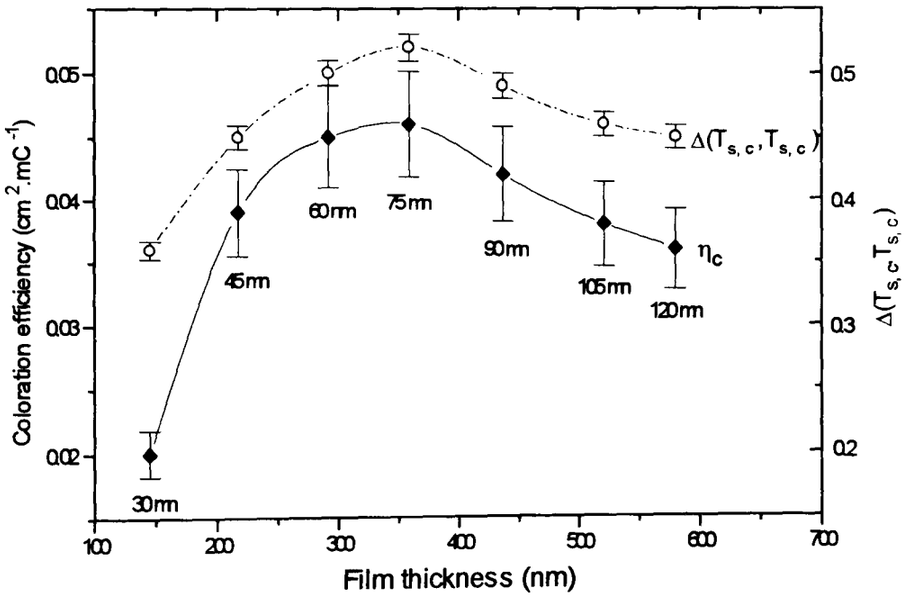

Figure 6.10 : Coloration efficiency of nickel oxide films in the solar range and difference of solar transmittance in the bleached state ($T_{s,b}$) and coloured state ($T_{s,c}$), as a function of film thickness, at 1.77 W/cm² power, 16 mT pressure, uncooled substrate and 7.5 % oxygen content. The corresponding sputtering time has been added. Standard error on thickness : ± 10 nm.

6.4.1.3 Nickel oxide films prepared at different sputtering times

Figure 6.10 shows the variation of coloration efficiency and the difference of transmittance in the bleached state and coloured state of films in the solar range as a function of film thickness. The substrate was uncooled. An optimum η_c is obtained at thicknesses in the range 300-350 nm. This is due to the fact that thin films can be totally bleached, but cannot reach an optimum coloration, and very thick films become very dark in the coloured state but cannot reach a fully bleached state. There is a compromise film thickness at which the coloured and the bleached states of sputtered nickel oxide films are acceptable.

For the sputtering conditions used in Figure 6.10, the optimum sputtering time was chosen to be 60 minutes. The deposition rate at the above sputtering conditions is 0.08 nm/s.

6.4.1.4 Summary of optimum nickel oxide sputtering parameters

The electrochromic properties of nickel oxide films seemed to be strongly influenced by the deposition process parameters. The optimum sputtering conditions are similar to the conditions obtained in previous work[18] of the laboratory as well as work published elsewhere[28].

However, optical properties in transmittance of NiO_x films have been significantly improved. The solar transmittance of R.F. diode[18] sputtered nickel oxide in the coloured state was not less than 0.3, whereas R.F. magnetron sputtered films showed a decrease to 0.1 (see section 6.5.3). Nevertheless, the nanocrystalline structure is shown to be very similar for films made by both diode and magnetron sputtering (see section 6.5.1).

Nickel oxide films formed by R.F. magnetron sputtering from a metallic nickel target in argon-oxygen atmospheres show good electrochromic properties when produced at low power densities (1.77 W/cm^2) and medium pressure (16 mT). Optimum electrochromic nickel oxide seems to be deposited at low oxygen content (7 %) onto a cooled substrate. These deposition process parameters are summarised in Table 6.2.

When sputtered onto a cold substrate, electrochromic properties of nickel oxide are significantly improved. However, voltammograms are seen to be slightly less reversible than when sputtered onto warm substrates.

Target material	Ni (99.9% pure)
Target size (cm^2)	10.2 x 30.5 (4"x12")
Power density range (W/cm^2)	1.5-2.0 (13.56 MHz)
Sputtering pressure range (mT)	15-17
Oxygen concentration range (%)	6-8
Substrate temperature	~ 150°C
Thickness range (nm)	300-400

Table 6.2 : Summary of R. F. magnetron sputtering process parameters used to deposit optimised electrochromic nickel oxide films.

One possible reason can be that films deposited onto a cold substrate exhibit a more amorphous structure, therefore, more charge can be inserted but also more charge can be trapped into the lattice (see section 6.5). Further investigations are required to identity the reasons of this irreversibility.

6.4.2 Anodically deposited nickel oxide films

6.4.2.1 General remarks

A few comments should be added to the previous investigation[29]; firstly, good film adhesion was only achieved with films freshly cleaned, and secondly the addition of a stabilising agent into the film deposition solution was seen to improve the electrochromic and mechanical properties of films only if the agent is not oxidised. Polyoxyethylene sorbitan monorolaurate is a detergent which was noticed to degrade very quickly when exposed to air. This degradation altered the stabilising properties of the detergent, producing nickel oxide with very poor electrochromic and mechanical properties.

Good anodically deposited nickel oxide produced in our previous study[20] shows repeatable optical and electrochemical properties when investigated a year later[29]. Owing to the quantity of water contained in anodic nickel hydroxide, it was noticed that films have lost water when exposed to air over a long period of time causing structural cracks. Figure 6.11 shows two micrograph pictures, one of a cracked nickel hydroxide film produced by McMeeking et al.[20] and one of a nickel hydroxide film freshly made. This loss of water can be seen in the microstructure of the aged film with a reduction in size of its interconnecting cylindrical rods and a more compact appearance of its surface morphology. Aged films showed nevertheless good electrochromic properties. This effect associated with water has to be considered when producing large area windows. It could lead to premature degradation as well as altering the uniformity of coloration. Problems could also occur if assembling devices require dried surfaces.

The deposition procedure of anodic nickel hydroxide was re-used in this study and produced films with similar optical properties and charge capacity. This preparation technique has been described to be an efficient and simple method of nickel hydroxide film formation.

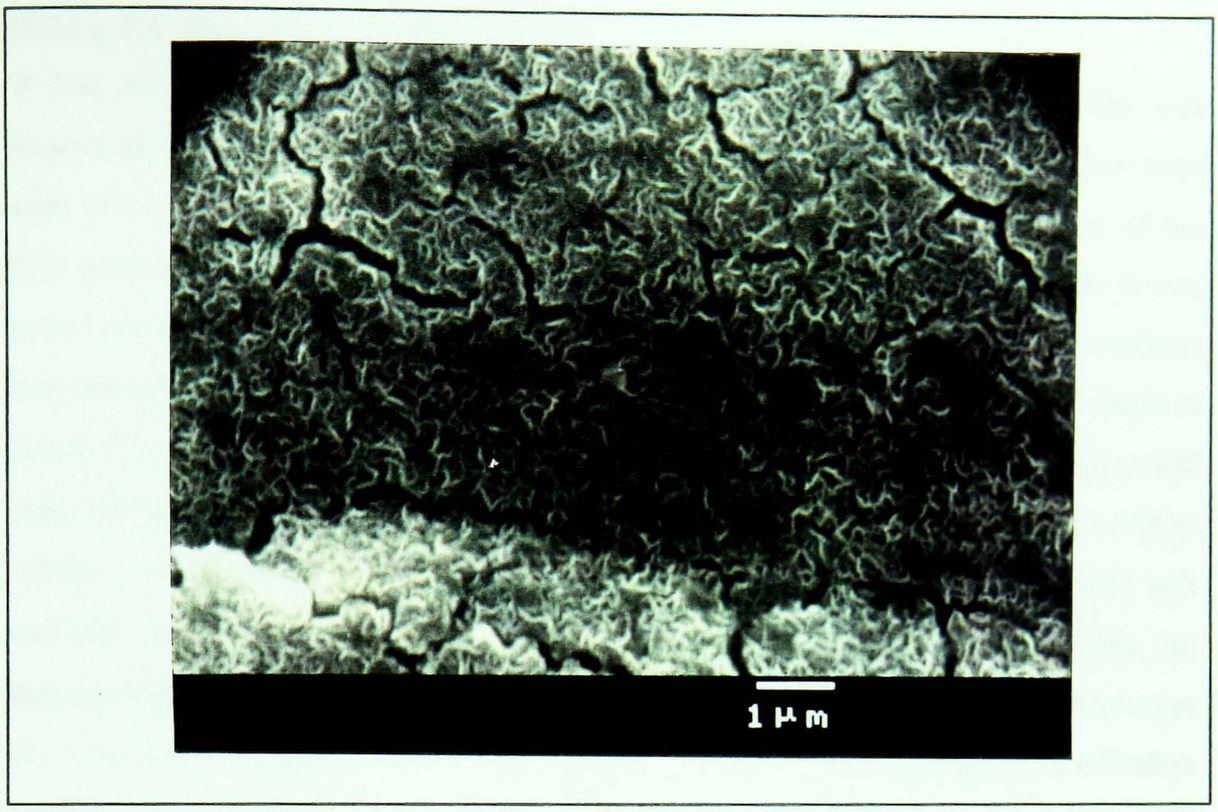

(a)

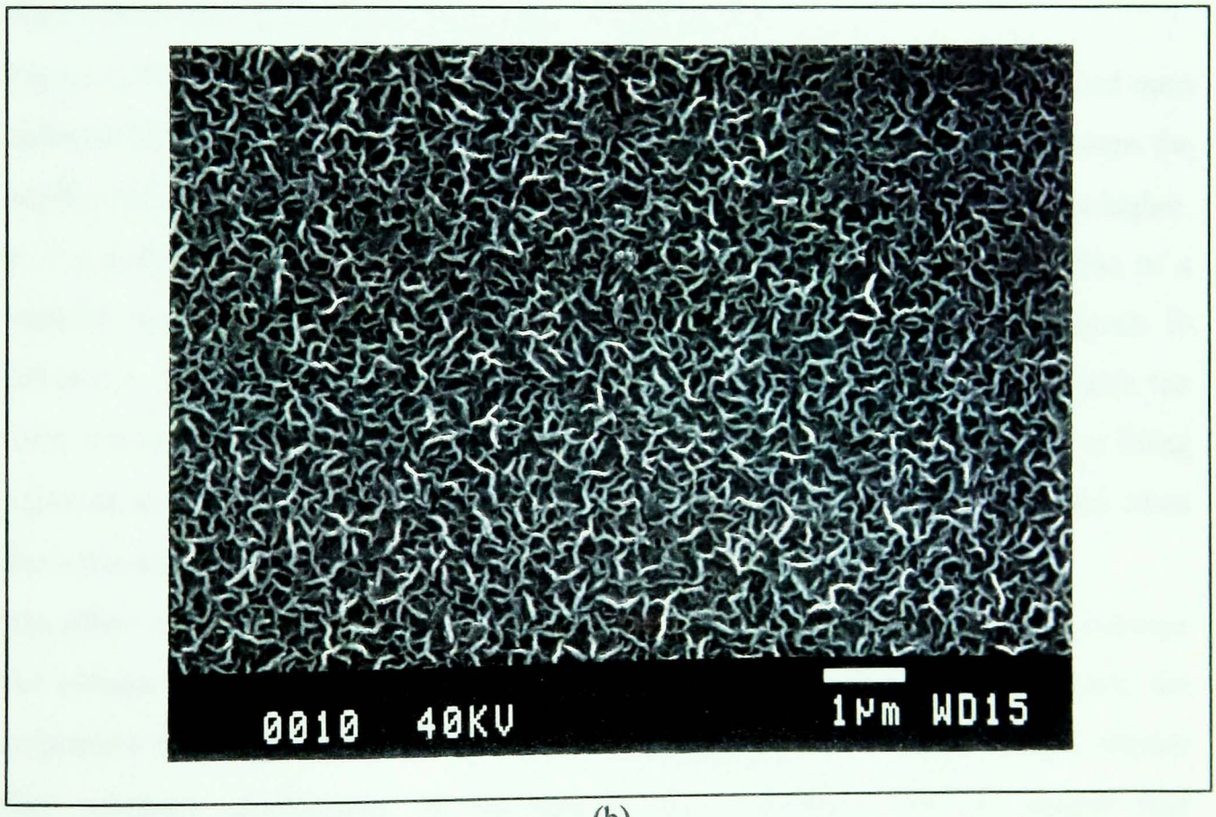

(b)

Figure 6.11 : Secondary electron micrographs of an aged anodic deposited nickel hydroxide film (a) and of a freshly anodically deposited nickel hydroxide film (b). Resolution x10 000.

6.4.2.2 The effect of substrate resistivity

It was also observed that the irreversible degradation of nickel hydroxide film was dependent upon the applied potentials. The real potential applied onto films has been seen to be a crucial parameter and consequently related to the sheet resistivity of the ITO substrate and the electrolyte concentration. Firstly, cyclic voltammetry was shown to be a very useful technique to determine the potentials of the electrochemical reactions that can occur at the working electrode. It allowed us to determine the potential limits in which the electrochromic film should be studied. Anodic nickel oxide was deposited onto substrates with different sheet resistivities. The electrochromic response of films showed a dependence on the conductivity of the substrate. Anodic films are very soft and high driving voltages will force ionic insertion (bleaching process) into layers. No degradation is observed if the force is within the mechanical strength of films. However like a membrane, anodic nickel oxide will crack, and films will eventually peel off when potentials are too high. Table 6.3 reports the safe potential limits used for nickel oxide films coated onto ITO with different sheet resistivities.

Figure 6.12 shows the voltammograms of two anodic nickel oxide films deposited onto different ITO coated glass. The principal effect observed is the separation between the anodic and cathodic peaks. The separation is greater when the sheet resistivity is higher. It is not due to an irreversibility of the electrochemical process, but simply due to a reduced speed of the electrochromic response[30]. Similar observation is given in Table 6.4, where solar transmittance of the nickel hydroxide layer corrected with the solar transmittance of the ITO substrate in the bleached and coloured states is being reported for fixed process parameters. The transmittance modulation is reduced when the substrate resistance is increased.

The effect of increasing the substrate resistance will be to increase the time and increase the voltage required for the ionic insertion/extraction process. As a consequence, the coloration and bleaching uniformity of films in large area window devices might require high substrate conductivity. In the case of high resistance, one can expect that electrochromic coating close to the electrical contact on the window will colour or bleach faster than material at larger distances from the edge.

ITO Substrate	Deposition potentials (mV)	Safe colouring potentials (mV)	Safe bleaching potentials (mV)
ITO 14 Ω/□	-250/+1100	+ 700	- 50
ITO 35 Ω/□	-250/+1100	+ 700	- 200
ITO 90 Ω/□	-500/+1500	+ 750	- 500

Table 6.3 : Optimised potentials used for deposition, colouring and bleaching of anodic nickel oxide films deposited onto ITO with different sheet resistivities.

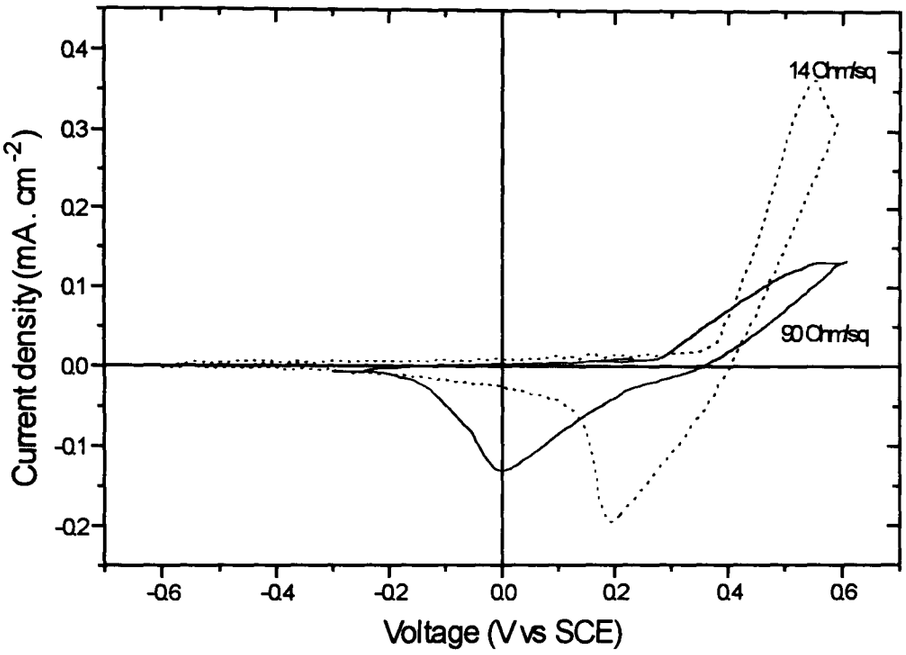

Figure 6.12 : Cyclic voltammograms of anodic nickel oxide films coated on ITO substrates with different sheet resistivites (14 Ω/□ and 90 Ω/□), in 0.1M KOH, at 20 mV/s scan rate.

Anodic nickel oxide on ITO	Solar Transmittance of nickel hydroxide layer without the effect of the ITO substrate in the bleached / coloured states +0.7 V / - 0.3 V	Difference in solar transmittance between the coloured and bleached states	Colouring and bleaching duration
ITO 14 Ω/□ $T_{s,ITO} = 0.75$	0.95 / 0.21	0.74	< 2 mn
ITO 35 Ω/□ $T_{s,ITO} = 0.80$	0.95 / 0.25	0.69	~ 2 mn

Table 6.4 : Solar transmittance of the bleached and coloured states of anodic nickel oxide films corrected with the solar transmittance of the ITO coated glass substrate using the following equation: $T_{s,ITO} \times T_{s,NiO} = T_{s,measured}$. Solar transmittance presented for ITO substrates with 2 different sheet resistivities.

6.5 Comparison of the electrochromic properties of sputtered nickel oxide and anodically deposited nickel oxide films

Optical and electrochemical performances of both anodic and R.F. magnetron sputtered films are presented and compared in this section. Reference to previous work on R.F. diode sputtered films is also mentioned in this part of the chapter.

6.5.1 Film composition and microstructure

Anodically-deposited films with a thickness of 200 nm were bleached in appearance in the as-deposited state compared to the grey/black appearance of the sputtered films with a thickness of about 300 nm. The surface morphology was studied by electron microscopy and representative micrographs of the two types of film are shown in Figures 6.13 and 6.14. Electrodeposited films are extremely brittle; film thickness is measured by removing enough coating from the ITO substrate with a knife to produce a step. Physically-deposited films are extremely robust and cannot be easily scratched. The SEM micrographs show this structure. Electrodeposited film in Figure 6.14 is more open and porous than the sputtered film in Figure 6.13. The surface structure consists of an open and porous structure consisting of randomly distributed interconnecting ligands. The size of these ligands is of the order of half a micron. Submicron-sized cavities can be observed which enable the ionic diffusion to take place, and also to enhance the fundamental absorption process by multiple reflection within the cavities to take place in the dark state. This type of structure would facilitate the diffusion of OH^- ions into the layer. A similar type of microstructural growth has been reported on electrodeposited cobalt oxide by the laboratory[31]. This differs significantly with the sputtered film, which exhibits a very compact and granular structure. Figure 6.15 shows a high magnification of an sputtered nickel oxide film[32]. The average grain structure is about 5-10 nm and most nickel oxide grains have a lattice image with a preferential orientation of (111) crystal planes. SEM micrographs show also a very similar structure in both cycled and as-deposited films.

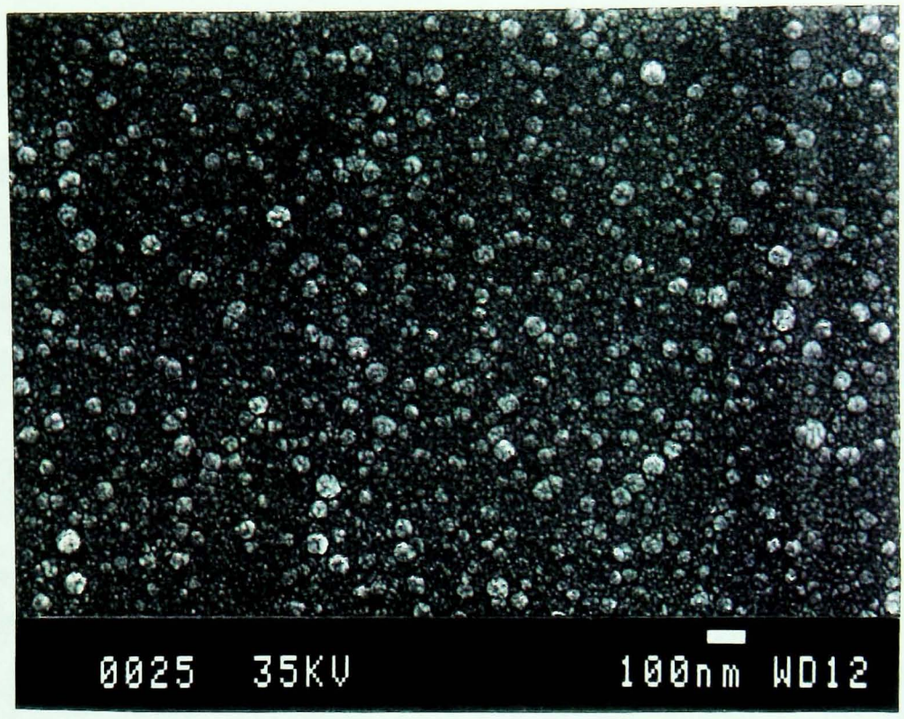

Figure 6.13 : SEM micrograph of an R.F. magnetron sputtered nickel oxide film. Magnification x 50000.

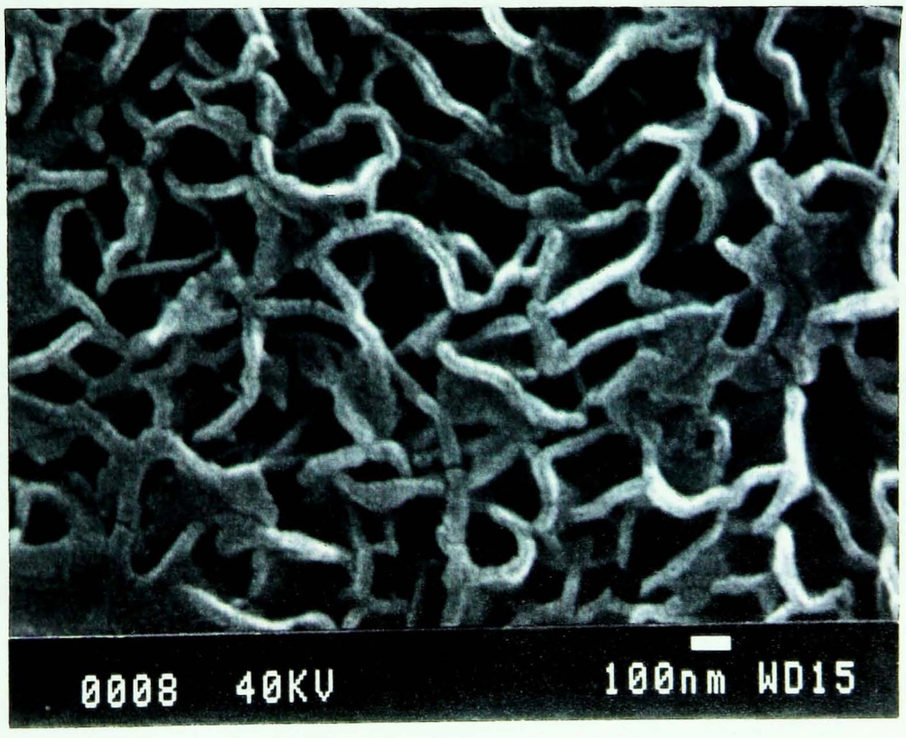

Figure 6.14 : SEM micrograph of an anodically-deposited nickel oxide film. Magnification x 50000.

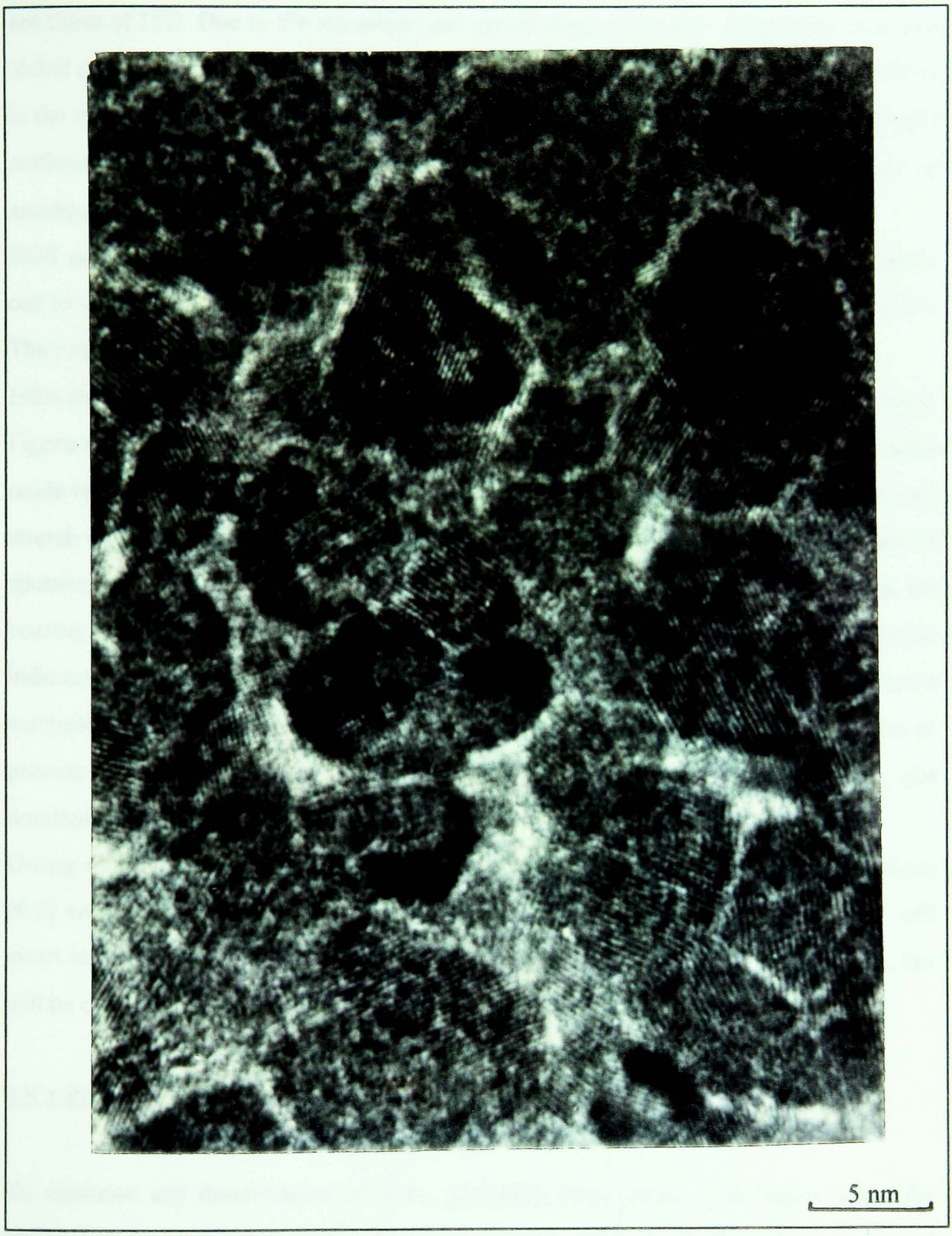

Figure 6.15 : HREM micrograph of an R.F. diode sputtered nickel oxide film[32].

Analysis of these coatings was studied by X-ray diffraction. The XRD pattern of the as-deposited sputtered nickel oxide films is shown in figure 6.16. The only peaks detected are those of ITO. Due to the nanostructural morphology of the R.F. magnetron sputtered nickel oxide films seen with the SEM pictures, it seems difficult to detect any crystallinity in the material. This can only indicate that sputtered nickel oxide films consist of crystals sufficiently small enough to not diffract a standard powered XRD beam. In the case of anodically deposited films, the XRD pattern shows an amorphous structure[33].

EDS analysis of as-deposited R.F. magnetron sputtered nickel oxide films was carried out to determine their composition. The nickel to oxygen ratio is shown to be about 2:3. The colour of this film is consistent with the colour of Ni_2O_3 and published work[26,34].

Infra-red spectroscopy also showed the presence of an OH^- stretch in the bleached state. Figure 6.17 and Figure 6.18 show the infra-red spectra of anodic and sputtered nickel oxide respectively, in their coloured and bleached states. The appearance of an hydroxyl stretch was evident for anodic films but required about 5 switching cycles in the case of sputtered films. In both films, the coloured state shows the presence of water within the coating. Infra-red spectra analysis of the bleached state of anodic nickel oxide seems to indicate the presence of nickel hydroxide[35] which therefore supports the fundamental mechanism of anodic nickel oxide reaction described in equation [6.1]. Two types of process mechanism are present in electrochromic sputtered nickel oxide films, one dominating the other.

Owing to the presence of water in the electrolyte, the reaction described in Equations [6.2] and [6.3] is still the most probable. After repetitive switching cycles, water will insert into the lattice and the reaction described in [6.2] will probably still dominate, but will be combined with the reaction described in Equation [6.1].

6.5.2 Electrochemical properties

To minimise any deterioration of films, potentials were chosen just below those for oxygen and hydrogen evolution in the cycling process. Voltammograms of an anodic and sputtered nickel oxide films are shown in Figures 6.19 and 6.20 respectively.

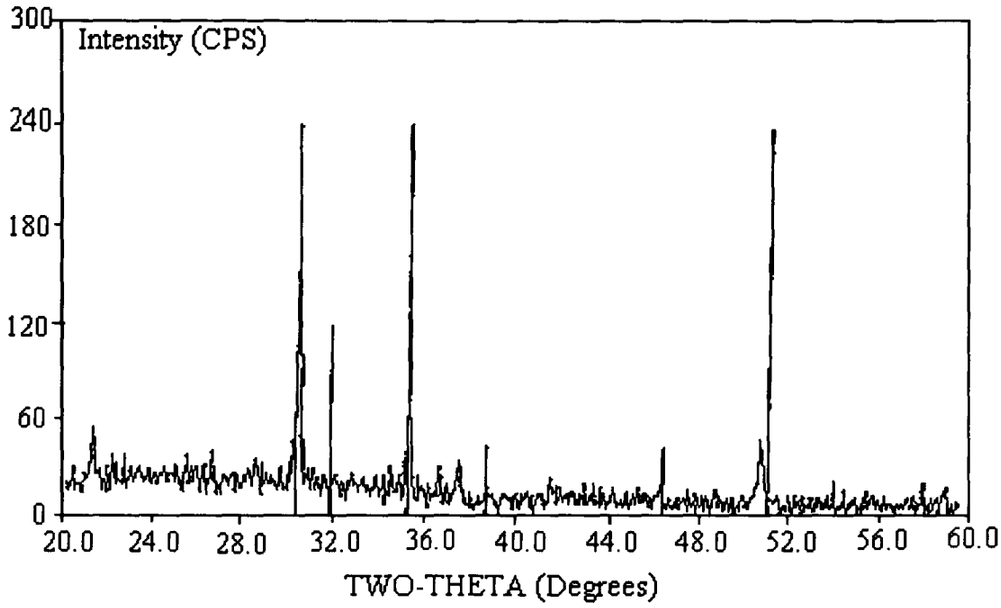

Figure 6.16 : XRD of an as-deposite R.F. magnetron sputtered nickel oxide film on ITO coated glass.

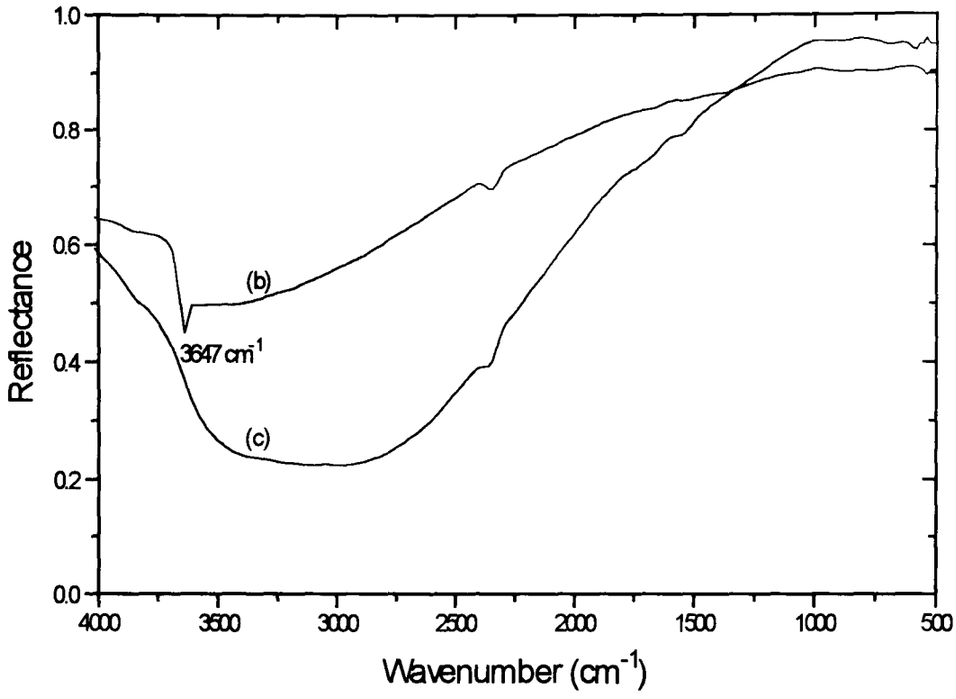

Figure 6.17 : Infra-red reflectance of the bleached (b) and coloured (c) states of an anodically deposited nickel oxide film.

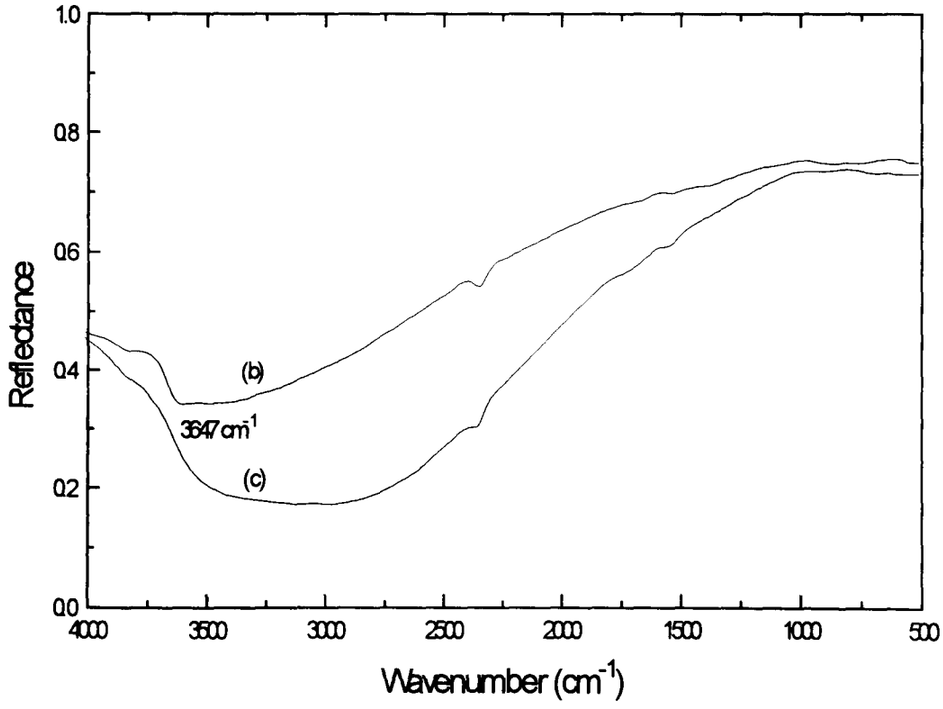

Figure 6.18 : Infra-red reflectance of the bleached (b) and coloured (c) states of a sputtered nickel oxide film.

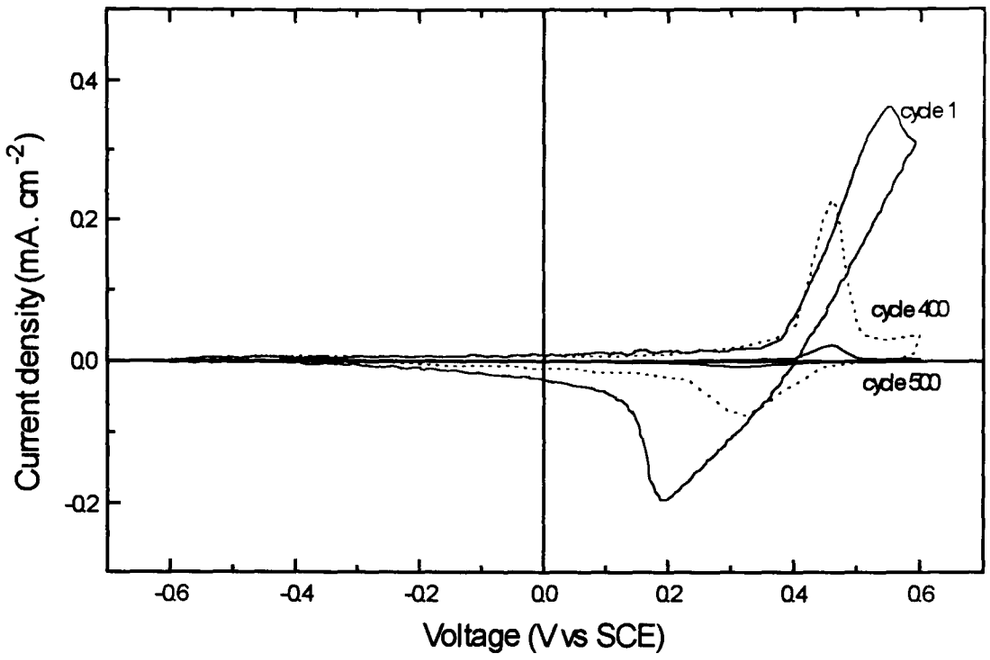

Figure 6.19 : Cyclic voltammograms of an anodic nickel oxide film initially, after 300 cycles in 0.1 M KOH, at 10 mV/s scan rate.

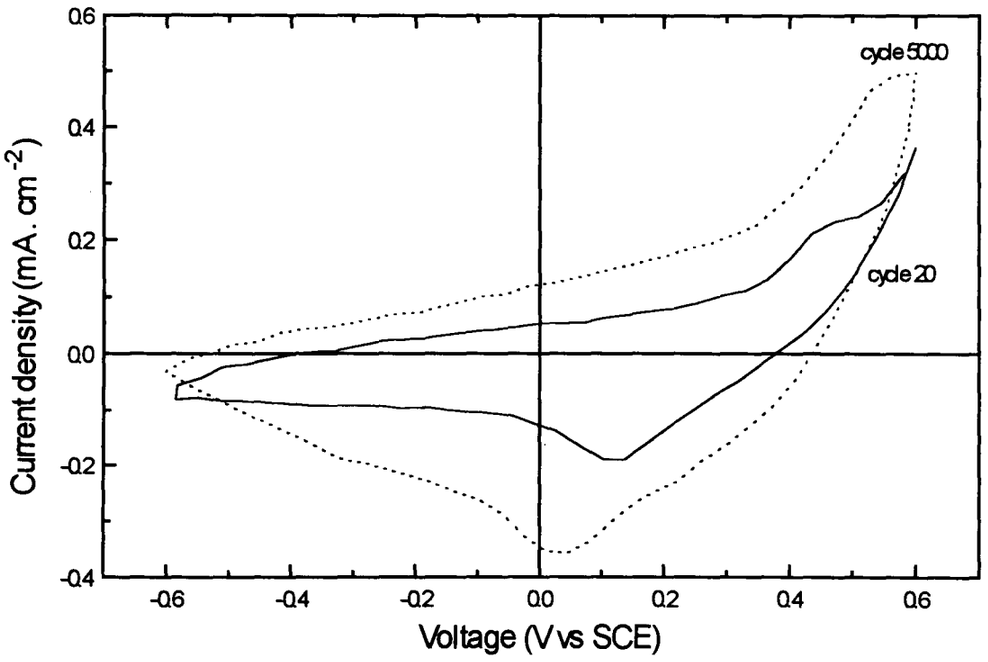

Figure 6.20 : Cyclic voltammograms of a sputtered nickel oxide film after 20 and 5000 cycles in 1 M KOH, at 10 mV/s scan rate.

They both show similar voltammetric behaviour: first, an anodic peak (positive current) is positioned at about 0.4 - 0.5 V associated with the diffusion limited reaction and the coloration process; then the onset of a second peak potentials at + 0.6 V, associated with oxygen evolution from the solvent but with little or no contribution to the coloration process. The onset of this last peak can increase during repetitive cycling. Finally, a cathodic peak (negative current) is seen at about 0.1 - 0.2 V on the reverse scan associated with the bleaching process.

Over different switching cycles, the anodic and cathodic peaks of the sputtered nickel oxide increased in size. There is almost no clear peak but broad peaks on the first scan. After ageing, peaks increased rapidly in the first 50 switching cycles then slightly grew in size for at least 1000 switching cycles. Then the cyclic voltammogram remained almost stable up to 5000 cycles, following which it started to decrease. The development of redox peaks is consistent with the gradual transformation of anhydrous nickel oxide to the hydrated phases $Ni(OH)_2$ and NiOOH, which explains the progressive appearance after repetitive cycling of an O-H stretch at 3647 cm^{-1} (see section 6.5.1).

On the contrary, electrodeposited nickel oxide films showed an opposite feature. Redox peaks were apparent on the first scan, but started to decrease in size after about 50 to 100 switching cycles. No films have been switched more than 500 times, above which they reached a state of complete degradation. The nature of the dominant process based on large cations such as OH^- ions might also be responsible for the degradation of the anodic films. Andersson's work[36] described results on the mechanical stress of nickel oxide films upon the insertion of charge into its lattice. A compressive stress was noticed during ionic intercalation which was then released upon ionic deintercalation. This could be one reason for the degradation of anodic films which possess a soft structure. Another reason might be the etching of the film surface occuring during the insertion and extraction process. These possible reasons would explain why films peel off the substrate surface over repetitive switching cycles.

Electrodeposited nickel hydroxide films showed a switching time of less than 20 seconds, whereas sputtered films required a minimum of 90 seconds between the two states. This is again due to the more open and porous microstructure of anodic films compared to the more compact structure of sputtered films.

The charge associated with these voltammograms was of the order of 35 mC/cm^2 for sputtered films. A charge imbalance of about 10 % was observed to be left in the film after the deintercalation process. This was maybe due to a side effect onto the film surface but more probably to an irreversible insertion charge into the film lattice. This can be seen with the optical properties. The charge capacity increased up to 49 mC/cm^2 over the 5000 scans. In the case of anodic films, the amount of charge involved at the beginning was 18 mC/cm^2. Due to the degradation process, it then decreased down to 5 mC/cm^2 on the 500 scans.

For both films, anodic and cathodic peaks moved and became broader over switching cycles. An anodic broad peak is seen for anodically-deposited films at lower voltages and distinct from the oxygen evolution peak after 50 cycles. At the same time the cathodic peak moved to higher voltages. Ageing also moved sputtered deposited anodic peaks to a higher potential, and the cathodic peak was moved to a lower voltage. However, the ageing effect is seen to not be so drastic for sputtered films as is observed for anodic nickel oxide films.

The sputtered films did not suffer the degradation in electrochemical response seen for the anodically deposited films. Degradation was the major deficiency of anodic deposited nickel oxide. This degradation was seen on the surface of films when it started to peel off. Possible reasons are thought to be the extremely porous and fragile microstructure of anodic nickel oxide films, and repetitive insertion/extraction of ions creating mechanical degradation. The number of switching cycles was increased by reducing potential limits, and by reducing the molarity of the electrolytic solution down to 0.1 M KOH.

6.5.3 Optical properties

Solar hemispherical transmittance spectra of sputtered and anodically-deposited nickel oxide films in different states are shown in Figures 6.21 and 6.22 respectively. Solar hemispherical reflectance spectra of sputtered and anodically-deposited nickel oxide films in different states are shown in Figures 6.23 and 6.24 respectively. Figure 6.25 shows the spectral absorptance of the sputtered and anodically-deposited films in their coloured and bleached states.

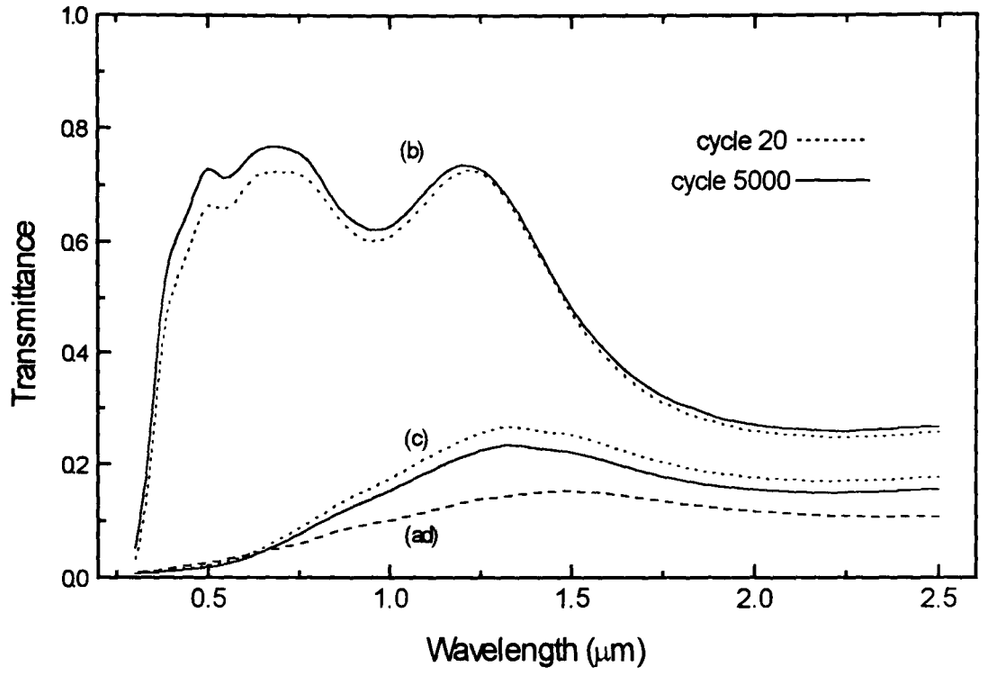

Figure 6.21 : Hemispherical transmittance of a sputtered nickel oxide film in the as-deposited(ad), coloured(c) and bleached(b) states respectively. Spectra shown after 20 and 5000 switching cycles.

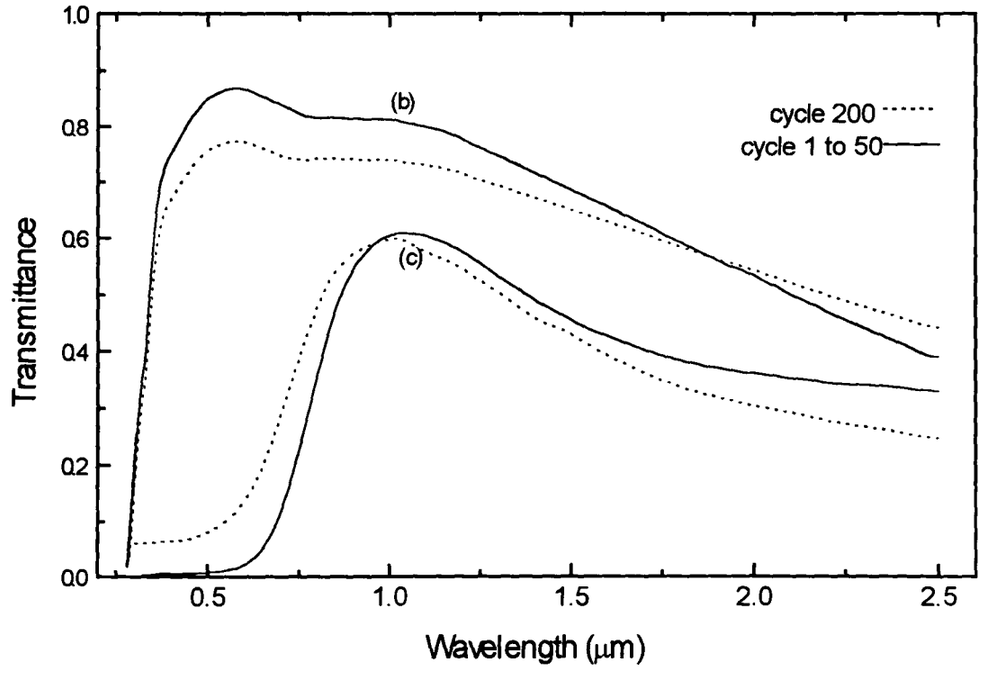

Figure 6.22 : Hemispherical transmittance of an anodic nickel oxide film in the coloured(c) and bleached(b) states respectively. Spectra shown after 1 and 200 switching cycles.

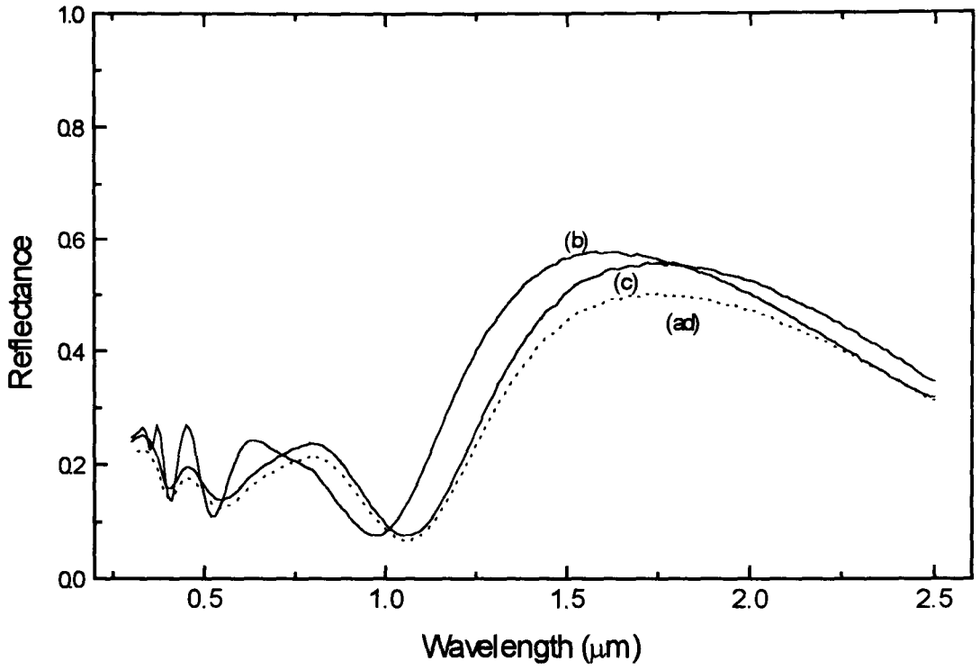

Figure 6.23 : Hemispherical reflectance of a sputtered nickel oxide film in the as-deposited(ad), coloured(c) and bleached(b) states respectively.

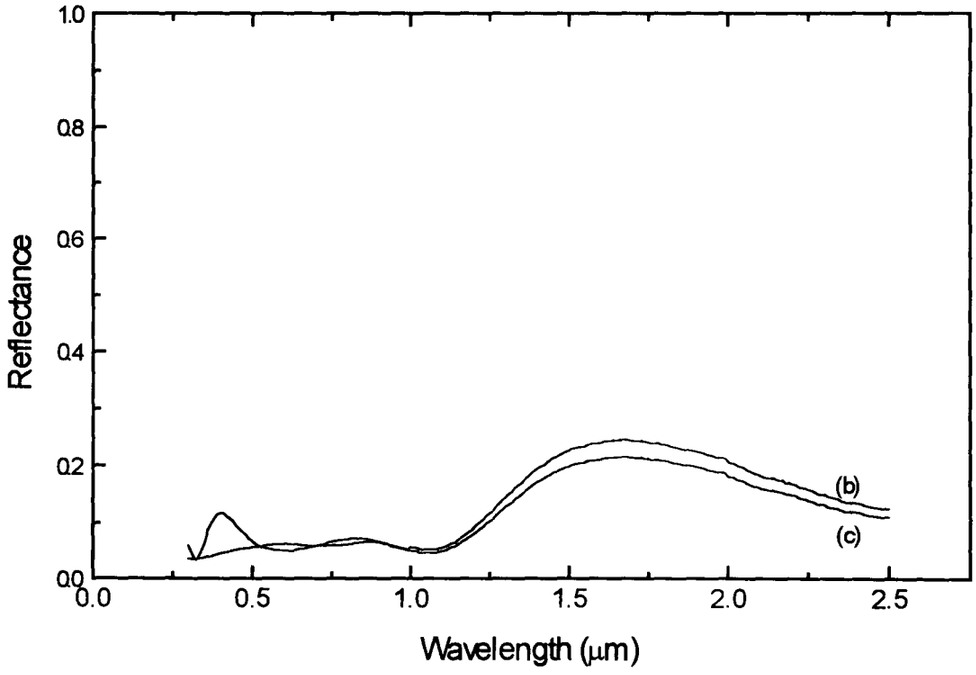

Figure 6.24 : Hemispherical reflectance of an anodic nickel oxide film in the as-deposited(ad), coloured(c) and bleached(b) states respectively.

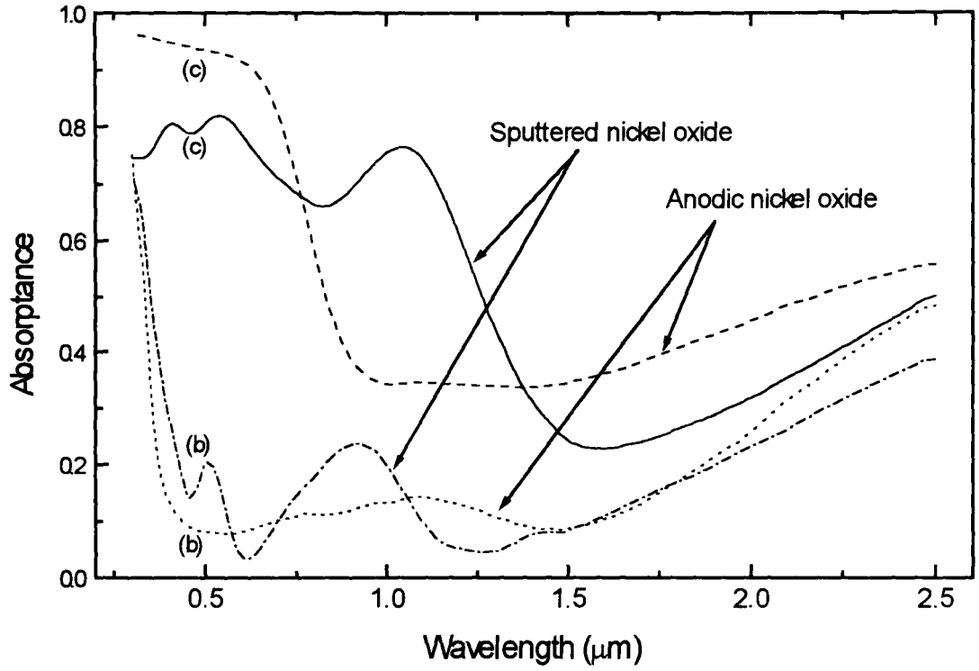

Figure 6.25 : Hemispherical absorptance of an anodic and of a sputtered nickel oxide film in the coloured(c) and bleached (b) states respectively.

Table 6.5 summarises all optimised optical properties of anodic and sputtered nickel oxide films. All the spectra and derived optical properties results include the properties of the ITO substrate.

The sputtered film is black in appearance in its as-deposited and coloured states with a visible transmittance of 3%. In the bleached state, the film has a visible transmittance of 74%. The transmittance modulation of R.F. magnetron sputtered nickel oxide is in the solar range equal to 56 %. This value is an improvement compared to the 40 % modulation obtained in the previous work made on R.F. diode sputtered nickel oxide[18] (see Figure 6.3). The most significant progress was made in the coloured state of sputtered nickel oxide films with a decrease in solar transmittance from 30 % down to 10 % . In both cases, films remain neutral in appearance (bronze/grey).

Anodic nickel oxide film also exhibits good optical properties in transmittance in the coloured state. These have been slightly improved compared to films made in previous studies[33] with a decrease in solar transmittance in the coloured state from 22 % down to 20 %. The chromaticity ordinates of the anodic film are very similar to the chromaticity ordinates of the sputtered film, both exhibiting a bronze black appearance (see Table 6.5).

The absorptance of the sputtered film seen in Figure 6.25 is very broad across the visible region compared to the sharp onset of absorptance in anodic films. The optical properties of this latter film are mainly due to its structural morphology: submicrometric cavities in which multiple reflection of visible light enhanced the fundamental absorption process. The roughness of the anodic film surface makes the reflection of light more diffuse. Table 6.5 shows that the reflectance of the sputtered nickel oxide film is similar to the reflectance of its ITO substrate, whereas the reflectance of the anodic film is lower than the reflectance of the ITO it was coated on.

The near infra-red region is strongly influenced by the ITO substrate, and as different qualities of ITO were used, limited comments can be made. Over the first 50 switching cycles, anodic and sputtered films showed very similar visible transmittance properties. Subsequent cycling of anodic films resulted in a continuous decrease in their visible performance. The electrochromic response can be quantified as a combination of charge capacity and change in spectral absorptance. Figure 6.26 shows the spectral coloration efficiency of the anodic and sputtered films respectively.

	ANODIC FILM		SPUTTERED FILM	
Solar Spectrum	**Transmittance**	**Reflectance**	**Transmittance**	**Reflectance**
ITO substrate	0.75	0.19	0.73	0.21
	cycle 1 / 200	**cycle 1 / 200**	**cycle 20 / 5000**	**cycle 20 / 5000**
As-deposited			0.07	0.22
Coloured	0.20 / 0.34	0.10 / 0.10	0.11/0.10	0.23 / 0.22
Bleached	0.68 / 0.64	0.12 / 0.11	0.63/0.67	0.23 / 0.23

Visible spectrum				
ITO substrate	0.80	0.15	0.81	0.16
	cycle 1 / 200	**cycle 1 / 200**	**cycle 20 / 5000**	**cycle 20 / 5000**
As-deposited			0.03	0.16
Coloured	0.01 / 0.11	0.06 / 0.05	0.04 / 0.03	0.18 / 0.17
Bleached	0.81 / 0.72	0.05 / 0.05	0.71 / 0.74	0.15 / 0.16

Charge capacity	**Cycle 1**	**Cycle 200**	**Cycle 20**	**Cycle 5000**
($mC.cm^{-2}$)	18	10	35	49

η_c	**Solar range cycle 1 / 200**	**Visible range cycle 1 / 200**	**Solar range cycle 20 / 5000**	**Visible range cycle 20 / 5000**
($cm^{-2}.C$)	29 / 27	106 / 81	22 / 18	36 / 28

Chromaticity coordinates	**Coloured state cycle 1 / 200**	**Bleached state cycle 1 / 200**	**Coloured state cycle 20 / 5000**	**Bleached state cycle 20 / 5000**
X (red)	0.40 / 0.38	0.31 / 0.32	0.38 / 0.38	0.32 / 0.32
Y(green)	0.35 / 0.35	0.34 / 0.33	0.36 / 0.36	0.33 / 0.33
Z(blue)	0.25 / 0.27	0.35 / 0.35	0.26 / 0.26	0.35 / 0.35

Table 6.5 : Summary table of solar and visible transmittance and reflectance values, and chromaticity coordinates for both electrodeposited and sputtered nickel oxide films.

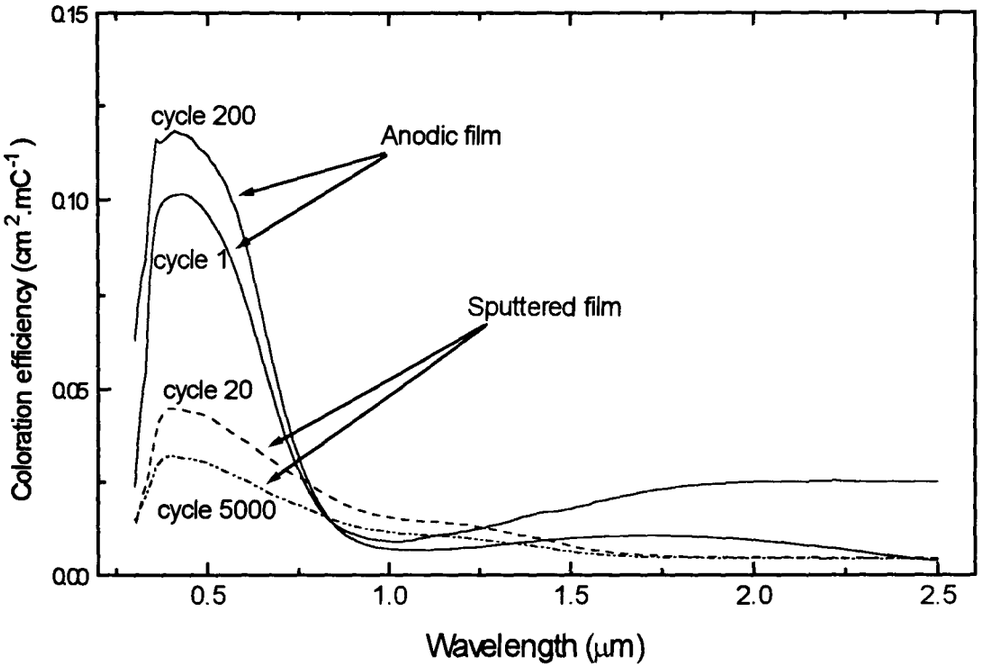

Figure 6.26 : Spectral coloration efficiency of an anodically deposited and of a sputtered nickel oxide film over different switching cycles.

Both films show a peak in coloration efficiency over the visible region of the spectrum, whereas the NIR remains almost equal to zero. The peak for the anodic film is almost 3 times bigger.

Optical properties of sputtered films in the coloured and bleached states remain almost unchanged after 5000 switching cycles. We can notice that the bleached state shows a slight increase in transmittance over ageing as well as a decrease in transmittance in the coloured state. This is also seen in Table 6.5. A decrease in coloration efficiency is noticeable between the cycle 20 and 5000. This is due to the increase of charge capacity of the sputtered nickel oxide film over stable optical properties. This is in sharp contrast to the anodic nickel oxide which shows severe optical deterioration. The onset of this deterioration is already visible after 50 switching cycles. Optical properties showed in Figure 6.22 were measured in the undamaged area of the coating. The increase in coloration efficiency for the anodic film is due to a reduction in the charge capacity created by the material degradation which is peeling off the ITO substrate and also due to the fact that optical properties were measured in the undamaged areas of the sample.

Chromaticity ordinates given in Table 6.5 show that both films are black/bronze in appearance in their coloured state. And that remains the same over the different switching cycles applied to them. The bleached state is seen to be relatively neutral in transmittance, or at least to show the appearance of the ITO underlayer.

Reflectance properties of the two films are seen to remain similar for both coloured and bleached states, and seem to have not been altered over the different switching cycles.

6.6 Electrochromic properties of sputtered nickel oxide for lithium intercalation/deintercalation

Most of the work carried out has concentrated on the proton insertion reaction in aqueous media, and deposition parameters have been investigated to get optimised electrochromic performance as counter electrode material. To avoid problems related to the presence of water, smart window devices are thought to be used with a lithium based

electrolyte. Recent work[37,38] reports on the intercalation of lithium ions into nickel oxide films.

Nickel oxide films were cycled in a lithium perchlorate 1M in propylene carbonate, with a platinum counter electrode and a lithium reference electrode. The scan rate was 10 mV/s and the voltage range 0.5 - 4.5 V.

The first, fifth and tenth cyclic voltammograms are presented in Figure 6.27. On the first cycle, the film shows 3 peaks in the anodic process, at 1.9 V, 2.2 V and 3.4 V, and 3 peaks in the cathodic process at 0.6 V, 0.9 V and 2.5 V. After 5 switching cycles, all the anodic peaks decrease and in particular the peak at 1.9 V comparative to the peak at 2.2 V. In the cathodic reaction, the process is seen in the [0.5 V - 0.8 V] region to change from a normal anticlockwise direction to a clockwise direction. This behaviour is similar to a redox process, indicating the growth of a new phase in the nickel oxide film. When switching cycles are extended (> 10 cycles), the anodic peaks disappear completely and only a broad peak remains. In the cathodic process, peaks at 0.9 V and at 2.5 V remain. It was found[39] that the peak currents of the remaining cathodic and anodic processes are dependent on the scan rate between 20-100 mV/s. The charge capacity passing through the films was initially 45 mC/cm^2 then 21 mC/cm^2 on the fifth and 5 mC/cm^2 on the tenth cycle. At lower scan rates, the amount of charge inserted increased, but resulted in the complete degradation of the active layer.

The visible transmittance was measured over the 5 first cycles and this is shown in Figure 6.28. Visible transmittance properties are clearly seen to become darker after each switching cycle. $T_{v,b}$ is continuously decreasing between 0.62 on the first cycle to 0.30 on the fifth. The coloured state is seen to reach a completely black state after the first cycle; $T_{v,c} < 0.07$. After 10 switching cycles, it was noticed that the adhesion of the coating on the ITO substrate was extremely weak, and the nickel oxide was irreversibly black.

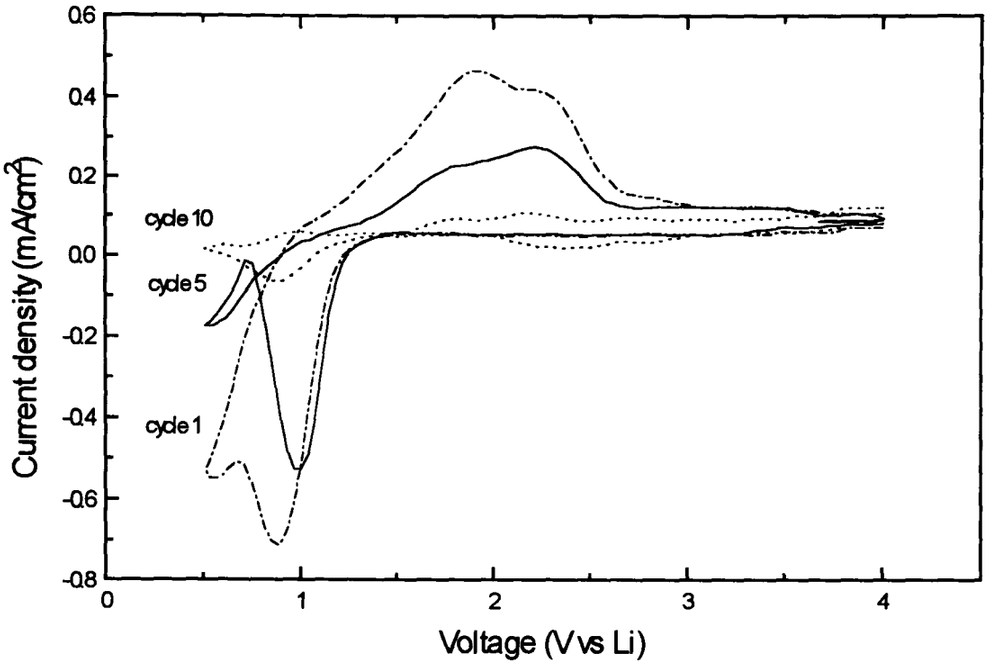

Figure 6. 27 : First, fifth and tenth cyclic voltammograms of a sputtered nickel oxide film in 1 M lithium triflate in PC.

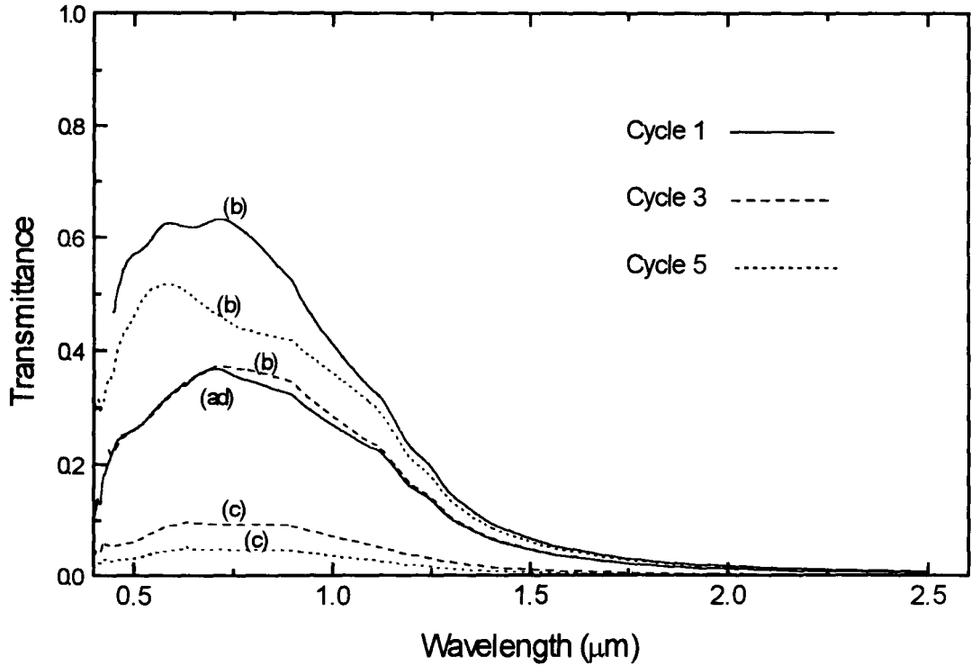

Figure 6.28 : Visible transmittance of a sputtered nickel oxide film in 1M lithium triflate in PC in the as-deposited (ad), coloured (c) and bleached (b) states. Cycle 1: $T_{s,b}$= 0.45, $T_{s,ad}$= 0.25 , $T_{v,b}$= 0.62, $T_{v,ad}$= 0.30;

Cycle 3: $T_{s,b}$= 0.36, $T_{s,c}$= 0.08 , $T_{v,b}$= 0.50, $T_{v,c}$= 0.07;

Cycle 5: $T_{s,b}$= 0.25, $T_{s,c}$= 0.03 , $T_{v,b}$= 0.30, $T_{v,c}$= 0.04.

6.7 The electronic mechanism in sputtered electrochromic nickel oxide

In Chapter 3, the geometric structure based on an octahedron unit was seen to be common to most of the inorganic electrochromic materials. Ions diffuse through channels and between layers, and ionic diffusion will be increased for nonstoichiometric amorphous materials. The only reason for ions to enter the materials is to attract an electron to maintain charge neutrality inside the crystal lattice. In that chapter, it was explained that electronic transitions inside the atomic bands or transitions between different atomic bands are the cause of absorption or non-absorption by materials. Therefore, the electrochromism mechanism is purely due to the insertion of electrons into the material electronic band structure. The objective of this section is to show that electrochromic behaviour of sputtered nickel oxide can essentially be based on electronic insertion into its lattice which is described by equations [6.2] and [6.3]. In these experiments, care has been taken to use aprotic electrolytes to avoid any involvement of hydroxyl ions contained in water. This section presents an experiment in which optical properties modulation of R.F. magnetron sputtered nickel oxide is studied as a function of the number of inserted ions. And this experiment is repeated for ions with different oxidation states.

6.7.1 Experimental procedure

All experiments were performed on similar nickel oxide materials. Three nickel oxide films were cut from a unique R.F. magnetron sputtered NiO_x batch. These samples, coated on ITO, originated from the sputtered optimised batches described in Section 6.5. The spectro-electrochemical cell was used simultaneously with the FTIR Bruker 66 spectrophotometer (see Chapter 4).

In order to slow down the intercalation/deintercalation process, experiments were carried out using low-concentration electrolytic solutions (0.1 Molar solutions) in propylene carbonate. The ionic solutions were chosen in accordance with the size of the radius of their ions. Due to the oxidation state of ions, ionic diffusion into a lattice is supposed to decrease with increasing oxidation state. For instance, Al^{3+} will diffuse more slowly than Li^{+}.

Electrolytes	Ions	Ionic radius[40] (nm)
Lithium Trifluoromethanesulfonate	Li^+	0.062
Magnesium perchlorate	Mg^{2+}	0.065
Aluminium Chloride	Al^{3+}	0.050

Table 6.6 : List of aprotic electrolytes and their ions used to study the mechanism of NiO_x.

Therefore, to expect a similar insertion behaviour, the size of the ions had to be smaller or more or less equal to the size of the lithium ion. Finally, the solutions chosen are non-aqueous in order to negate the effect of water. All the solutions were transparent in appearance in the visible range of the spectrum. The preparation procedure of the electrolytes is described in Chapter 4. Table 6.6 shows the different non-aqueous electrolytes used in this experiment.

6.7.2 Results

Results are shown in Figure 6.29. The relative visible transmittance is shown as a function of the number of inserted ions. The first remark is that all films exhibited a reversible optical modulation under ionic intercalation/deintercalation. Nickel oxide films exhibited a modulation over the whole visible region which was also reported by Corrigan et al.[41]. The fully bleached and coloured states were different for each electrolyte used, therefore only the relative visible transmittance was calculated for the purpose of this study. The charge passed into the films was considered to be directly related to the oxidation state of the ions, in other words related to the combined electrons inserted to maintain the material neutrality. The number of ions inserted into the nickel oxide layer was therefore equal to the charge passed, divided by the oxidation state of the ion and divided by the charge of an electron.

It is clear from Figure 6.29 that the modulation in relative transmittance increases more quickly under insertion of an high oxidation state ion. Magnesium or aluminium ions are inserted into the material instead of lithium ions. To preserve the overall neutrality of the material, this insertion is simultaneously combined with the insertion of electrons which fill the valence band and the intermediate bands. The lower bands are filled up much more quickly when high oxidation states ions are inserted, therefore the optical gap of the material varies accordingly.

No attempt has been made to investigate these experiments further. Both films showed some electrochromic behaviour over a few cycles, but no investigation has been made over a wide range of switching cycles. There is also no attempt to explain the exact mechanism when inserting these different ions, e.g. how the electronic configuration could be rearranged due to the probable creation of Ni^{2+}, Ni^{3+} and O^{2-} centres.

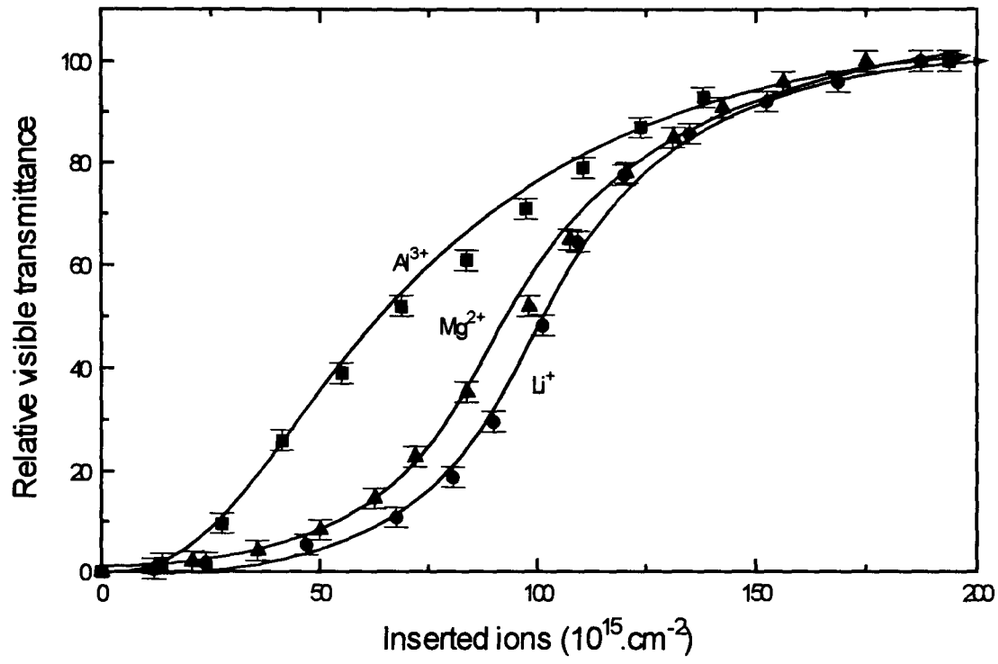

Figure 6.29 : Relative visible transmittance as a function of inserted lithium, magnesium and aluminium ions.
Estimated error on number of inserted ions ± 10 %.

The ionic intercalation of Mg^{2+} and Al^{3+} can be considered similar to the physical insertion mechanism of Li^{+}. Because magnesium and aluminium ions have almost the same sizes as lithium ions, they will move into the lattice at similar places. One can assume that in the site they occupy, ions might interact with neighbouring atoms in a similar way. The host material behaves like an ion storage layer. Therefore, it is easy to consider that the electronic band structure of doped nickel oxide with lithium, magnesium or aluminium ions could move to similar electronic band positions. Experiments show a transmittance modulation; consequently, one can assume that the optical gap might only be due to similar electronic transitions which are present in the lithium case. This result would then give evidence for the mechanism described in equations [6.2] and [6.3], where the inserted ion is only a charge carrier. Nickel oxide has been the subject of intense discussion concerning its mechanism.

This experiment would confirm that without the presence of water, the sputtered electrochromic nickel oxide mechanism can be simply described by a protonic insertion. More experimental investigations are required to confirm all the above speculation.

However, equations [6.2] and [6.3] could eventually be further developed to even more general reactions.

A simplified representation of reaction for a cathodic colouring material would be :

$$MeO_x\ (transparent) + yM^{z+} + (y+z-1)e^- \Leftrightarrow M_yMeO_x\ (coloured) \qquad [6.4]$$

and for an anodic colouring material would be :

$$M_yMeO_x\ (transparent) \Leftrightarrow MeO_x\ (coloured) + yM^{z+} + (y+z-1)e^- \qquad [6.5]$$

where M = $Li^+, H^+, Na^+, Fe^{2+}, Fe^{3+}, Mg^{2+}, Al^{3+}$... and Me = *Transition Metal*.

6.8 Conclusion

This Chapter presented the electrochromic properties of electrochemically-deposited nickel oxide and of R.F. magnetron sputtered nickel oxide. This work, based on aqueous electrolytic solutions, was the continuation of previous research studies of the laboratory. Deposition of these two types of film was optimised and significant improvements were made concerning their optical and electrochemical properties. Most noticeable progress was achieved with the lowering of the visible transmittance in the coloured state to values of 1% for the anodic film and 4 % for the sputtered material. The charge storage of both films was also studied and showed to be equal or greater than 20 or 30 mC/cm^2 for the anodic and sputtered nickel oxide films respectively. Those were in agreement with values required by ideal counter-electrode layers.

On the other hand, long-term cycling in a potassium hydroxyde electrolyte revealed greater differences between the two types of film. Nickel oxide films prepared by sputtering exhibited little degradation in electrochromic response over switching cycles, whereas anodic material showed a rapid destruction of the deposited film. Electrodeposited nickel hydroxide films have shown very good optical and electrochemical properties over the first switching cycles but require further studies to improve their long term stability in order to fulfil any electrochromic applications. As well as the optical and electrochemical properties, the durability of the film is a key point for an improved electrochromic window.

Both films exhibited two very different types of structure. The anodic film is a very soft material made of submicron-sized cavities. The microstructure is very open and porous, and it undergoes a high mechanical stress under ionic intercalation. In the case of anodically-deposited films, the hydroxyl mechanism was seen to dominate, making the tensile stress high, considering the size of the cation. On the other hand, the sputtered film is very hard and compact. It was seen to be made of nanocrystals in which mostly potassium ions will be responsible for the coloration/decoloration mechanism. However, hydroxyl ions will also intercalate when cycled in an aqueous electrolyte. The robustness of such film does not seem to be affected by the stress caused by the ionic intercalation, making it much more durable.

Sputter-deposited nickel oxide films produced in this work are shown to be far better candidates for ion storage layers in a protonated environment than the anodically-deposited nickel oxide. And a reason for that is principally due to the robustness of its nanocrystalline structure.

However, the presence of water inside an electrochromic device does not make it attractive to manufacturers. This is mainly due to possible oxygen and hydrogen evolution during the deintercalation or intercalation reaction process, putting the long-term durability of the device at risk. Nevertheless, devices with protonic conductor electrolytes seem to have been successfully fabricated using hydrated niobium pentoxide or antimony pentoxide as a solid-state electrolyte[42].

Alternatively, nickel oxide electrodes have been used in a lithium-based electrolyte. Xingfang et al.[21] showed that sputtered nickel oxide could be bleached under lithium ion bombardment. This Chapter showed the electrochemical reaction occurring on the sputtered deposited nickel oxide when used in lithium triflate. Nickel oxide film behaviour was seen to vary drastically under lithium ion intercalation or deintercalation, compared to the highly reproducible behaviour of films studied in a protonic electrolyte. It is thought that films undergo different stages, exhibiting different reactions. It was seen to degrade extremely quickly. Further studies should be carried out to investigate the reasons of the failures presented in this Chapter. At this stage, three possible explanations can be given. Firstly, the presence of water in concentrations less than 0.16% was seen to increase the redox processes, and was seen to decompose species[39]. Secondly, Brotherston et al.[43] reported that the most probable reaction was a reduction of Ni^{+2} to Ni^{0} in the cathodic process which is then reversed in the anodic region. A redox process observed in the CV indicates the growth of a new phase in the nickel oxide film. This is probably why reduced nickel oxide (black in appearance), starts peeling off the substrate in the cathodic process. Finally, sputtered nickel oxide used under lithium ion insertion was prepared and optimised for protonic intercalation and it was seen that the deposition conditions strongly influenced the electrochromic properties of these oxide films. It is possible that these deposition conditions are not the same for electrochromic films with a lithiated electrolyte. It is also possible that the range of deposition conditions are much narrower for lithium ions than for protons.

The result of this study has shown that nickel oxide produced in this work seems suitable for protonic insertion but seems unsuitable for lithium-based EC devices. Chapter 8 presents the performance of a laminated prototype based on a polymer containing lithium ions. Protonated devices based on an solid-state electrolyte have been successfully produced by other research laboratories making the work presented in this Chapter still relevant.

Chapter 7

DEPOSITION AND CHARACTERISATION OF COUNTER ELECTRODE FILMS OF VANADIUM/TITANIUM MIXED-OXIDE

7.1 Introduction

Vanadium oxide and titanium oxide based materials are known to display chromogenic effects and can be of interest for transmittance modulation in "smart windows". Different vanadium oxides can be used as an ion storage layer, and much work has been done on lithium ion intercalation in V_2O_5, V_4O_9, VO_2 and V_3O_8[1,2,3]. Among these, V_2O_5 and VO_2 have been employed as optically-passive counter electrodes in prototype smart windows. They can store a relatively large quantity of ions and exhibit a clear yellow or bluish coloration depending on the deposition conditions. Titanium oxide[4,5] has been shown to exhibit a rapid and reversible neutral coloration under a relatively small insertion of lithium ions.

VO_x and TiO_x oxide are known transition metal oxides which exhibit some electrochromism, and the possibility exists that a mixture of both might have some use as a counter electrode. Doping has been widely used in the semiconductor industry, and doped VO_x and doped VO_x are expected to produce interesting effects. The electrochromism of doped TiO_x has already been studied with different metal oxides such as cerium oxide[6,7], molybdenum oxide[8] and also with impurities such as fluorine[9]. VO_x has also been studied with dopant such as molybdenum oxide[10] or CF_4[11]. Doping VO_x films can produce interesting effects, for instance : vanadium pentoxide films doped with fluoro-carbon have their optical absorption lowered[11], and vanadium dioxide films doped with tungsten have their thermochromic switching temperature decreased[12,13].

On their own, both VO_x and TiO_x films do not exhibit all the required properties of an electrochromic counter electrode material. TiO_x films show good optical properties but bad charge-storage capabilities whereas vanadium oxide films have good charge-storage capabilities but exhibit an unfavourable coloration appearance. By mixing the oxides of two transition metals, it is expected that the coloration will change as well as the charge-storage capacity due to defects caused by the mixture. It was felt that investigating the properties of mixed metal oxides such as VO_x and TiO_x might produce a suitable film for a counter electrode application.

The aim of this Chapter is to study the charge-storage capability and the optical properties of the mixed oxides of V and Ti metals. Both oxides are separately produced and studied to optimise their sputtering process parameters. Mixed-metals targets were produced using a simple and quick method of making cheap mixed-metals sputtering targets. Mixed-metal oxide films were produced as a potential EC device counter electrode, and their electrochromic properties investigated.

7.2 Making mixed-metal targets

Mixed-metal targets of varied concentrations of the two metals were prepared by sputtering different areas of metallic vanadium onto hot-pressed metallic titanium targets. This was shown to be a cheap and quick technique to investigate a wide range of composition of the mixed-metal oxide.

7.2.1 Sputtering yields of metallic vanadium and metallic titanium produced from metallic targets

Metallic films were sputtered using the LCS-100 CVC sputter coater. Metallic V and metallic Ti films were prepared by D.C. magnetron sputtering from pure vanadium (99.9%) and titanium (99.9%) targets in an argon atmosphere. Sputtering was performed as a function of power, pressure, oxygen concentration and duration.

Details of the sputtering conditions used for metallic V and metallic Ti films are summarised in Table 7.1.

Target material	Ti (99.9% purity) & V (99.9% purity)
Target size	152 mm diameter
Power densities (W/cm^2) standard error : ±10 %	1.65, 2.75, 3.85, 4.9, 6.65, 7.8 (13.56 Mhz)
Sputter pressures (mT) standard error : ±10 %	2, 5, 7, 10, 15, 20, 30
Duration (mn) standard error : ±1 mn	5, 10, 20, 30

Table 7.1 : Sputter conditions used for the deposition of metallic vanadium and metallic titanium films.

Figure 7.1 shows the thickness of metallic vanadium and titanium films as a function of power density at a constant working pressure and duration.

7.2.2 Making of the mixed-metals targets

Areas of the titanium targets were masked with heat-resistant tape[14]. The masks were arranged as sectors of a circle to achieve the required ratio between the 2 metals. Vanadium was then sputtered onto the masked titanium plate by D.C. magnetron sputtering from a vanadium target. The vanadium layer deposited onto the titanium target was about 10 μm thick.

A typical arrangement for target production is shown in Figure 7.2. Targets were prepared with the following V/Ti surface area ratios : 90/10, 75/25, 60/40, 50/50, 40/60, 35/65, 30/70, 25/75.

7.2.3 Composition analysis of oxide films produced from mixed-metal targets

Atomic absorption spectroscopy was carried out on reactively-sputtered films deposited from targets prepared with different V to Ti surface area ratios. Relatively thick films of the order of 2 μm of the oxide of each target was deposited onto a 10 x 10 cm^2 glass plate. Each film was then dissolved off in aqua-regia (3 parts of HCl to 1 part of HNO_3) and the mass of both V and Ti measured[15].

Table 7.2 presents the composition analysis of the mixed oxide films produced from 5 different mixed metal targets with 80/20, 60/40, 50/50, 40/60, 20/80 V to Ti surface area ratios. These ratios were calculated using the atomic weight of titanium (47.9 g)[16] and of vanadium (50.942 g) [16]. An overall standard error on the V/Ti atomic ratio was estimated equal to 0.08.

Figure 7.3 shows the ratio of vanadium atoms to titanium atoms in mixed-metal oxide films produced from mixed-metal targets as a function of the metallic vanadium ratio of the mixed-metal targets. This graph shows that the ratios in the mixed oxide films can be considered almost proportional to the ratio of the V/Ti metallic target they were produced with.

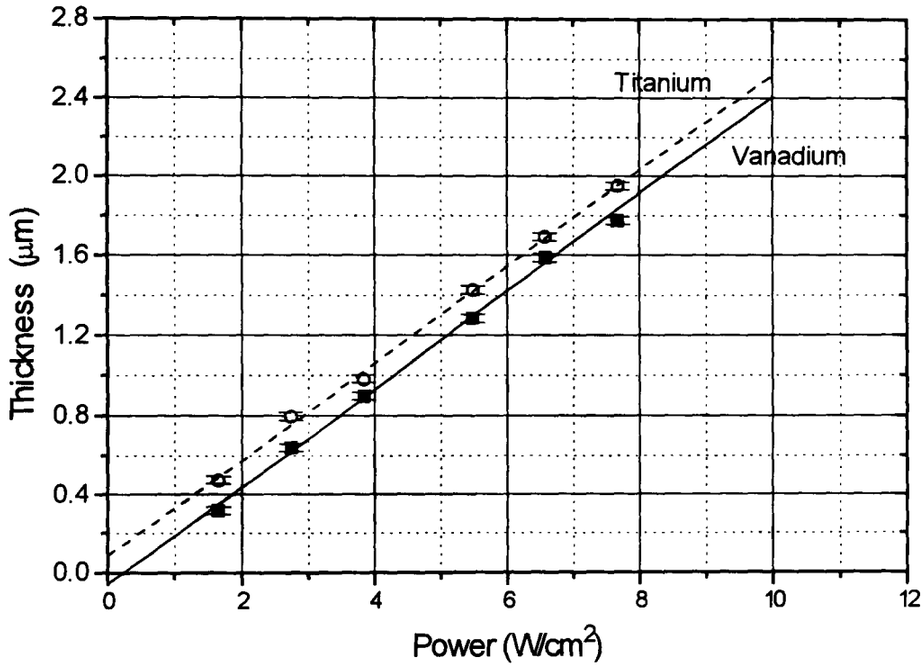

Figure 7.1 : Thickness of metallic vanadium and metallic titanium as a function of power density at a constant working pressure of 5 mT and 15 minutes duration.

Standard error on power densities : ± 10 %.

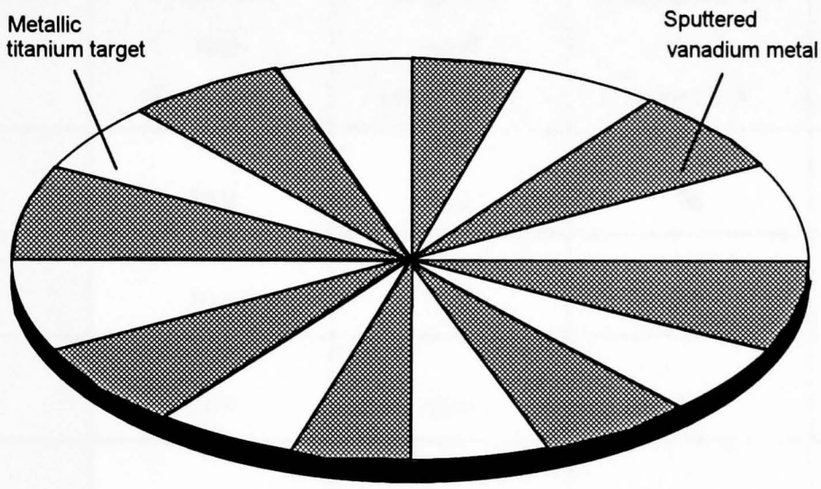

Figure 7.2 : Sector division for the preparation of mixed-metal targets. The sector areas were varied to achieve different vanadium to titanium ratios for subsequent preparation of the mixed-metal oxides.

Metallic Vanadium ratio on mixed metal target (%)	**Mass of Vanadium in the sputtered mixed oxide film** (mg) error : ± 0.5	**Mass of Titanium in the sputtered mixed oxide film** (mg) error : ± 0.5	**Vanadium to titanium ratio on sputtered mixed oxide film** (%) error : ± 8	**Vanadium to titanium Atomic ratio on sputtered mixed oxide film** (%) error : ± 8
80	20.9	6.5	76	75
60	10.6	5.8	65	63
50	11.9	10.6	53	51
40	10.6	14.1	43	41
20	6.5	14.2	31	30

Table 7.2 : Atomic absorption spectroscopy composition analysis of vanadium/titanium mixed oxide thick films produced from different mixed-metal targets.

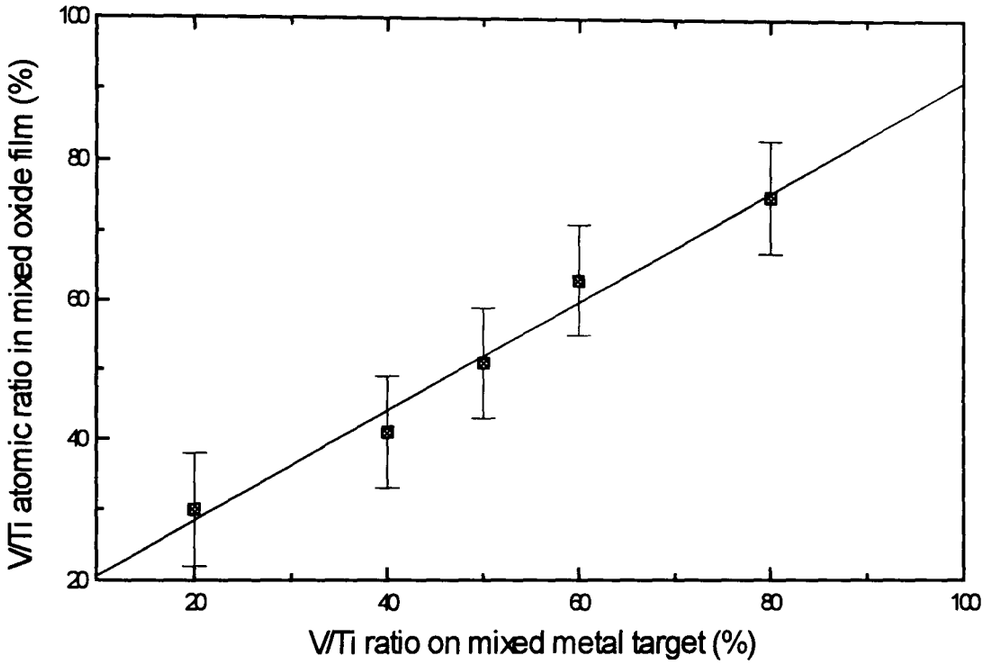

Figure 7.3 : The ratio of vanadium atoms to titanium atoms in mixed-metal oxide films produced from mixed-metal targets as a function of metallic vanadium ratio of the mixed-metal targets.
Standard error on V/Ti metallic ratio on target ± 3 %.

This line is used in this Chapter to evaluate the V/Ti ratio of $V_zTi_yO_x$ sputtered films. These results show that this technique of producing mixed-metal targets is not only cheap and quick but also reliable for producing mixed-metal oxide films.

An alternative method was studied. Mixed-metal targets were produced by sputtering metallic V and metallic Ti at different concentration ratios onto hot-pressed titanium targets. Consequently, the mixed-metal oxide film was produced from an all-sputtered mixed-metal target. However, composition analysis of the mixed oxide films did not show any major difference with previous methods. Due to the time taken to produce these latter targets, the technique was not used in further work.

7.3 Deposition of vanadium oxide and titanium oxide films

In order to understand the mixed oxide, it was necessary to understand the properties of the single oxides separately. In this section, VO_x and TiO_x films were deposited by R.F. magnetron sputtering and were characterised.

Both oxides exhibit electrochromic properties for applications in a lithium-based system. The results found for the two oxides are presented in this section.

7.3.1 Experimental Method

Vanadium oxide and titanium oxide thin films of undetermined stoichiometry were deposited by reactive R.F. magnetron sputtering using the CVC equipment. Lithium ions were inserted into vanadium oxide and titanium oxide films by cyclic voltammetry in an electrochemical cell containing 1M lithium perchlorate ($LiClO_4$) in propylene carbonate (PC). An EG&G Condecon 310 was used to operate a standard 3 electrode electrochemical cell with the oxide film as the working electrode, a platinum wire as a reference electrode and a 6 cm circumference platinum wire as a counter electrode. The active sample area was about 4 cm^2. The cell was prepared and assembled in a controlled atmosphere glove box. To reach an electrochemically stable condition, the samples were cycled for at least 10 insertions/extractions at a scan rate of 10 mV/s and at potentials between + 1.0 V and + 4.0 V.

Optical transmittance in the visible range of the spectrum (T_v) was measured by placing the electrochemical cell inside the Bruker 66 spectrophotometer compartment (see Chapter 4).

Sputtering was performed at different powers, pressures, oxygen concentrations and duration. Each sample was masked with a heat-resistant tape during the sputtering deposition process leaving an uncoated area of ITO.

Details of sputtering conditions for both vanadium oxide and titanium oxide films are summarised in Table 7.3.

After deposition, film thickness and as-deposited visible transmission were measured for each film. The electro-optical properties were measured simultaneously with the electrochemical cell placed inside the spectrophotometer.

7.3.2 Experimental results

7.3.2.1 Growth-rate of sputtered titanium oxide and vanadium oxide films

Figure 7.4 shows the dependence of growth rate as a function of sputtering pressure and power for VO_x and TiO_x thin films. Figure 7.5 shows the dependence of growth-rate as a function of oxygen concentration.

In both figures, the sputtering rate of TiO_x is lower than the rate of VO_x. The growth rate of TiO_x is also seen independent of pressure and oxygen concentration. On the other hand, the sputtering rate of VO_x films seems more dependent on process pressure than TiO_x films.

At high sputtering power, the growth-rate is seen to reach a maximum for pressures in the range 7-10 mT. The rate is also strongly dependent on the oxygen content. One can expect that the films go through different oxidation states for oxygen contents below 5 %. Above this concentration, the growth-rate does not vary significantly.

These graphs show that the sputtering rates of TiO_x films do not vary significantly with R.F. magnetron process parameters, whereas VO_x films seem more dependent on them.

The reproducibility of the deposition rates of VO_x and TiO_x thin films was within $\pm$ 10 %.

Target material	V (99.9% purity) & Ti (99.9%)
Target size	152 mm diameter
Power densities(W/cm^2) standard error : ± 10 %	0.55, 1.65, 2.75, 3.85, 4.9 (13.56 MHz)
Sputter pressures (mT) standard error : ± 10 %	02, 5, 7, 10, 20
Oxygen concentrations (%) standard error : ± 20 % of concentration value	1, 1.5, 2, 2.5, 3, 5, 10, 30, 40, 50
Substrate temperature standard error : ±10 °C	~180 °C
Duration (mn) standard error : ±1 mm	30

Table 7.3 : Deposition conditions employed to prepare vanadium oxide and titanium oxide thin films by reactive R.F. magnetron sputtering.

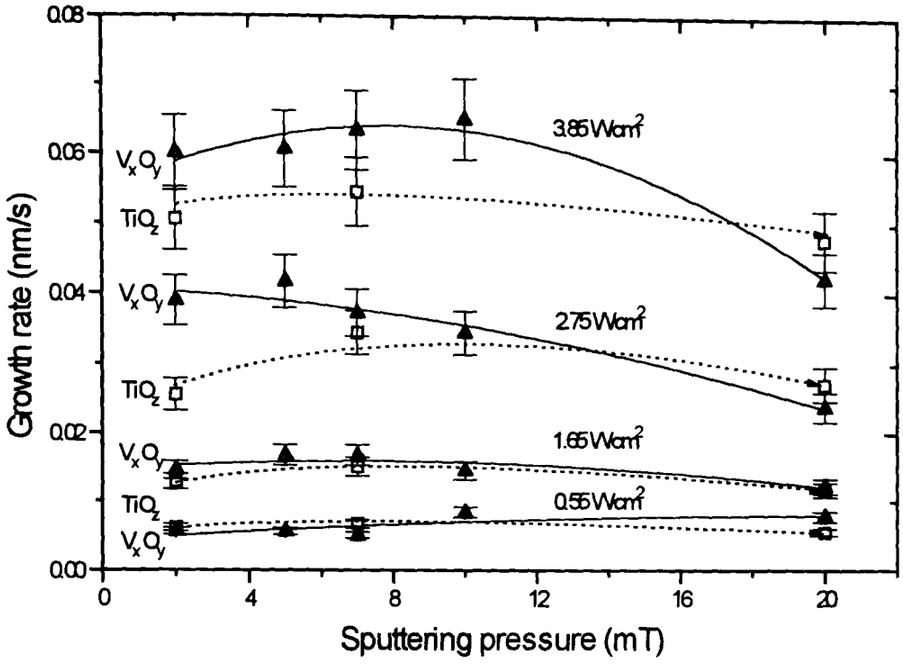

Figure 7.4 : Growth rates of vanadium oxide (—) and titanium oxide (.....) at different sputtering pressures and powers, and at 20 % oxygen content. Standard error on sputtering pressure : ± 10 %.

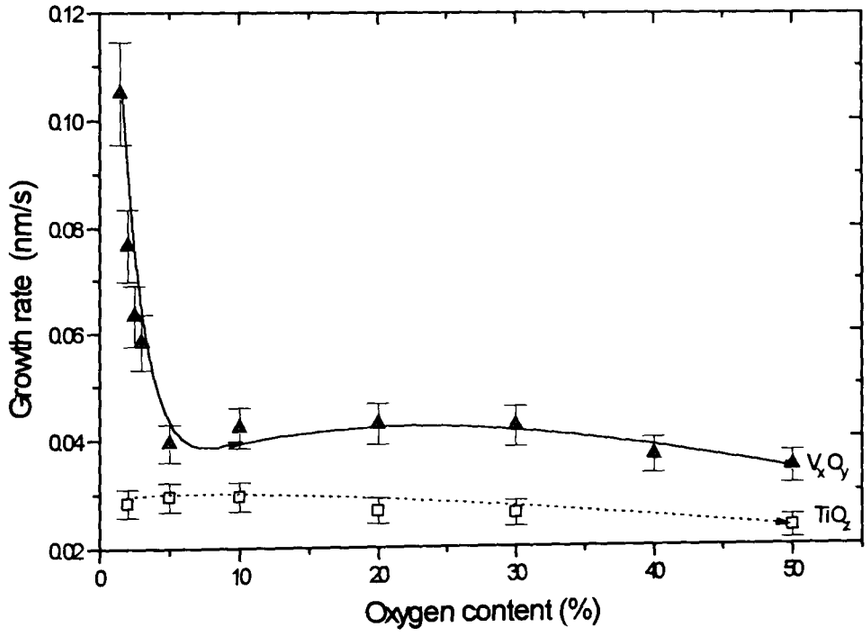

Figure 7.5 : Growth rates of vanadium oxide (—) and titanium oxide (.....) at different oxygen contents, at 2.75 W/cm² power and 7 mT pressure. Standard error on oxygen content : ± 15 % of content value.

7.3.2.2 TiO_x and VO_x prepared at different working pressures

Table 7.4 shows the variation of chromaticity coefficients of vanadium oxide and titanium oxide films at different deposition pressures.

Figure 7.6 shows the quantity of charge transferred into titanium oxide and vanadium oxide films as a function of working pressure used during the deposition process.

Figures 7.7 and 7.8 show the visible transmittance of vanadium oxide and titanium oxide films respectively at different deposition pressures in charged (or inserted) and uncharged (extracted) states.

VO_x films are yellow in coloration in the uncharged state and blue/grey under lithium insertion. Films produced at different deposition pressures do not show any particular variation in their appearance in either the charged or uncharged states. The charge capacity is seen to be 3 times higher than the charge capacity of TiO_x films. The charge storage of VO_x films do not strongly depend on the sputtering pressure used during the process. There is also no significant variation in T_v for charged and uncharged films deposited under different sputtering pressures. The charged state is seen to have a high $T_{v,ch}$ (80 %) and the difference ($T_{v,u}$ - $T_{v,ch}$) remains equal to 10 % at all pressures.

TiO_x films are blue/grey in their uncharged state and transparent under lithium insertion. Films produced at different deposition pressures do not show any variation in their coloration appearance in either the inserted or extracted states. All films show a high T_v as well as a very small modulation in the visible range of the spectrum between the 2 states. The charge transferred remains constant for films produced at all pressures and was seen to be very low in comparison with vanadium oxide films.

TiO_x thin films exhibit characteristic neutral coloration and charge storage capability which seem independent of the total pressure used during the sputtering deposition process. On the other hand, the charge capacity of VO_x thin films seem slightly higher at pressures below 10 mT. For this reason, the optimum sputtering pressure was chosen to be in the range [7 - 10 mT].

	Charged state Pressures 2 mT / 7 mT / 20 mT	**Uncharged state** Pressures 2 mT / 7 mT / 20 mT
Vanadium oxide		
X (red)	0.37 / 0.37 / 0.37	0.32 / 0.32 / 0.32
Y (green)	0.41 / 0.41 / 0.40	0.34 / 0.32 / 0.32
Z (blue)	0.22 / 0.22 / 0.23	0.34 / 0.36 / 0.36
Titanium oxide		
X (red)	0.30 / 0.30 / 0.30	0.30 / 0.30 / 0.30
Y (green)	0.30 / 0.30 / 0.29	0.30 / 0.29 / 0.29
Z (blue)	0.40 / 0.40 / 0.41	0.40 / 0.41 / 0.41

Table 7.4 : Chromaticity coefficients of vanadium oxide and titanium oxide thin films in the charged and uncharged states. Films were R.F. magnetron sputtered at different pressures, at 2.75W/cm^2 power density, 30 minutes duration and at 20 % O_2 content.

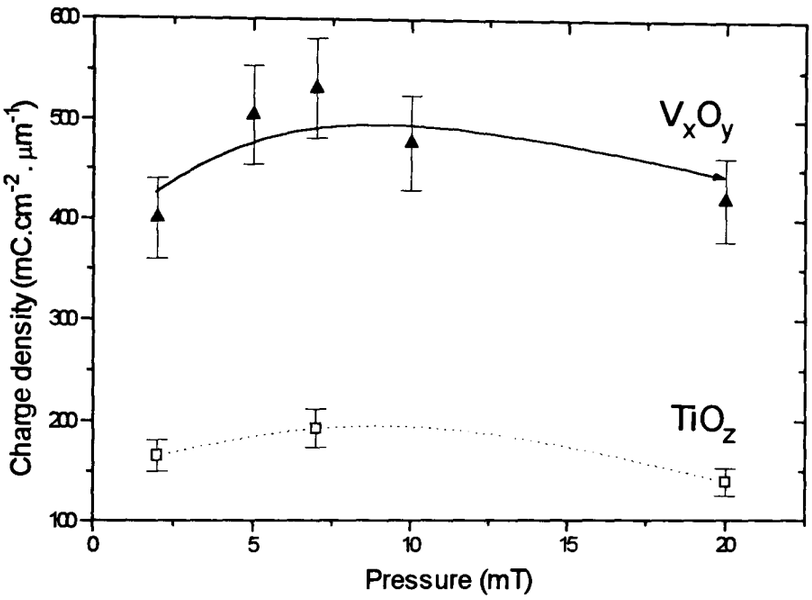

Figure 7.6 : Charge density of titanium oxide and vanadium oxide thin films as a function of sputtering pressure, at 3.75W/cm^2 power density, 30 minutes duration and 20 % O_2 content.

Standard error on pressure : ± 10 %.

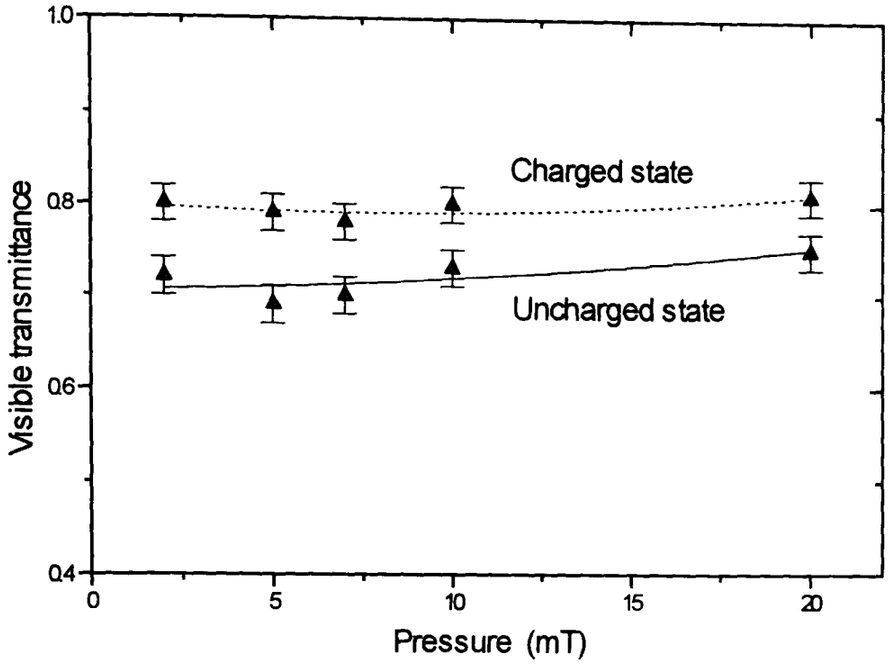

Figure 7.7 : Visible transmittance of vanadium oxide thin films as a function of sputtering pressure, at 2.75W/cm^2 power density, 30 minutes duration and 20 % O_2 content.
Standard error on pressure : ± 10 %.

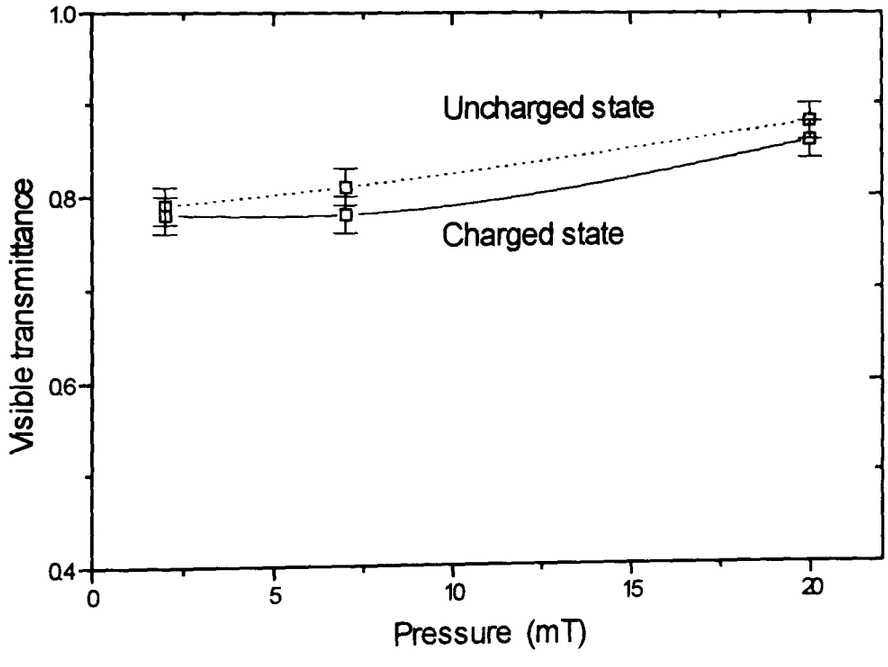

Figure 7.8 : Visible transmittance of titanium oxide thin films as a function of sputtering pressure, at 2.75W/cm^2 power density, 30 minutes duration and 20 % O_2 content.
Standard error on pressure : ± 10 %.

7.3.2.3 TiO_x and VO_x prepared at different power densities

Figures 7.9 and 7.10 show the visible transmittance of titanium oxide and vanadium oxide thin films respectively as a function of the deposition power density in the charged and uncharged states.

Figure 7.11 shows the charge storage capacity of vanadium oxide and titanium oxide thin films as a function of the power density.

VO_x and TiO_x thin films made under different power densities do not show any particular variation in their respective appearance in either charged and uncharged states. Figure 7.9 shows that the difference in T_v between the two states is almost constant and is equal to ~ 10 %. The increase of power density increases the film thickness for a constant deposition time, which results in a decrease in the T_v of the film. These variations in optical properties are in the order of 15 %, which is low compared to results found with vanadium oxide.

Figure 7.10 shows a proportional decrease in the T_v of VO_x film with the increase of film thickness which is itself directly related to the increase of power density. There is a clear contrast in T_v modulation of VO_x films compared with TiO_x films as a function of film thickness. Figure 7.10 shows an increase from 5 % to 20 % between 0.5 to 4.0 W/cm^2 power density whereas TiO_x remains constant.

On the other hand, the charge storage capacity of VO_x films is in sharp contrast with TiO_x films. It increases proportionally with the power used during the process, and is therefore proportional to the thickness of films. For power densities higher than 2.0 W/cm^2, the charge storage capacity of VO_x films is seen to be higher than 25 mC/cm^2, which is an acceptable value for counter electrode applications.

The variation of the sputtering power or film thickness is seen to influence the optical and electrochemical properties of VO_x thin films whereas TiO_x films remain insensitive to this deposition parameter.

7.3.2.4 TiO_x and VO_x prepared at different oxygen concentrations

Figures 7.12 and 7.13 show the visible transmittance of titanium oxide films and vanadium oxide films respectively as a function of oxygen concentration for films in the charged and uncharged states.

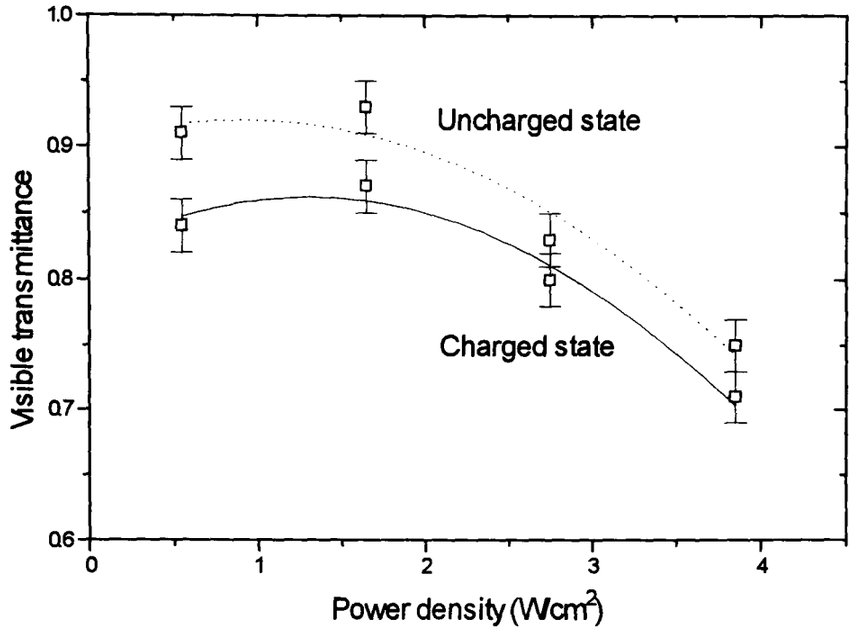

Figure 7.9 : Visible transmittance of titanium oxide films in the charged and uncharged states as a function of power densities, at 7 mT working pressure, 30 minutes deposition and at 20 % O_2 content. Standard error on power density : ± 10 %.

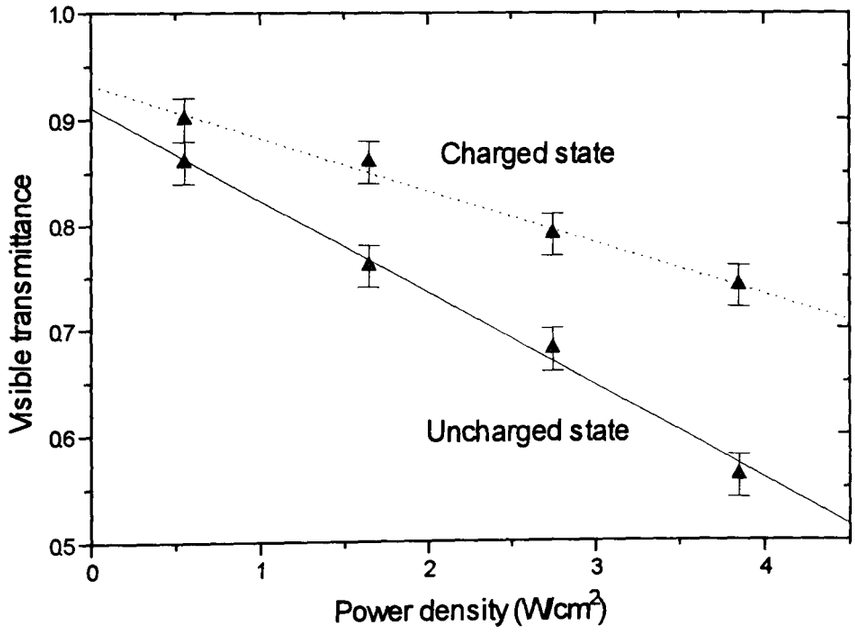

Figure 7.10: Visible transmittance of vanadium oxide films in the charged and uncharged states as a function of power densities, at 7 mT working pressure, 30 minutes deposition and 20 % O_2 content. Standard error on power density : ± 10 %.

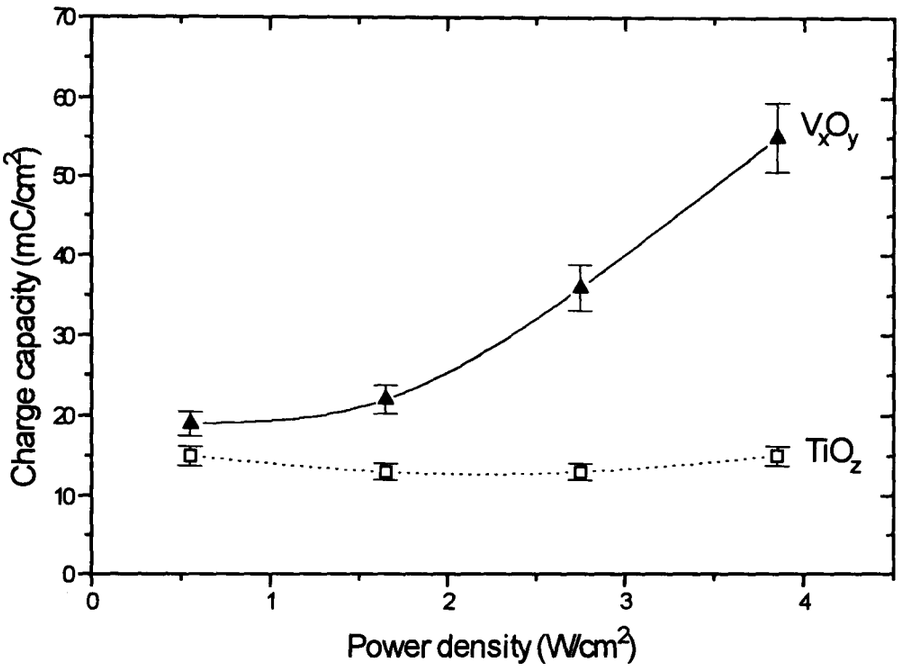

Figure 7.11: Charge storage capacity of titanium oxide and vanadium oxide films as function of deposition power, at 7 mT a working pressure, 30 minutes deposition and 20 % O_2 content. Standard error on power density : ± 10 %.

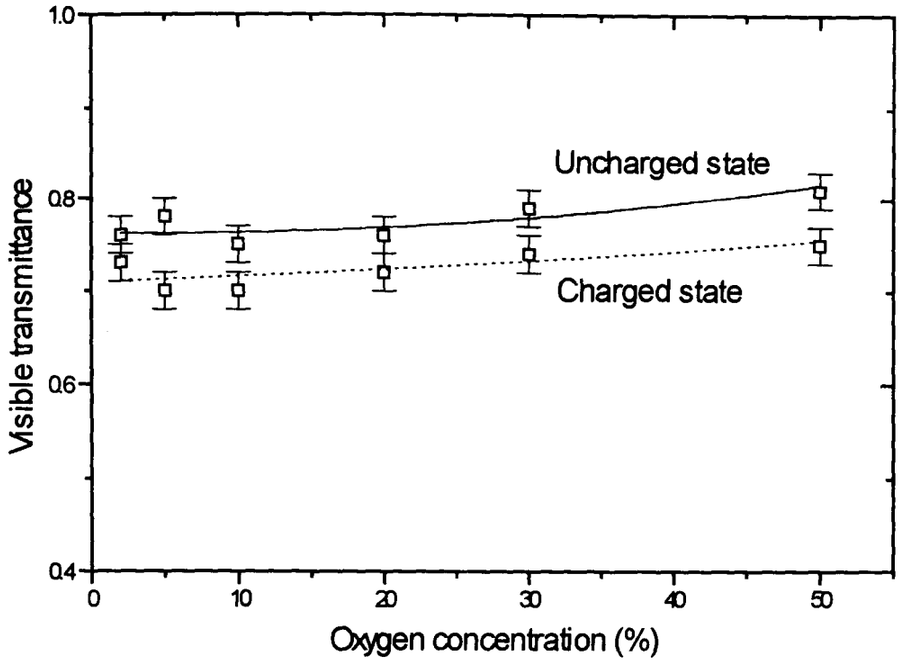

Figure 7.12 : Visible transmittance of titanium oxide films in the charged and uncharged states as a function of oxygen concentration, at 7 mT working pressure, 30 minutes deposition and 2.75 W/cm^2 power density. Standard error on oxygen concentration : ± 20 % of concentration value.

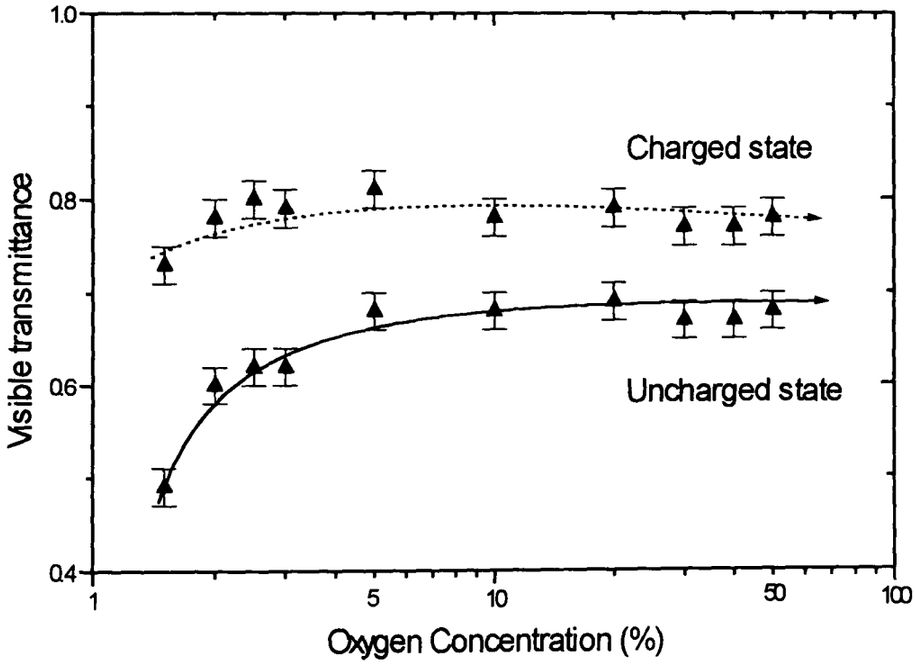

Figure 7.13 : Visible transmittance of vanadium oxide films in the charged and uncharged states as a function of oxygen concentration, at 7 mT working pressure, 30 minutes deposition and 2.75 W/cm^2 power density. Standard error on oxygen concentration : ± 20 % of concentration value.

Table 7.5 shows the chromaticity coefficients at different oxygen concentrations for vanadium oxide and titanium oxide films respectively.

Figure 7.14 shows the charge density of vanadium oxide and titanium oxide thin films as a function of oxygen concentration.

The visible transmittance of TiO_x films in both charged and uncharged states remains constant for all oxygen concentrations used during the deposition process. A constant difference of 5 % between the two states is also seen in Figure 7.12.

Similarly, the charged state of VO_x films exhibit no significant variations for all oxygen concentrations whereas the uncharged state increases for concentrations in the range [1.5 - 10 %]. Above 10 %, the visible transmittance remains unaffected, and the difference between the two states is within 10 %. Titanium seems fully oxidised at concentrations above 2 %, whereas vanadium seems to exhibit different oxidation states up to 10 %.

Table 7.5 shows that TiO_x films are grey or slightly bluish in appearance in both uncharged and charged states for the different concentrations of oxygen. VO_x films appear grey / bluish in the uncharged state and clearly yellow in the charged one. At low O_2 contents (~ 2 %), these latter films are also seen to be slightly brownish, but then appear identical at contents above 5 %.

The charge storage density of TiO_x films is shown to be independent of oxygen content, whereas VO_x charge density increases up to 10 % and then remains unaffected.

Optical and electrochemical properties of VO_x and TiO_x films are unaffected by oxygen/argon ratios above 10-15 %. For this reason, 20% was chosen as the optimum concentration for studying the mixed-metal oxides.

7.3.3 Summary of results

In this section, no attempt has been made to study in great depth the electrochromic response of VO_x and TiO_x thin films under lithium ion intercalation. However, it was clear that both oxides are well-suited for lithium intercalation/deintercalation.

	Uncharged state Oxygen content 2 % / 5 % / 40 %	**Charged state** Oxygen content 2 % / 5 % / 40 %
Vanadium oxide		
X (red)	0.31 / 0.30 / 0.31	0.35 / 0.33 / 0.34
Y (green)	0.31 / 0.31 / 0.31	0.39 / 0.35 / 0.35
Z (blue)	0.38 / 0.39 / 0.38	0.26 / 0.32 / 0.32
Titanium oxide		
X (red)	0.30 / 0.31 / 0.31	0.31 / 0.32 / 0.32
Y (green)	0.31 / 0.30 / 0.31	0.31 / 0.31 / 0.32
Z (blue)	0.39 / 0.39 / 0.38	0.38 / 0.37 / 0.36

Table 7.5 : Chromaticity coefficients of titanium oxide and vanadium oxide films at different oxygen concentrations, at 7 mT working pressure, 30 minutes deposition and 2.75 W/cm^2 power density.

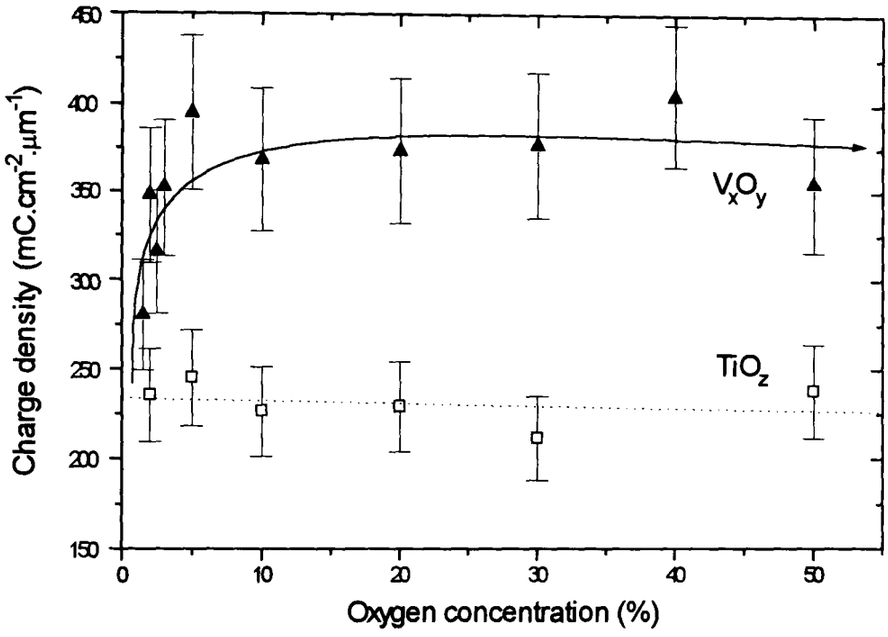

Figure 7.14 : Charge storage capacity into titanium oxide and vanadium oxide films as a function of oxygen concentration at 7 mT working pressure, 30 minutes deposition and 2.75 W/cm^2 power density. Standard error on oxygen concentration : ± 20 % of concentration value.

This section showed that titanium oxide films are relatively easy to produce at any sputtering condition, and their electrochromic properties are not shown to be strongly dependent on R.F. magnetron sputtering parameters. On the other hand, VO_x thin films are seen to be more strongly influenced by the process parameters used.

Figure 7.15 and Figure 7.16 show the hemispherical transmittance and reflectance of the optimised vanadium oxide film and of a titanium oxide film respectively.

Table 7.6 presents all optical and electrochemical properties of titanium oxide and vanadium oxide films as well as the optimised deposition process parameters.

In this table, the optical bandgaps of VO_x and TiO_x oxide thin films are calculated using Equation [4.11] with n = 2 as for tungsten oxide films[17].

Figure 7.17 and Figure 7.18 show the cyclic voltammograms of the optimised vanadium oxide and titanium oxide films respectively.

The coloration of VO_x films appeared very yellow in the as-deposited and uncharged state. On lithium intercalation, the films'appearance evolved through a yellow-colourless-blue or yellow-blue optical transition depending on the film. On lithium intercalation, the optical absorption edge is shifted to a higher energy. This is due to the filling or at least partial filling of the conduction band so that the lowest electron states are blocked[17]. An irreversible 0.7 eV shift of the bandgap to higher energies is seen between the as-deposited and the uncharged states of VO_x films. The charged state of VO_x films shows an increase of 0.5 eV in the gap energy relative to the uncharged state, whereas the TiO_x film bandgap shows a very low variation between the different states (~ 0.1 eV). This shift is reversible. Similar bandgap energies were found for as-deposited VO_x and TiO_x thin films sputter-deposited by different authors[17].

TiO_x films appeared transparent in the as-deposited and uncharged states, whereas the inserted state appeared grey/bluish. Electrochromic TiO_x films are easy to produce and are not strongly influenced by sputtering-deposition parameters. They show neutral coloration and high visible transmittance ($T_{v,u}$ = 0.81 and $T_{v,ch}$ = 0.78) under very small amount of charge insertion Q_{TiOx} = 13 $mC.cm^{-2}$. They exhibit the required appearance for counter electrode applications. It was also noticed that TiO_x films charge capacity remains constant at any thickness of the deposited film.

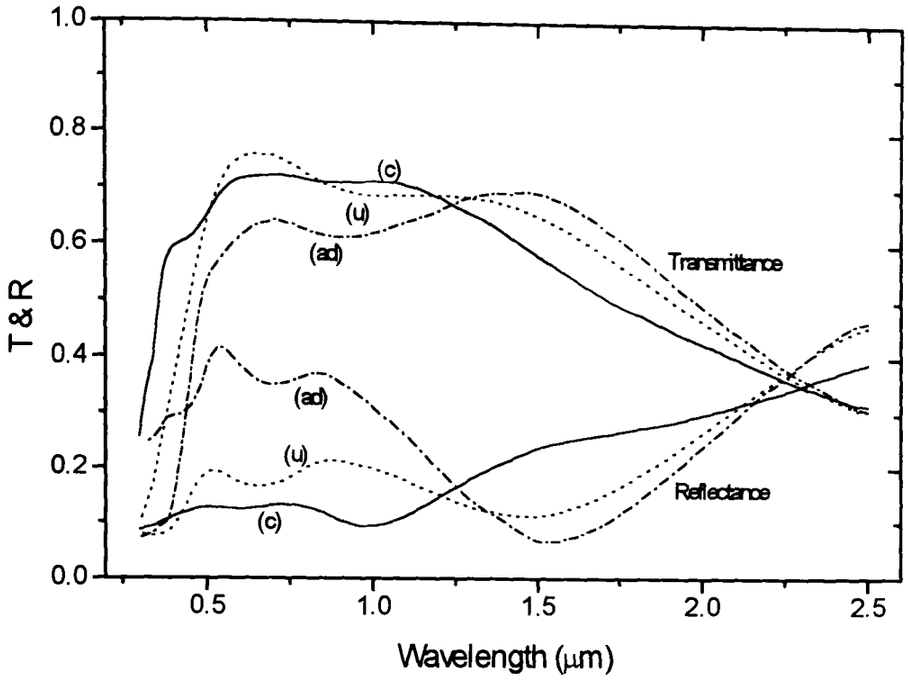

Figure 7.15 : Hemispherical transmittance and reflectance in the solar range of a vanadium oxide thin film in the as-deposited (ad), charged (c) and uncharged (u) states. Film produced at 7 mT, 2.75 W/cm^2, 20 % oxygen concentration and 30 mn duration. Film thickness : 67 nm.

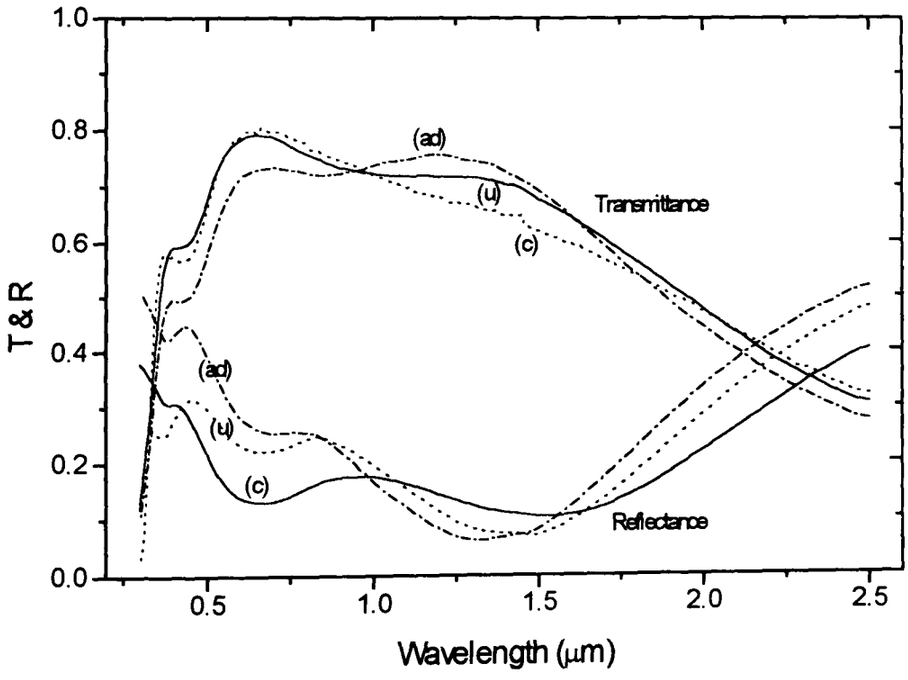

Figure 7.16 : Hemispherical transmittance and reflectance in the solar range of a titanium oxide thin film in the as-deposited (ad), charged (c) and uncharged (u) states. Film produced at 7 mT, 2.75 W/cm^2, 20 % oxygen concentration and 30 mn duration. Film thickness : 62 nm.

	TiO_2 film as-deposited/uncharged /charged	V_2O_5 film as-deposited/uncharged /charged
T_s	0.70 / 0.70 / 0.70	0.64 / 0.66 / 0.66
T_v	0.70 / 0.80 / 0.78	0.66 / 0.78 / 0.70
Optical bandgap (eV)	3.5 / 3.5 / 3.6	2.2 / 2.9 / 3.4

Q ($mC.cm^{-2}$)	13 ± 1	34 ± 3
Film thickness (nm)	62 ± 10	67 ± 10
η_c ($cm^2. C^{-1}$) Visible range	0.8 ± 0. 1	1.4 ± 0.1
Switching potentials	+ 1 V / + 4 V vs Li	+ 1 V / + 4 V vs Li
Charging time (s)	< 120	< 120
Lifetime (cycles)	> 500	> 500

	Optimised R.F. magnetron sputtering parameters
Target material Target size	Ti and V (99.9 % purity) 15.2 cm diameter
Power density Sputter pressure Oxygen content Temperature	2.75 W/cm^2 7 - 10 mT 20 % 180 °C
Time	30 mn

Table 7.6 : Summary of the electrochromic properties and optimised deposition process parameters of R.F. magnetron sputtered titanium oxide and vanadium oxide films under lithium intercalation/deintercalation.

This is probably due to the compactness of films into which a maximum quantity of lithium ions can intercalate. This would mean that a definite layer depth of the film is active and allows ionic insertion.

When compared to VO_x, TiO_x cyclic voltammograms exhibit a very low intercalation/deintercalation activity per unit volume. The current density scale of Figure 7.18 is 20 times smaller than the scale of Figure 7.17. Ti oxide is seen to be stable over cycling, whereas the two cathodic peaks in VO_x voltammograms decrease between the first and the fourth cycle.

One can expect that higher stability might be obtained when mixed with Ti. For instance, the addition of titanium is known to have a stabilising effect on WO_3 films[18,19], the mixed Ti/W oxide film exhibits a more stable coloration over time and traps less charge than pure WO_3 films.

This section shows that VO_x films are influenced by the deposition process parameters. They can store a much larger quantity of charge per volume Q_{VOx} = 34 $mC.cm^{-2}$ and exhibit a very characteristic coloration in their uncharged state. On its own, VO_x material is less desirable for counter electrode applications.

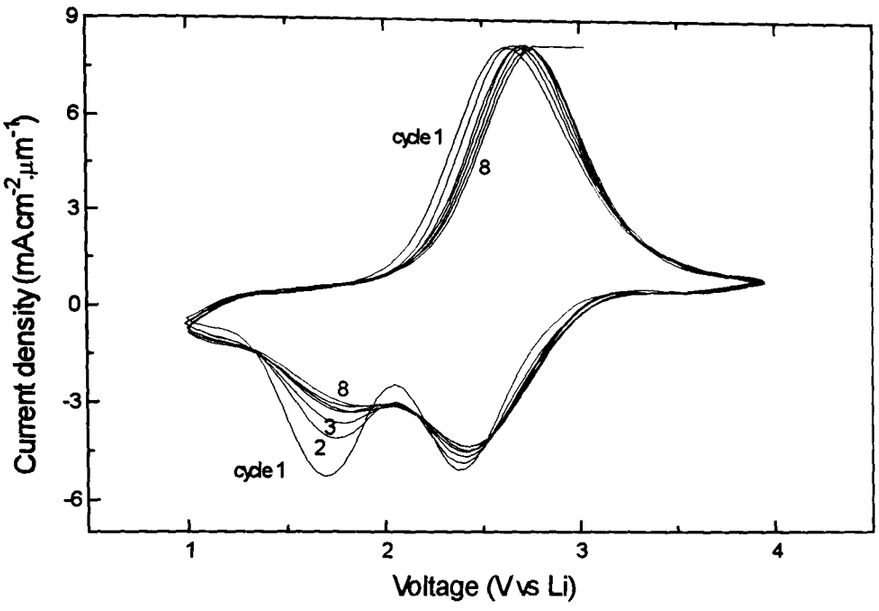

Figure 7.17 : Cyclic voltammograms 1 to 10 of a vanadium oxide thin film in 1M lithium perchlorate, at 10 mV/s scan rate, 3.5 cm^2 working area. Film produced at 7 mT, 2.75 W/cm^2, 20 % oxygen concentration and 30 mn duration.

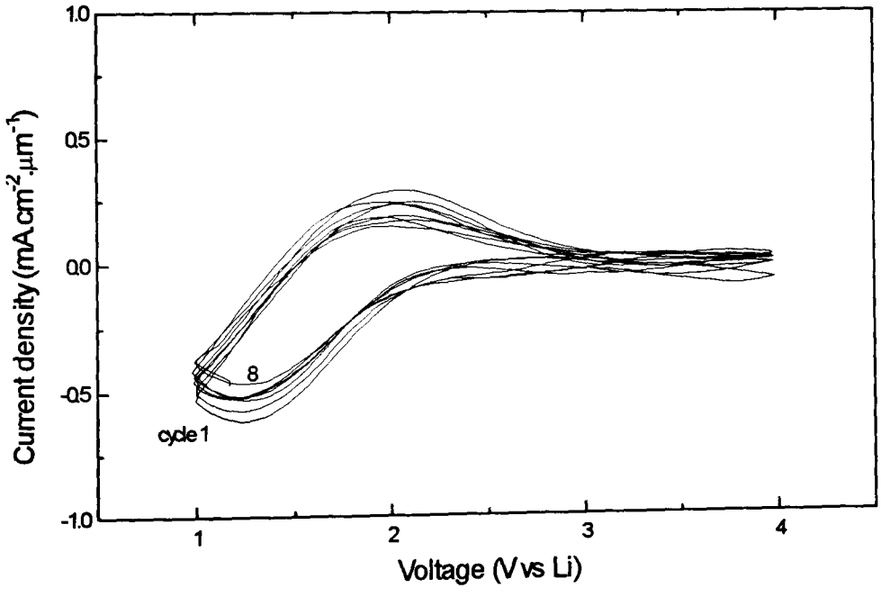

Figure 7.18 : Cyclic voltammograms 1 to 8 of a titanium oxide thin film in 1M lithium perchlorate, at 10 mV/s scan rate, 3.5 cm^2 working area. Film produced at 7 mT, 2.75 W/cm^2, 20 % oxygen concentration and 30 mn duration.

7.4 Deposition of vanadium/titanium mixed oxide thin films

The work undertaken in the previous section on the two oxides enables work on mixed-metal oxides to be carried out. A set of R.F. magnetron sputtering conditions were chosen for which vanadium oxide films exhibited optimum performance for counter electrode applications. These parameters are; working pressures in the range 7-10 mT, power densities in the range 1.6-4.0 W/cm^2 and 20 % oxygen concentrations.
This section presents the electrochromic characteristics of vanadium/titanium mixed-oxide films prepared by R.F. magnetron sputtering. The metallic vanadium/titanium ratios used were 25%, 30%, 35%, 40%, 50%, 60%, 75% and 90%. However, these are the results of an initial study which is still under investigation. For this reason, all results presented below have to be confirmed with more experimental data.

7.4.1 Experimental method

The mixed-metal targets were sputtered onto 2" x 2" Pilkington Aerospace ITO-coated glass with a resistance of 13 Ω/□. The substrates were cleaned prior to deposition using the technique described in Chapter 4. After a target presputtering of 15 minutes in pure argon, deposition was commenced. Film thickness was recorded by surface profilometry. Lithium ions were inserted into the mixed-oxide films by cyclic voltammetry in an electrochemical cell containing 1M lithium perchlorate ($LiClO_4$) in propylene carbonate. To reach an electrochemically stable condition, the samples were cycled for at least 8 insertions/extractions at a scan rate of 10 mV/s and at potentials +1 V/ +4.5 V .
Optical transmittance in the visible range of the spectrum was simultaneously measured with the electrochemical cell placed inside the Bruker IFS66 spectrophotometer.

7.4.2 Experimental results

The growth-rates of $V_zTi_yO_x$ films produced from targets with different V to Ti surface ratios are shown in Figure 7.19. The variation of growth-rate seems to be very similar to the results obtained by the collaborating laboratory[15].

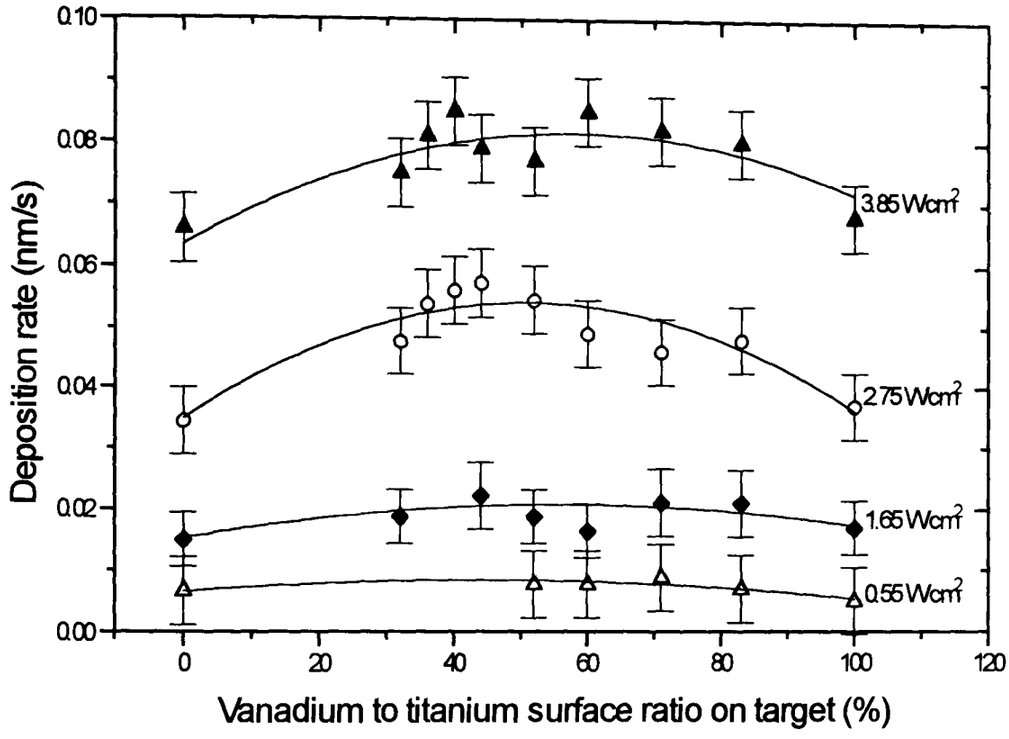

Figure 7.19 : Growth-rates of reactively-sputtered vanadium and titanium mixed oxide films deposited from metallic titanium targets coated with different ratio areas of metallic vanadium at different working powers, 20 % oxygen concentration and 7 mT pressure. Standard error on V/Ti ratio : ± 8%.

7.4.2.1 Electrochemical properties

Figures 7.20 (a), (b) and (c) show cyclic voltammograms 1 to 9 of mixed oxide films produced with 3 different V/Ti ratios : 83 %, 52 % and 32 % respectively. Films were studied in the spectro-electrochemical cell in the same way that single oxides were (see Section 7.3). The same potentials and scan rates were used for all films. It was noticed that intercalation potentials for mixed films are sensitive to their composition: the more Ti is present in films, the higher the potential difference (relative to the equilibrium value) which is needed to insert the same quantity of charge in each of them.

The shape of the voltammograms show a gradual evolution as the quantity of Ti is increased between pure VO_x and pure TiO_x. At V/Ti = 83 %, the voltammograms are essentially the same as for pure VO_x. The cathodic peak at 1.7 V for pure VO_x shifts towards 2 V after 4 cycles, while the peak at 2.4 - 2.5 V is still present. For V/Ti = 52 %, a broad cathodic peak is seen hiding those previously seen, whereas on the anodic process a peak below 2 V can be guessed. This anodic peak is clearly seen at 1.5 V for V/Ti = 32 % as well as one at 1.2 V approximately. One can observe that the voltammograms in Figure 7.20 (c) look like a combination of features for pure TiO_x and pure VO_x. These peaks are not attributed to any specific process reaction known to us. This might suggest that the mixed-metal oxide films behave as mixtures of the two oxides and not as new compounds.

The density of charge intercalated/deintercalated for the 3 films is reduced for the increasing proportion of Ti : Q_a = 49 $mC.cm^{-2}$ for V/Ti = 83 % 86 nm thick; Q_b = 44 $mC.cm^{-2}$ for V/Ti = 52 % 82 nm thick; and Q_c = 33 $mC.cm^{-2}$ for V/Ti = 32 %, 86 nm thick.

The stabilising property of Ti noticed in the previous section is seen on these cyclic voltammograms. After the fifth intercalation/deintercalation, voltammograms show a more stable reaction for high Ti ratios. In the case of Figure 7.20 (c), the process stabilises to a more reproducible process after the second switching cycle (notice the magnified scale; four times smaller than for Figure (a)).

Figure 7.21 shows the charge capacity of $V_zTi_yO_x$ films at different ranges of thickness. To fulfil one of the counter electrode applicability in an EC device, the charge capacity of $V_zTi_yO_x$ films has to balance the charge capacity of WO_3 to ensure its full discharge.

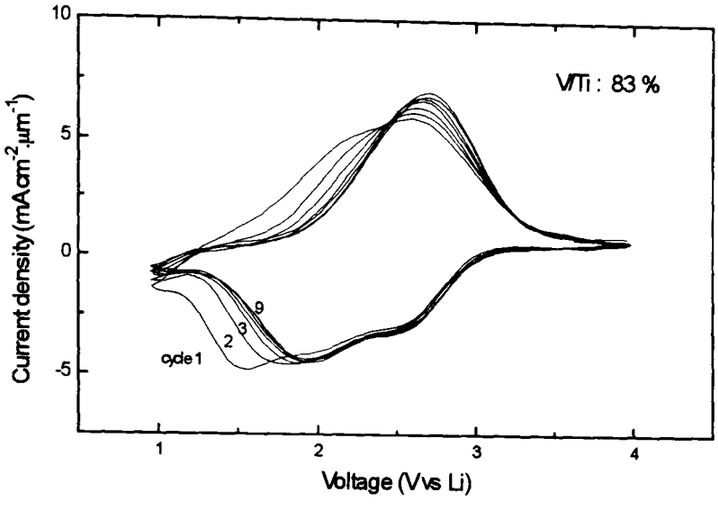

(a)

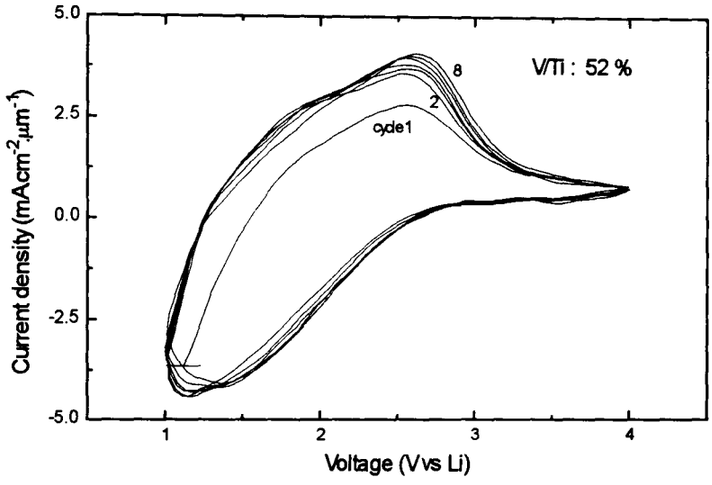

(b)

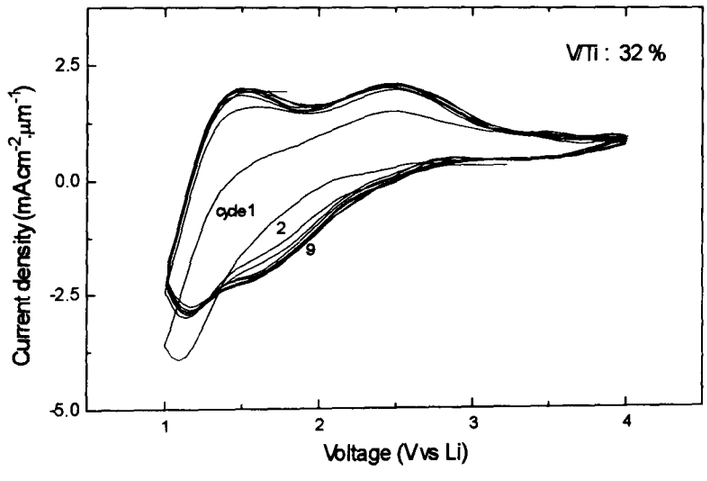

(c)

Figure 7.20: Cyclic voltammograms 1 to 9 of mixed oxide films with vanadium/ titanium ratios of (a) 83 %, (b) 52 % and (c) 32 %. Films were cycled in 1M $LiClO_4$ in PC, at a scan rate of 10 $mV.s^{-1}$.

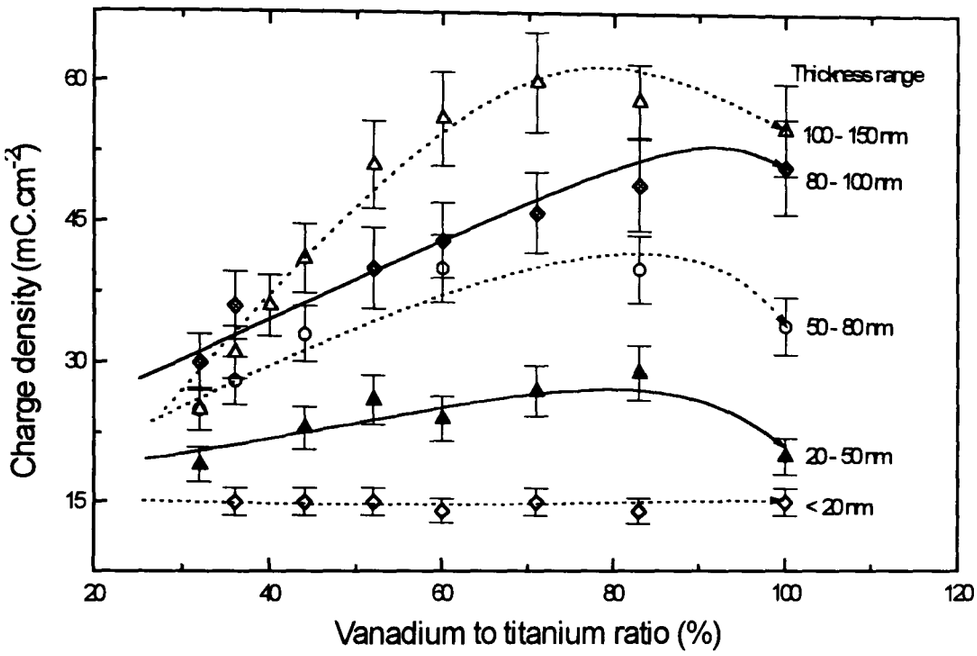

Figure 7.21 : Charge capacity of sputter-deposited $V_zTi_yO_x$ films at different thickness ranges. Films deposited at different power densities, 7 mT, 20 % oxygen concentration and 30 mn duration. Standard error on V/Ti : ± 8 %.

Therefore, the charge capacity of the mixed-metal oxide counter electrode has to be ≥ 40 mC/cm^2, and this is obtained for films of thickness ≥ 80 μm and for V/Ti ratio ≥ 40 %. The graphs also show that the charge capacity of vanadium oxide is increased when doped with Ti atoms. For films in the range 100 - 150 μm, the charge capacity of films with V/Ti > 60 % is higher than pure VO_x with a maxima at $V_{0.8}Ti_{0.2}O_x$ approximately. Below 60 %, the charge capacity of $V_zTi_yO_x$ films is lowered upon an increasing proportion of Ti atoms.

Slow scan cyclic voltammetry[20] was used to study the Li intercalation into $V_{0.52}Ti_{0.48}O_x$ films produced at different oxygen concentrations (5 %, 10 %, 20 % and 30 %), 7 mT, 2.75 W/cm^2, for 30 minutes, from the same mixed-metal target. Figure 7.22 shows the cyclic voltammograms (1 to 3) at 0.1 mV/s in 0.5 M lithium triflate in PC between 1.8 V and 4.5 V for these samples. They are all very similar, and the first cathodic cycles show an irreversible lithium insertion. The amplitude and the position of these peaks seem to be correlated with the oxygen concentration used during the deposition. Figure 7.22 (d) shows the CV of a film produced at an oxygen content of 30 %: a very pronounced peak is observed on the first cycle at a potential close to 3 V. On the other hand, Figure 7.22 (a) shows the CV of a film produced at an oxygen content of 5 % : a less pronounced peak is observed at a lower potential (2.5 V). These results show that there is a correlation between the charge loss during the first cycle and the oxygen content in the plasma during deposition. The activity of oxygen decreases with decreasing oxygen content during the deposition. Michalak et al.[20] suggested that a possible reason might be a reaction with lithium to form LiO_2 for instance. This reaction would explain the high irreversibility of the intercalation process during the first scan. Such behaviour might be similar to the one observed with the sputtered tungsten oxide samples. This needs to be further investigated.

7.4.2.2 Optical properties

Figures 7.23 (a), (b) and (c) show the hemispherical transmittance and reflectance of $V_zTi_yO_x$ at different V/Ti ratios : 85 %, 47 % and 36 % respectively, in the as-deposited, coloured and bleached states.

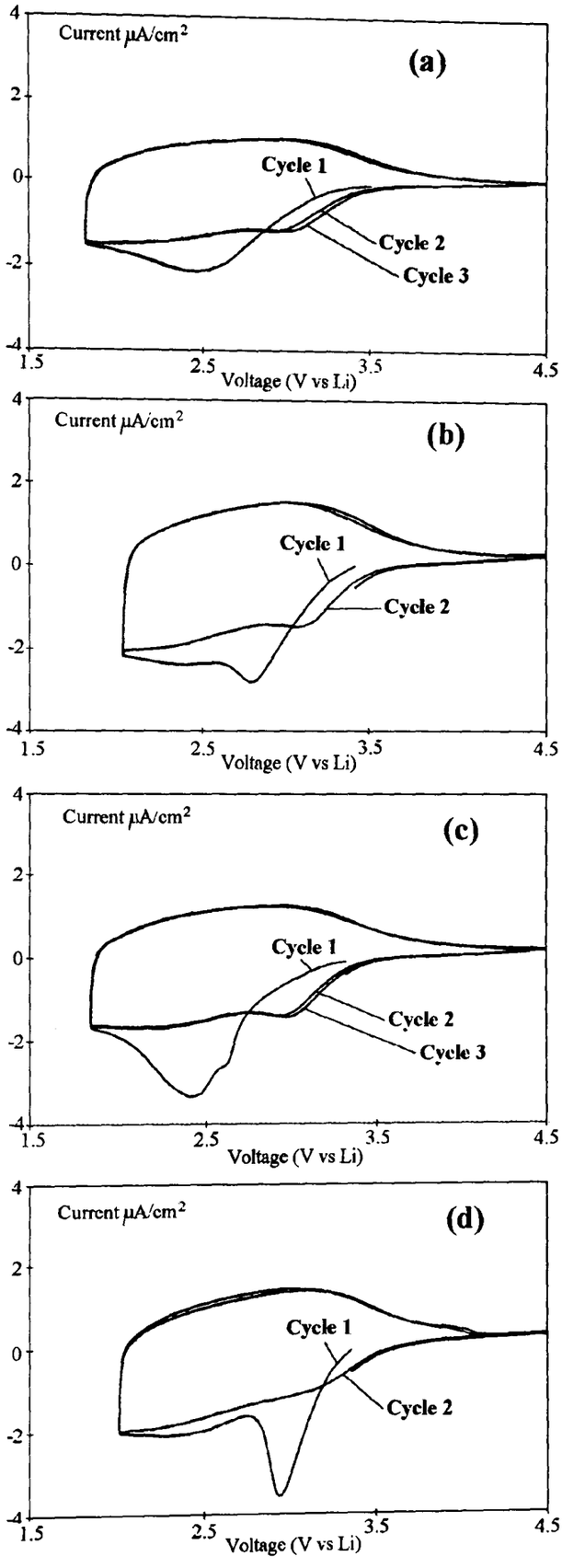

igure 7.22 : Cyclic voltammograms[20] of $V_{0.52}Ti_{0.48}O_x$ films deposited with an oxygen concentration of 5 % (a), 10 % (b), 20 % (c) and 30 % (d). Films produced at 7 mT, 2.75 W/cm^2 and 30 mn duration and cycled in 0.5 M lithium perchlorate, at 0.1 mV/s scan rate, 1 cm^2 working area.

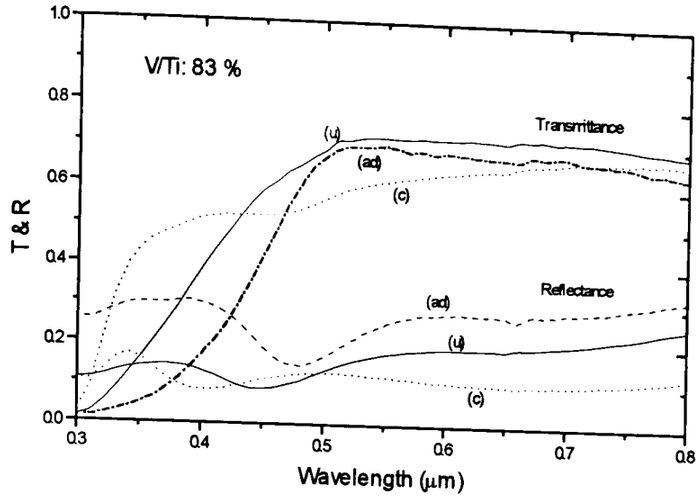

(a)

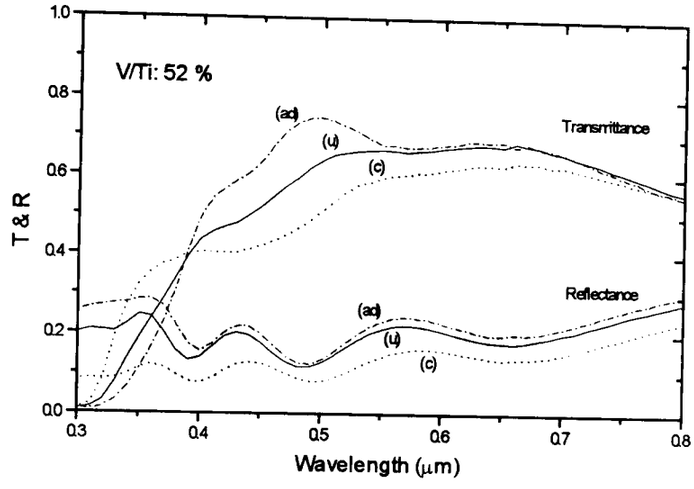

(b)

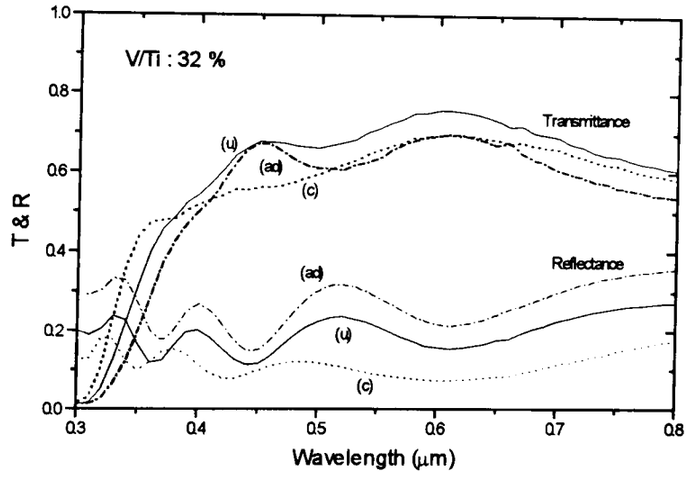

(c)

'igure 7.23 : Hemispherical transmittance and reflectance of $V_zTi_yO_x$ at different V/Ti ratios: (a) 83 %, (b) 52 % and (c) 32 %, in the as-deposited (ad), charged (c) and uncharged (u) states respectively. Films were produced at 3.75 W/cm^2, 7 mT, 20 % oxygen concentration and 30 mn duration.

In these figures, optical reflectance and transmittance measurements were carried out by taking the films out of the cell and placing them on the side of the sphere. They also include T_λ and R_λ of the ITO-coated glass substrate; e.g. the reflectance spectra shown in these figures are principally due to the ITO coating.

The reflectance of films at different V/Ti ratios does not vary very strongly. A modulation between $R_{v,u} = 0.20$ and $R_{v,ch} = 0.15$ can be observed for all films. Films are mainly transparent in the visible spectrum. Differences between the sets are due to different qualities of ITO.

On the other hand, transmittance modulation between the uncharged and charged states is seen to vary more strongly at the short wavelength edge. The shape of the spectra show a gradual evolution as the quantity of Li is inserted into the films. This indication of strong absorption at the material bandgap is also gradually seen as more Ti is incorporated into the mixed-oxide films.

Figure 7.24 shows the spectral absorption coefficient of $V_zTi_yO_x$ films at different ratios. These spectra are used to calculate the optical bandgaps using the method described in Chapter 4. Results for as-deposited films are shown in Figure 7.25. An apparent regression line has been fitted to guide the eye. It is clear from Figure 7.25 that there is an almost proportional shift in the optical bandgap energy upon an increasing Ti ratio, between pure VO_x (E_g = 2.26 eV) and pure TiO_x (E_g = 3.5 eV). These results are well below the optical bandgap of the ITO substrate used for these films ; E_g = 3.7 eV. The bandgap widening of $V_zTi_yO_x$ films clearly shows that the Ti ratio is effectively being proportionally incorporated into the film, making the sputtering method described earlier very reliable and efficient, and that films are effectively reaching a more neutral or titanium-like appearance.

Figure 7.26 shows the E_g modulation of $V_zTi_yO_x$ films in the as-deposited, charged and uncharged states, as a function of the V/Ti ratio. The colour appearance of the films is given in Table 7.7. The chromaticity ordinates of films with V/Ti $\leq$ 52 % show a totally neutral and colourless appearance in the uncharged state and a neutral grey appearance in the charged state. Above 52 % V/Ti ratio, films exhibit a clear yellow appearance in both uncharged and charged states.

Figure 7.27 shows the visible transmittance of $V_zTi_yO_x$ films in the uncharged and charged states respectively as a function of the V/Ti ratio.

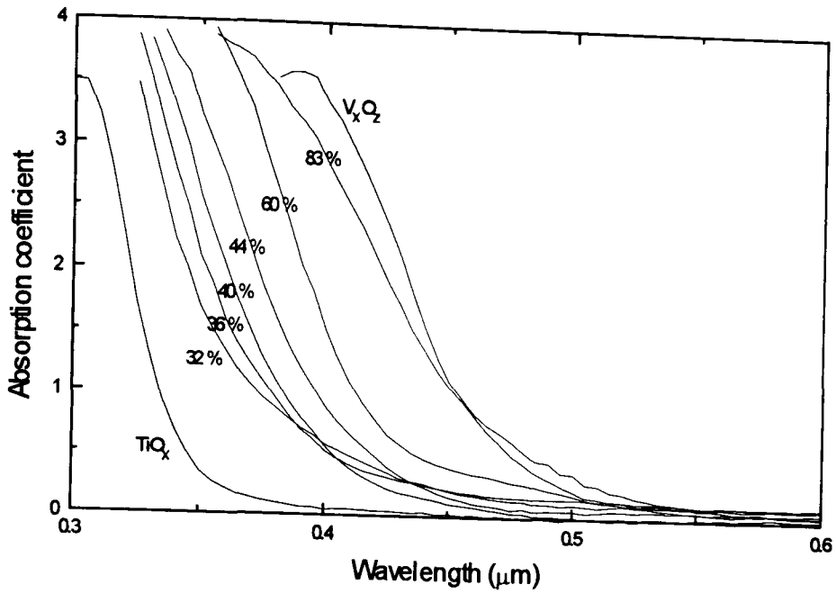

Figure 7.24 : Spectral absorption coefficient of as-deposited VO_x, TiO_x films and $V_zTi_yO_x$ films at different V/Ti ratios. Films were produced at 3.75 W/cm^2, 7 mT, 20 % oxygen concentration and 30 mn duration. Standard error on V/Ti ratio : ± 8 %.

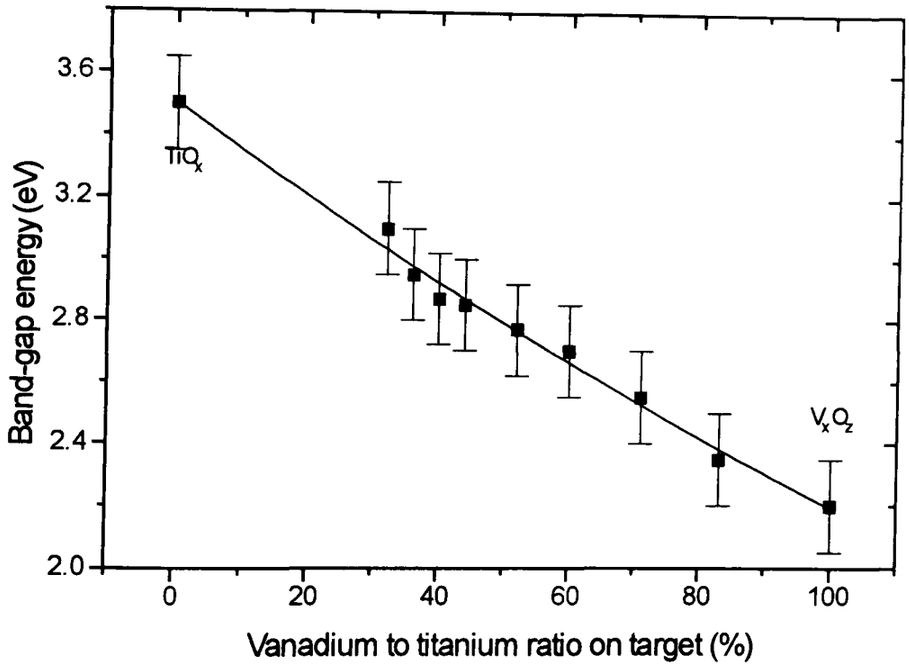

Figure 7.25 : Optical bandgap of as-deposited VO_x, TiO_x films and $V_zTi_yO_x$ films at different V/Ti ratios. Films were produced at 3.75 W/cm^2, 7 mT, 20 % oxygen concentration and 30 mn duration. Standard error on V/Ti ratio : ± 8 %.

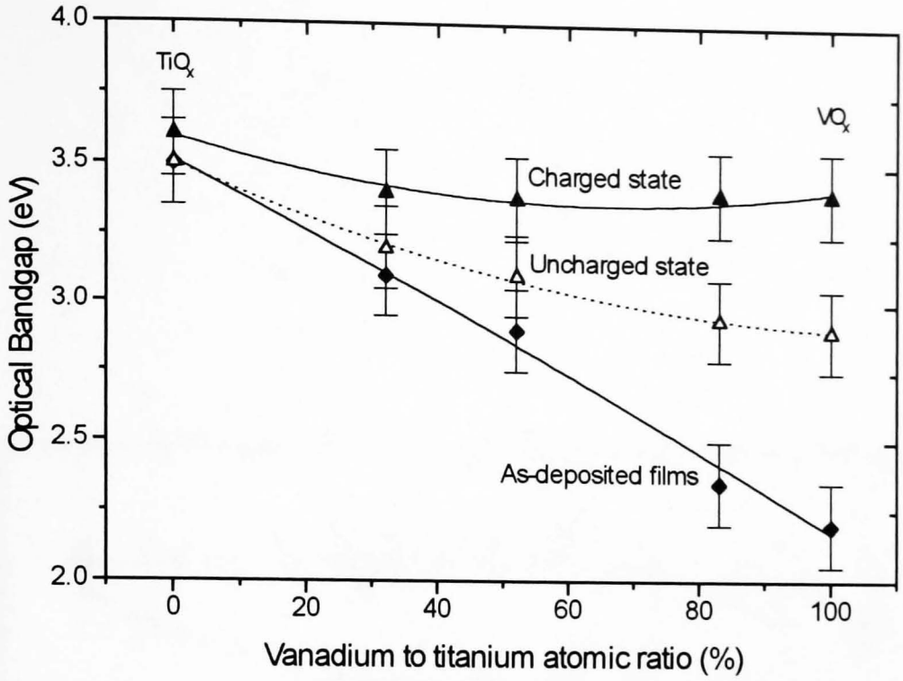

Figure 7.26 : Optical bandgap energies of $V_zTi_yO_x$ films in the as-deposited, charged and uncharged states as a function of V/Ti atomic ratios. Films were produced at 3.75 W/cm^2, 7 mT, 20 % oxygen concentration and 30 mn duration.
Standard error on V/Ti ratio : ± 8 %.

	Charged state Chromaticity coefficients X(red) / Y (green) / Z (blue)	**Uncharged state Chromaticity coefficients X(red) / Y (green) / Z (blue)**
Vanadium oxide	0.34 / 0.35 / 0.31	0.37 / 0.41 / 0.22
52 % vanadium	0.33 / 0.33 / 0.34	0.35 / 0.35 / 0.30
32 % vanadium	0.32 / 0.33 / 0.35	0.33 / 0.33 / 0.34
Titanium oxide	0.32 / 0.32 / 0.36	0.30 / 0.30 / 0.40

Table 7.7 : Chromaticity coefficients of VO_x and TiO_x films and of $V_zTi_yO_x$ films at different V/Ti ratios in the charged and uncharged states. Films were produced at 3.75 W/cm^2, 7 mT, 20 % oxygen concentration and 30 mn duration.

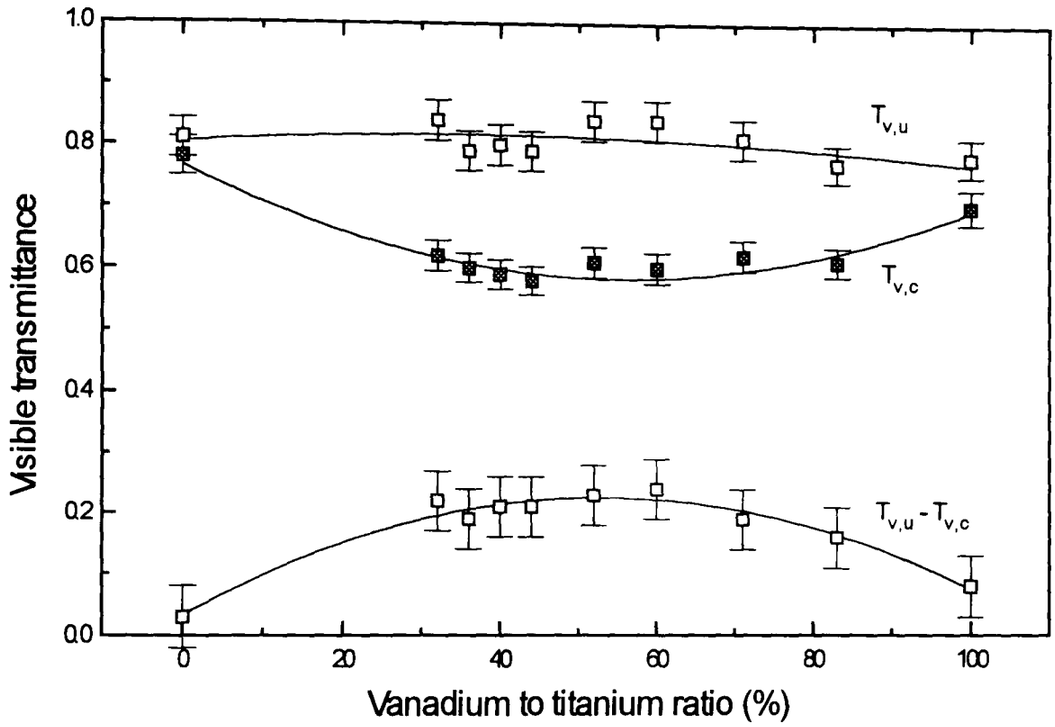

Figure 7.27: Visible transmittance of VO_x and TiO_x films and of $V_zTi_yO_x$ films at different V/Ti ratios in the charged and uncharged states. Films were produced at 3.75 W/cm^2, 7 mT, 20 % oxygen concentration and 30 mn duration.

Standard error on V/Ti ratio : ± 8 %.

Optical measurements including the transmittance properties of the ITO substrate were carried out with films placed inside the electrochemical cell. These results show that the uncharged state is transparent $T_{v,u} < 0.80$ at any V/Ti ratio, whereas $T_{v,ch}$ decreases upon a higher proportion of dopant in films. The difference between $T_{v,u}$ and $T_{v,ch}$ is shown in Figure 7.27 and a clear maximum is obtained at V/Ti = 50%. TiO_2 is a wide bandgap transition metal oxide and is oxygen-deficient when nonstoichiometric. Undoped thin films of TiO_2 are n-type semiconductors and are most stable as Ti^{+4}. Doped with pentavalent ions acting as a donor type, the conductivity of doped TiO_x has been reported to increase[21]. One can expect that doping with vanadium might introduce free carriers into the mixed-metal oxide and increase the light absorption into the visible region. It is obvious in Figure 7.27 that increasing concentration of dopant creates stronger absorption in the material. At V/Ti = 40 %, the absorption of the counter electrode layer is ($T_{v,u}$ - $T_{v,ch}$) = 0.2 for a charge transferred in the order of 40 $mC.cm^{-2}$.

7.5 Discussion and conclusions

Vanadium oxide and titanium oxide films have been separately deposited in order to gain an understanding of their electrochromic properties as a function of their R.F. magnetron sputtering parameters. Titanium oxide electrochromic properties were not strongly dependent on the process parameters, whereas VO_x showed a greater dependence. Both oxide films possessed the expected optical and electrochemical properties; TiO_x films can store a limited quantity of charge Q_{TiOx} = 13 $mC.cm^{-2}$, are very transparent in both charge and uncharged states $T_{v,u} \approx T_{v,ch} > 0.80$, and are very stable upon charge insertion/extraction; VO_x films store a much larger quantity of charge Q_{VOx} = 35 $mC.cm^{-2}$, $T_{v,u}$ and $T_{v,ch} > 0.70$, however the charge insertion /extraction is seen to evolve during the initial cycles.

Electrochromic R.F. magnetron sputtered mixed-metal oxides of vanadium and titanium produced in this work have been successfully deposited: films of all compositions exhibit electrochromism. The technique of making mixed-metal has been seen to be a reliable and efficient method of producing oxide films with different metallic ratios. One can use this technique for mixing more than 2 oxides. The addition of Ti in $V_zTi_yO_x$ has the

advantage of stabilising pure VO_x and, by creating more defects into the lattice, it increases the charge capacity. The $V_zTi_yO_x$ films optical bandgap is widened upon increasing incorporation of Ti, making films more neutral in appearance. However, the drawback is the rise of absorption of visible radiation due to a probable creation of free carriers. The choice for the optimum $V_zTi_yO_x$ film has to be a trade-off between the highest quantity of Ti and the minimum material requirement to be economically cheaper; the highest visible transmittance in the charged state and the highest charge capacity, to match counter electrode application. Table 7.8 presents the optical and electrochemical properties of a $V_{0.52}Ti_{0.48}O_x$ film which gives the best compromise for EC device needs.

Mixed oxides of vanadium and titanium are promising materials for transparent and colourless counter electrodes to be used with WO_3 electrochromic materials and lithium conducting electrolytes. This chapter presented the end of thin films deposition. Three primary layers have been R.F. magnetron sputtered, optimised and characterised for a designated application in an all-solid-state device. The next chapter presents the fabrication and characterisation of laminated electrochromic devices made with these different films.

	$V_{0.52}Ti_{0.48}O_x$ film as-deposited / uncharged / charged
T_v	0.88 / 0.82 / 0.62
Optical bandgap (eV)	2.9 / 3.1 / 3.4

Q ($mC.cm^{-2}$)	43 ± 3
Film thickness (nm)	82 ± 10
η_c ($cm^2.C^{-1}$) **Visible range**	2.8 ± 0.3
Switching potentials	+ 1 V / + 4 V vs Li
Charging time (s)	< 120
Lifetime (cycles)	> 500

	Optimised R.F. magnetron sputtering parameters
Target material **Target size**	Ti and V (< 99.9 % purity) 15.2 cm diameter
Power density **Sputter pressure** **Oxygen content** **Temperature**	2.75 W/cm^2 7 - 10 mT 20 % ~ 180 °C
Time	30 mn

Table 7.8 : Summary of the electrochromic properties and of optimised deposition process parameters of R.F. magnetron sputtered $V_{0.52}Ti_{0.48}O_x$ film under lithium intercalation/deintercalation.

PART C

ELECTROCHROMIC DEVICES

Chapter 8

FABRICATION AND CHARACTERISATION OF EC DEVICES

8.1 Introduction

The need for solar-gain control advanced glazings, such as electrochromic smart windows in particular, was reviewed in the first Chapters. Different electrochromic devices have been considered and the 5-layer laminated design retained our attention because of its high potential for commercial development. This Chapter presents the results obtained when investigating the performance of different prototype electrochromic devices comprising electrochromic materials produced in this work. Optimised electrochromic tungsten oxide films were used as the working electrode and two potential counter electrode materials, the optimised nickel oxide and vanadium/titanium oxide films, are evaluated as possible ion storage layers in electrochromic devices. Prototypes were assembled with a lithiated polymer electrolyte and switched between safe potentials. General characteristics have been identified for comparison between the different devices to assess their potential applicability for commercial smart windows devices.

8.2 The electronic and ionic transparent conductors

Both electronic and ionic conductors were supplied by collaborating laboratories. This Section is a description of their principal physical and optical properties. The production of these materials is also briefly reviewed.

8.2.1 The transparent electrical conductor

The ITO coated glass used in this work was provided by a collaborative laboratory[1].

ITO can be deposited by many techniques, usually done by magnetron sputtering onto a heated glass substrate[2] (~ 300°C) or by spray hydrolysis (pyrolysis)[3], which is simpler and cheaper. The properties of ITO are based on the quantity of doping and the thickness of the deposited layer. A low thermal emissivity is obtained only at thicknesses above 0.2 μm[4]. If the coating thickness equals a fraction of the wavelength for visible light, optical interference will appear, and any minor variations in thickness will cause iridescence. The thickness control is therefore of great importance during the deposition process.

The ITO used in this thesis was prepared by R.F. magnetron sputtering from a $(In_{0.9}Sn_{0.1})_2O_3$ target. Studies[5,6] have shown that electrical properties are sensitive to tin content and optimisation was obtained for a tin to indium ratio of 1 to 9.

The investigation of sputtering-deposition conditions have indicated[7,8] that the substrate temperature is the critical deposition parameter for both conductivity and visible transmittance performance of the coating. The carrier concentration and the mobility are increased with increasing temperatures, mainly up to 300 - 350 °C. As a consequence, electrical conductivity is also increased. Above this temperature, the carrier concentration will be over 10^{21} cm^{-3}, therefore decreasing the visible transmittance of the film.

When sputtering from an oxide target, resistivity is also seen to increase with oxygen content. Best results are obtained at an oxygen to argon content in the range 0.05 to 0.5 %. The sputtering rate has to be low, and optimum electrical performance seems to be reached at about 9 nm per minute. In the same way, sputtering pressures are giving best electrical properties in the range 4-8 mT.

The film thickness does not have any strong effect on the conductivity (when above 20 nm) but will be directly related to a decreasing visible transmittance (when above 100 nm).

Figure 8.1 shows a typical representation of optical properties (0.3 - 20 μm) of a 0.2 μm sputter-coated ITO film material used in this work.

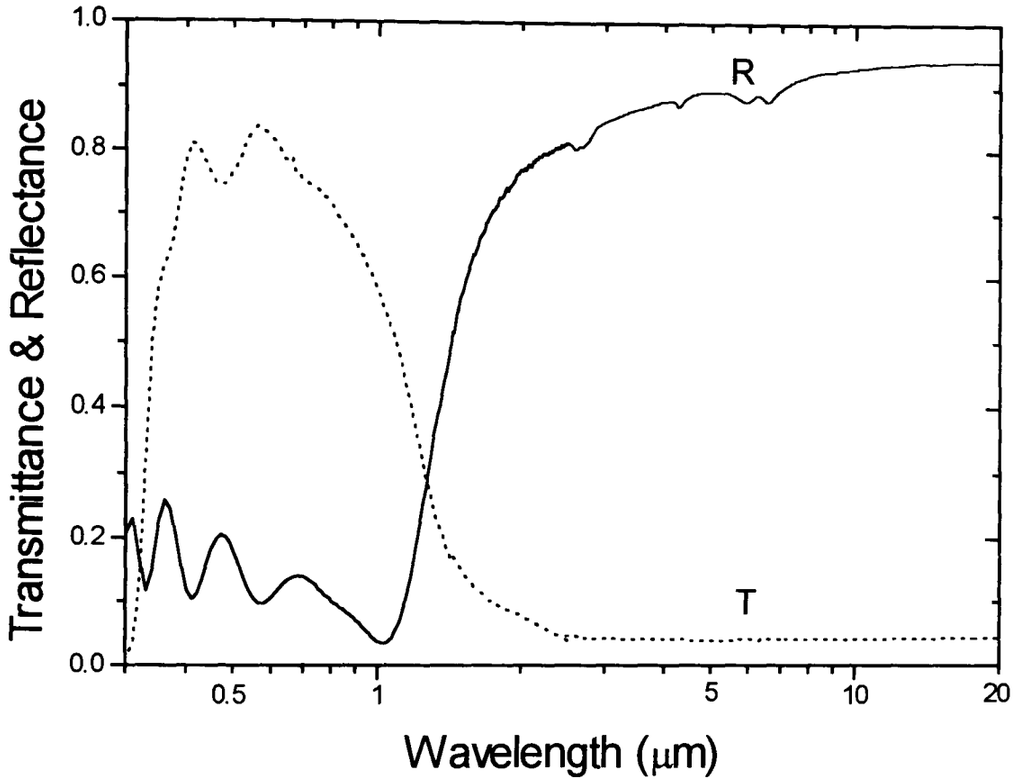

Figure 8.1 : Hemispherical transmittance and reflectance (0.3 - 20 μm) of a 10 Ω/□ ITO coated glass. $T_s = 0.70$, $T_v = 0.81$, $R_s = 0.21$, $R_v = 0.12$, $\varepsilon_{300°K} = 0.11$.

8.2.2 The PAAUA polymeric transparent ionic conductor

The polymer network is based on a mixture of two acrylate monomers which are polyether(1) acrylate and aliphatic-urethane (1) acrylate (PAAUA) at a ratio of 0.4[9].
They are shown in Figure 8.2 (a) and Figure 8.2 (b) respectively. The chain of the network will be formed by carbon to carbon cross-linking. The acrylate C=C bonds of each polymer can easily cross-link with one another. The structure of this polymer shows several ether-oxygen groups used as donor sites for electrons to favour ionic conductivity.
To improve the conductivity of the solid electrolyte (10^{-5} to 10^{-6} $S.cm^{-1}$), lithium salt is added in the form of lithium trifluoromethansulfonate ($LiCF_3SO_3$)[10]. Lithium triflate is a transparent and stable electrochemical electrolyte. The lithium ion is an acceptor and is solvated by coordination with an oxygen. As with PEO polymer[11], the lithium ion will hop between available sites and will be responsible for the conduction.
The characterisation of the polymer has to include the addition of a plasticizer that does not lower the conductivity and gives a good electrochemical stability. In the present case, glymes which are in the family of ethyl dimethyl ether have been used to polymerise this ionic-conducting solid electrolyte. Conductivity in the range 10^{-4} - 10^{-5} $S.cm^{-1}$ is obtained[12]. At temperatures between -20°C to 85°C, the ionic conductivity of the polymer remained within the above range and mechanical and adhesive properties also seemed to be preserved[12,13].
The film sandwiched between the electrochromic layer and the ion storage layer is about 1mm thick. Figure 8.3 shows the optical transmittance of the polymer in the solar range of the spectrum. The film is almost invisible to the human eye and a sudden increase in absorption is seen for wavelengths higher than 2 μm, and 90 % of the infrared radiation is absorbed by the polymeric layer.
Finally, in practical applications, the chemical and electrochemical stability of the polymer electrolyte is of crucial importance. Figure 8.4 shows the cyclic voltammogram of the polymerised PAAUA between two platinum electrodes at a voltage range 1 V - 4 V vs Li. It is clear from this figure that the PAAUA electrolyte shows very little electrochemical activity within the potential range.

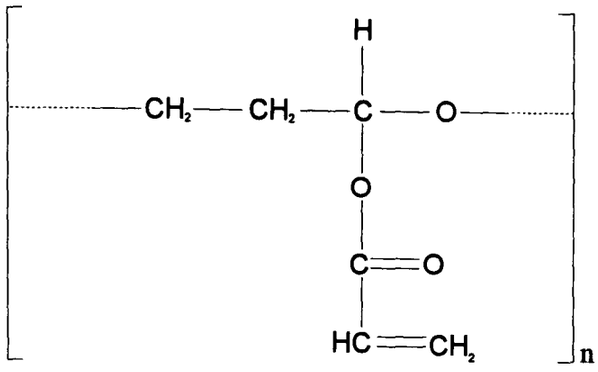

Figure 8.2 (a) : Backbone structure of polyether-1 acrylate.

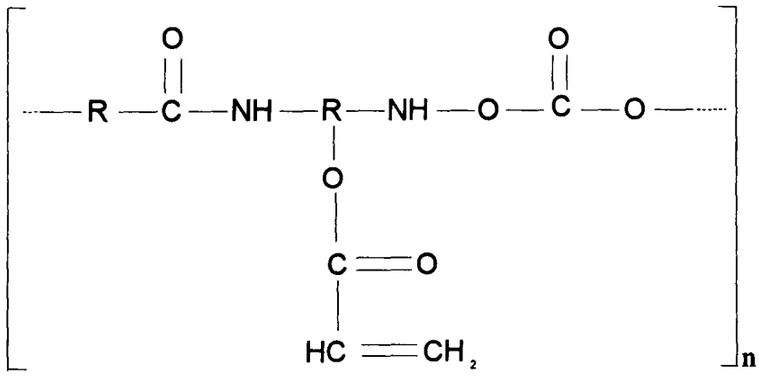

Figure 8.2 (b) : Backbone structure of aliphatic-urethane (1) acrylate.

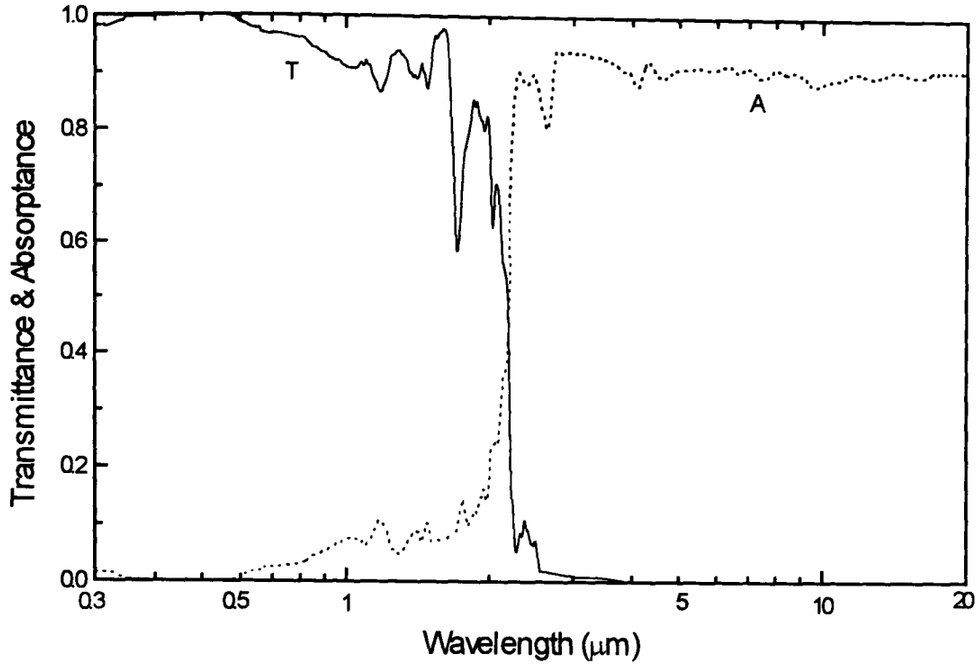

Figure 8.3 : Hemispherical transmittance and absorptance (0.3 - 20 μm) of the polymer electrolyte. $T_v = 0.99$, $T_s = 0.90$, $\varepsilon_{300°K} = 0.89$.

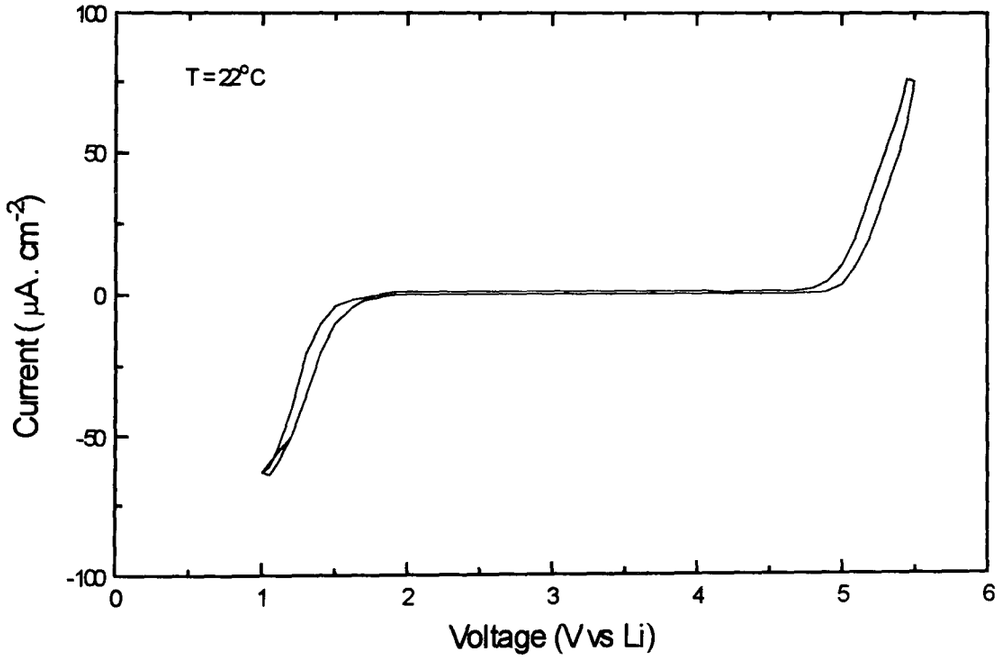

Figure 8.4 : Cyclic voltammogram of the PAAUA polymer measured between two platinum electrodes at 10 mV/s, and at room temperature.

The limiting potential is 5 V, which is beyond the electrochemical limits of the electrochromic electrodes[13]. Such stability remains very low at temperatures below 60°C[13]. The PAAUA polymer seems to fulfil the temperature stability and potential limits requirements for EC device applications.

8.3 Assembling electrochromic devices

8.3.1 Laminated EC design

In this section, the device assembly procedure is described. Figure 8.5 shows a schematic cross-section of the design of the prototype EC device assembled in this work. This device is composed of two electrochromic layers facing each other : a WO_3 film deposited onto an ITO-coated glass, and an ion storage layer which is either a NiO_x or a $V_zTi_yO_x$ film. These layers can be either active, such as NiO_x, or be purely a charge-reserve layer, such as $V_zTi_yO_x$. Each of these layers has been coated on a 5 x 5 cm^2 masked ITO substrate, leaving an uncoated area (approximately 0.5 x 5 cm^2) for electrical contact. To improve these contacts, the ITO uncoated area and the glass substrate (see Figure 8.5) are covered with a copper tape coated with a highly conducting adhesive[14]. The two pieces of coated glass are fixed together using a 1 mm thick double sided-adhesive tape[15]. This tape is 0.5 cm wide and is placed all around the edges of the electrochromic layer, leaving a cavity between the two panes. This cavity is filled with the PAAUA ion-conducting polymer using a syringe. To further improve the air tightness of the cavity, and to protect the polymer from moisture, a layer of silicon sealant is spread on the edge of the EC device.

8.3.2 The working and counter electrode states on device assembly

The optical modulation of the EC device depends on the amount of charge that is reversibly transferred between the WE (working electrode : WO_3) and CE (counter electrode). This charge is limited by the charge capacity of both electrodes.

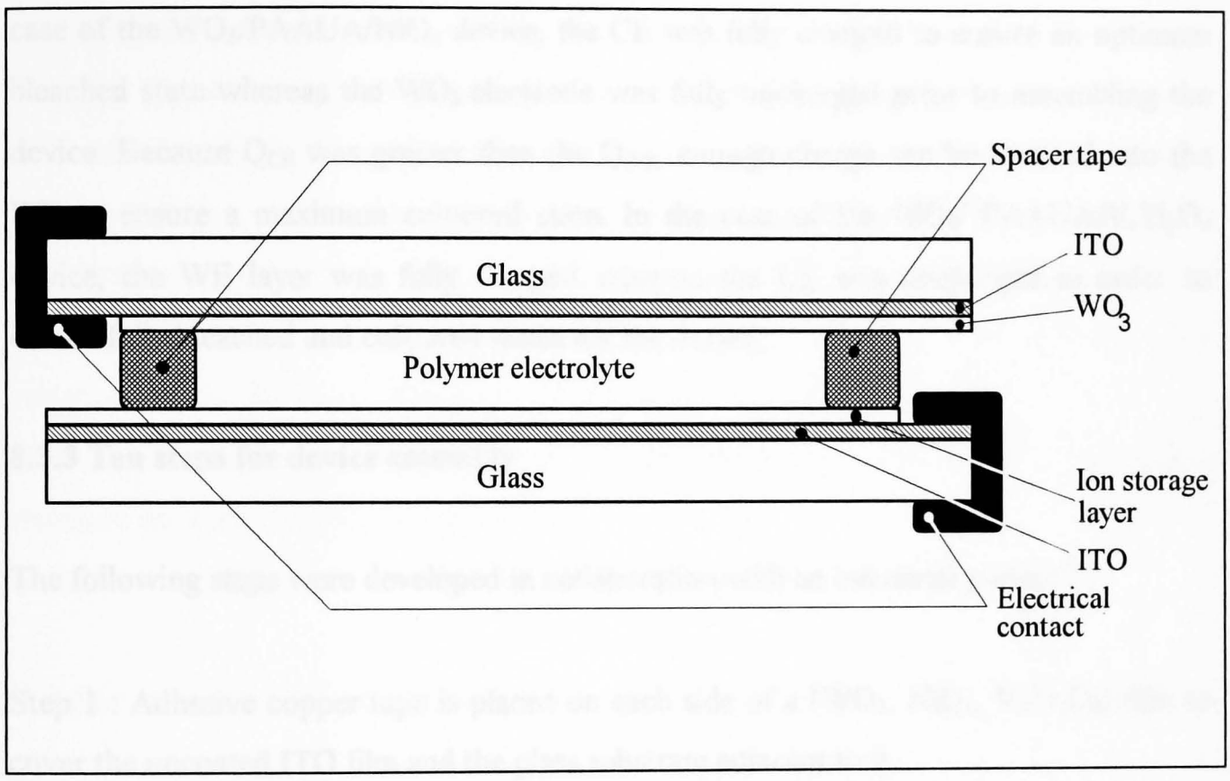

Figure 8.5 : Cross-section of the laminated electrochromic device design.

Care has to be taken to have an optimum balanced system, e.g. the charge transferred between the electrodes should not be limited by the charge capacity of one of the layers. Ideally, the full charge capacity of the two layers should be utilised in order for the electrochromic device to be fully bleached and coloured[16]. This problem is important when using an active CE such as NiO_x. It is difficult to balance both electrodes. However, as a way to ensure optimum bleached and coloured states, the counter electrode was chosen with higher charge capacity (Q_{CE}) than the Q_{WO3} counterpart. In the case of the WO_3/PAAUA/NiO_x device, the CE was fully charged to ensure an optimum bleached state whereas the WO_3 electrode was fully uncharged prior to assembling the device. Because Q_{CE} was greater than the Q_{WE}, enough charge can be inserted into the WE to ensure a maximum coloured state. In the case of the WO_3/ PAAUA/$V_zTi_yO_x$ device, the WE layer was fully charged whereas the CE was uncharged in order to ensure fully bleached and coloured states for the device.

8.3.3 Ten steps for device assembly

The following steps were developed in collaboration with an industrial partner[17].

Step 1 : Adhesive copper tape is placed on each side of a (WO_3, NiO_x, $V_zTi_yO_x$) film to cover the uncoated ITO film and the glass substrate adjacent to it.

Step 2: The WE and CE films are cycled in 1M lithium triflate between +1 V and + 4 V until a reversible reaction process is obtained.

Step 3 : When a reversible reaction is reached, films are fully charged or uncharged as follows : for the WO_3/PAAUA/$V_zTi_yO_x$ device, the WO_3 layer is fully charged whereas the $V_zTi_yO_x$ film is uncharged; and for the WO_3/PAAUA/NiO_x device, the WO_3 layer is uncharged whereas the NiO_x film is fully charged.

Step 4 : Films are then dry-blown with nitrogen. This is to ensure a good adhesion of the electrolyte to the surface of the thin films as well as ensuring good adhesion of the double sided tape.

Step 5 : A (3.5 x 4.5 cm^2) piece of double-sided tape is cut in the middle of a (4 x 5 cm^2) piece, leaving a 0.5 cm wide squared frame of the material. This is fixed onto one of the two electrodes. The two pieces of coated glass are then firmly fixed together, creating an air-tight cavity between them.

Step 6 : The PAAUA polymer is outgassed for one hour under vacuum (see Chapter 4, Section 4.2.2) to prevent the formation of gas bubbles during curing.

Step 7 : Unpolymerised polymer is injected into the cavity using a syringe. A second unloaded syringe is also used to allow air to escape.

Step 8 : The device is then left for 12 hours without curing to allow the tape to swell with the electrolyte. Then some more PAAUA electrolyte can be added to prevent bubbles forming and ease the tensile stress which may be caused by the electrolyte shrinking upon curing.

Step 9 : The PAAUA electrolyte is cured or polymerised for 10 minutes under ultra-violet radiation (88 $W.m^{-2}$, Philips) with the CE uppermost.

Step 10 : Finally the device is sealed around the edges with an epoxy sealant to prevent moisture entering through the tape.

8.4 The WO_3/PAAUA/NiO_x device

A tungsten oxide - nickel oxide complementary device using the PAAUA polymeric electrolyte was assembled. This section presents the optical and voltammetric characteristics of the glass-ITO/WO_3/PAAUA/NiO_x/ITO-glass prototype.

8.4.1 Cyclic voltammetry

The long-term performance of EC devices depends critically on the stability of the electrochromic WE and CE layers. A triangular waveform (- 1.5 V, + 1.5 V) with a ramp rate of 10 mV/s was used to cycle the device between coloured and bleached states. Figure 8.6 shows different cyclic voltammograms (1, 3, 10 and 20) of the WO_3/PAAUA/NiO_x prototype. One can see that the current and consequently the charge injected into the CE in the anodic process is decreasing as the cycling continues.

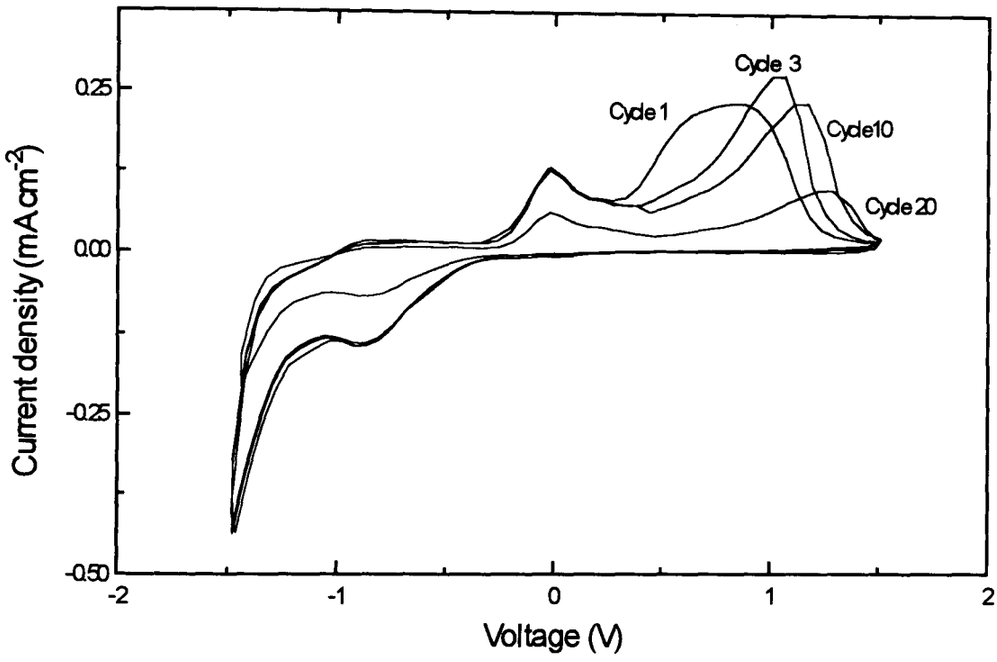

Figure 8.6 : Cyclic voltammograms of the WO_3/PAAUA/NiO_x electrochromic device at a scan rate of 10 mV/s between +/- 1.5 V.

Gas evolution was also observed after the third switching cycle, causing delamination. It disappeared after a few hours when no potential was applied to the device. It is supposed that the gas bubbles were dissolved back into the polymer. However, it reappeared after the fifth switching cycle and irreversibly stayed inside the device. After 20 cycles the device was almost completely delaminated.

For applications in windows, it is necessary to have long-term stability in excess of several thousand cycles. Several modes of degradation are possible: these include the trapping of charge due to irreversible chemical reactions between WE and CE and chemical reactions of films which cause delamination and cracking of films under insertion/extraction of ions. In the present case, it is clear that a reaction occurs at the surface of the NiO_x electrode under lithium intercalation/deintercalation. Delamination is clearly observed on the CE side of the device. The anodic peak at 0.75 V moves to higher voltages as cycling is carried on. The quantity of charge inserted into both WE and CE layers is almost constant over the 10 first cycles and is equal to 15 mC/cm^2. A charge imbalance is noticed and is equal to about 10 % of the overall charge moved between the two layers. At higher switching cycles, the charge inserted into the CE layer in the cathodic reaction is seen to start decreasing, and above 20 cycles the delamination is such that the intercalation/deintercalation process reaction is drastically reduced.

8.4.2 Optical measurements

The spectral transmittance of the WO_3/PAAUA/NiO_x device in the initial state (after assembling) and in both coloured and bleached states on the 3rd cycle is shown in Figure 8.7. The prototype exhibits a visible transmittance modulation of about 40 %. The chromaticity ordinates show a very neutral appearance of the device in the bleached state whereas the coloured state appears clearly blue. In the solar range, the transmittance modulation of the device is of the order of 52 %.

Figure 8.8 shows the visible transmittance modulation of the prototype as a function of the applied voltage. After the 10th switching cycle, optical properties measurements were difficult to carry out due to bubble formation inside the device.

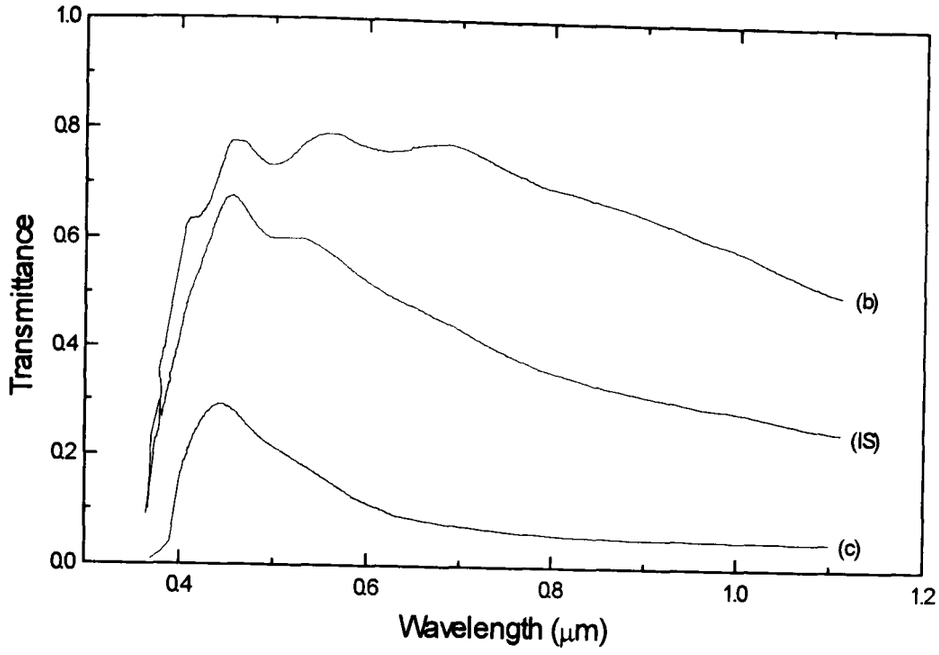

Figure 8.7 : Spectral transmittance of the WO_3/PAAUA/NiO_x electrochromic device in the initial (IS) bleached (b) and coloured (c) states on the 3rd cycle. Optical properties : $T_{v,is}$ = 0.59, $T_{s,is}$ = 0.36, $T_{v,b}$ = 0.75, $T_{s,b}$ = 0.60, $T_{v,c}$ = 0.24, $T_{v,c}$ = 0.08. Chromaticity ordinates: X_b = 0.32, Y_b = 0.33, Z_b = 0.35, X_c = 0.24, Y_c = 0.25, Z_c = 0.51.

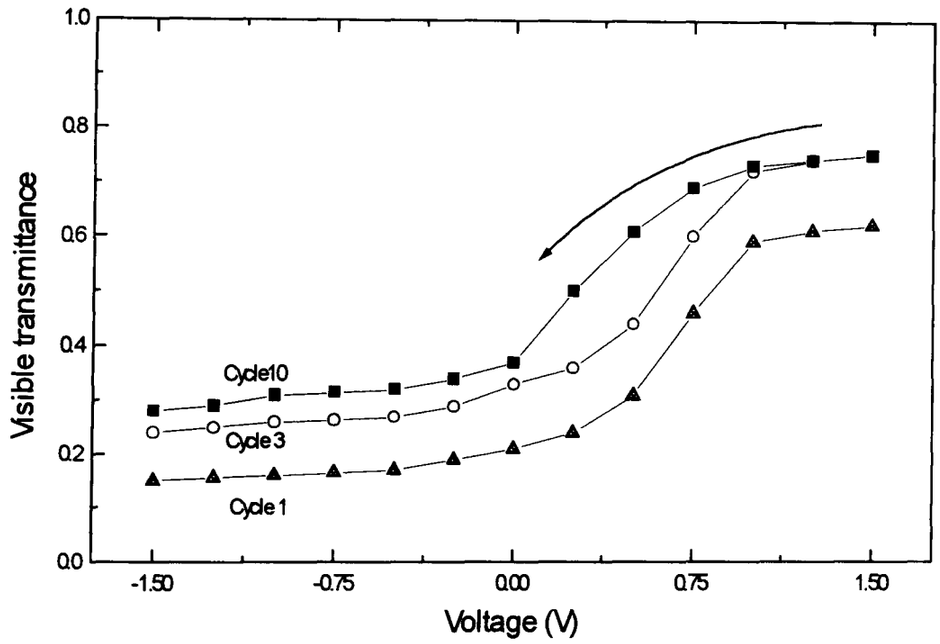

Figure 8.8 : Visible transmittance of the WO_3/PAAUA/NiO_x device as a function of the applied potential for different cycles, at 5 mV/s scan rate, ± 1.5 V.

However, one can see that $T_{v,b}$ of the device reaches an optimum value of 0.75 after the 3rd cycle, whereas the coloured state evolves to clearer appearances after each cycle. Between the 1st and 10th switching cycle, $T_{v,c}$ increases from 0.15 to 0.3 respectively. The visible coloration efficiency of the device is equal to 33 cm^2/C on the 3rd cycle. The switching time was greater than 5 minutes and a memory higher than 12 hours in both states was measured.

Figure 8.9 shows a photograph of the delaminated WO_3/PAAUA/NiO_x device.

The failure of NiO_x films under lithium ion insertion/extraction was previously observed in Chapter 6 using a liquid electrolyte. The failure of the NiO_x film under lithium ions does not make this system attractive for future development of electrochromic windows.

8.5 The WO_3/PAAUA/$V_zTi_yO_x$ device

Improved smart window device performance has been demonstrated with the glass-ITO/WO_3/PAAUA/$V_zTi_yO_x$/ITO-glass configuration. Different devices have been assembled using optimised vanadium/titanium mixed-metal oxide films produced in Chapter 7 as a passive ion-storage layer. $V_zTi_yO_x$ films used were made with an atomic ratio of 48 % titanium and 52 % vanadium. This Section presents the results obtained for an EC device exhibiting best electrochromic properties.

The optical and electrochemical properties of this device are compared with a glass-SnO_2:F/WO_3/PAAUA/$V_zTi_yO_x$/SnO_2:F-glass device produced by a collaborating laboratory. The polymer used in both devices is the same. The WE and CE layers of this latter device were deposited using similar R.F. magnetron sputtering conditions and the V to Ti ratio of the ion-storage layer is close to the ratio used for the CE described in this thesis. The only difference is the use of a SnO_2:F electron conducting layer, or K-Glass™, (see Chapter 1) instead of ITO. The working area of the devices is equal to approximately 10 cm^2 (3 x 3.3 cm^2) for the glass-ITO/WO_3/PAAUA/$V_zTi_yO_x$/ITO-glass system and 64 cm^2 (8.3 x 7.7 cm^2) for the glass-SnO_2:F/WO_3/PAAUA/$V_zTi_yO_x$/SnO_2:F-glass system.

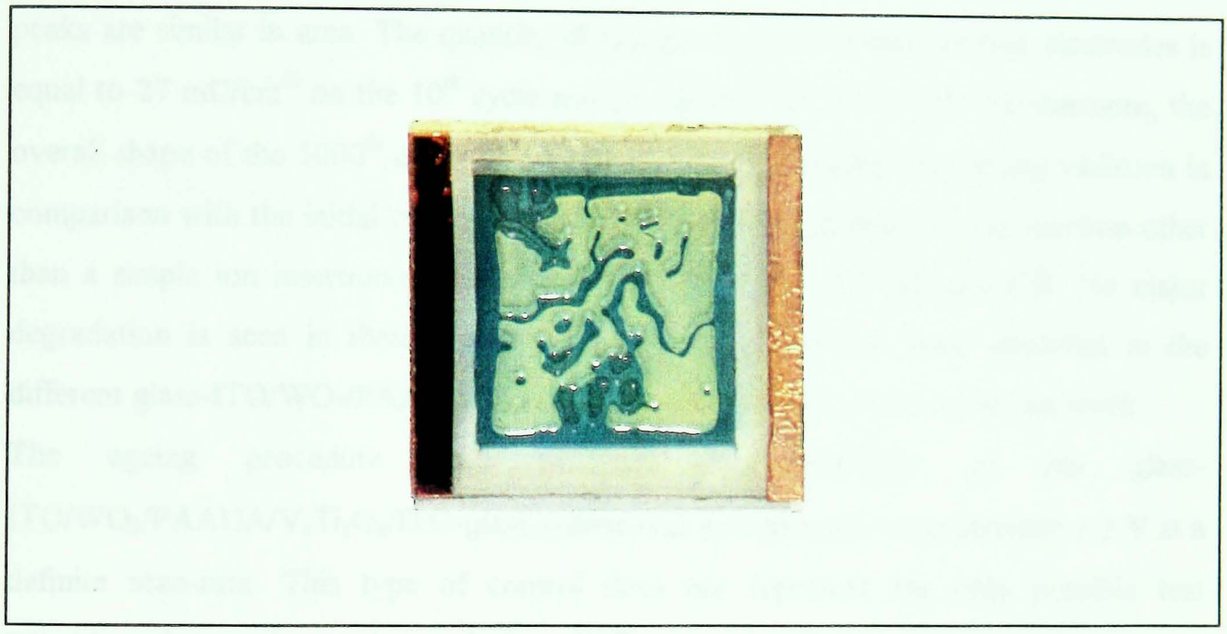

Figure 8.9 : The delaminated WO_3/PAAUA/NiO_x device after 30 switching cycles. The photographs show the actual size of the prototype.

8.5.1 Cyclic voltammetry

Several glass-ITO/WO_3/PAAUA/$V_zTi_yO_x$/ITO-glass EC devices have been assembled in this work and were switched between ± 3 V at a scan rate of 20 mV/s using the equipment described in Chapter 4. They all exhibited similar features in their electrochemical behaviour throughout the switching cycles. Figure 8.10 shows the 10^{th} and the 5000^{th} cyclic voltammograms of glass-ITO/WO_3/PAAUA/$V_zTi_yO_x$/ITO-glass. The ionic intercalation/extraction process between WE and CE layers is seen over each of the two voltammograms to be very reversible i.e. the area of both cathodic and anodic peaks are similar in area. The quantity of charge moved between the two electrodes is equal to 27 mC/cm^{-2} on the 10^{th} cycle and 24 mC/cm^{-2} on the 5000^{th}. Furthermore, the overall shape of the 5000^{th} cyclic voltammogram does not show any strong variation in comparison with the initial cyclic voltammogram, which suggests that no reaction other than a simple ion insertion/extraction process occurs at both WE and CE. No major degradation is seen in these results and no delamination has been observed in the different glass-ITO/WO_3/PAAUA/$V_zTi_yO_x$/ITO-glass devices produced in this work.

The ageing procedure used to test the durability of the glass-ITO/WO_3/PAAUA/$V_zTi_yO_x$/ITO-glass system was a continuous ramp between ± 3 V at a definite scan-rate. This type of control does not represent the only possible test procedure that can be applied to devices. Different types of signal can be used to control the ionic transfer inside the EC device. For instance, square potentials can be used instead of triangular waveforms, and can also include a relaxing time between the application of colouring and bleaching potentials. This latter control procedure has been used with glass-SnO_2:F/WO_3/PAAUA/$V_zTi_yO_x$/SnO_2:F-glass devices. The colouring and bleaching potentials have been applied for periods of time ranging from 30s to 120s with a 30s relaxing period.

Figure 8.11 shows the cyclic voltammograms (using a triangular potential) of a glass-SnO_2:F/WO_3/PAAUA/$V_zTi_yO_x$/SnO_2:F-glass device after 50 cycles and after 250000 cycles (using squared potential and relaxing time). The quantity of charge transferred is 21 mC/cm^2 after 50 cycles and 14 mC/cm^2 after 250000 cycles. The shape of the voltammograms seem similar to the shape of $V_zTi_yO_x$ film shown in Figure 7.20.

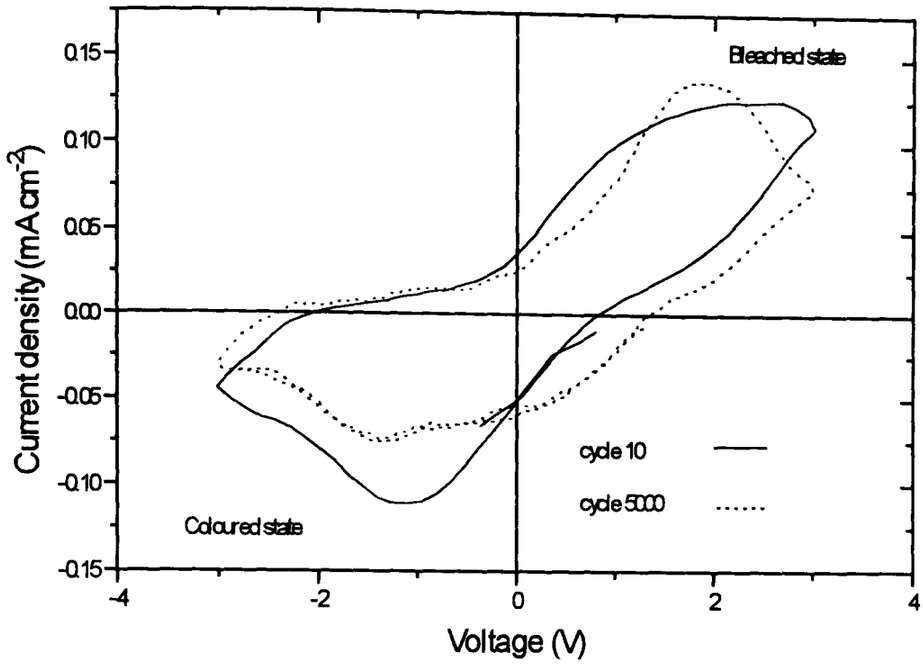

Figure 8.10 : Cyclic voltammogram 10 and 5000 of a 10 cm^2 glass-ITO/WO_3/PAAUA/$V_zTi_yO_x$/ITO-glass device at 20 mV/s scan rate.

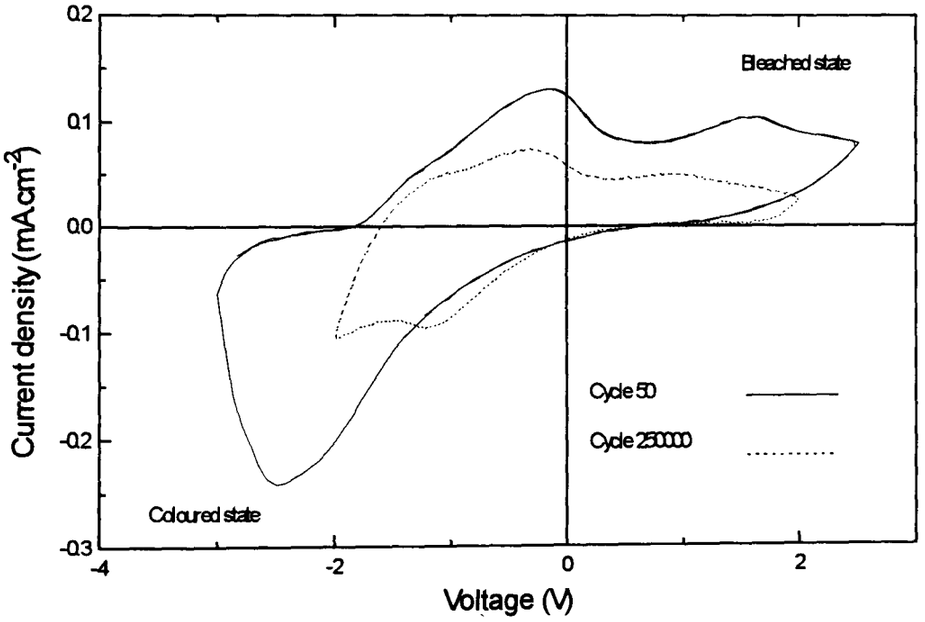

Figure 8.11 : Cyclic voltammograms (triangular potential) of a 64 cm^2 glass-SnO_2:F/WO_3/PAAUA/$V_zTi_yO_x$/SnO_2:F-glass device at 20 mV/s after 50 cycles and after 250000 cycles (square potential and relaxing time).

Over continuous switching cycles, charge is being irreversibly inserted inside CE and WE layers, which explains the smaller anodic and cathodic peaks of cycle 250000. If no delamination was observed, a strong edge-effect appeared during the ageing. The effect makes the edge of the device more brown in colour. However, delamination started to appear on the edge when a continuous slow scan-rate ramp (10 mV/s) was applied to the system. After 5 cycles, the delamination had irreversibly reduced the effective working area of the device to about 38 cm^2 in the middle. On the contrary, no delamination appears on a 50-cycle aged device. This shows the limits of the electrochromic performance of a smart window device when controlled with different waveforms.

8.5.2 Optical properties

The optical properties measurements of all solid-state devices in a spectrophotometer can be carried out with either the WE or CE facing the incident beam. Figure 8.12 shows the variation of spectral absorptance of a glass-SnO_2:F/WO_3/PAAUA/$V_zTi_yO_x$/SnO_2:F-glass device in the bleached and coloured states measured with the WE and CE facing the beam. The device was bleached at + 2.5 V for 100 s and coloured at - 3 V for 120s. The optical properties of this device are summarised in Table 8.1. It is clear from these results that the solar absorptance is slightly greater when the WE is facing the beam. For energy-efficient glazings, solar absorptance by the EC-device layers has to be minimised and therefore it seems better for the CE layer to face the incident radiation. As a consequence, all optical properties measurements are being carried out with the CE facing the spectrophotometer beam.

The total hemispherical spectral transmittance properties of the glass-ITO/WO_3/PAAUA /$V_zTi_yO_x$/ITO-glass and glass-SnO_2:F/WO_3/PAAUA/$V_zTi_yO_x$/SnO_2:F-glass devices are shown in Figure 8.13 and Figure 8.14 respectively, in the bleached and coloured states.

The total hemispherical spectral reflectance properties of the glass-ITO/WO_3/PAAUA /$V_zTi_yO_x$/ITO-glass and glass-SnO_2:F/WO_3/PAAUA/$V_zTi_yO_x$/SnO_2:F-glass devices before and after their respective ageing are shown in Figure 8.15 and Figure 8.16 respectively, in the bleached and coloured states.

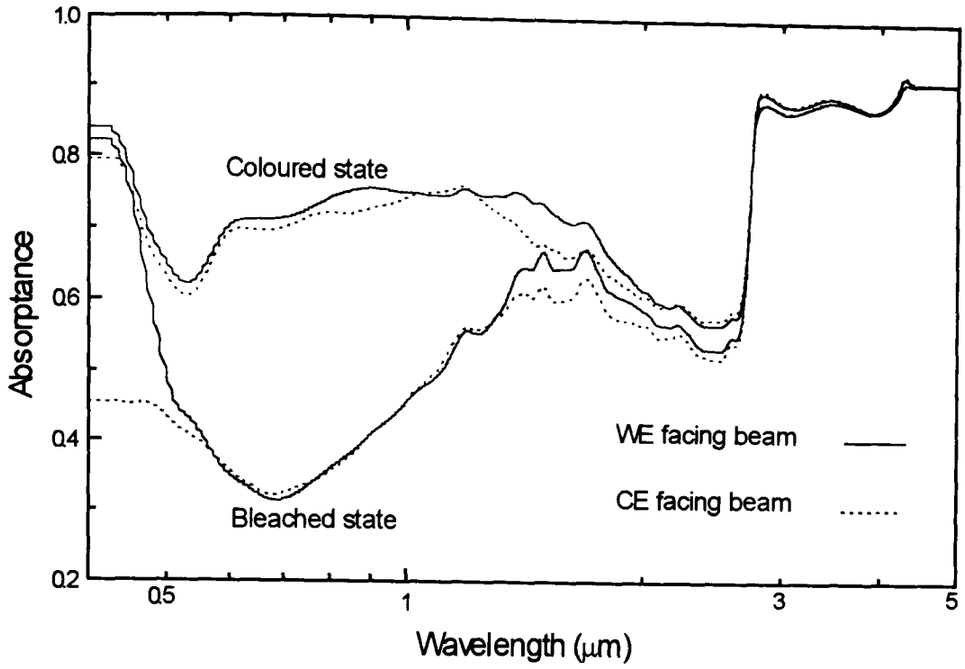

Figure 8.12 : Total hemispherical spectral absorptance of both glass-SnO_2:F/WO_3/PAAUA/$V_zTi_yO_x$/SnO_2:F-glass in the bleached and coloured states measured with the WE and the CE layer facing the beam . The device was bleached at + 2.5 V for 100 s and coloured at - 3 V for 120s.

Solar range	CE / WE facing incident beam	Visible range	CE / WE facing incident beam
$T_{s,b}$	0.41 / 0.41	$T_{v,b}$	0.50 / 0.50
$T_{s,c}$	0.18 / 0.18	$T_{v,c}$	0.27 / 0.27
$R_{s,b}$	0.15 / 0.14	$R_{v,b}$	0.12 / 0.11
$R_{s,c}$	0.13 / 0.11	$R_{v,c}$	0.09 / 0.07
$A_{s,b}$	0.44 / 0.45	$A_{v,b}$	0.38 / 0.39
$A_{s,c}$	0.69 / 0.71	$A_{v,c}$	0.64 / 0.66

Table 8.1 : Optical properties of a glass-SnO_2:F/WO_3/PAAUA/$V_zTi_yO_x$/ SnO_2:F-glass in the bleached and coloured states measured with the WE and the CE facing the incident beam. The device was bleached at + 2.5 V for 100 s and coloured at - 3 V for 120s.

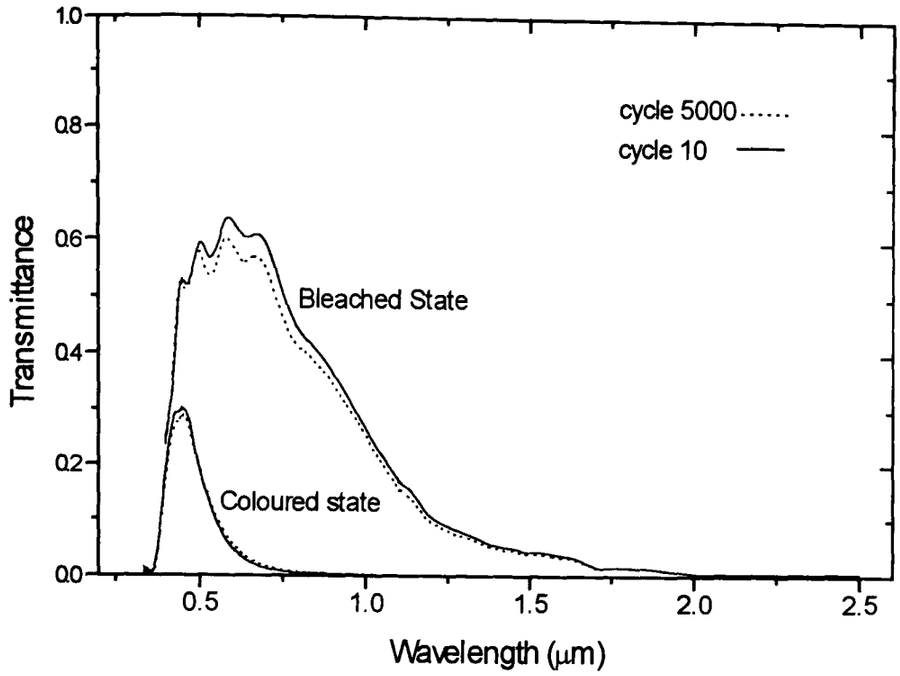

Figure 8.13 : Spectral transmittance of the glass-ITO/WO_3/PAAUA/$V_zTi_yO_x$/ ITO-glass device, after 10 and 5000 cycles. The device was bleached at + 3 V for 2 mn and coloured at - 3 V for 2 mn.

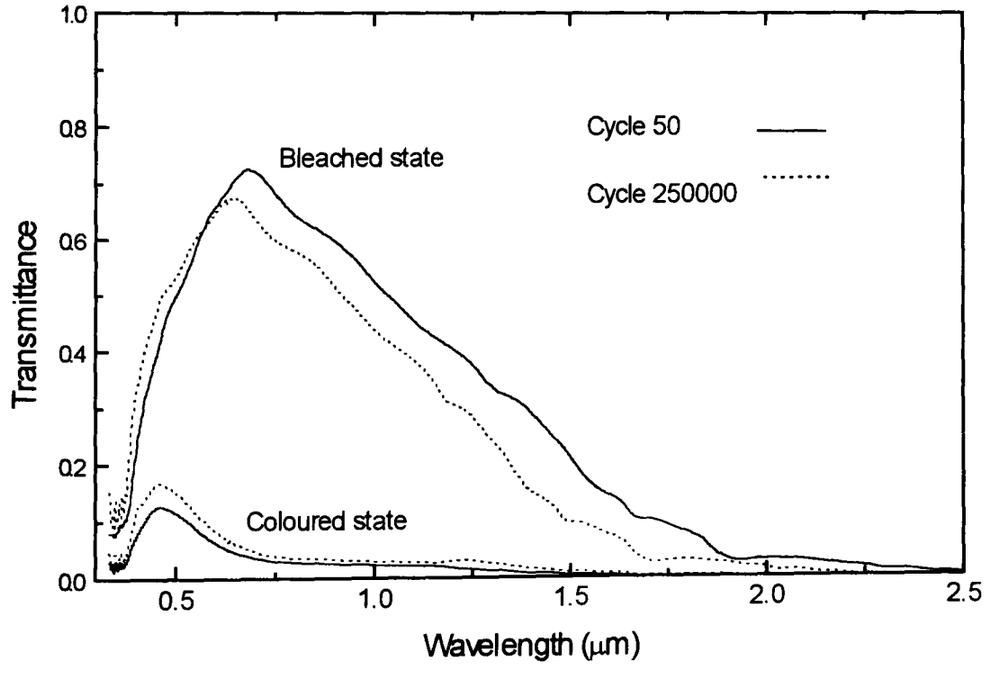

Figure 8.14 : Spectral transmittance of the glass-SnO_2:F/WO_3/PAAUA/ $V_zTi_yO_x$/ SnO_2:F-glass device, after 10 and 5000 cycles. The device was bleached at + 3 V for 2 mn and coloured at - 3 V for 2 mn.

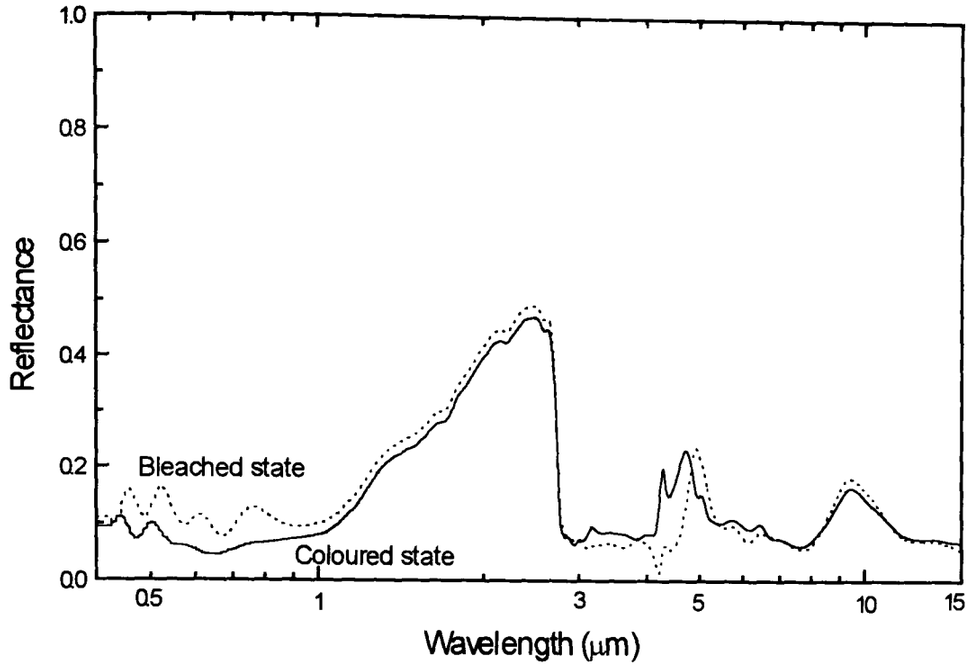

Figure 8.15 : Spectral reflectance of the glass-ITO/WO_3/PAAUA/$V_zTi_yO_x$/ ITO:F-glass device in the bleached and coloured states. The device was bleached at + 3 V for 2 mn and coloured at - 3 V for 2 mn.

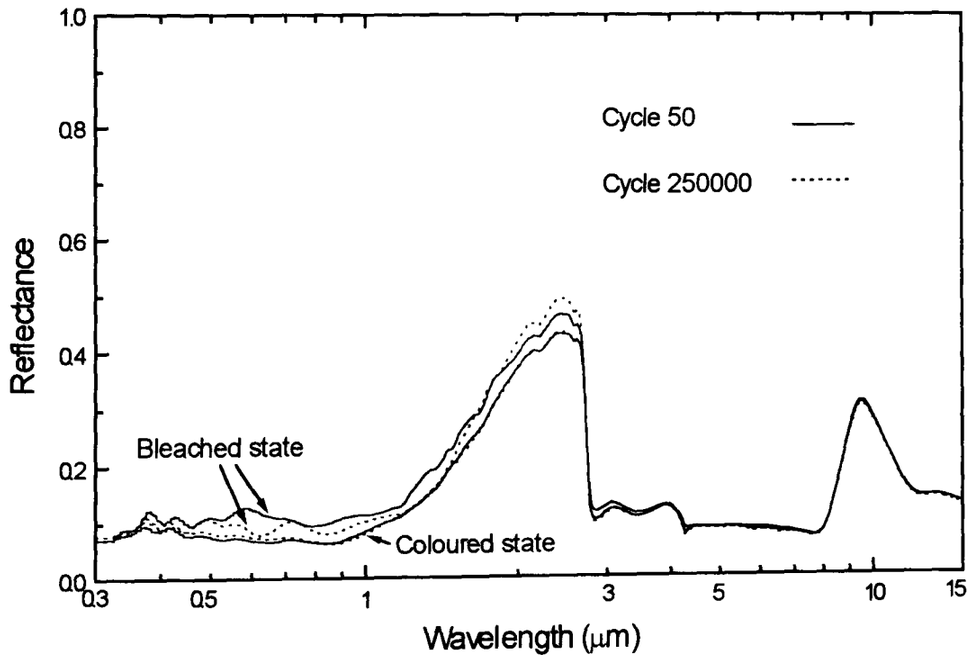

Figure 8.16 : Spectral reflectance of the glass-SnO_2:F/WO_3/PAAUA/$V_zTi_yO_x$/ SnO_2:F-glass device, after 50 and 250000 cycles. The device was bleached at + 3 V for 2 mn and coloured at - 3 V for 2 mn.

The hemispherical spectral absorptance of the glass-ITO/WO_3/PAAUA/$V_zTi_yO_x$/ITO-glass and glass-SnO_2:F/WO_3/PAAUA/$V_zTi_yO_x$/SnO_2:F-glass devices after ageing are shown in Figure 8.17 and Figure 8.18 respectively in the bleached and coloured states.

All optical properties of both EC prototype devices are summarised in Table 8.2.

The glass-SnO_2:F/WO_3/PAAUA/$V_zTi_yO_x$/SnO_2:F-glass device exhibits a T_v and a T_s modulation of about 52 % and 43 % respectively. This is seen to reduce to 49 % and 40 % after 250000 cycles, ageing due to a decrease of $T_{v,b}$ and an increase of $T_{v,c}$. A direct effect of this is the increase of both $A_{v,c}$ and $A_{s,c}$ principally and a decrease of $A_{v,b}$ and $A_{s,b}$.

Similar results are also obtained for the glass-ITO/WO_3/PAAUA/$V_zTi_yO_x$/ITO-glass prototype. The modulation of T_v and T_s are equal to 50 % and 37 % respectively. $A_{s,c}$ and $A_{s,c}$ are also seen to increase over switching cycles.

The NIR and thermal IR absorptance properties of both devices are seen to be very high in the coloured state, meaning that modulation behaviour occurs between transparent and absorbing states. The solar absorptance is modulated between $A_{s,b} \sim 0.40$ and $A_{s,c} \sim 0.80$ for both devices, and the thermal emittance is ≈ 0.90.

These optical results confirm those repeated above; solid-state EC devices having a WO_3/PAAUA/$V_zTi_yO_x$ structure exhibit good electrochromic behaviour. Their transmittance properties are clearly modulated under ionic intercalation/deintercalation between $T_{v,b} \sim 0.60$ and $T_{v,c} \sim 0.10$. Both luminous and solar radiation can be altered, gradually and reversibly between a transparent and an absorbing state. Such behaviour is also seen to be reasonably stable over ageing, and clearly demonstrates good potential for commercial development. The open circuit memory is greater than 12 hours and their colouring and bleaching time less than 5 minutes.

Figure 8.19 and Figure 8.20 show photographs of the glass-ITO/WO_3/PAAUA /$V_zTi_yO_x$/ITO-glass and of the glass-SnO_2:F/WO_3/PAAUA/$V_zTi_yO_x$/SnO_2:F-glass devices respectively in the bleached and coloured states. These photographs show the actual size of the prototypes.

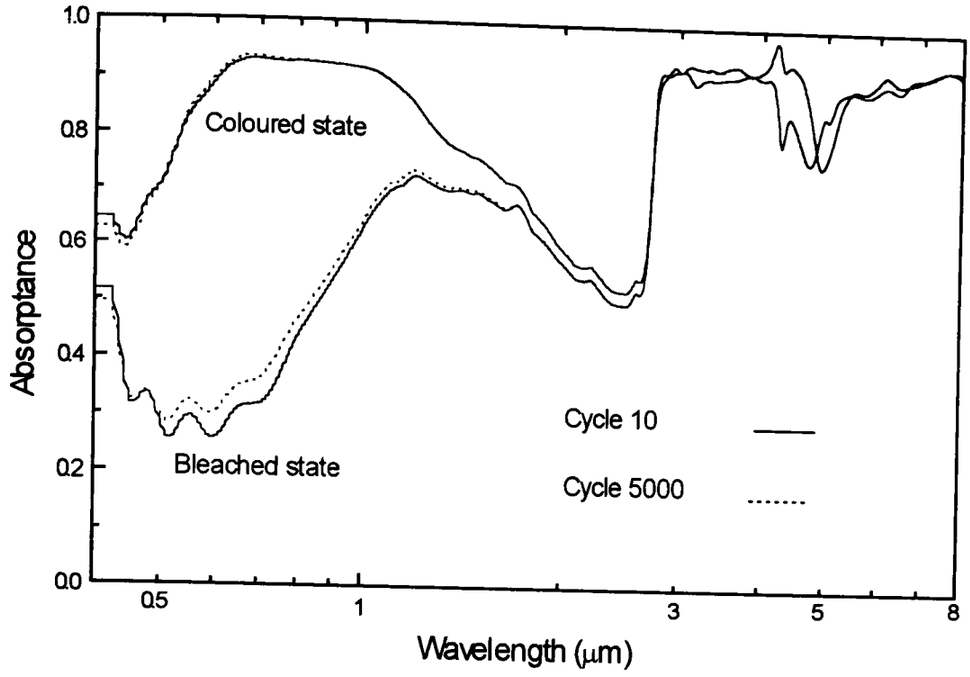

Figure 8.17 : Hemispherical spectral absorptance of the glass-ITO/WO_3/ PAAUA /$V_zTi_yO_x$/ITO-glass devices, after 10 and 5000 cycles. The device was bleached at + 3 V for 2 mn and coloured at - 3 V for 2 mn.

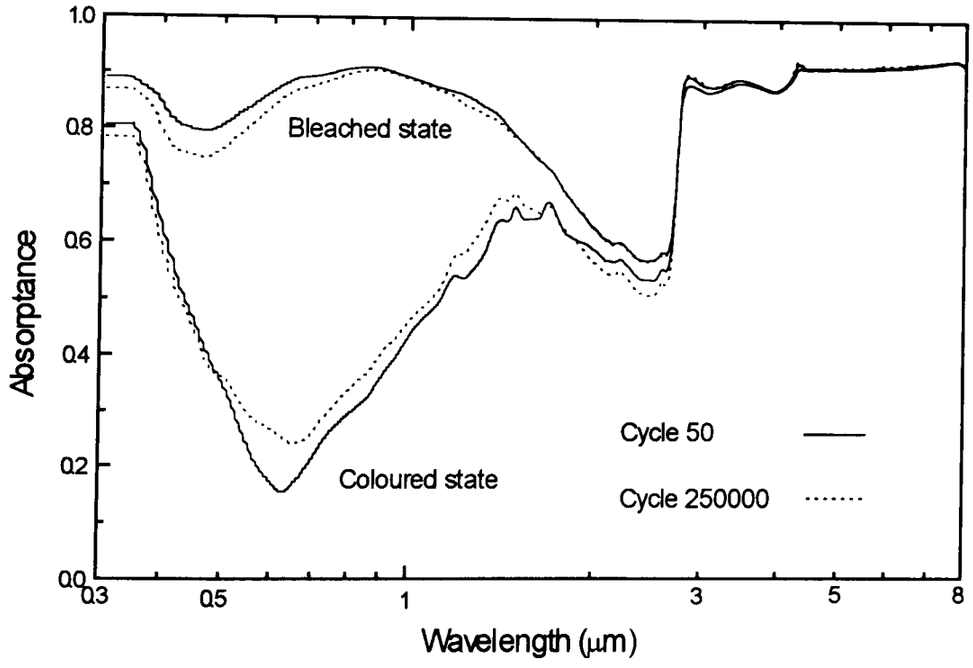

Figure 8.18 : Hemispherical spectral absorptance of the glass-SnO_2:F/WO_3/ PAAUA/$V_zTi_yO_x$/SnO_2:F-glass device, after 10 and 5000 cycles. The device was bleached at + 3 V for 2 mn and coloured at - 3 V for 2 mn.

	SnO_2:F/WO_3/PAAUA/$V_zTi_yO_x$/SnO_2:F		ITO/WO_3/PAAUA/$V_zTi_yO_x$/ITO	
	Cycle 50	cycle 250000	Cycle 10	cycle 5000
Solar spectrum				
$T_{s,b}$	0.48	0.46	0.43	0.41
$T_{s,c}$	0.05	0.06	0.07	0.07
$R_{s,b}$	0.15	0.14	0.16	0.16
$R_{s,c}$	0.13	0.13	0.14	0.14
$A_{s,b}$	0.38	0.40	0.41	0.43
$A_{s,c}$	0.82	0.81	0.79	0.79
Visible spectrum				
$T_{v,b}$	0.63	0.60	0.60	0.55
$T_{v,c}$	0.09	0.11	0.10	0.10
$R_{v,b}$	0.13	0.13	0.13	0.13
$R_{v,c}$	0.09	0.09	0.07	0.07
Emissivity	Near-normal hemispherical / 300°K		Near-normal hemispherical / 300°K	
$\varepsilon_{n,b}$	0.86	0.86	0.91	0.91
$\varepsilon_{n,c}$	0.85	0.86	0.90	0.90
Q (mC/cm^2)	21	14*	27	24
$\eta_{c\,/solar}$ (cm^2/C)	47	63*	30	32
$\eta_{c\,/visible}$(cm^2/C)	40	53*	29	31
Response time	< 4 mn		< 4 mn	
Voltage (V)	± 3 V		± 3 V	
Memory (hr)	> 12 hr		> 12hr	

Table 8.2 : Summary table of electrochromic properties of glass-ITO/WO_3/PAAUA/$V_zTi_yO_x$/ITO-glass and glass-SnO_2:F/WO_3/PAAUA/$V_zTi_yO_x$/SnO_2:F-glass devices.
(*Device partially damaged ; the result is estimated)

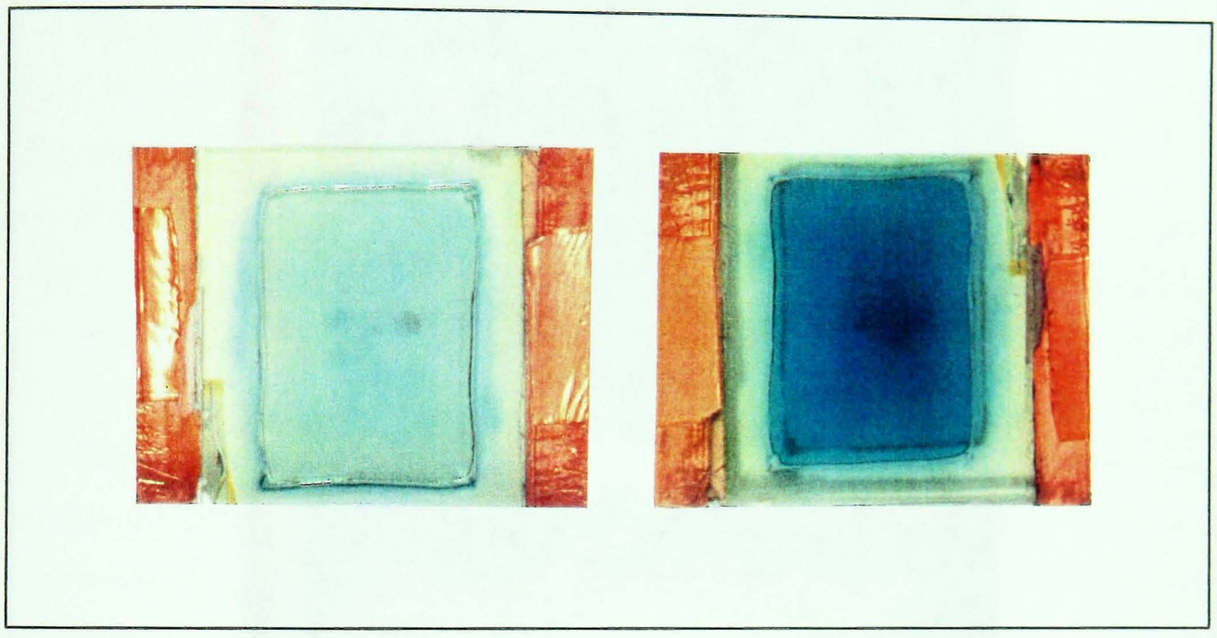

Figure 8.19 : The glass-ITO/WO_3/PAAUA /$V_zTi_yO_x$/ITO-glass device in the bleached and coloured states. The photographs show the actual size of the prototype.

Figure 8.20 : The glass-SnO_2:F/WO_3/PAAUA/$V_zTi_yO_x$/SnO_2:F-glass device in the bleached and coloured states. The photographs show the actual size of the prototype.

8.6 Conclusion

In this Chapter, two different structures of electrochromic devices have been assembled and investigated, using the different candidate materials produced in this work. The irreversible behaviour of the WO_3/PAAUA/NiO_x structure has been observed. The rapid degradation of the NiO_x layer under lithium intercalation/deintercalation was seen to be the main reason for the device delamination and is consistent with results observed in liquid electrolytes.

The relative success of the WO_3/PAAUA/$V_zTi_yO_x$ device structure has been confirmed and it is believed that the 5-layer laminated design is a viable option for electrochromic window devices. This device was seen to modulate the whole range of solar radiation between a fairly transparent and an absorbing state due to ion insertion/extraction. Under specific conditions of use, the WO_3/PAAUA/$V_zTi_yO_x$ device was seen to be very durable and almost stable over ageing. Criteria have been identified to limit degradation and increase the stability and durability of EC devices over ageing. For instance, the use of a continuous triangular waveform to drive the device between bleached and coloured states has been seen to degrade devices more quickly than a rectangular waveform that includes a relaxing time. Colouring potential and colouring time in particular have also been noticed to be important parameters to be defined for the long-life stability of the device, i.e. high potential or long colouring time could mean high $T_{v,c}$ but could also mean irreversible insertion of lithium and lower stability of the device.

The limits on the optical, electrochemical and mechanical performance and the durability of EC smart window devices remain to be explored, though they can already be assessed on the basis of different degradation categories[18].

Degradation stresses observed with our devices were the results of imposed conditions. These are usually predictable or controllable, and repeatable ageing parameters. These can be electrical parameters imposed, such as scan rate and colouring and bleaching potentials and times. They can also be natural parameters such as UV radiation, humidity, temperature, wind and any different climate conditions. Now we are able to produce devices, further systematic investigation needs to be carried out to assess the effect of such conditions. These are distinct to other types of degradation processes that can repeat themselves in totally chaotic ways, such as thermal shocks, elevated

temperatures and electrochemical instability. The third type of degradation process observed in this work refers to problems occurring at a molecular level. These usually include gas evolution, secondary reactions, photoreactions, volume changes and formation of water, for instance. In our case, such problems were minimised by using lithium-based instead of a protonic-based electrolyte. Nevertheless, this type of degradation is the most probable one occurring on the NiO_x electrode which makes it potentially unsuitable for EC applications. Further work on NiO_x electrode might relate film degradation to identified physical and chemical processes such as film dissolution and corrosion. In the case of the WO_3/PAAUA/$V_zTi_yO_x$ device, irreversible insertion of ionic species into layers is a degradation process that can diminish electrochromic response. This is usually provoked by high and/or long applied potentials.

This Chapter shows the relatively good electrochromic behaviour of the WO_3/PAAUA/$V_zTi_yO_x$ structure to be used as a variable transmittance device. New devices need to be assembled and limits of electrochromic performance and durability tests need to be explored in future work to demonstrate their applicability for commercial development.

It is also shown that such electrochromic devices do not exhibit good solar energy efficiency. Further improvements are required to increase the NIR reflectance of the electronic conductor to limit the thermal absorptance of solar radiation.

Chapter 9

CONCLUSIONS

In this work, the optical, electrochemical and chromogenic properties of some inorganic transition metal oxides thin films were investigated with the aim of realising a practical 5-layer all-solid state electrochromic device for use as a variable transmission window in buildings.

Different candidate materials were made by R.F. magnetron sputtering and studied. Nickel oxide films made from a metallic target were shown to have transmittance modulation properties similar to electrodeposited films when studied under proton insertion/extraction: $\Delta(T_{v,b}, T_{v,c}) = 0.70$ for sputtered films and 0.80 for electrodeposited films were observed. Anodic films exhibited a very high visible coloration efficiency (100 $cm^2.C^{-1}$) compared to sputtered films (35 $cm^2.C^{-1}$). However, chemically-deposited nickel oxide films were extremely porous and soft. Under the mechanical stresses of ionic insertion/extraction, anodic films would degrade more quickly than the very compact nanostructure of physically-deposited films. Electrodeposited NiO_x films were not seen to be potential candidates for EC device applications.

Similarly, due to possible gas evolution, the use of a water-based electrolyte was found to be a source of difficulties for the development of practical EC prototypes. As a consequence no further study was carried out using such electrolytes, even though proton-based devices have been shown to work[1], making our early work on NiO_x thin films still relevant. Widely used in battery technology, lithium-based electrolytes were seen as a more suitable alternative for EC applications.

Most of the work in this thesis was then concentrated on the study of potential electrochromic films under lithium intercalation/deintercalation. Experimental techniques and procedures were adapted as well as an electrochemical cell which was designed and built to fulfil all the necessary requirements for working with lithiated electrolytes.

The electrochromic behaviour of WO_3 thin films has been intensively studied and they appear to be well-understood electrochromic materials with well-established properties. The colour of tungsten oxide-based glazing systems was not considered to be a major problem for a future EC device development. WO_3 has been shown to be a suitable material for use as an active electrochromic layer in EC devices. WO_3 thin films were therefore deposited by R.F. magnetron sputtering and studied under Li^+ intercalation/deintercalation. Optimised films produced in this work exhibited a high visible transmittance modulation of $\Delta(T_{v,b}, T_{v,c}) = 0.82$, a visible η_c of about 49 $cm^2.C^{-1}$ for a thickness of 450 nm.

When studied under lithium insertion/extraction, sputtered NiO_x films optimised for proton insertion/extraction were seen to degrade extremely quickly. Brotherston et al.[2] reported that the most probable reaction was a reduction of Ni^{+2} to Ni^0 in the cathodic process which is then reversed in the anodic region. A nucleation loop was observed in cyclic voltammetry indicating the growth of a new phase in the nickel oxide film. At that point, nickel oxide (black in the reduced state) was clearly seen to peel off the surface of the film. At narrower and higher potential ranges, the reaction process could have been more reversible, but almost no charge was being inserted, and these potential conditions did not match those required for optimum response of the WO_3 layer. It was clear that NiO_x thin films deposited and optimised in this work were not suitable for any EC device applications using a lithium-based electrolyte. A possible reason is that reversible proton insertion/extraction is possible over a wider range of NiO_x structures, whereas for Li^+ the range of deposition conditions is narrower. This would mean that electrochromic properties of sputtered nickel oxide films may be very sensitive to deposition process parameters when studied with lithium. This would probably explain why some authors[3,4] have succeeded in reversibly intercalating Li^+.

Following the observed limitations of NiO_x, alternative ion-storage layers made of vanadium oxide and titanium oxide were studied. Electrochromic properties of TiO_x films were seen to not strongly depend on the R.F. magnetron sputtering process parameters whereas VO_x showed a greater dependence. TiO_x films are able to store a limited quantity of charge Q = 13 $mC.cm^{-2}$ at any thickness greater than 10 nm, they are very transparent in both charged and uncharged states $T_{v,u}$ and $T_{v,ch} > 0.80$, and are very stable upon charge insertion/extraction. VO_x films can store a much larger quantity of

charge Q = 35 $mC.cm^{-2}$ for a thickness of 70 nm, and they are relatively transparent in both charged and uncharged $T_{v,u}$ and $T_{v,ch} > 0.70$. However, they appear yellow in the uncharged state and bluish in the charged state and the charge insertion /extraction was seen to evolve during the initial cycles.

The main achievement of this work was the development of highly durable vanadium/titanium mixed oxide thin films. Work was carried out on different V/Ti ratios using specific deposition techniques developed for that purpose. Films with a vanadium to titanium ratio of about 50 % showed optimum performance characteristics for passive ion-storage layer applications. Such layers deposited on ITO exhibited high visible transmittance ($T_{v,ch} > 0.62$) and a relatively low modulation: $\Delta(T_{v,u}, T_{v,ch}) = 0.20$, with high storage capacity Q > 40 mC/cm^{-2} for a thickness of 80 nm.

Electrochromic devices were assembled using a laminated 5-layer configuration with a polymer electrolyte. This design was seen to have at present the highest practical use for commercial development. The WO_3/PAAUA/$V_zTi_yO_x$ EC device structure was assembled and exhibited encouraging electrochromic properties. Under specific switching conditions, the visible transmittance modulation remained greater than $\Delta(T_{v,b}, T_{v,c}) > 0.50$ over more than 10^5 cycles. However, $T_{v,b}$ was seen to be limited at 0.60. Also, such devices were seen to exhibit solar absorptance modulation ($A_{s,c} > 0.85$) instead of solar reflectance modulation which would be more favourable for energy-efficient applications. More work is necessary to optimise and fully characterise these devices. Greater understanding is needed on the ionic intercalation/deintercalation process and on the irreversible processes between electrolyte and electrodes in particular for the $V_zTi_yO_x$ ion-storage layer.

The addition of Ti in $V_zTi_yO_x$ was seen to stabilise pure VO_x and by creating more defects into the lattice, it increases the charge capacity. The optical bandgap was seen to widen upon increasing incorporation of Ti, making the film more neutral in appearance. However the drawback was the rise of absorption of visible radiation in the charged state due to a probable creation of free carriers. Titanium oxide was seen to possess a rutile lattice structure where the low-lying bands (2p) are completely full and all the other states remain empty. The Fermi level sits in a large bandgap between the 2 states (O2p and T_{2g}). Rutile structure is shown to be a good insulator, therefore transparent. It is possible to produce non-stoichiometric TiO_2 by losing oxygen or by doping it with

another material such as vanadium oxide. This introduces charge carriers into the t bands. VO_x has an additional electron which can be accommodated in the t levels. When cations are inserted into the lattice, electrons will move into the oxide and make the lower part of the t band populated. The excess electrons can easily jump from one site to another by absorbing photons. The peak absorption lies in the near infrared and is relatively broad for the $V_zTi_yO_x$ material in the charged state to exhibit a bluish coloration which is a significant performance deficiency for EC applications.

This work showed that the electrochromic properties of $V_zTi_yO_x$ films for CE applications are better than properties of VO_x and TiO_x, and possess much higher charge storage capacities than single oxides. They are more stable than NiO_x and when assembled with WO_3, the EC devices are very stable and reversible. Mixed-metal oxide films seem to exhibit great potential use for CE applications. Future work lies in the study of alternative mixed-metal oxides other than $V_zTi_yO_x$. Compositions using more than two electrochromic metal oxides might exhibit better electrochromic properties than $V_zTi_yO_x$ such as $W_kV_zTi_yO_x$ for instance. One can also expect to produce alternative colours of electrochromic WO_3. Further work can also concentrate on the study of possible Li^+ conducting inorganic ion-conducting layers and on solar reflectance modulation devices using crystalline WO_3 for instance to make smart windows more energy efficient.

ABBREVIATIONS,

ACRONYMS, AND SYMBOLS

A (mm^{-2})	electrode area
$\mathbf{A_\lambda}$	spectral absorptance coefficient
α_λ	absorption coefficient of a film
AM0	Air mass zero is the path length of solar radiation above atmosphere
AM2	Air mass two is the path length of solar radiation at ground level
$\mathbf{A_s}$	solar absorptance of a film
$\mathbf{A_{s,b}}$, $\mathbf{A_{s,c}}$, $\mathbf{A_{s,u}}$, $\mathbf{A_{s,ch}}$	solar absorptance in the bleached state, solar absorptance in the coloured state, solar absorptance in the uncharged state, solar absorptance in the charged state
$\mathbf{A_v}$	visible absorptance of a film
$\mathbf{A_{v,b}}$, $\mathbf{A_{v,c}}$, $\mathbf{A_{v,u}}$, $\mathbf{A_{v,ch}}$	visible absorptance in the bleached state, visible absorptance in the coloured state, visible absorptance in the uncharged state, visible absorptance in the charged state
c ($m.s^{-1}$)	speed of light in vacuum
C	spectrophotometer amplification
$\mathbf{C_i}$ ($mole.l^{-1}$)	concentration of species in electrolyte
CV	cyclic voltammetry
d (nm)	film thickness
δ (V)	electrochemical overpotential
δ_a (V)	anodic overpotential
δ_c (V)	cathodic overpotential

D_λ	relative power distribution of illuminant D_{65}
D_{65}	illuminant defined in C.I.E. No. 152, Vienna, 1986.
d^n, d^{n+1}, d^{n-1}	d atomic orbital at different ionisation states
e (C)	electronic charge
e^-	electron
ε	emissivity
E (V)	potential between working and counter electrodes
E^a_e (V)	potential at the anode
E^c_e (V)	potential at the cathode
$E_{b,\lambda}$ ($W.m^{-2}.\mu m^{-1}$)	blackbody spectral emissive power
ECD	electrochromic device display
E_F (eV)	Fermi energy
e_g	degeneracy doublet of 2d atomic orbital
E_g (eV)	energy gap
E_λ(eV)	energy of a photon (= hc/λ)
ε_λ	spectral emittance coefficient
ϕ_λ	spectral distribution characteristic
g_n or SHGC	sum of the solar transmittance and the longwave input of the solar radiation absorbed within the glazing that enters the building, also called solar heat gain coefficient
G_λ($W\ m^{-2}.\mu m^{-1}$)	spectral solar irradiance
h (J.s)	Planck's constant
$\hbar$ (J.s)	$h/2\pi$
HREM	high resolution electronic microscope

i (A)	current
I ($A.m^{-2}$)	current density
$\mathbf{I_i}$	intensity of spectrophotometer incident beam
IR	infrared radiation (> 3 μm)
ITO	Indium tin oxide
k ($J.K^{-1}$)	Boltzmann's constant
λ (μm)	wavelength
λ_p (μm)	plasma wavelength
n	type of optical transitions
η_c ($cm^2.C^{-1}$)	coloration efficiency
NIR	near-infrared radiation [0.8 μm - 3 μm]
$\mathbf{M_y}$	guest element in an electrochromic
$\mathbf{MeO_x}$	metal oxide
OD	optical density
2p	2p atomic orbital
PC	propylene carbonate
Q ($mC.cm^{-2}$) or ($mC.cm^{-2}.\ \mu m^{-1}$)	charge capacity or charge density
R (Ω)	electrolyte resistance
ρ (Ω)	D.C. electrical resistivity
$\mathbf{R_{Al}}$	spectral reflectance of the aluminium standard
R.F.	Radio Frequency (13.56 MHz) power applied to a sputtering electrode.
$\mathbf{R_\lambda}$	spectral reflectance coefficient, visible reflectance

R_s	solar reflectance of a film
$R_{s,b}$, $R_{s,c}$, $R_{s,u}$, $R_{s,ch}$	solar reflectance in the bleached state, solar reflectance in the coloured state, solar reflectance in the uncharged state, solar reflectance in the charged state
R_{sample}	spectral reflectance of a sample
ρ_s ($\Omega/\square$)	sheet resistivity
R_v	visible reflectance of a film
$R_{v,b}$, $R_{v,c}$, $R_{v,u}$, $R_{v,ch}$	visible reflectance in the bleached state, visible reflectance in the coloured state, visible reflectance in the uncharged state, visible reflectance in the charged state
2s	2s atomic orbital
S_{sample}	signal measured by the integrating sphere detector with a sample
$S_{reference}$	signal measured by the integrating sphere detector with aluminium reference standard
SEM	scanning electron microscope
t (s)	time
TEM	transmission electronic microscope
t_{2g}	degeneracy triplet of the 2d atomic orbital
T_λ	spectral transmittance coefficient
T_{sample}	spectral transmittance of a sample
T_s	solar transmittance of a film
$T_{s,b}$, $T_{s,c}$, $T_{s,u}$, $T_{s,ch}$	solar transmittance in the bleached state, solar transmittance in the coloured state, solar transmittance in the uncharged state solar transmittance in the charged state
T_v	visible transmittance of a film
$T_{v,b}$, $T_{v,c}$, $T_{v,u}$, $T_{v,ch}$	visible transmittance in the bleached state, visible transmittance in the coloured state, visible transmittance in the uncharged state, visible transmittance in the charged state
T (K)	temperature

UV		ultra violet radiation (<0.4 μm)
U-value	($W.m^{-2}.^{o}C^{-1}$)	total heat transfer coefficient of a window system, which includes conductive, convective and radiative heat transfer
V (V)		potential
V_{λ}		relative sensitivity or photopic response of the human eye
VIS		visible radiation [0.4 μm- 0.8 μm]
ω		angular frequency
ω_p		plasma frequency
X		stimulus value for the red
$X_{\lambda i}$		radiative property coefficient
$X_{\lambda 1, \lambda 2}$		radiative property of a film
XRD		X-ray diffraction
Y		stimulus value for the green
Z		stimulus value for the blue
Z_i		valence of ion

REFERENCES

Chapter 1

(1) IEA, Solar Heating & Cooling Programme, Task 18, Task leader Prof M. G. Hutchins, Oxford Brookes University, SEMRL, Oxford, U.K, 1992-1997.

(2) D. Aresteh, " *Advances in Window Technology: 1973-1993*", LBL, University of California for the U.S. Department of Energy under Contract DE-AC03-76SF00098, February 1995.

(3) Advanced Glazing Industry Club, Prof M. G. Hutchins. Oxford Brookes University, Oxford, U.K.

(4) M. G. Hutchins, " *Recent Advances in the Development and Use of Electrochromic Glazing*", Feature Article, IEA, Solar Heating & Cooling Programme, Annual Report, p. 7, Ed. Sheila Blum, USA, February 1995.

(5) R. Siegel, J. R. Howell, "*Thermal Radiation Heat Transfer*", Second Edition, Hemisphere Publishing Corporation, New York, p. 412, 1981.

(6) G. Wyszecki, " *Handbook of Optics* ", Edition W.G. Driscott and W. Vaugham, New York, 1978.

(7) International Standard ISO 90/50, ISO/TC 160, " *Glass in Building, Determination of Light Transmittance, Solar Direct Transmittance, Energy Transmittance and Ultra-violet Transmittance, and Related Glazing Factors*", Genève, Switzerland, 1990.

(8) C.C. Figgures, " *The sputtering of Zinc Oxide Thin Films for Spectrally Selective Solar Energy Material Applications*", PhD Thesis, Oxford Polytechnic, September 1989.

(9) IEA, Solar Heating & Cooling Programme, Task 18, Advanced Glazing and Associated Materials for Solar and Building Applications, Subtask B9, " *Frame and Edge Seal Technology*", and Subtask B14 " *Measurement of the U-Value of Advanced Glazing systems*", M. G. Hutchins Operating Agent, Oxford Brookes University, 1992-1997.

(10) G. Haacke, " *Materials for Transparent Heat Mirror Coatings*", S.P.I.E. Proceedings, Vol. 324, p. 10, 1982.

(11) C. G. Granqvist, " *Optical Coatings for Energy Efficiency and Solar Applications : Some Recent Developments*", S.P.I.E. Proceedings, Vol. 401, p. 330, 1983.

(12) C. G. Granqvist, " *Transparent Conductive Electrodes for Electrochromic Devices : A Review*", Applied Physics, Vol. A 57, p. 19, 1993.

(13) C. G. Granqvist, " *Materials Science For Solar Energy Conversion Systems*", p. 125, Pergamon Press, Oxford, 1991.

(14) Ipasol™ is a trade mark of Interpane, Germany.

(15) B. Stjerna, " *Electrical and Optical Properties of Doped Tin Oxide Films*", Doctorate Thesis, Göteborg, Sweden, 1992.

(16) Z. C. Jin, I. Hamberg, C. G. Granqvist, "*Optical-Properties Of Sputter-Deposited ZnO-Al Thin-Films*", Journal of Applied Physics, Vol.64, No.10, p. 5117, 1988.

(17) Y. Igasaki, H. Saito, " *The Effects Of Zinc Diffusion On The Electrical And Optical-Properties Of ZnO-Al Films Prepared By RF Reactive Sputtering*", Thin Solid Films, Vol. 199, No. 2, p.223, 1991.

(18) K-Glass™ is a trade mark of Pilkington, U.K.

(19) Window Version 4.1, " *Fenestration Product Thermal Analysis Program*", Windows and Daylighting Group, Energy and Environment Division, Lawrence Berkeley Laboratory, California, 1994.

(20) EASE Project for the European Communities, Section 3.1 by W. Platzer, *"Advanced Glazings and Transparent Insulation*", 1996.

(21) D.A. Clugston, R.E. Collins, " *Pump Down of Evacuated Glazings*", Journal of Vacuum Science & Technology A- Vacuum Surfaces and Films, Vol. 12, No. 1, p. 241, 1994.

(22) R.E. Collins, C.A. Davis, C.J. Dey, S.J. Robinson, J.Z. Tang, G.M. Turner, *" Measurement of Local Heat-Flow in Flat Evacuated Glazing*", International Journal of Heat and Mass Transfer, Vol. 36, No. 10, p. 2553, 1993.

(23) W. J. Platzer, P. O. Braum, " *Transparent Insulation Technology for Buildings- A Review*", Conference Proceedings, Window Innovations' 95, Toronto, p. 588, June 1995.

(24) S.E. Selkowitz, M. Rubin, E.S. Lee, R. Sullivan, " *A Review of Electrochromic Performance Factors*", S.P.I.E. Proceedings, Vol. 2255, p. 227, 1994.

Chapter 2

(1) J.R Platt, " *Electrochromism, a Possible Change of Color Producible in Dyes by and Electric Field*", Journal of Chemical Physics, Vol. 32, No. 3, p. 862, 1961.

(2) C.G Granqvist, C.M. Lampert, " *Science and Technology of Electrochromics* ", EUROPTO series, Toulouse, France, 1992.

(3) C.G. Granqvist, " *Handbook of Inorganic Electrochromic Materials*", p. 413, Elsevier, Amsterdam, 1995.

(4) C.G. Granqvist, " *Handbook of Inorganic Electrochromic Materials*", Elsevier, Amsterdam, 1995.

(5) W. Xu, G. X. Wan, " *Electrochromic Effect of Vinyl Viologenacetate Copolyether Solid*", Journal of Macromolecular Science Pure and Applied Chemistry, Vol. A30, No. 5, p. 373, 1993.

(6) M. C. Bernard, A. Hugot le Goff, " *Electrochromic performance of Polyaniline Films during their Cycling in a PH 3 Electrolyte*", Journal of the Electrochemical Society, Vol. 141, No. 10, p. 2682, 1994.

(7) K. Hyodo, " *Electrochromism of Conducting Polymers*", Electrochemica Acta, Vol. 39, No. 2, p. 265, 1994.

(8) T. Saika, T. Iyoda, K. Honda, T. Shimidzu, " *Multimode Chemical Transducers .2. Electrochromic and Photochromic Properties of Azoquinone Compounds*", Journal of the Chemical Society - Perkin Transactions 2, No. 6, p. 1181, 1993.

(9) R. Taguchi, T. Kobayashi, J. Muto, " *Characteristics of Electrochromic Magnesium Phthalocyanine Films for Initial Oxidation-Reduction Cycling*", Journal of Materials Science Letters, Vol. 13, p. 1320, 1994.

(10) D. J. Moore, T. F. Guarr, " *Electrochromic Properties of Electrodeposited Lutetium Diphthalocyanine Thin-Films* ", Journal of the Electroanalytical Chemistry, Vol. 314, p.313, 1991.

(11) G. D. McMeeking, " *Deposition and Characterisation of Nickel Oxide Based Coatings for Advanced Glazing Applications*", PhD Thesis, Oxford Brookes University, Oxford, UK, 1996.

(12) S. M. Christie, " *Optical and Electrochromic Properties of Reactively Sputtered Tungsten Oxide Films for Window Glazings* ", Mphil Thesis, Oxford Polytechnic, 1989.

(13) P. M. S. Monk, R. J. Mortimer, D. R. Rosseinsky, " *Electrochromism: Fundamentals and Applications*", VCH, Weinheim, 1995.

(14) N. R. Lynam, " *Automotive Applications of Chromogenic Materials*", S. P. I. E. Proceedings, Institute Series, Vol. IS4, p. 47, 1988.

(15) F. H. Smith, " *Apparatus for Use as an Antidazzle and Fog-Penetrating Device for Use in Conjunction with Motor Car Headlamps*", British Patent Specification 328,017, November 16, 1929.

(16) S. K. Deb, "*A Novel Electrophotographic System*", Applied Optics, Supplement on Electrophotography, Vol. 8, p. 193, 1969.

(17) T. Alfrey, E. F. Gurnee, "*Organic Polymers*", Edt John Dorn, Prentice-Hall Series in Materials Science, New Jersey, U. S. A., 1967.

(18) D. Bloor, "*Plastics that Conduct Electricity*", New Scientist, p. 577, March 1982.

(19) F. E. Bailey, J. V. Koleske, "*Poly(ethylene oxide)*", Academic Press, New York, 1976.

(20) B. Scrosati, " *Polymer Electrolyte Reviews - 1*", Eds J. R. MacCallum and C. A. Vincent, Elsevier, London, p. 315, 1987.

(21) M. Gauthier, D. Fauteux, G. Vassort, A. Belanger, M. Duval, P. Ricoux, J. M. Chabagno, D. Muller, P. Rigaud, M. B. Armand, D. Deroo, "*Assessment of Polymer-Electrolyte Batteries For EV and Ambient_Temperature Applications*", Journal of the Electrochemical Society, Vol. 132, p. 1333, 1985.

(22) C. M. Lampert, S. J. Visco, M.M. Doeff, Y.P. Ma, Y. He, J. C. Giron, "*Characteristics of Laminated Electrochromic Devices Using Polyorganosulfide Electrodes*", Solar Energy Materials and Solar Cells, Vol. 33, No. 1, p. 91, 1994.

(23) H. Tada, Y. Bito, K. Fujino, H. Kawahara, " *Electrochromic Windows using a Solid Polymer Electrolyte*", Solar Energy Materials and Solar Cells, Vol. 16, p. 509, 1987.

(24) H. Ohno, " *Applications of Polymer Electrolytes - Electrochromics, Sensors and Biology*", Electrochemica Acta, Vol. 37, No. 9, p. 1649, 1992.

(25) A. Magistris, K. Singh, " *PEO-Based Polymer Electrolytes*", Polymer International, Vol. 28, No. 4, p. 277, 1992.

(26) F. M. Gray, " *Solid Polymer Electrolytes*", VCH, p. 2, 1991.

(27) F. M. Gray, " *Solid Polymer Electrolytes*", VCH, p. 85, 1991.

(28) S. Pantaloni, S. Passerini, B. Scrosati, " *Solid-State Thermoelectrochromic Display*", Journal of the Electrochemical Society, Vol. 134, No. 3, p. 753, 1987.

(29) O. Bohnke, C. Bohnke, " *Polymer-based Solid Electrochromic Cell for Matrix-Addressable Display Devices*", Journal of the Electrochemical Society, Vol. 138, No.12, p. 3612, 1991.

(30) H. Ohno, H. Yamazaki, " *Preparation and Characteristics of All Solid State Electrochromic Display with Cation-Conductive Polymer Electrolytes*", Solid State Ionics, Vol. 59, No. 3-4, p. 217, 1993.

(31) J. Li, A. Mintz, I. M. Khan, " *Poly(ethylene oxide)/Poly(2-vinylpyridine)/Lithium Perchlorate Blends. New Materials for Solid Polymer Electrolytes*", Journal of the American Chemical Society, Vol. 4, p. 1131, 1992.

(32) D. W. Kim, J. K. Park, M. S. Gong, H. Y. Song, " *Effect of Grafting Degree and Side PEO Chain-Length on the Ionic Conductivities of NBR-G-PEO based Polymer Electrolytes*", Polymer Engineering and Science, Vol. 34, No. 17, p. 1305, 1994.

(33) J. Nagai, M. Mizuhashi, T. Kamimori, " *Large Area Chromogenics: Materials and Devices for Transmittance Control*", S.P.I.E. Institute Series, Vol. IS4, p. 378, 1990.

(34) O. Bohnke, C. Rousselot, P. A. Gillet, C. Truche, " *Gel Electrolyte for Solid-State Electrochromic Cell*", Journal of the Electrochemical Society, Vol. 139, No. 7, p. 1862, 1992.

(35) J. Nagai, M. Mizuhashi, T. Kamimori, " *Polymeric Ion Conductors*", S.P.I.E. Institute Series, Vol. IS 4, p.378, 1988.

(36) P. Ageorges, M. G. Hutchins, " *Assessment of the Gentex EC Window Device No. 4 Based on a Viologen Electrolyte*", IEA Solar Heating and Cooling Programme, Task 18, Report T18/B3/UK2/95, Oxford Brookes University, 1995.

(37) C. M. Lampert, S. J. Visco, M. M. Doeff, Y. P. Ma, Y. He, J. C. Giron, "*Characteristics of Laminated Electrochromic Devices Using Polyorganodisulfide Electrodes*", Solar Energy Materials and Solar Cells, Vol. 33, No. 1, p. 91, 1994.

(38) M Andrei, A. Roggero, L. Marchese, S. Passerini, " *Highly Conductive Solid Polymer Electrolyte For Smart Windows*", Polymer, Vol. 35, No. 17, p. 3592, 1994.

(39) M. Green, K.S Kang, " *Solid State Electrochromic Cells: the M-Alumina WO_3 System*", Thin Solid Films, Vol. 40, L19, 1977.

(40) Y. F. Y. Yao, J. T. Kummer, " *Ion Exchange Properties of and Rates of Ionic Diffusion in Beta-Alumina*", Journal of Inorganic Nuclear Chemistry, Vol. 29, p. 2453, 1967.

(41) Vo-Van Truong, F. E. Girouard, P. V. Ashrit, " *Inorganic Ion Conductors*", S.P.I.E. Institute Series, Vol. IS 4, p. 386, Hamburg, 1988.

(42) M. Kitao, H. Akram, K. Urabe, S. Yamada, " *Properties of Solid-State Electrochromic Cells Using Ta_2O_5 as Electrolyte*", Journal of Electronic Materials, Vol. 21, No. 4, p. 419, 1992.

(43) S. Tanemura, " *Energy Benefit of Smart Windows and the State-Of-Art of their R&D in Japan*", Proceedings of the 5th Int. Sym. on New Glass, Tokyo, 16-17 October 1995.

(44) R. B. Goldner, T. E. Haas, G. Seward, K. K. Wong, P. Norton, G. Foley, G. Berera, G. Wei, S. Schulz, R. Chapman, " *Thin Film Solid State Ionic Materials for Electrochromic Smart Window™ Glass*", Solid State Ionics, Vol. 28-30, p. 1715, 1988.

(45) M. Miyamura, S. Tomura, A. Imai, S. Inomata, " *Electrochemical Studies of Lithium Nitride Solid Electrolyte for Electrochromic Devices*", Solid State Ionics, Vol. 3-4, p. 149, 1981.

(46) T. Saito, Y. Ushio, M. Yamada, T. Niwa, " *Properties of Tantalum Oxide Thin-Film for Solid Electrolyte*", Solid State Ionics, Vol. 40-1, p. 499, August, 1990.

(47) Y. Sone, A. Kishimoto, T. Kudo, "*Proton Conductivity of Spin-Coated Ta_2O_5-Center-Dot-NH_2O Amorphous Thin-films From Peroxo-polytantalate Solution*", Solid State Ionics, Vol. 66, No. 1-2, p. 53, 1993.

(48) K. Kuwabara, K. Sugiyama, M. Ohno, " *All-Solid State Electrochromic Device .1. Electrophoretic Deposition Film of Proton Conductive Solid Electrolyte*", Solid State Ionics, Vol. 44, No. 3-4, p. 313, 1991.

(49) K. Kuwabara, M. Yamada, " *Early Cycling Processes in a Variable Transparency ECD Utilising Antimony Hydrogen Phosphate Thin-Film Electrolyte*", Solid State Ionics, Vol. 59, No. 1-2, p. 25, 1993.

(50) B.W. Faughnan, R.S. Crandall, P. M. Heyman, " *Electrochromism in WO3 Amorphous Films*", RCA Review, Vol. 36, p. 177, 1975

(51) K. Yamanaka, " *Tungsten Trioxide Liquid Electrolyte Electrochromic Devices with Amorphous Iron Tungstate Counter Electrodes - Response Characteristics and Cell Reliability*", Japanese Journal of Applied Physics, Part 1, Vol. 25, No. 7, p. 1073, 1986.

(52) K. West, "*High conductivity Ionic Conductors; Recent Trends and Applications*", by Takahashi, Edt. World Scientific Publishing Company, Singapore, 1989.

(53) S. E. Selkowitz, M. Rubin, E. S. Lee, R. Sullivan, " *A Review of Electrochromic Performance Factors*", S. P. I. E. Proceedings, Vol. 2255, p. 227, 1994.

(54) M. G. Hutchins, " *Recent Advances in the Development and Use of Electrochromic Glazing*", Feature Article, IEA, Solar Heating & Cooling Programme, Annual Report, p. 7, Ed. Sheila Blum, USA, February 1995.

Chapter 3

(1) J. E. Huleey, " *Inorganic Chemistry; Principles of Structure and Reactivity* ", Third Edition, Chapters 3 & 4, Harper International SI Edition, New York, 1983.

(2) J.D. Lee, " *Concise Inorganic Chemistry*", Fourth Edition, Chapters 2-5, Chapman & Hall, 1991.

(3) P.G. Dickens, M.S. Whittingham, " *Quarterly Review*", Chem. Soc. Lond., Vol. 22, p. 30, 1968.

(4) P. Hagenmuller, " *Les Bronzes Oxygénés*", Progress in Solid State Chemistry, Edt Reiss, Pergamon Press, Oxford, Vol.5, p. 71, 1971.

(5) C. G. Granqvist, C. M. Lampert, " *Science and Technology of Electrochromics*", Europto Series, Professional Development Programme, Toulouse, 1992.

(6) F. Wöhler," *Sur le Tungsten*", Annales de Chimie et de Physique, Vol. 23, p. 43, 1823.

(7) C. G. Granqvist, " *Electrochromic Oxides: Systematics, Materials, and Applications to Smart Windows*", Renewable Energy, Vol. 5, Part I, p. 141, 1994.

(8) P. A. Cox, "*Transition Metal Oxides; An Introduction to their Electronic Structure and Properties*", Chapter 1, Clarendon Press, Oxford, 1992.

(9) J.D. Lee, " *Concise Inorganic Chemistry*", Fourth Edition, Chapman & Hall, p. 59, 1991.

(10) V. E. Heinrich, P. A. Cox, " *The Surface Science of Metal Oxide*", Chapter 2, Cambridge University Press, Cambridge, 1994.

(11) S. Geller, " *Solid Electrolytes*", Chapter 2, Springer-Verlag, New York, 1977.

(12) J.B. Goodenough, " *Metallic Oxides* ", Progress in Solid State Chemistry, Edt Reiss, Pergamon Press, Oxford, Vol. 5, p. 149, 1971.

(13) M.S. Whittingham, R.A. Huggins, " *Fast Ion Transport in Solids*", W. Van Gool Editions, North Holland Publication, Amsterdam, p. 645, 1973.

(14) P. Hagenmuller, W. van Gool, " *Solid Electrolytes: General Principles, Characterisation, Materials, Applications*", Academic Press, New York, p. 370, 1973.

(15) C. Pisani, R. Dovesi, C. Roetti, " *Hartree-Fock Ab Initio Treatment of Crystalline Systems*", Springer-Verlag, Berlin, 1988.

(16) P. A. Cox, "*Transition Metal Oxides; An Introduction to their Electronic Structure and Properties*", p. 57, Clarendon Press, Oxford, 1992.

(17) V. E. Heinrich, P. A. Cox, " *The Surface Science of Metal Oxide*", p. 23, Cambridge University Press, Cambridge, 1994.

(18) P. A. Cox, "*Transition Metal Oxides; An Introduction to their Electronic Structure and Properties*", Chapter 2, Clarendon Press, Oxford, 1992.

(19) V. E. Heinrich, P. A. Cox, " *The Surface Science of Metal Oxide*", Chapter 5, Cambridge University Press, Cambridge, 1994.

(20) S. Trasatti, " *Electrodes of Conductive Metallic Oxides, Part A*", Elsevier, p. 24, Amsterdam, 1980.

(21) P. A. Cox, "*Transition Metal Oxides; An Introduction to their Electronic Structure and Properties*", p. 192, Clarendon Press, Oxford, 1992.

(22) P. A. Cox, "*Transition Metal Oxides; An Introduction to their Electronic Structure and Properties*", p. 195, Clarendon Press, Oxford, 1992.

(23) C. G. Granqvist, " *Electrochromic Oxides: a Bandstructure Approach*", Solar Energy Materials and Solar Cells, Vol. 32, p. 369, 1994.

(24) J.G. Bednorz, K. A. Müller, " *Possible High-TC Superconductivity in the Ba-La-Cu-O System*", Z. Physi, B-Condensed Matter, Vol. 64, No. 2, p. 189, 1986.

(25) S. Hüfner, "*Electronic Structure of NiO and Related 3d-Transition-Metal Compounds*", Advances in Physics, Vol. 43, No. 2, p. 183, 1994.

(26) N. F. Mott, "*The Metal Insulator Transition*", Taylor & Francis, London, 1974.

(27) J. Zaanen, G. A. Savatzky, J. W. Allen, " *Band-Gaps and Electronic Structure of Transition Metal Compounds* ", Physical Review Letters, Vol. 55, No. 4, p. 418, 1985.

(28) F. Reinert, P. Steiner, S. Hüfner, H. Schmitt, J. Fink, M. Knupfer, P. Sand, E. Bertel, " *Electron and Hole Doping in NiO*", Z. Phys. Vol. B 97, p. 83, 1995.

(29) H. H. Kung, " *Transition Metal Oxides: Surface Chemistry and Catalysis*", Elsevier, Amsterdam, p. 61, 1989.

(30) V. E. Heinrich, P. A. Cox, " *The Surface Science of Metal Oxide*", Chapter 6, Cambridge University Press, Cambridge, 1994.

(31) D. G. Aitken, P. A. Cox, R. G. Egdell, M. D. Hill, I. Sach, Vaccum, " *The Adsorption of Water on Tungsten Bronze (001) Surfaces- A Study by HREELS and Photoemission*", Vol. 33, No.10-1, p. 753, 1983.

(32) V. E. Heinrich, P. A. Cox, " *The Surface Science of Metal Oxide*", p. 361, Cambridge University Press, Cambridge, 1994.

Chapter 4

(1) H.K. Pulker " *Coatings on Glass*", Elsevier Science Publishing Company Inc., Amsterdam, p. 215, 1984.

(2) H.K. Pulker " *Coatings on Glass*", Elsevier Science Publishing Company Inc., Amsterdam, p. 228, 1984.

(3) P. Ageorges, " *Nordiko Sputter Coater Carousel Control System*", Internal Report, Solar Energy Materials Research Laboratory, Oxford Brookes University, 1994.

(4) Kapton™ film is a trade mark of Dupont de Nemours, France.

(5) J.A.J. Jacquez, H. F. Kuppenheim, " *Theory of the Integrating Sphere*", Journal of the Optical Society of America, Vol. 45, p. 460, 1955.

(6) D. G. Goebel, " *Generalised Integrating Sphere Theory*", Applied Optics, Vol. 6, p. 125, 1967.

(7) Window Version 4.1, " *Fenestration Product Thermal Analysis Program*", Windows and Daylighting Group, Energy and Environment Division, Lawrence Berkeley Laboratory, California, 1994.

(8) International Energy Agency Solar Heating and Cooling Programme: Task *18 "Advanced Glazing and Associated Materials for Solar and Building Applications"*; Task *12 "Building Energy Analysis and Design Tools for Solar Applications"*, Annual Report, International Planning Associates, Inc, 1993.

(9) Technical foundations for Fenestration: Rating and Labelling Procedures, National Fenestration Rating Council, U.S. Department of Energy, 1993.

(10) M. G. Hutchins, P. Ageorges, " *Intercomparison of Measurements of Spectral Transmittance and Reflectance at Different Angles of Incidence*", Final Report, Commission of the European Communities, Community Bureau of Reference, Oxford, May 1992.

(11) M. G. Hutchins, P. Ageorges, " *Angular Dependent Spectral Optical Properties of Architectural Glazings: Results of An Inter-Laboratory Comparison of Measurements*", S.P.I.E Proceedings, Vol. 2017, p. 13, 1993.

(12) Aluminium reference standard, Reference QO03/1/93/064B, Mirror JV93, National Physical Laboratory, U.K.

(13) T. J. Muriss, " *Operational Manual for the OPUS Macros*", SEMRL Internal Report 95/86, Oxford, 1995.

(14) J.A Wiebelt and J.B Henderson " *Selected Ordinates for Total Solar Radiant Property Evaluation from Spectral Data* ", Journal of Heat Transfer, Vol. 101, p. 101, 1979..

(15) Publication C.I.E. No. 152, "*Colorimetry*" (second Edition), Vienna, 1986.

(16) International Standard ISO 9050, ISO/TC 160, " *Glass in Building Determination of Light transmittance, Solar Direct Transmittance, Total Energy Transmittance, Ultraviolet Transmittance and Related Glazing Factors*", Genève, Switzerland, 1990.

(17) Beckman UV 5240, UV-VISIBLE-NIR spectrophotometer," *Beckman Instruction manual"*, Beckman Instrument Inc, U.S.A., 1977.

(18) F. Demichelis, G. Kaniadakis, A. Tagliaferro, E. Tresso, " *New Approach to Optical Analysis Absorbing Thin Solid Films*", Applied Optics, Vol. 26, No. 9, p. 1737, 1987.

(19) F. Wooten, " *Optical Properties of Solids*", Academic Press, New York, p. 48, 1972.

(20) D. L. Wood, J. Tauc, " *Weak Absorption Tails in Amorphous Semiconductors*", Physical Review B, Vol. 5, No. 8, p. 3145, 1972.

(21) A. Nakamura, S. Yamada, " *Fundamental Absorption Edge of Evaporated Amorphous WO_3 Films*", Applied Physics, Vol. 24, p. 55, 1981.

(22) Southampton Electrochemistry Group " *Instrumental Methods in Electrochemistry*", Ellis Horwood Series in Physical Chemistry, Chapter 1, England, 1990.

(23) Fluke calibrated multimeter, N.A.M.A.S. calibrated, Serial No. 5865269, Certificate No. 12800, November 1993.

(24) M. G. Hutchins, P. Ageorges, T. J. Muriss, Second Periodic Report for Contract JOU2-CT92-0048, "*Solid State Variable Transmission Window*", for The Commission of the European Communities, JOULE II Programme, Oxford, March 1994.

(25) C.M. Lampert, Vo-Van Truong, N. Nagai and M.G. Hutchins " *Characterisation parameters and test methods for electrochromic devices in glazing applications*", IEA task X-C, Interim Report.

(26) M. A. Hayat, " *X-Ray Microanalysis in Biology*", Edt M.A. Hayat, Macmillan Press, Cambridge, 1975.

(27) F. M. Smiths, " *Measurements of Sheet Resistivities with the Four-Point Probe*", The Bell System Technical Journal, p. 711, May, 1958.

Chapter 5

(1) T. Naba, T. Takahashi, J. Takada, A. Osaka, Y. Miura, I. Yasui, A. Kishimoto, T. Kudo, " *Characterisation of Amorphous Tungsten Trioxide Thin-films Prepared by RF Magnetron Sputtering Method*", Journal of Non-Crystalline Solids, Vol. 178, p. 233, 1994.

(2) C. Bohnke, O. Bohnoke, " *Heat Treatment of Amorphous Electrochromic WO_3 Thin Films Deposited onto Indium-Tin Oxide Substrates*", Journal of Applied Electrochemistry, Vol. 18, p. 715, 1988.

(3) H. Kaneko, K. Miyake," *Estimation of the Composition Parameter of Electrochemically Coloured Amorphous Hydrogen Tungsten Oxide Films*", Journal of Applied Physics, Vol. 66, Part 2, p. 854, 1989.

(4) J. Arakaki, R. Reyes, M. Horn, W. Estrada, " *Electrochromism in NiO_x and WO_x Obtained by Spray Pyrolysis*", Solar Energy Materials and Solar Cells, Vol. 37, p. 33, 1995.

(5) D. C. Green, J. M. Bell, G. B. Smith, " *Microstructure and Stoichiometry Effect in Electrochromic Sol-Gel Deposited Tungsten Oxide Films*", S.P.I.E. Proceedings, Vol. 1728, 1992.

(6) S. A. Agnihotry, R. Ramchandran, S. Chandra," *Pre-Existence of H_xWO_3 in e-Beam Deposited WO_3 Films*", Solar Energy Materials and Solar Cells, Vol. 36, No. 3, p. 289, 1995.

(7) T. Maruyama, S. Arai," *Electrochromic Properties of Tungsten Trioxide Thin-Films Prepared by Chemical Vapour Deposition*", Journal of the Electrochemical Society, Vol. 141, No. 4, p. 1021,1994.

(8) S. E. Selkowitz, M. Rubin, E. S. Lee, R. Sullivan, " *A Review of Electrochromic Window Performance Factors*", S.P.I.E. Proceedings, Vol. 2255, p. 227, Freiburg, 1994.

(9) S.M. Christie, " *Optical and Electrochromic Properties of Reactively Sputtered Tungsten Oxide Films for Window Glazings*", Mphil, Oxford Polytechnic, 1989.

(10) M.G. Hutchins, A.A. Ramadan, S.A. Aly, " *Electrochromism of D.C. Sputtered WO_3 Films*", presented at the XVIII Conference on Solid State Science for The Egyptian Society of Solid State Science and Applications, January 22 - 26, 1995.

(11) A. Deneuville, P. Gerard, " *Influence of Substoichiometry, Hydrogen Content and Crystallinity on the Optical and Electrical Properties of the H_xWO_y Thin Films*", Journal of Electronic Materials, Vol. 7, No. 4, p. 559, 1978.

(12) OCLI (Santa Rosa, California, USA) supplied sputtered tungsten oxide films for the IEA Task 18 Subtask B3.

(13) B. Chevalier, " *Optical and Microstructure Properties of Different Electrochromic Samples*". IEA Solar Heating and Cooling Programme, Task 18, Report T18/B3/FRA1/95, CSTB France. 1995.

(14) K. Yoshimura, " *Characterisation of OCLI Electrochromic samples* ", IEA Solar Heating and Cooling Programme, Task 18, Report T18/B3/JAP/95, National Industrial Research Institute of Nagoya, Japan, 1995.

(15) P. Schlotter, L. Pickelmann, " *The Xerogel Structure of Thermally Evaporated Tungsten Oxide Layers*", Journal of Electronic Materials, Vol. 11, No. 2, p. 207, 1982.

(16) M. F. Daniel, B. Desbat, J. C. Lassegues, B. Gerand, M. Figlarz, " *Infrared and Raman Study of WO_3 Tungsten Trioxides and WO_3,H_2O Tungsten Trioxide Hydrates*", Journal of Solid State Chemistry, Vol. 67, No. 2, p.235, 1987.

(17) J. Nagai, G. D. McMeeking, Y. Noutomi, " *Optical and Electrochemical Properties of OCLI WO_3 Films*", IEA Solar Heating and Cooling Programme, Task 18, Report T18/B3/JAP1/95, Asahi Glass, Japan, 1995.

(18) P. Ageorges, M. G. Hutchins, " *Reflection, transmission and absorption measurements of 3 different types of electrochromic tungsten oxide films*", IEA Solar Heating and Cooling Programme, Task 18, Report T18/B3/UK1/94, Oxford Brookes University, 1995.

(19) B. Reichman, A. J. Bard, " *The Electrochromic Process at WO_3 Electrodes Prepared by Vacuum Evaporation and Anodic Oxidation of W*", Journal of the Electrochemical Society, Vol.126, No. 126, p. 583, 1979.

(20) N. Yoshiike, y. Mizuno and S. Kondo, '*Behaviour of the evaporated WO_3 film in Li-salt PC electrolyte*', Journal of the Electrochemical Society, Vol. 131, p. 2634, 1984.

(21) K. Michalak, Department of Chemistry, University of Southampton, UK, private information.

(22) F. Kanai, S. Kurita, S. Sugioka, H. Li, Y. Mita, " *Optical Characteristics of WO_3 Electrochromic Cells under Heavy Li Ion Injection* " Journal of the Electrochemical Society, Vol. 129, p. 2633, 1982.

(23) P. V. Ashrit, G. Bader, F. E. Girouard, Vo-Van Truong, " *Electrochromic Materials for Smart Window Applications*", S.P.I.E., Vol. 1401, p. 119, 1990.

(24) A. M. Andersson, " *Electrochemical and Optical Measurements on OCLI WO_3 Samples*", IEA Solar Heating and Cooling Programme, Task 18, Report T18/B3/SWE1/95, Chalmers University of Technology, Sweden, 1995.

(25) P. V. Ashrit, Vo-Van Truong, " *Reflection, Transmission and Absorption Measurements of OCLI Electrochromic Samples*", IEA Solar Heating and Cooling Programme, Task 18, Report T18/B3/CAN1/94, University of Moncton, Canada, 1995.

(26) H. Akram, M. Kitao, S. Yamada, "*Electrochromic properties of rf-sputtered tungstic oxide film prepared from a W metal target*", Journal of Applied Physics, Vol. 66, No. 9, p. 4364, 1989.

Chapter 6

(1) T. Maruyama, S. Arai, "*The Electrochromic Properties of Nickel Oxide Thin Films Prepared by Chemical Vapor Deposition* ", Solar Energy Materials and Solar Cells, Vol. 30, p. 257, 1993.

(2) C. M. Lampert, R. S. Caron-Popowich, " *Electron Microscopy and Electrochemistry of Nickel Oxide Films for Electrochromic Devices Produced by Different Techniques*", S.P.I.E. Proceedings, Vol. 1149, p. 46, 1989.

(3) R. M. Torresi, M. V. Vasquez, A. Gorenstein, S. I. Cordoba-Torresi, "*Infrared Characterisation of Electrochromic Nickel Hydroxide Prepared by Homogenous Chemical Precipitation* ", Thin Solid Films, Vol. 229, p. 180, 1993.

(4) P.C Miller and U.B Thomas, '*Advances in Electrochemistry and Electrochemical Engineering*', Edt. C.W. Tobias, Interscience, Vol. 5, p. 1, 1967.

(5) U. Falk, A. J. Salkind, " *Alkaline Storage Batteries*", Wiley, New York, 1969.

(6) B.E. Conway, M.A Sattar and D.Gilroy, " *Electrochemistry of the Nickel Oxide Electrode - V. Self Passivation Effects in Oxygen Evolution Kinetics*", Electrochim. Acta, Vol. 14, p. 677, 1969.

(7) M.A Sattar and B.E. Conway, " *Electrochemistry of the Nickel Oxide Electrode - VI. Surface Oxidation of Nickel Anodes in Alkaline Solution*", Electrochim. Acta, Vol. 14, p. 695, 1969.

(8) B.E. Conway, M.A Sattar and D.Gilroy, " *Electrochemistry of the Nickel Oxide Electrode - VII. Potentiostatic Step Method For Study of Adsorbed Intermediates* ", Electrochim. Acta, Vol. 14, p. 711, 1969.

(9) E. Buder, " *Oxygen Evolution during Recharging of Positive Nickel Oxide Sinter Electrodes*", J. Appl. Electrochem., Vol. 2, p. 301, 1972.

(10) D.M. MacArthur, " *The Hydrated Nickel Oxide Electrode Potential Sweep Experiments*", J. Electrochem. Soc., Vol. 117, No. 4, p. 422, 1970.

(11) P. Oliva, J. Leonardi, J. F Laurent, C. Delmas, J.J. Braconnier, M. Figlrz, F. Fievet, A. de Guibert, " *Review of the Structure and the Electrochemistry of Nickel Hydroxides and Oxy-Hydroxides*", Journal of Power Sources, Vol. 8, No. 2-3, p. 229, 1982.

(12) C. G. Granqvist, " *Handbook of Inorganic Electrochromic Materials*", p. 339, Elsevier Science, Amsterdam, 1993.

(13) F.P Kober, " *Infrared Spectroscopic Investigation of Charge Nickel Hydroxide Electrodes*", J. Electrochem. Soc., Vol. 114, No. 3, p. 215, 1967.

(14) C. Johnson, P. R. Graves, " *In Situ Raman Spectroscopy Study of the Nickel Oxy-Hydroxide Electrode (NOE) System*", AEA Harwell, AERE R 13466, April 1989.

(15) F.P Kober, " *Analysis of the Charge Discharge Characteristics of Nickel Oxide Electrodes by Infrared Spectroscopy*", J. Electrochem. Soc., Vol. 112, No. 11, p. 1064, 1965.

(16) S. A. Aleshkevich, E.I. Golovchenko, V.P. Morozov, and L.N. Sagoyan, " *Proton Behaviour in an Oxide-Nickel Electrode*", Soviet Electrochem., Vol. 4, No. 530, p. 1117, 1968.

(17) M.G. Hutchins, G. D. McMeeking and Z. Crnjak Orel, " *Infrared Analysis of Electrochromic Nickel Oxide Coating* ", SPIE, Vol. 1728, Optical Materials Technology for Energy Efficiency and Solar Energy Conversion XI, 1992.

(18) M. G. Hutchins, G. McMeeking, H. Xingfang, " *R.F. Diode Sputtered Electrochromic Nickel Oxide Films*", S.P.I.E. Conference Proceedings, Vol. 1272, p. 139, 1990.

(19) G. D. McMeeking, " *The Deposition of Nickel Oxide Films for Novel Electrochromic Devices*", Mphil to PhD transfer report, Oxford Polytechnic, Solar Energy Materials Research Laboratory, 1991.

(20) G. McMeeking, Z. Orel, "*Comparison of the Electrochromic Properties of Nickel Oxide Films Formed by R.F. Sputtering and Anodic Electrodeposition Process*", S.E.M.R.L. Internal Report, Oxford Brookes University, 1991.

(21) H. Xingfang, C. Xiaofeng and M. G Hutchins,' *Study on the Electrochromic Mechanism of RF Diode Sputtered Nickel Oxide Films*', S.P.I.E. Proceedings, Vol. 1728, p. 73, 1992.

(22) M. Fantini and A. Gorenstein, ' *Electrochromic Nickel Hydroxide Films on Transparent/Conducting Substrates* ', Sol. Energy Mat., Vol. 16, p. 487, 1987.

(23) R. M. Bendert and D.A. Corrigan,' *Effect of Coprecipitated Metal Ions on the Electrochromic Properties of Nickel Hydroxide.*', J. Electrochem. Soc., Vol. 136, No. 5, p. 1369, 1989.

(24) P. Pramanik and S. Bhattacharya,' *A Chemical Method for the Deposition of Nickel Oxide Films*', J. Electrochem. Soc., Vol. 137, No.12, p. 3869, 1990.

(25) J. Joseph, H. Gomathi and G.P Rao,' *A Simple Novel Method of Preparing Thin Surface Films of Electrochromic* $Ni(OH)_2/NiOOH$', Sol. Energy Mat., Vol. 23, p. 1, 1991.

(26) A. K. Tolstikhina, V. N. Petrov, S. S. Olevskii, A. V. Koschchienko, S. O. Semiletov, B. I. Kozyrkin, " *Structure and composition of Nickel Oxide Films*", Inorganic Materials, Vol. 23, No. 6, p. 863, 1987.

(27) J. S. E. M. Svensson, C. G. Granqvist, " *Sputter Deposited Nickel-oxide-Based Electrochromic Coatings*", S.P.I.E. Institute Series, Vol. IS 4, p. 285, 1989.

(28) R. S. Connell, D. A. Corrigan, B. R. Powell, " *The electrochromic Properties of Sputtered Nickel Oxide Films*", Solar Energy Materials and Solar Cells, Vol. 25, p. 301, 1992.

(29) P. Ageorges, " *Physical Deposition and Characterisation of Electrochromic Nickel Oxide Films*", MPhil to PhD Transfer Report, Oxford Brookes University, 1994.

(30) A. Gorenstein, F. Decker, M. Fantini, W. Estrada, "*Hydrated Nickel Oxide Films: Electrochemical and Related Physical Properties*", S. P. I. E. Institute Series, Vol. IS 4, p. 272, 1989.

(31) M. G. Hutchins, P. J. Wright, P. D. Grebenik, " *Comparison of Different Forms of Black Cobalt Selective Solar Absorber Surfaces*", Solar Energy Materials, Vol. 16, p. 113, 1987.

(32) Hu Xingfang, Chen Xiaofeng, Song Xiangyun, " *Structure Study on Electrochromic Films of Nickel Oxide* ", S.P.I.E. Proceedings, Vol. 2017, p. 172, 1993.

(33) G. D. McMeeking, " *Deposition and Characterisation of Nickel Oxide Based Coatings for Advanced Glazing Applications*", PhD thesis, Oxford Brookes University, September 1995.

(34) M. G. Hutchins, T. P. Murphy, " *Oxidation States in Nickel Oxide Electrochromism*", Sol. En. Mat. and Sol. Cells, Vol 39, p. 111, 1995.

(35) J. Desilvestro, D. A. Corrigan, M. J. Weaver, " *Spectroelectrochemistry of Thin Nickel-Hydroxide Films on Gold Using surface Enhanced Raman Spectroscopy*", Journal of Physical Chemistry, Vol. 90, No. 24, p. 6408, 1986.

(36) A. M. Andersson, " *Electrochromic Materials: Optical, Electrophysical and Structural Properties*", PhD Thesis, University of Göteborg, Sweden, p. 70, 1992.

(37) T. Ohzuku, A. Ueda, M. Nagayama, " *Electrochemistry and Structural Chemistry of $LiNiO_2$ for 4 Volt Secondary Lithium Cells*", Journal of the Electrochemical Society, Vol. 140, No. 7, p. 1862, 1993.

(38) T. Ohzuku, A. Ueda, M. Nagayama, Y. Iwakoshi, H. Komori, " *Comparative Study of $LiCOO_2$, $LiNi_1/2CO_1/2O_2$ and $LiNiO_2$ for 4 Volt Secondary Lithium Cells*", Electrochemica Acta, Vol. 38, No. 9, p. 1159, 1993.

(39) I. Brotherston, Z. Cao, J. R. Owen, First Periodic Report for Contract JOU2-CT92-0048, "*Solid State Variable Transmission Window*", for The Commission of the European Communities, JOULE II Programme, October 1993.

(40) Sargent-Welch Scientific Company, "*Table of Periodic Properties of the Elements*", Chicago, 1978.

(41) D. A. Corrigan, M. K. Carpenter, " *Electrochromic Nickel Hydroxide Films and the Effects of Foreign Metal Ions*", S.P.I.E. Intitute Series, Vol. IS4, p. 298, 1988.

(42) S. Tanemura, " *Energy Benefit of Smart Windows and the State of the Art of their R&D in Japan*", Proceedings of the 5th Intl. Sym. on New Glass, Tokyo, p. 37, 1995.

(43) I.D. Brotherston, Z. Cao, G. Thomas, P. Weglicki, J. R. Owen, " *Counterelectrode Films for Electrochromic Windows*", Solar Energy Materials and Solar Cells, Vol. 39, p. 257, 1995.

Chapter 7

(1) S.F. Cogan, M. N. Nguyet, S. J. Perrotti, R. D. Rauh, " *Optical Properties of Electrochromic Vanadium Pentoxide*", Journal of Applied Physics, Vol. 66, No. 3, p. 1333, 1989.

(2) N. Machida, R. Fuchida, T. Minami, " *Behavior of rapidly Quenched V_2O_5 Glass at Cathode in Lithium Cells*", Journal of the Electrochemical Society, Vol. 136, No. 8, p. 2133, 1989.

(3) M. S. R. Khan, K. A. Khan, W. Estrada, C. G. Granqvist, " *Electrochromism and Thermochromism of Li_xVO_2 Thin Films*", Journal of Applied Physics, Vol. 69, No. 5, p. 3231, 1991.

(4) J.L. Ord, D.J. Desmet, D. J. Beckstead, " *Electrochemical and Optical Properties of Anodic Oxide Films on Titanium*", Journal of Electrochemical Society, Vol.136, No. 8, p. 2179, 1989.

(5) A. Hagfeldt, N. Vlachopoulos, S. Gilbert, M. Grätzel, " *Electrochromic Switching with Nanocrystalline TiO_2 Semiconductor Films*", S.P.I.E. Proceedings, Vol. 2255, p. 297, 1994.

(6) U. Lavrencic Štangar, B. Orel, I. Grabec, B. Ogorevc, K. Kalcher, " *Optical and Electrochemical Properties of CeO_2 and CeO_2-TiO_2 Coatings*", Solar Energy Materials and Solar Cells, Vol. 31, No. 2, p. 171, 1994.

(7) D. Camino, D.Deroo, J. Salardenne, N. Treuil, " *$(CeO_2)_x$-$(TiO_2)_{1-x}$: Counter Electrode Materials for Lithium Electrochromic Devices*", Solar Energy Materials and Solar Cells, Vol. 39, p. 349, 1995.

(8) L. Kullman, A. Azens, A. Gutarra, C. G. Granqvist, " *D.C. Magnetron Sputtered Mo-Ti Oxide Films for Colour Neutral Electrochromic Devices*", not published yet, 1995.

(9) A. Gutarra, A. Azens, B. Stjerna, C. G. Granqvist, " *Electrochromism of Sputtered Fluorinated Titanium Oxide Thin Films*", Applied Physics Letters, Vol. 64, No. 13, p. 1604, 1994.

(10) Y. Li, T. Kudo, " *Properties of Mixed-Oxide MoO_3/V_2O_5 Electrochromic Films Coated from Peroxo-Polymolybdovanadate Solutions*", Solar Energy Materials and Solar Cells, Vol. 39, p. 179, 1995.

(11) A. Talledo, B. Stjerna, C. G. Granqvist, " *optical Properties of Lithium-Intercalated V_2O_5-based Films Treated in CF_4 Gas*", Applied Physics Letters, Vol. 65, No. 22, p. 2774, 1994.

(12) P. Jin, M. Tazawa, K. Yoshimura, T. Miki, K. Igarashi, S, Tanemura, " *Thermochromism of Metal-Doped VO_2 Films Deposited by Dual Target Sputtering*", S.P.I.E. Proceedings, Vol. 2255, p. 423, 1994.

(13) M. A. Sobhan, R. T. Kivaisi, B. Stjerna, C. G. Granqvist, " *Reactively Sputtered Thermochromic Tungsten Doped VO_2 Films*", S.P.I.E. Proceedings, Vol. 2255, p. 423, 1994.

(14) Kapton™ film backed by a silicone adhesive. This is a trade mark of Dupont de Nemours, France.

(15) J.M. Gallego, J. R. Siddle, M. S. Burdis, R.A. Batchelor, Fourth Periodic Report for Contract JOU2-CT92-0048, "*Solid State Variable Transmission Window*", for The Commission of the European Communities, JOULE II Programme, April 1995 .

(16) Sargent-Welch Scientific Company, " *Table of Periodic Properties of the Elements*", Chicago, 1978.

(17) C. G. Granqvist, " *Handbook of Inorganic Electrochromic Materials*", p. 271 and p. 325, Elsevier Science, Amsterdam, 1995.

(18) J. Göttsche, A. Hinsch, V. Wittwer, " *Electrochromic Mixed WO_3-TiO_2 Thin Films Produced by Sputtering and the Sol-gel Technique : A Comparison*", Solar Energy Materials and Solar Cells, Vol. 31, p. 415, 1993.

(19) S. Hashimoto, H. Matsuoka, " *Lifetime of Electrochromism of Amorphous WO_3-TiO_2 Thin Films*", Journal of the Electrochemical Society, Vol. 38, p. 2403, 1991.

(20) F. Michalak, Final Periodic Report for Contract JOU2-CT92-0048, "*Solid State Variable Transmission Window*", for The Commission of the European Communities, JOULE II Programme, not published yet .

(21) A. Bernasik, M. Radecka, M. Rekas, M. Sloma, " *Electrical properties of Cr- and Nb- doped TiO_2 Thin Films*", Applied Surface Science, Vol. 65/66, p. 240, 1993.

Chapter 8

(1) Joule II-Programme, DG XIII, Commission of the European Communities, Contract CT92-0048, March 1993 - March 1996.

(2) T. Maruyama, S. Arai, "*Electrochromic Properties of Conductive Thin-Films Prepared by Radiofrequency Magnetron Sputtering Method* ", Applied Physics Letters, Vol. 63, p. 869, 1993.

(3) L. A. Ryabova, V.S. Salun, I.A. Serbinov, "*Transparent Conductive Films of In_2O_3-Sn Prepared by the pyrolysis Method*", Thin Solid Films, Vol. 92, p. 327, 1982.

(4) C. G. Granqvist, " *Materials Science For Solar Energy Conversion Systems*", p. 126, Pergamon Press, Oxford, 1991.

(5) J. Gallego, Pilkington Technology Centre Ltd, private communication, unpublished work.

(6) G. Frank, H. Kostlin, " *Electrical Properties and Defect Model of Tin-Doped Indium Oxide Layers* ", Journal of Applied Physics, A-Solids and surfaces, Vol. 27, No. 4, p. 197, 1982.

(7) J.C.C. Fan, F. J. Nachner, " *Properties of Sn-Doped In_2O_3 Films Prepared by R. F. Sputtering*". Journal of the Electrochemical Society, Solid-State Science and Technology, Vol. 122, No. 12, p. 1719, 1978.

(8) G. Cochrane, Z. T. Zheng, G. B. Smith, " *Optimization of the Electrical and Optical Properties of ITO Layers Deposited by Magnetron Sputtering*", S. P. I. E Proceedings, Vol. 2017, p. 68, 1994.

(9) M. Consigny, A. Wensjo, S. Yde-Andersen," *Solid State Variable Transmission Windows*", Second Periodic Report for Contract CT92-0048, Joule II-Programme, Commission of the European Communities, March 1994.

(10) M. Consigny, S. Yde-Andersen," *Solid State Variable Transmission Windows*", First Periodic Report for Contract CT92-0048, Joule II-Programme, Commission of the European Communities, September 1993.

(11) F. M. Gray, " *Solid Polymer Electrolytes*", VCH, p. 83, 1991.

(12) A. Wendsjo, M. Consigny, S. Y. Yde-Andersen, "*Solid State Variable Transmission Window*", Third Periodic Report for Contract CT92-0048, Joule II-Programme, Commission of the European Communities, September 1994.

(13) A. Wendsjo, M. Consigny, S. Y. Yde-Andersen, "*Solid State Variable Transmission Window*", Fourth Periodic Report for Contract CT92-0048, Joule II-Programme, Commission of the European Communities, March 1995.

(14) Copper coated with a highly conductive adhesive acrylic supplied by RS.

(15) Double sided extra bond 4910F adhesive tape supplied by 3M.

(16) D. Rauh, " *Design and Fabrication of Electrochromic Light Modulators*", Solar Energy Materials and Solar Cells, Vol. 39, p. 145, 1995.

(17) Work in collaboration with Dr Mark Burdis, Pilkington Technology Centre, Lathom, UK, under Joule II-Programme for the Commission of the European Communities.

(18) A. W. Czanderna, C. M. Lampert, " *Evaluation Criteria and Test Methods for Electrochromic Windows*", Report for the U.S. Department of Energy under contract No. DE-AC02-83CH10093, July 1990.

Chapter 9

(1) S. Tanemura, " *Energy Benefit of Smart Windows and the State-of-the-Art of their R & D in Japan*", Proc. of the 5th Intl. Sym. on New Glass, p. 37, October 1995.

(2) I.D. Brotherston, Z. Cao, G. Thomas, P. Weglicki, J. R. Owen, " *Counterelectrode Films for Electrochromic Windows*", Solar Energy Materials and Solar Cells, Vol. 39, p. 257, 1995.

(3) A. M. Andersson, " *Electrochromic Materials: Optical, Electrophysical and Structural Properties*", PhD Thesis, Department of Physics, University of Göteborg, 1992.

(4) S. Passerini, B. Scrosati, A. Gorenstein, " *The Intercalation of Lithium in Nickel Oxide and its Electrochromic Properties*", Journal of the Electrochemical Society, Vol. 137, No. 10, p. 3297, October 1990.

STUDIES ON ELECTROCHROMIC MATERIALS AND DEVICES

by

Philippe Ageorges

A thesis submitted in fulfilment of the requirements
for the degree of Doctor of Philosophy

STUDIES ON ELECTROCHROMIC MATERIALS AND DEVICES

by

Philippe Ageorges

A thesis submitted in fulfilment of the requirements
for the degree of Doctor of Philosophy

Solar Energy Materials Research Laboratory
School of Engineering
Oxford Brookes University
Gipsy Lane
Oxford OX3 0BP
United Kingdom

May 1996

Adsuefacte ad ea etiam, de quibus desperas.

Marci Antonini, imperatoris,

De seipsos et ad seipsum, Libri XII.

PREFACE

The objective of this thesis is devoted to technologies that can be used for advanced energy-efficient fenestration systems. A better understanding of energy impacts can make more efficient use of advanced fenestration technologies. Solar passive technologies, including low-e coatings, gas fills and insulating frames have helped to increase the overall thermal resistance of fenestration products. However, they do not consider natural season and daily variations. Switchable glazing technologies and electrochromism in particular are the focus of international research interests for both academic and industrial institutions.

A growing interest has been shown in studying new electrochromic materials and in understanding their fundamental mechanisms. International research activities are concentrated on the development and optimisation of the different materials and layers that may comprise future commercial electrochromic products. There is an increasing number of materials available, though their suitability in an ECD remains to be studied.

This work concentrates on the deposition and performance of two different types of complementary layers which may be used in the construction of electrochromic devices. These layers can act as active or as passive materials such as nickel oxide and titanium oxide doped with vanadium respectively. The films as well as the active tungsten oxide electrochromic layer were produced by R.F. magnetron sputtering techniques and their optical and electrochemical properties were optimised. Their electrochromism was studied under protonic and lithiated electrolytes. Prototype devices were assembled and tested under lithium ion insertion and extraction using an acrylate polymer. Finally, the different prototypes were characterised and compared to match the performance of an ideal EC device of interest for energy efficiency.

ACKNOWLEDGEMENTS

I would like to acknowledge and give thanks to all those who have helped with the development of this research. I would especially like to thank Prof M.G. Hutchins, my supervisor, for his support during all these years and his guidance throughout this thesis.

I wish to thank Dr Zorica Crnjak Orel (National Institute of Chemistry, Ljubljana, Slovenia) and Dr Alla Cordery for their continuous guidance and friendship during this work.

Special thanks to my colleague and friend Mrs Theresa-Jane Squire for all her work on the scanning electron microscope and her assistance with the spectroscopy measurements.

Thanks also to the members of the Solar Energy Materials Research Laboratory as well as all the academic and non-academic staff of the School of Engineering, Oxford Brookes University.

I am also extremely grateful to Dr Keith Refson (Department of Earth Sciences, Oxford University) for his explanations and assistance in writing Chapter 3 and Chapter 6 of this thesis, and to Dr Mark Burdis (Pilkington) for his help in Chapter 7 and Chapter 8.

Finally, I am very grateful to Mr Richard Holland for proofreading this thesis.

This work was funded in part by an award from the Commission of the European Communities, DG XII, Non-Nuclear Energies Programme, Joule I, in collaboration with Pilkington Technology Centre Ltd, Lathom, UK; the Department of Chemistry, University of Southampton, UK; and Danionics, Denmark.

ABSTRACT

This thesis investigates electrochromic thin films needed to construct a variable transmission electrochromic device. Such a device is made of 5 layers sandwiched between 2 pieces of glass: two electronic transparent conducting layers, an optically active electrochromic layer (WO_3), a ion-conducting polymer electrolyte and an ion-storage layer (NiO_x, TiO_x, VO_x, $V_zTi_yO_x$) .

Electrochromic NiO_x thin films were produced by R.F. magnetron sputtering and electrodeposition techniques and studied under proton intercalation. A visible transmittance modulation of 0.70 and 0.80 and a visible coloration efficiency of 35 and 100 $cm^2.C^{-1}$ for a thickness of 300 and 200 nm were obtained for sputtered and chemically-deposited NiO_x films respectively. Anodic films are extremely porous and soft. Under the mechanical stresses of ionic insertion/extraction they degrade more quickly than the compact nanostructure of physically deposited films. When studied under lithium intercalation, sputtered NiO_x films exhibit a nucleation loop observed in cyclic voltammetry indicating the growth of a new phase and are seen to degrade quickly. NiO_x films were not seen to be potential candidates for EC applications using Li^+ intercalation.

WO_3, TiO_x and VO_x thin films were deposited by R.F. magnetron sputtering and studied under Li^+ intercalation/deintercalation. Optimised WO_3 films exhibited good electrochromic properties: a visible transmittance modulation of 0.82 and a visible coloration efficiency of 49 $cm^2.C^{-1}$ for a thickness of 450 nm.

Electrochromic properties of TiO_x films were seen to not strongly depend on the sputtering process parameters whereas VO_x films showed a stronger dependence. TiO_x films are able to store a limited quantity of charge Q = 13 $mC.cm^{-2}$ for thicknesses greater than 13 nm. They are transparent in both charged and uncharged states $T_{v,u}$ and $T_{v,ch} > 0.80$, and are stable upon charge insertion/extraction. VO_x films can store a much larger quantity of charge Q = 35 $mC.cm^{-2}$ for a thickness of 70 nm. They are yellow in

the uncharged state and bluish in the charged state: $T_{v,u}$ and $T_{v,ch} > 0.70$, and the charge insertion/extraction process is seen to evolve during the initial cycles. Both TiO_x and VO_x films did not show all the required electrochromic properties for EC applications.

The main achievement of this work was the development of highly durable vanadium/titanium mixed oxide thin films. Work was carried out on different V/Ti ratios using specific deposition techniques developed for that purpose. Films with a vanadium to titanium ratio of about 50 % showed optimum performance characteristics for passive ion storage layer applications. Such layers deposited on ITO exhibited high visible transmittance: $T_{v,ch} > 0.62$, and a relatively low visible modulation (0.20), with high storage capacity $Q > 40$ mC.cm^{-2} for a thickness of 80 nm.

The laminated WO_3/PAAUA/$V_zTi_yO_x$ EC device was assembled and exhibited under specific switching conditions encouraging properties: a visible transmittance modulation > 0.50 over more than 10^5 cycles.

Table of Contents

PART A

FUNDAMENTAL CONCEPTS

Chapter 1

INTRODUCTION

1.1 Background

Over the past 25 years, a growing interest has been expressed by both research and industrial communities in the thermal performance and optical behaviour of glazings. More recently, in the face of energy implications and associated environmental problems, international organisations[1] and countries[2,3] have increased research and development activities in the field of energy efficient buildings. Today's commercial and residential architecture incorporates large areas of glass walls and fenestration for lighting and aesthetics. With such modern designs, traditional glazings with low thermal resistance would increase heating loads in winter, while in summer the transmission of solar radiation would increase the cooling loads. Space conditioning in developed countries represents 40 % to 60 % of the annual energy consumption used in heating, lighting and cooling[2].

Thermal losses through traditional single glazed windows account for some 10 % of the total heat loss of a building[2]. Energy efficient windows involve the control of the incoming radiation and of the heat gains or losses due to radiation, conduction and convection. Different climates require different approaches to regulate the throughput of radiant energy[4]. Windows should be designed such that the solar gains are greater than the energy losses. Among the different possibilities to reduce heat losses without blocking visible radiation, passive solar glazings offer an alternative technology to insulating shutters. Specific techniques have been developed over the past 20 years to achieve a static control of solar and heat gain, and they are already commercially available.

For residential and commercial buildings in cold climates, priority is given to heating energy insulation. Advanced window designs, such as multiple glazings, have been developed to reduce heat losses by a factor of two in *U-values*. By using low-emittance coatings or heat mirrors alone, it is possible to reduce the U-value significantly. In practice, combinations of techniques are used and for instance, the U-value can be further reduced with the use of a gas filling.

For cooling-dominated climates, solar gains through windows must be offset by cooling the building. Such a problem is again solved by the use of heat mirrors, that can filter solar gains. These advanced glazings selectively transmit visible light and reflect the near infrared component of the solar radiation.

The heating and cooling demands of buildings vary seasonally. The use of heat mirrors assists in reducing heat gains, by preventing the admission of solar radiation that may be present at certain times of the year. Thus a dynamic control of glazing properties seems to be an attractive alternative. Switchable systems can have their optical properties modulated in response to the demands of the building environment. Such materials are called *chromogenic*. There are 3 different chromogenic classes; *photochromic* materials which change their optical properties in response to the intensity of incident light; *thermochromic* materials which modulate their optical properties with temperature; and *electrochromic* materials which reversibly alter their optical properties as a function of an applied voltage. Promising results have been obtained for these materials which show a reversible change in the visible spectrum between dark and transparent states. Incorporated into a building, dynamic fenestration technologies could make a more positive contribution to energy saving throughout the year[2]. Such systems allow excessive solar gains to be rejected during periods of high solar radiation, while still allowing the window to admit as much solar radiation as possible during periods of lower daylight availability.

1.2 Optical properties of materials for solar energy conversion

The basic understanding of solar energy efficiency lies in the radiative properties of our natural surroundings. The radiation which prevails in our ambience is confined at specific and well-defined wavelengths. Figure 1.1(a) illustrates the solar spectral distribution[5,6] above the atmosphere (denoted Air Mass 0 or *AMO*) and at ground level (*AM2*) on the horizontal to the sun under clear weather conditions.

The terrestrial solar spectrum is seen to be confined in the range 0.3 - 3 μm. Figure 1.1(a) shows that about 45% of the sun's energy lies in the visible region, about 52% lies in the near infra-red and the remaining 3% is in the ultra-violet. The radiation that reaches the Earth has been attenuated and scattered by absorption in the atmosphere, and this is mainly due to the presence of carbon dioxide, water vapour and ozone. The integrated area under the solar spectrum (AM0) curve gives a solar intensity (or irradiance) constant of 1353 $W.m^{-2}$. After absorption in the atmosphere the maximum solar irradiance (AM2) is limited to less than 1000 $W.m^{-2}$.

Visible light is in the narrow range $0.4 < \lambda < 0.7$ μm, covering about half the energy of the solar radiation that reaches the Earth. Figure 1.1(c) shows the photopic response (V_λ) of the human eye.

All matter above absolute zero emits radiation. It is convenient to look at the ideal blackbody spectrum, called the Planck spectrum. Planck's law is a consequence of the quantum nature of electromagnetic radiation. Figure 1.1(b) also shows the spectral emissive distributions of four blackbodies (100°C, 50°C, 0°C and -50°C) derived from Planck's law which are of interest for most glazing applications. The spectra are confined in the range 2 - 100 μm. At room temperature the peak lies at about 10μm and will move towards shorter wavelengths as the temperature increases.

The blackbody spectral emissive power is equal to :

$$E_{b,\lambda} = \frac{2\pi h c^2}{\lambda^5 e^{hc/kT} - 1} \qquad [1.1]$$

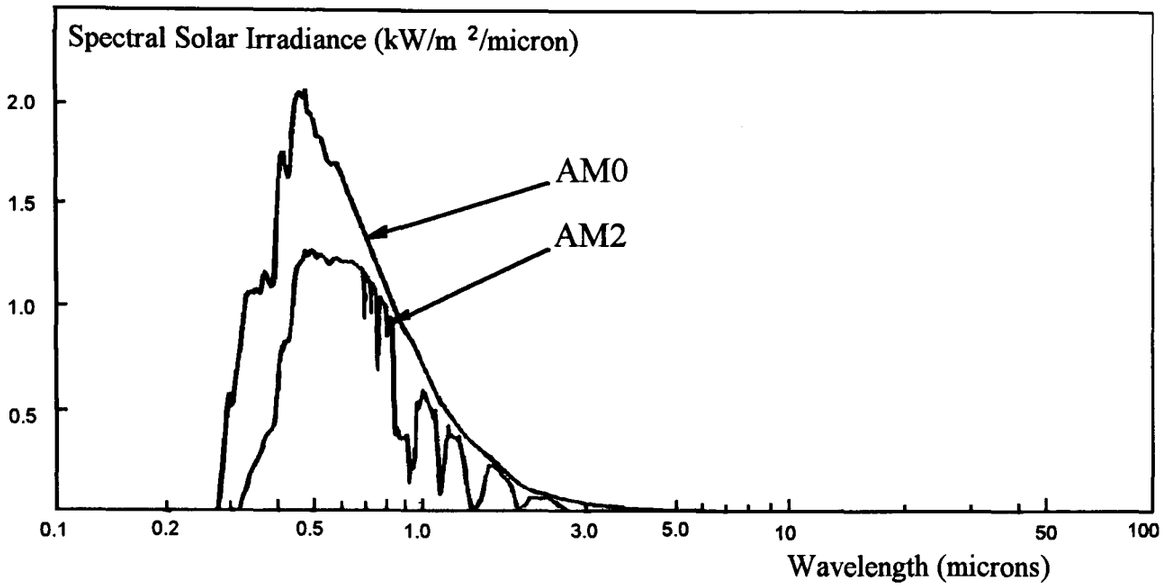

Figure 1.1(a) : Spectral distribution (G_λ) of solar spectrum for *AMO* and *AM2* at normal incidence.

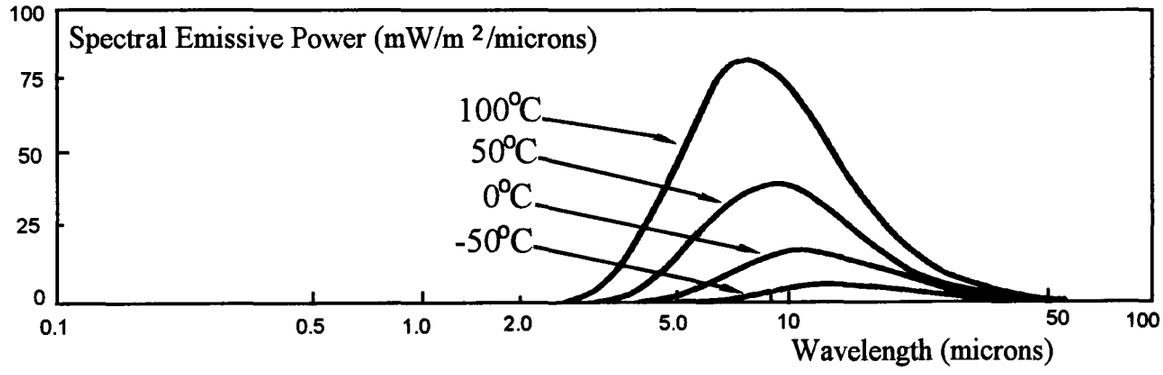

Figure 1.1(b) : Blackbody emissive power ($E_{b,\lambda}$) at different temperatures.

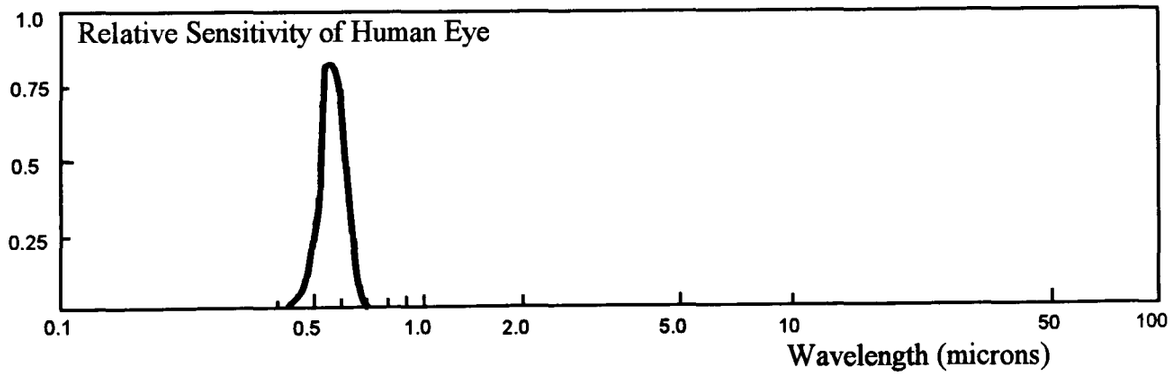

Figure 1.1(c) : Photopic response of the human eye (V_λ).

The wavelength of maximum emission λ_{max}, can be found from the above equation in equating its derivative to zero. The result is given by Wien's law :

$$\lambda_{max} \cdot T = 2897.8\ \mu m \qquad [1.2]$$

Thermal radiation for building and solar heating applications lies between 2.5 - 50 μm and in this range quantitative performance parameters are defined to describe the properties of energy efficient windows. Monochromatic radiation that is incident on a surface can either be absorbed, reflected or transmitted. From Kirchhoff's law and the law of conservation of energy this can be expressed as :

$$A_\lambda = \varepsilon_\lambda \qquad [1.3]$$

$$T_\lambda + R_\lambda + A_\lambda = 1 \qquad [1.4]$$

Where A_λ, R_λ, T_λ and ε_λ are respectively spectral absorptance, reflectance, transmittance and emittance coefficients.

To be able to describe the overall response of a surface to all relevant wavelengths in solar energy applications, it is necessary to define a set of optical properties integrated with respect to a defined spectral distribution (ϕ_λ) over a specific range of the spectrum (λ_1, λ_2). The integrated optical properties are angular dependent, and θ is the angle from the surface normal for the incident or emitted radiation.

The evaluation of the transmittance (T_s, T_v), reflectance (R_s, R_v) or absorptance (A_s, A_v, ε) of glazing materials requires a knowledge of the spectral distribution ϕ_λ. For calculation in the visible region of the spectrum ($\lambda_1 = 0.38\mu m$, $\lambda_2 = 0.78\mu m$), the distribution ϕ_λ is equal to the product of the relative spectral power distribution of an illuminant[7] and the photopic response of the human eye (V_λ).

For calculation in the solar range (λ_1= *0.3 μm*, λ_2= *2.5 μm*), the distribution ϕ_λ is equal to the solar irradiance G_λ for AM0 or AM2. For calculation in the thermal range of the spectrum (λ_1= *2.5 μm*, λ_2= *25 μm*), the function ϕ_λ is equal to the black body emissive power $E_{b,\lambda}$. The radiative properties ($X_{\lambda 1,\lambda 2}$ = T_s, T_v, R_s, R_v, A_s, A_v *or* ε) of films can be calculated from the general formula[7] :

$$X_{\lambda_1,\lambda_2}(\theta) = \frac{\int_{\lambda_1}^{\lambda_2} X_\lambda(\theta,\lambda)\phi_\lambda(\theta)d\lambda}{\int_{\lambda_1}^{\lambda_2} \phi_\lambda(\lambda)d\lambda} \qquad [1.5]$$

where X_λ can be T_λ, R_λ, A_λ, or ε_λ; and ϕ_λ represents the appropriate spectral distribution for the luminous, solar and thermal range.

Solar and thermal radiation are each confined in specific wavelength ranges. The key concept for energy efficiency is spectral selectivity which implies that the radiative properties of glazings differ in different wavelength ranges. It is, for instance, the possibility to combine the transmittance of visible radiation with the reflectance of thermal radiation. Figure 1.2 shows the spectral selectivity of a ZnO film[8] doped with aluminium over the solar spectrum.

1.3 Insulating glazings

Historically, fenestration products have always been a key part of any architectural design. The basic reason for an improved energy efficient glazing lies in the properties of the standard glass window itself.

Figure 1.3 shows the spectral transmittance and reflectance of a 6 mm thick glass. The spectrum shows a very high visible transmittance, which is a key property for advanced glazing development. Glass is also seen to be opaque in the thermal range. Some of the absorbed energy will increase the temperature of the glass, and the thermal emittance is high.

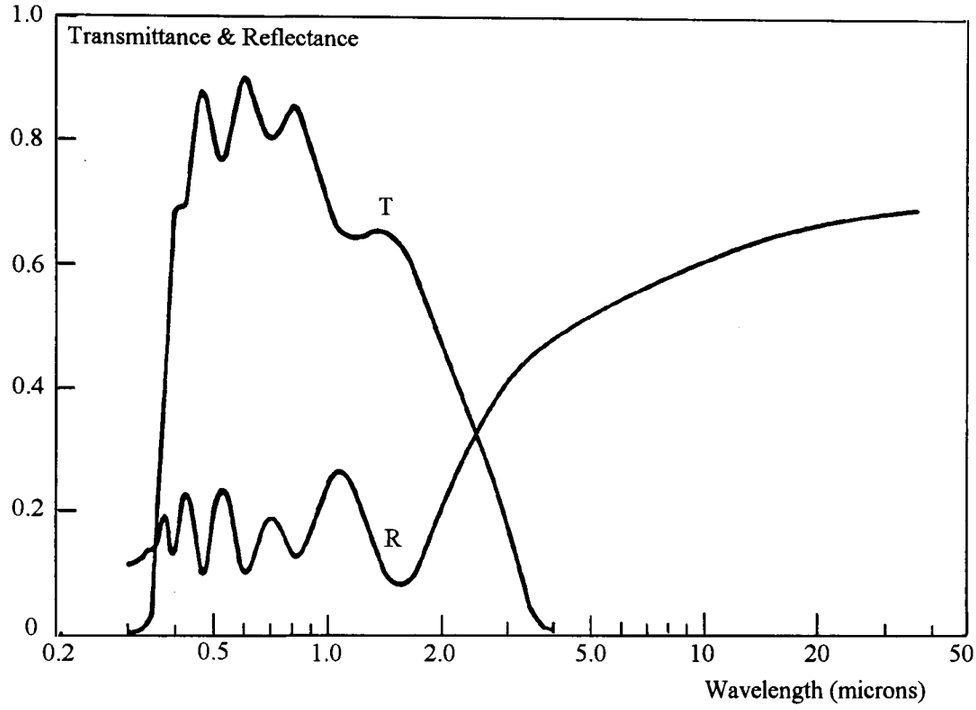

Figure 1.2 : Spectral transmittance and reflectance of a zinc oxide film doped with aluminium[8]: $T_v = 0.84$, $T_s = 0.70$, $R_s = 0.14$ and $\varepsilon_{300°K} = 0.30$.

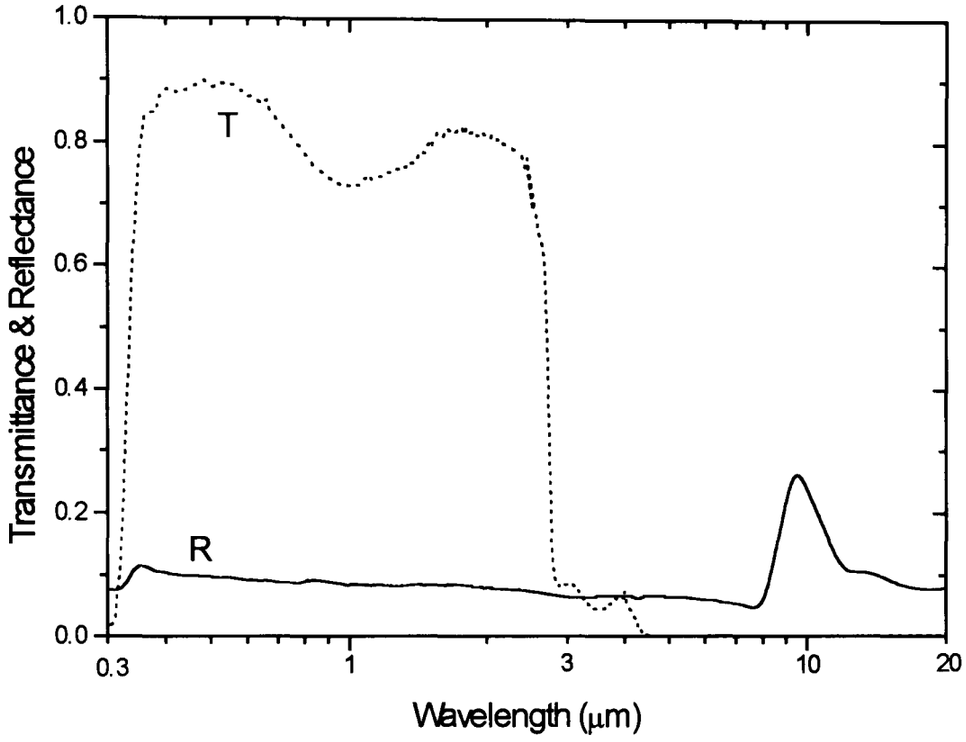

Figure 1.3 : Hemispherical transmittance and reflectance (0.3 - 20 μm) of a 6 mm thick float glass. $T_s = 0.79$, $T_v = 0.89$, $R_s = R_v = 0.07$, $E_{300°K} = 0.87$.

The method used to produce modern float glass was developed by Pilkington, where the glass solidifies on a bath of molten tin. The technique is very well developed and gives a very good uniformity and flatness of the pane. The design of high performance window products is based on understanding heat transfer and optics of window systems. In the past, total heat transfer was based on the glazed areas only. Recent research has demonstrated the importance of the frame and the edge on overall window thermal properties[9]. The total heat transfer coefficient (or *U-value*) of the total window system includes conductive, convective and radiative heat transfer. The solar heat gain coefficient (g_n *or SHGC*) of the total window system represents the solar heat gain through the window system relative to the incident solar radiation and is the sum of the solar transmittance and the longwave input of the solar radiation absorbed within the glazing that enters the building. Heat transfer through window systems can be separated into a heat transfer through the centre of glass areas and through the frame and edge areas. Also different environmental effects strongly influence window heat transfer such as : the solar spectrum, indoor and outdoor radiative temperatures, wind speed and direction and air flow inside the building.

For many years, northern European buildings have been using two sets of glass windows containing an air interlayer. This system could alter heat transfer by thermal radiation conduction or convection. After single glass windows, this glazing system was the first to combine high transmittance with a reduction in energy losses.

Technologically advanced windows are generally composed of more than one pane of transparent material (glass usually), and the radiative heat transfer is defined as an infrared radiation exchange from one layer to another. The radiative heat transfer across a gap is proportional to the effective emittance. Consequently, reducing the emittance of surfaces would reduce the radiative heat transfer through the whole system. Radiative properties of glazings can be altered by thin coatings called low-emissivity (or *low-e*) coatings[10] deposited on a glass surface.

1.3.1 Noble-metal coatings

If a metal is thin enough, it will be partially transparent to visible and solar radiation, but it will still show good infrared reflectance. Extremely thin layers of metal (0.03 μm) can

be used to reduce thermal loss[11]. These coatings are called noble-metal coatings or coinage metal films[12] due to the free electron and they are the simplest technique to increase long wavelength reflectance combined with a relatively good short wavelength transmittance. Heat mirrors are obtained with Cu, Ag and Au or with alternative materials such as TiN, ZrN and Al[12].

To be transparent such layers must be very thin. When deposited onto glass the coating goes through a series of different stages. Metallic materials will be formed at certain sites on the substrate surface like metal islands[12]. When deposition continues, more and more islands appear, then the growing coating forms a metallic network. The space between the metallic islands becomes smaller and smaller until a uniform layer is formed. Noble-metal films are reasonably uniform for thicknesses greater than 0.01 μm. The metallic conduction of such coatings is only possible when a sufficient thickness including a large network is obtained. The visible transmittance decreases with increasing thickness.

The interest of these coatings are : they can be produced at high deposition rate without control of the stoichiometry; they are good electronic conductors to be used in an electrochromic device. The disadvantages are : they are soft, porous, strongly oxidising, chemically reactive and their electrical resistance depends on their thickness to which the optical absorption will be directly proportional.

1.3.2 Dielectric/metal/dielectric coatings

The limited transmittance through reasonably uniform noble-metal layers is caused by reflection at the surfaces of the coating, and the transmittance can be improved by additional layers which stop the reflection of the metal[11,13]. Then dielectric/metal or dielectric/metal/dielectric multilayers are considered to overcome the problem. Dielectrics with high refractive indices such as Bi_2O_3, In_2O_3, TiO_2, SnO_2, ZnS and Al_2O_3 are the most widely used coatings. Fabrication of such coatings requires a precise control of the stoichoimetry and the deposition rate is usually low. In comparison to noble-metal films, these films are hard, compact, chemically resistant and anti-reflecting. Their thickness can be tuned to make coatings anti-reflecting and cause T_v to peak at different wavelength ranges. By selecting the appropriate thickness of a three layer system, it can be used to optimise the energy efficiency. For a warm climate, a maximum thermal

reflectance is a priority compared to the level of visible transmittance, and for a cold climate luminous transmittance has to be maximised as well as having a low emissivity. Figure 1.4 shows the hemispherical transmittance and reflectance of an Interpane Ipasol™ product which is a $BiO_2/Ag/BiO_2$ multilayer[14].

Another advantage of this multilayered system is the protection of the metallic film from chemical reactions and oxidation.

1.3.3 Doped oxide coatings

Alternative to the noble-metal based coatings are doped semiconductors. The semiconductor must possess a wide band-gap to allow high transmission in the luminous and solar ranges and the doping level must be high enough to allow the material to be metallic therefore conducting and infrared reflecting.

The unique transparent properties of heat mirrors are based on the existence of a forbidden energy gap in their band structure and the possibility to generate free electrons or holes by doping. The energy gap and the plasma wavelength (λ_p) define the transparency region of the heat mirror. λ_p is given by the concentration N of the dopant and will increase with an increasing N. In a metal, N is large enough to move λ_p to the UV/VIS region of the spectrum. In the case of semiconductors, N needs to be in the range (10^{19} - 10^{21} cm^{-3}) to bring λ_p to the near infrared[13].

Several materials based on Zn, Cd, In, and Sn have been used. The doping is achieved with the addition of a foreign element (extrinsic doping) or it can be achieved with a deficiency of oxygen (intrinsic doping). Like dielectric/metal/dielectric multilayers, these films are chemically resistant and mechanically durable and their resistivity is independent of thickness. Strict control of film stoichiometry during deposition is also necessary. They can be easily used on glass surfaces inside the glazing cavity.

Good results have been obtained with SnO_2 doped[15] with F, Sb and Mo; and ZnO[16,17] doped with In or Al. Another commonly used heat mirror is indium oxide doped with tin. Figure 1.5 shows the optical spectra of Pilkington K-Glass™ (SnO_2-F)[18]. The luminous transmittance is shown to be very high as well as the thermal reflectance. This type of coating is useful for energy efficient windows to be applied in a cold climate.

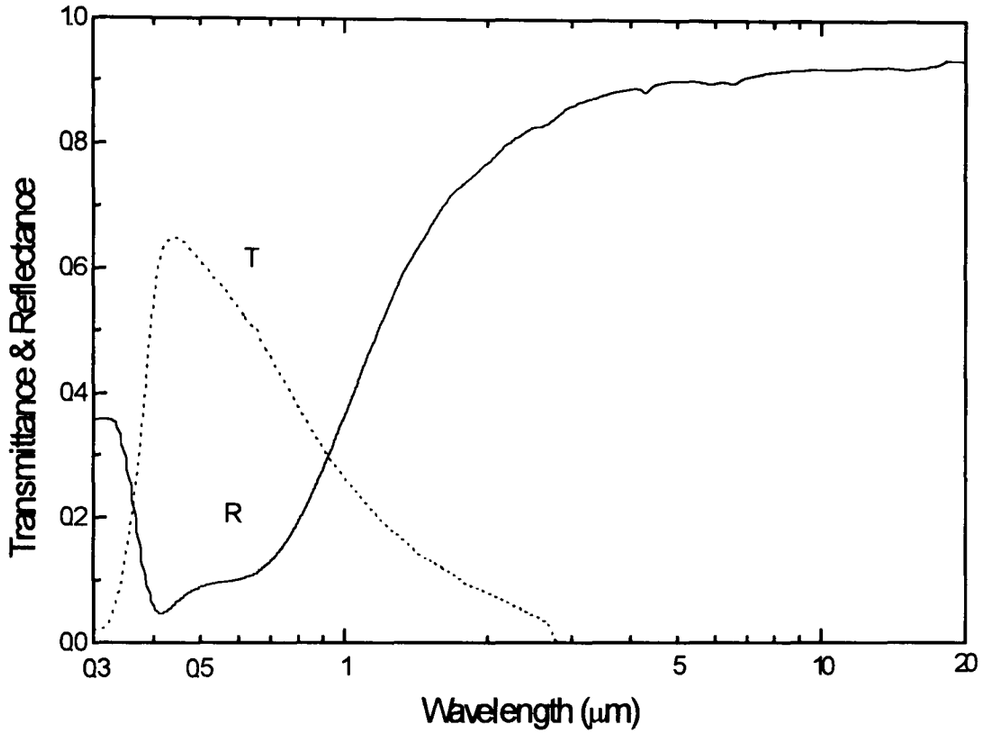

Figure 1.4 : Hemispherical transmittance and reflectance (0.3 - 20 μm) of an Interpane Ipasol™ (BiO_2/Ag/BiO_2) [14]. $T_s = 0.37$, $T_v = 0.57$, $R_s = 0.29$, $R_v = 0.10$, $E_{300°K} = 0.06$.

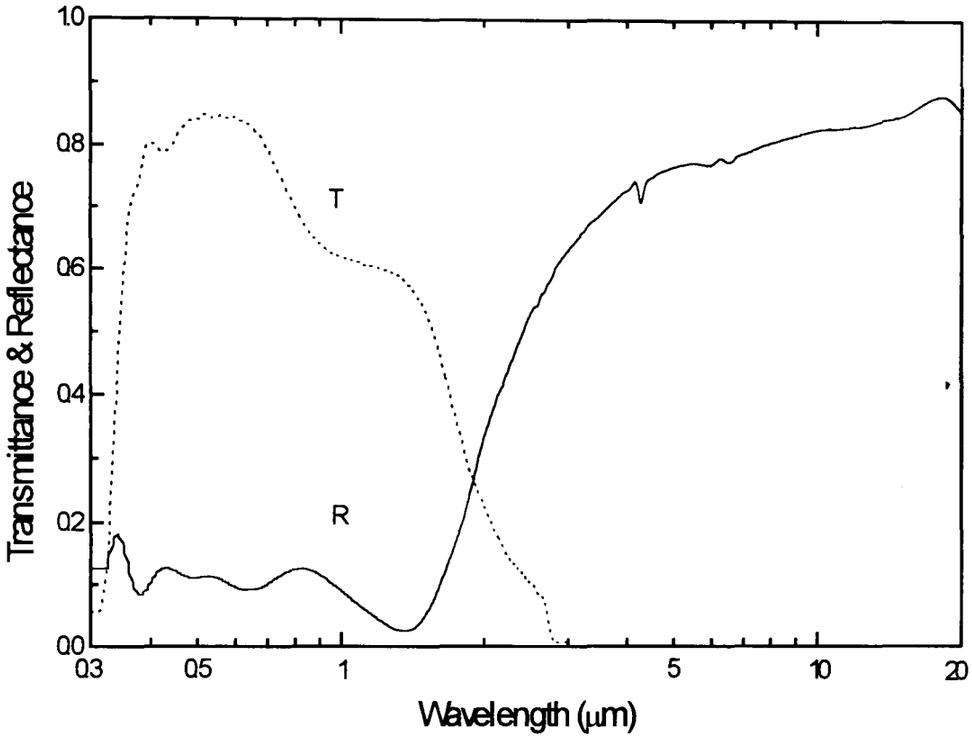

Figure 1.5 : Hemispherical transmittance and reflectance (0.3 - 20 μm) of a Pilkington K-Glass™(SnO_2-F)[18]. $T_s = 0.68$, $T_v = 0.84$, $R_s = R_v = 0.11$, $E_{300°K} = 0.16$.

It is also useful for electrochromic glazings because of their high electronic conductance combined with a high visible transmittance.

1.3.4 Solar gain control

Infrared reflecting thin films behave differently in respect of incident solar radiation. Heavily doped semiconductor materials where the plasma frequency (ω_p) is in the NIR transmit visible and near-infrared radiation. In contrast, noble-metal based coatings with high free electrons density transmit only the visible radiation. Semiconductor heat mirrors are used in cold climates where solar gain is required to be high. Noble-metal based solar gain control coatings have greater values of T_v coupled with lower values of T_s and low emissivity. As such they may have significant advantages in applications such as commercial buildings where solar gain is to be restricted to prevent overheating while providing high visible transmittance.

1.3.5 Gas filling

The use of low emissivity coatings can reduce heat transfer across a gap by a factor of two, which makes the conductive and convective heat transfer dominant. Heat transfer inside the gap is then due to conduction and natural convection. Air is a relatively good insulator, though conduction can be further reduced by filling the gap with lower conductivity inert (or noble) gases. Also, the use of a relatively high viscosity gas can limit convection. Suitable gases used in windows must also be non-toxic, inert, and the most commonly used[2] are listed in Table 1.1.

1.3.6 Edge seal and frames

High performance insulating glass units can be maximised with the use of a third low-e layer unit with two gas gaps. Significant improvements in centre of glass thermal performance make heat losses through the frame and the edge of a traditional window comparatively more important.

Gas	Thermal conductivity ($W.m^{-1}.°C^{-1}$)
Air	0.241
Argon	0.0162
CO_2	0.0146
Krypton	0.0086
Xenon	0.0049

Table 1.1 : Thermal conductivity of different gases[2].

The design of new energy efficient products raises the need to represent the performance of the whole window. Heat transfer through window frames is similar to heat transfer through windows e.g. convection, conduction and radiation effects. Modelling tools are used to examine temperatures and heat flows through different materials containing different air spaces. To reduce heat transfer, crucial improvements need to be focused on the thermal bridging effects of frame components. The solar heat gain through frame areas is a function of the solar absorptance and heat resistance of the material used but more significant is the infiltration through the window. The opening mechanism is usually the main reason for the infiltration and it should be adapted to climatic conditions (wind, rain, large temperature variations). The frame made of aluminium or vinyl should be designed for optimum thermal efficiency which incorporates different cavities filled either with air or with an insulating foam[2]. The window spacers should also be carefully chosen to limit bridging heat transfer. It includes foam or butyl spacers, U-shaped spacers or thermally broken metal[3].

All the above technologies are already widely commercially available. Computing tools are available to model and predict the energy performance and the optical characteristics of any type of glazing unit[19]. Table 1.2 gives an indication of typical performances for different combinations of glazing systems.

1.3.7 Alternative or complementary technologies

More recently, research efforts have also concentrated on future highly insulating and non-conventional window technologies. Evacuated windows are a possible alternative solution[21,22]. Another promising means to reduce conductive, convective and radiative heat transfer through window systems is to fill the space between the glass panes with transparent insulating media[23]. These materials can be flexible polymer foils, honeycomb materials, bubbles, foams, fibres and silica aerogels. They can be almost transparent to the eye (aerogels, polymers) or highly scattering (honeycomb, foams, bubbles, fibres). The characteristics of such media are to be almost transparent or translucent to the human eye, and to possess a structure in which air is trapped. However, optical properties are usually different from conventional insulating glass units, with transmitted light being often scattered.

Glazing type	Gas filling	Thickness of layers (mm)	T_v	g_n or SHGC	Total U-value ($W.m^{-2}.°K^{-1}$)
DGU with no coating	Air	5 - 16 - 5	0.81	0.76	2.9
DGU + hard heat mirror	Argon	5 - 14 - *5	0.75	0.72	1.9
DGU + soft heat mirror	Argon	5 - 14 - *5	0.74	0.61	1.3
DGU + soft heat mirror	Xenon	5 - 8 - *5	0.76	0.58	0.9
TGU + soft heat mirror	Krypton	4* - 8-4-8 - *4	0.63	0.55	0.7
TGU + soft heat mirror	Xenon	5* - 8-5-8 - *5	0.64	0.42	0.4

Table 1.2 : Typical key parameters for different glazing systems[20].
Legend : DGU: Double Glazed Unit; TGU : Triple Glazed Unit.

An energy efficient window is a device capable of providing sufficient natural lighting during the day[24] to minimise the use of artificial lighting and also thermal comfort during both day and night. Thermal comfort implies a control of overheating to minimise the use of a cooling system as well as limiting heat losses by radiation, conduction or convection to minimise the use of an heating or cooling load. The impact of solar gains will vary with building type and use, climate, season and the time of day. When minimising U-values are always better, this is different for solar heat gain coefficients. For some applications it needs to be maximised, and for others, it needs to be as low as possible.
For buildings in cooling-dominated climates, it may be important to minimise the solar radiation entering rooms through glazing units.

1.4 Variable solar gain control

Energy efficient windows can incorporate a system which enables a dynamic throughput of radiant energy. This solution is of particular interest in temperate and cooling-dominated climates when there is sometimes a need for preventing overheating during the hot season and when solar gain can reduce heating demands at other times of the year. This can be achieved by some form of reversible, variable transmittance window. Such an advanced system is called "chromogenic glazing" or "smart window". In addition to energy and thermal comfort benefits, the control of solar gain can enhance visual comfort by reducing glare.
For heating-dominated climates, window systems must be designed to limit the energy losses when solar gain has to be maximised. The use of multi-glazings will decrease losses due to conduction and convection. The use of "heat mirrors" or passive insulators can lower the heat transfer and provide maximum gain of solar radiation. Again, chromogenic glazings offer the opportunity to control the building's energy savings.
There are currently different types of switchable glazings, and three control mechanisms exist : they can be light sensitive or photochromic, heat sensitive or thermochromic and electrically activated or electrochromic.

Thermochromic, for instance, can respond well to thermal effects, but may not allow the proper transmittance of daylight, and might not distinguish both inside and outside temperatures or take into account the quantity of incident solar radiation. Photochromic glazings controls daylighting but are inappropriate to control solar heat gains. Electrochromic glazings offer the highest degree of control. Such windows can be integrated into building energy-management systems to permit a direct optimisation of lighting and cooling consumption.

Finally, the window should be integrated as one component of a building system to enable and control further energy savings. Such a window system integrated with the surrounding wall should allow the wall to have a better thermal performance and improve the performance of the window. This system uses solar shadings above the window and wall cavities with high infrared insulation. Cooling and heating systems, lighting and smart glazing systems could then be monitored by a computerised control system with the help of photo sensors, comfort sensors and thermostats. Because electrochromics can be controlled by a system which best suits each application, they are viewed by manufacturers as having greater potential for energy savings and user comfort than any other chromogenics.

Chapter 2

ELECTROCHROMIC MATERIALS AND ELECTROCHROMIC DEVICES

2.1 Introduction

The dynamic window described in Chapter 1 controls incoming radiation and regulation is climate-dependent. Among the different possibilities in chromogenics glazings, the most probable alternative uses of electrochromic thin films are to vary the amount of incoming radiant energy.

This Chapter presents a review of the electrochromism principle and materials known to exhibit electrochromic properties. Different electrochromic device designs are described with the aim of practical utilisation for energy control glazings. Among these, the five-layer laminated design presents particular advantages for future window applications. Most work in this thesis concerns materials of interest for the development of an all-solid state electrochromic window with good characteristics for energy efficiency. Ideal performance characteristics of such materials and devices are presented in this Chapter.

2.2 Electrochromism and electrochromic materials

Electrochromic materials have gradual and reversible optical properties at solar wavelengths achieved by the application of an external electric field. A clear statement of the electrochromic effect was published in 1961 by J.R. Platt[1] where the author reported: "*The absorption and emission spectra of certain dyes may be shifted by hundreds of Angstroms upon application of a strong electric field. The effect could be called 'electrochromism' in analogy to 'thermochromism' and 'photochromism'...*

It appears that [..] dyes and other organic and inorganic compounds might turn up phenomena of considerable interest and value. "

The electrochromic phenomenon was discovered in tungsten oxide films which have been the most studied material. There are two major categories of electrochromic materials: transition metal oxides including intercalated compounds, and organic compounds[2].

Table 2.1 presents some of the most common transition metal oxides which are coloured by oxidation or reduction, and Table 2.2 presents some of the most common organic materials that exhibit electrochromism.

All the well known transition metal oxide (*MeO*) materials which exhibit electrochromism possess similar features[3]. Particular crystal structures, composed of MeO_6 octahedra with corner-sharing and edge-sharing arrangements seem well suited for electrochromic behaviour. MeO_6 units can be arranged in cluster-type or columnar microstructures. Many electrochromic materials have defect perovskite, rutile or layered structures and the electronic bandstructure of these ionic arrangements explains the presence of cathodic or anodic electrochromism. Optical absorption can be due to intraband effects, interband transitions and polaron hopping (see Chapter 3).

These materials have their largest technological applications as ion insertion electrodes in solid-state batteries. Electrochromic metal oxides can be considered as intercalation compounds which change their optical properties.

A simplified representation of the reaction for a cathodic colouring material is :

$$MeO_x\,(transparent) + yM^+ + ye^- \rightleftharpoons M_yMeO_x\,(coloured) \qquad [2.1]$$

and for an anodic colouring material is :

$$M_yMeO_x\,(transparent)^- \rightleftharpoons MeO\,(coloured) + yM^+ + ye^- \qquad [2.2]$$

where M = Li^+,H^+,Na^+... and Me = *Transition Metal*.

Materials	Coloured state	Bleached state
Cathodic materials:		
Tungsten Oxide (WO_3)	*Blue*	*Colourless*
Molybdenum Oxide (MoO_3)	*Grey-Purple*	*Yellow*
Titanium Oxide(TiO_2)	*Blue*	*Colourless*
Niobium Oxide (Nb_2O_5)	*Bronze*	*Colourless*
Vanadium Oxide (V_2O_5)	*Blue, Grey, Black*	*Yellow*
Tantalum Oxide (Ta_2O_5)	*Neutral*	*Colourless*
Anodic materials:		
Nickel Oxide (NiO_x)	*Bronze*	*Colourless*
Iridium Oxide (IrO_2)	*Black*	*Colourless*
Rhodium Oxide(Rh_2O_3)	*Green, Brown, Purple*	*Yellow*
Cobalt Oxide (CoO_x)	*Purple, Grey, Black*	*Red*
Chromium Oxide (Cr_2O_3)	*Dark brown*	*Pale brown*
Manganese Oxide (MnO_2)	*Colourless*	*Colourless*
Iron Oxide (FeO_x)	*Red*	*Colourless*
Vanadium Oxide (VO_2)	*Blue, Grey*	*Yellow, brown*

Table 2.1 : List of cathodic and anodic inorganic electrochromic materials[4].

Materials	Coloured state	Bleached state
Viologens	*Blue, Violet, Red*	*Colourless*
Polyaniline	*Green, Blue, Purple*	*Colourless*
Polypyrrole	*Brown*	*Yellow*
Polythiophene	*Blue*	*Red*
Polysiothianaphene	*Black*	*Colourless*
Anthraquinones	*Blue, Green*	*Red*
Magnesium Phthalocyanines	*Green*	*Red, Violet, Blue*
Lutetium Diphthalocyanines	*Green*	*Red, Violet, Blue*
Tetrathiafulvalenes	*Yellow*	*Green, Purple*
Pyrazoline	*Yellow*	*Yellow, Blue*

Table 2.2 : List of some organic electrochromic materials[2,5,6,7,8,9,10].

More detailed consideration of the reaction is given in Chapter 3 and in chapters related to the transition metal oxide materials studied in this work.

With organic electrochromic compounds, coloration is achieved by an oxidation-reduction reaction, which may be coupled to a chemical reaction.

Detailed reviews of organic and inorganic electrochromic materials and more generally of chromogenic materials have been produced by the laboratory[11,12] and published by different authors[2,4,13].

2.3 Electrochromic devices for variable transmission control

To date the first large-scale commercialisation of electrochromic technology was for the car industry[14]. The earliest electrochromic patent, dating back to 1929, concerned an antidazzle and fog-penetrating device for car headlamps using aqueous electrochemichromic solutions[15]. In 1969, the first electrochromic display device was reported by Deb[16] using inorganic oxides such as amorphous WO_3 films as the colour centre. Technology evolved and electrochromic devices can now be constructed in several different ways. Various designs are possible including assemblies with 3 to 7 layers[14]. This Section presents some of the possible designs including a device with favourable commercial applications.

2.3.1 Smart window designs

The earliest electrochromic device for car application was designed with 3 layers. Figure 2.1(a) shows a simple three-layer configuration[14]. An electrochemichromic solution contains a redox couple responsible for a colour change when a potential is applied between the two transparent conducting layers. However, like liquid crystals, the system comes back to its original state when the potential is turned off.

A 4-layer configuration is shown in Figure 2.1(b). A liquid or polymeric electrolyte is sandwiched between a transparent conductor and an electrochromic WO_3 film coated on a second transparent conductor.

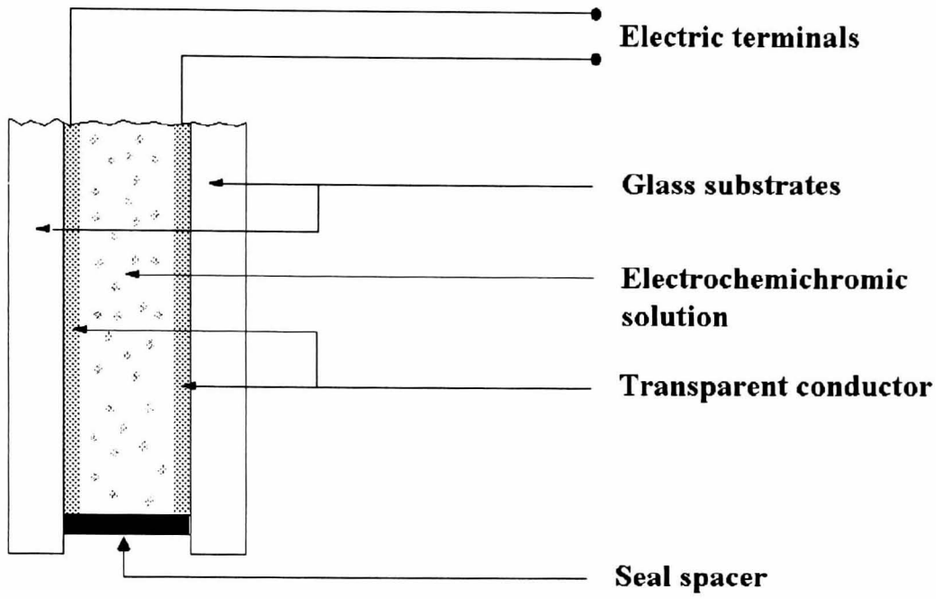

Figure 2.1 (a): A three-layer configuration of an electrochromic window device[14].

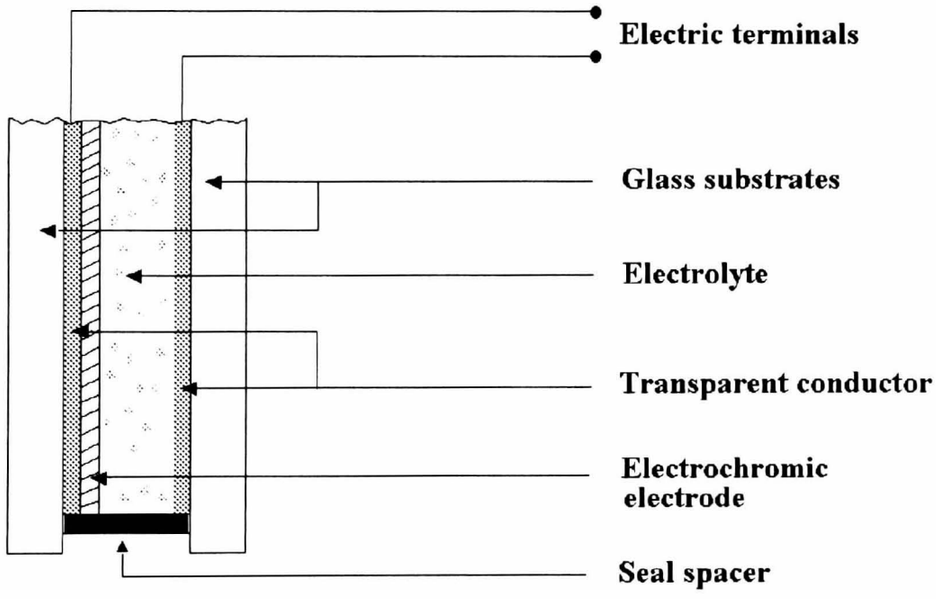

Figure 2.1 (b): A four-layer configuration of an electrochromic window device[14].

The ions responsible for the oxidation and the reduction of the WO_3 must have a redox reaction in the electrolyte or in the transparent conductor. A problem in this type of device is that a long lifetime may be hard to accomplish.

In his paper, Lyman[14] also reports a 7-layer reflective device. This system is symmetrically constructed using two 4-layer systems located on each side of a reflector layer. This configuration does not present any real advantage over the 4-layer design, and its manufacturing time and cost may be much higher.

Another possible electrochromic device system is the 5-layer configuration. This is shown in Figure 2.2, where a fifth ion-storing layer is added to the construction of the 4-layer device. As a consequence, a charge balanced process can take place. The different layers may be sandwiched between two glass panes and are therefore protected from the outside environment. The outermost layers are two transparent conducting films which drive the ions. These transparent conducting layers are usually highly doped semiconductors, such as In_2O_3 :Sn. The sheet resistivity of the layer is in the order of 1 - 30 Ω/□. This semiconductor is typically 0.1 to 0.3 μm thick. The second layer is the electrochromic layer. Usually this is 50 to 300 nm thick. Then follows a fast ion conductor or electrolyte which can be a transparent polymer such as a polymer based on polyethylene oxide or an all-solid state inorganic material. This layer exhibits ionic conduction but little or no electronic conduction. If a polymer is used, the device is laminated and the polymer layer is typically 5 to 50 μm thick. The fourth layer is the ion storage layer or counter electrode material which can be another electrochromic material. Its thickness is about that of the electrochromic layer. This layer can be optically passive and act purely as an ion storage layer or can serve as a complementary layer to the working electrode layer, e.g. one material is anodic and the other is cathodic. They work in such a way that they colour and bleach together. The 5-layer design is the most favoured system due to its similarity with solid-state batteries.

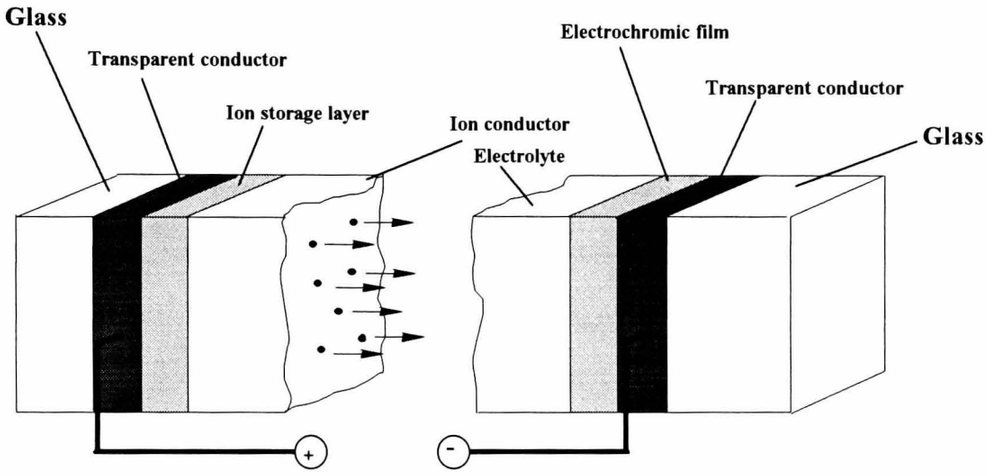

Figure 2.2 : Basic design of an electrochromic device (from Granqvist[2]).

2.3.2 Organic ion conductors

Over the past 30 years, conducting polymer technology has been rapidly developed mainly for battery applications. Polymers provide materials which are relatively light-weight; most of them are optically colourless or transparent; electrically insulating; and they possess a wide capacity for mechanical robustness and flexibility[17].

2.3.2.1 Ionic conduction in polymers

The useful properties of polymers are due to their long and repeating groups of atoms called monomers. Two types of chemical reaction can produce polymers[18]. The addition reaction will break a double or triple bond between two carbon atoms in the monomer to form new bonds that link the polymer chain. Such a method requires the generation of free radicals, which are molecules with free electrons. This can be achieved with the use of an initiator such as benzoyl peroxide. The use of radiation will enhance such a reaction. The condensation reaction will join two molecules together to make a larger one by removing some of the constituent atoms which themselves will create a stable molecule such as water.

The polymer chain is formed by atoms which are held together by strong chemical bonds involving the sharing or exchange of electrons[18]. Laterally they are weak. When polymer chains are formed from a solution, they fold back on themselves forming microscopic plate-like crystals. The random nature of the initiation and termination of the polymerisation produces molecules with a wide range of lengths. So the structure is a complex mixture of microscopic ordered and disordered elements. The folding of the polymer molecules masks the anisotropy of the individual molecules to produce a material with isotropic properties.

Polymers have saturated chemical structures. All the outer electrons are used in forming bonds between carbon atoms. Consequently, they are electrical insulators because there are no free electrons to carry charge through the material. The simplest polymer is poly(ethylene) which possesses a complete saturated chain and its backbone is shown in Figure 2.3 (a). To be conducting, some electrons must be less strongly localised in the chemical bonds. This is the case of poly(ethylene oxide)[19] shown in Figure 2.3 (b). The oxygen will be regarded as the donor sites for electrons.

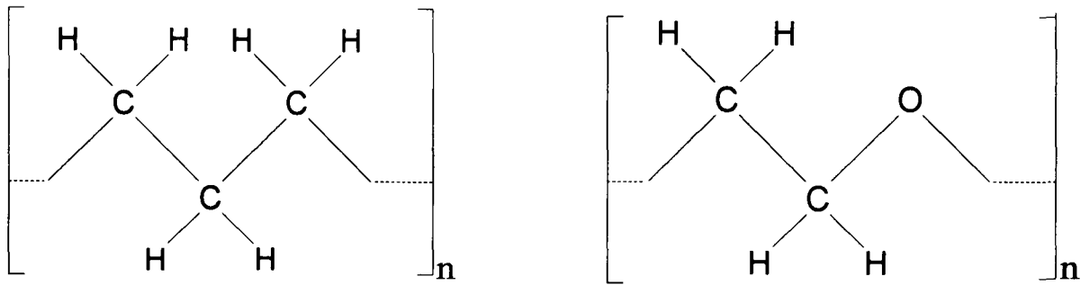

(a) **(b)**

Figure 2.3 : The backbone of poly(ethylene) (a) and of poly(ethylene oxide) (b)

To date, poly(ethylene oxide) (PEO) has been the most studied polymer primarily for batteries[20,21] and secondly for electrochromic displays[22,23] and sensors[24]. This macromolecule possesses groups of atoms with sufficient electron donor properties to form bonds with cations; the barrier to allow bond rotation is relatively low so that segments of the polymer can easily move. Finally they possess a suitable distance between "coordinating centres" to allow the formation of intra-polymer ion bonds.

The conductive performance of the polymer can be improved with the addition of a salt[25]. In this case the essential feature of the polymer is to act as a network to host a salt. The ionic motion takes place without long-range displacement of the solvent[16]. The ionic transport is created by the combination of ion motion coupled with the local motion of polymer segments and inter and intra-polymer transitions between ion sites. However the role of the polymer remains secondary as a conducting medium compared to the conduction of the salt.

The fabrication of the polymer electrolyte film involves the preparation of a solution with the salt. The quantity of salt added to the polymer is crucial for a good conductivity but too high a quantity can affect the polymerisation of the solution[27]. Usually a catalyst is added and then cured at high temperature or by the use of UV radiation to polymerise the material.

2.3.2.2 Ionic-conducting polymers for electrochromic devices

Complexes based on PEO-salt have been the most reported polymers but seem to show some limitations[28] for glazing applications. At temperatures below 65°C the polymer is shown to be crystalline and therefore a bad conductor. This is also shown at lower temperatures in polymers such as poly(propylene oxide) (PPO), poly(vinyl pyridine) (PVP)[29] and oligo(oxyethylene) methacrylate (MEO)[30] with lithium perchlorate as the salt.

A lot of efforts are being made to develop a solid polymer electrolyte with an amorphous structure at room temperature. This problem has been overcome by developing mixtures of different polymers. Several blends based on (PEO) have shown some promising results[31,32].

To obtain higher conductivity at room temperature, gel electrolytes have also been used as an alternative polymer-solvent-salt system. The polymer acts as a stiffener for the

solvent which dissolves the salt[33], for instance poly(methymethacrylate) (PMMA)[34]. Polyvinylidene fluoride (PVdF), polyacrylonitrile (PAN) and polyvinyl acetate (PVAc)[35] have been used to increase the viscosity of lithium perchlorate diluted in propylene carbonate.

Polymer electrolyte films have been produced in a very controlled manner in order to construct devices which take advantage of their unique properties. A large number of recent papers report the preparation and the characterisation of prototype devices composed of conductive polymer electrolytes. Although the lifetime of polymers can be irreversibly affected by environmental conditions[36] (temperature, UV radiation and humidity), intense progress is being made to overcome these problems, and many prototype smart windows have already been successfully fabricated[37,38].

2.3.3 Inorganic ion conductors

Solid state materials exhibiting ionic conduction are also known as superionic conductors. One of the first all-solid state electrochromic devices reported used sodium-β-alumina (Na^+ in β-Al_2O_3) as the solid electrolyte[39]. Initially reported by Yao and Kummer[40], this material has been extensively studied in the field of electrolytes for solid state batteries.

In Chapter 3, it is explained that in nearly-perfect crystals, ionic diffusion is always connected to the existence of lattice defects. Diffusion can take place through vacancies and through interstitial sites in ionic crystals. Such motion of ions is created under the influence of an external field. Ionic motion will increase in disordered structures where the existence of available sites is greater than the number of available ions.

A problem with β-alumina is the very slow diffusion of sodium ions into the electrochromic layer. Furthermore, it is a ceramic which makes the fabrication of large areas impractical[39], and it is an opaque material.

To date, inorganic ion conductors have been mainly studied in the field of solid-state batteries, fuel cells, electronic displays and memory devices. As a consequence, studies on these materials do not investigate the visible properties.

A detailed review of possible candidates was reported by Truong et al.[41] with some emphasis on smart window applications. Physically deposited inorganic ion conductors

are shown to conduct a wide range of cations such as Li^+, H^+, Na^+, K^+, Ag^+ and Cu^+. Only a few all-solid state devices have been reported where inorganic films such as $Ta_2O_5.xH_2O$[42,43], $LiNbO_3$[44] and Li_3N[45] have been incorporated as the ionic conducting layer.

More recently, alternative preparation methods such as electrochemical techniques or spraying processes have been used to deposit inorganic ion conductors. Devices based on electrochromic tungsten oxide films showed reversible EC characteristics with an electrodeposited[46] or spin-coated[47] $Ta_2O_5.xH_2O$ proton conductor. Electrophoretic deposition[48] has also been used to coat SnP (acetone used for the dispersion) as a solid electrolyte in an amorphous WO_3 device. Vacuum evaporation has also been employed in the deposition of AHP (Antimony Hydrogen Phosphate) thin films[49].

Although having an all solid-state electrochromic device that could be physically deposited with one technique presents a technological improvement, and some prototypes seem to have been successfully fabricated[42,43,44], important problems relating to device failures remain unsolved.

2.3.4 The laminated 5-layer design

2.3.4.1 Advantages of the 5-layer configuration

The advantage of the 5-layer configuration is the possibility of a charge-balanced operation, in which ions will intercalate/deintercalate a compound. The largest technological interest of intercalation compounds as ion-insertion electrodes is in solid-state batteries. The simple reaction implies a reversible intercalation using a highly electropositive alkali metal as the intercalated species, e.g. lithium. Owing to their crystal structure (see Chapter 3), transition metal oxides can intercalate ions, which is generally followed by a charge transfer in the host lattice. Consequently, their optical properties may change gradually upon ion insertion. This charge transfer is created by an applied potential and this gives the possibility to directly control the change in optical properties, and to leave the system at any state between a fully inserted state and a fully extracted one when reversing the applied potential, e.g. such system is said to have a memory.

2.3.4.2 Advantage of a laminated system

The problem associated with a liquid electrolyte in an EC device is based on the large area displays. If, for instance, there is a 0.5 mm gap between two glass panes of 2 x 2 square meters, 2 litres of electrolyte will be needed. A liquid electrolyte cannot only represent a potential safety hazard, but the pressure due to gravitational force on the glazing can deform the glass panes and the joints.

A solid-state inorganic electrolyte offers a promising alternative technology. Although several prototype windows have been successfully fabricated, important problems remain unsolved, which are : their very low optical response for glazing applications, their susceptibility to mechanical and thermal stresses, the problem of interfacial resistances and short circuits between the electrodes.

Polymer-based electrolytes offer the advantages of being flexible and robust at the same time and these properties can eliminate several problems associated with liquid or rigid solid ionic conductors. Films can easily be deposited on large surfaces and their mechanical robustness makes them well suited to large area fabrication.

2.3.4.3 Advantages of the electrochromic device based on WO_3 and lithium ions

Despite the interest in other transition metal oxides, which has resulted in hundreds of scientific and technical papers, tungsten oxide remains the most studied and the most understood electrochromic material. It may be used pure or doped with other metal oxides or even used in combination with another active electrochromic material. Therefore there is no doubt that this material promises to have a prominent role as the working electrode in commercial switchable windows.

Some early devices were reported using an aqueous electrolyte with electrochromic tungsten oxide[50]. However, quick degradation was observed mainly due to the dissolution of the tungsten oxide layer. The other main problem is the narrow potential range available above which oxygen and hydrogen evolution will occur in the system.

When using liquid electrolytes, improved durability was achieved with lithiated ion conductors[51]. The technology of solid-state batteries based on lithiated high ion conductors has been extensively developed and is well-understood[52]. Although lithiated systems are very moisture-sensitive, such technology represents today the most attractive solution for commercial applications.

2.4 Performance criteria of electrochromic materials and devices

In Chapter 1, it was indicated that electrochromic technology incorporated into an advanced glazing system can reduce energy loads (lighting, cooling and heating) as well as provide glare control and improve thermal comfort. In Section 2.3, the 5-layer laminated device was described to be the most promising device for large scale development, and consequently is the device of interest in this thesis.

The performance criteria of electrochromic windows are the key information to be defined for the development of commercial glazing. Electrochromic glazings are complex multilayers which can be incorporated into a solar-efficient window system. Only small potential differences, typically 1-5 V are required to alter a change in state. A continuous change between a bleached state to a coloured state is operated as long as charge is being transferred. This is of great interest in building energy management systems where glazings could be controlled for a particular environment and for the users comfort.

2.4.1 The optimum performance properties of electrochromic devices

The properties required for a good electrochromic window system are to be transparent in one state and coloured in the other state.

The lifetime of the device must be a minimum of 10 years of use, which means that it must tolerate 10^5-10^6 colour/bleach cycles without degradation. It must also be stable against solar radiation and temperature variations.

There are three types of ideal switchable electrochromics glazings[53]. Transmittance of the coating can be switched over the entire solar spectrum, only over the visible range or only over the infra-red spectrum. For any change in transmittance, a corresponding change in reflection and absorption will occur. An increase in reflection will reject solar heat, but might increase the effect of glare. The most probable effect of decreasing the transmittance will be the increase of heat absorption by the coating.

In hot countries where daylight carries heat energy, or in cold climates where heating loads have to be preserved, heat gains of the glazing will have to be minimised to achieve maximum energy saving. This can be achieved in a double glazing system where the

electrochromic is used in conjunction with heat mirrors. The effect of such coating would be to reflect both daylight heat and heat generated inside the buildings. The transmittance would be directly controlled by the electrochromic layer. The absorption should be broad over the visible region to give a neutral appearance of the glazing in its dark state and should be minimum in the near-infrared range. This is shown in figure 2.4.

In temperate climates, where solar heat gain could however mean extra energy consumption savings, reflectance over the infrared range can be modulated between 10-20% in the bleached state to 70% in the coloured state.

Durability is another important criterion for large-area chromogenic devices and UV radiation and temperature will be the two major stresses affecting electrochromic technology in a building. Table 2.3 and Figure 2.4 show the ideal performance characteristics of an electrochromic glazing which could have the highest impact in most parts of the world as an energy saving product. Nevertheless the problem should not be limited to the device optimisation but must also address the application of energy-saving systems combined with human comfort quality (see Chapter 1).

2.4.2 The optimum performance properties of the ECD individual layers

To obtain the ideal performance characteristics described in Section 2.4.1, ideal characteristics for every individual layer have to be defined. Each of the 5 layers plays a part in one or several of the overall characteristics of the device.

Most of the work in this thesis is about electrochromic materials to be used as active and passive electrodes. Table 2.4 presents the ideal properties of these materials.

Although they are not the object of this work, electronic and ionic transparent conductors have been developed by collaborative laboratories. The ideal characteristics of these layers are presented in Table 2.5.

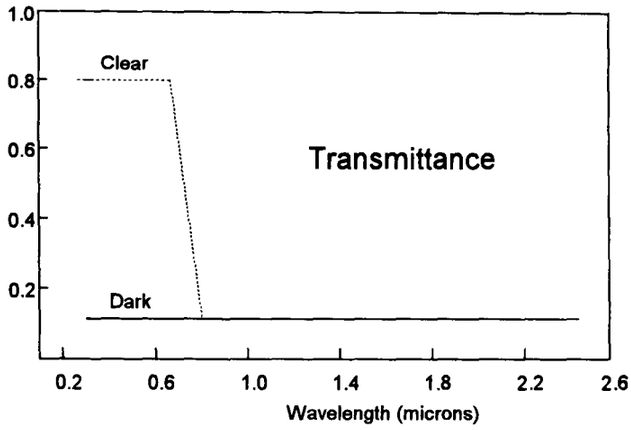

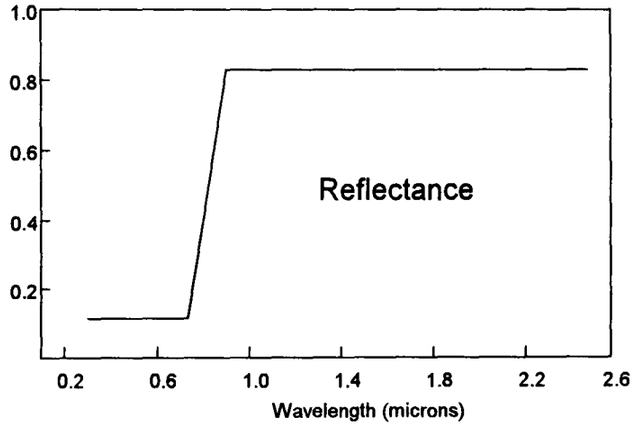

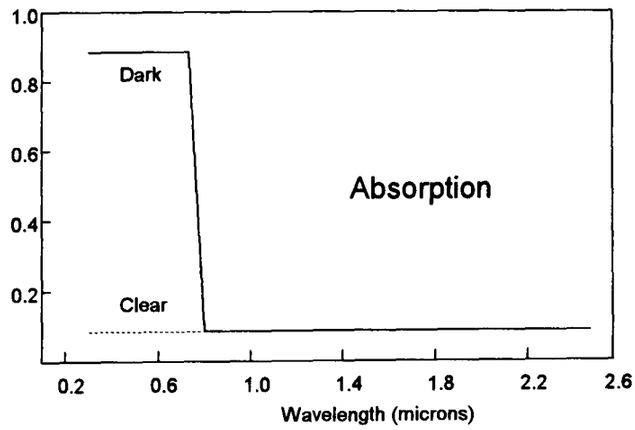

Figure 2.4 : Transmittance, reflectance and absorptance ideal spectra of a smart window system in the dark and clear states.

	Laminated 5-layer electrochromic device
Solar Transmittance	$T_{s,b} \geq 60 - 70\ \%$ $T_{s,c} \leq 10 - 20\ \%$
Visible Transmittance	$T_{v,b} \geq 70\ \%$ $T_{v,c} \leq 10\ \%$
Near IR Reflectance	$\geq 70\ \%$
Voltage Switching	- 5 V - + 5 V
Memory	> 12 hours
Switching Speed	1 - 5 mn
Lifetime	10 - 20 years
Cyclic Lifetime	$> 10^5$ cycles
Operating temperatures	- 30°C - +80°C

Table 2.3 : The optimum performance properties of an electrochromic smart window device[54].

	Active electrochromic layer	Passive ion storage layer
Solar Transmittance	$T_{s,b} \geq 60$ - 70 % $T_{s,c} \leq 10$ - 20 %	Uncharged/charged states > 70 %
Visible Transmittance	$T_{s,b} \geq 70$ % $T_{s,c} \leq 10$ %	Charge/uncharged states > 80 %
Near IR Absorptance	$A_{ir,c} < 10$ %	< 10 %
Voltage Switching	1 - 5 V	1 - 5 V
Switching Speed	1-5 mn	1-5 mn
Charge reversibility	> 95 %	> 95 %
Charge storage capacity	~ 30 mC/cm^2	> 30 mC/cm^2
Coloration efficiency	> 45 cm^2/C	< 10 cm^2/C
Cyclic Lifetime	> 10^5 cycles	> 10^5 cycles

Table 2.4 : The optimum performance properties of electrochromic materials.

	Electron conducting layer	Ion conducting layer
Visible Transmittance	> 90 % with a neutral appearance	> 90 % with a neutral appearance
Near IR Reflectance	> 90 %	> 90 %
Electronic resistivity **Sheet resistivity**	$< 10^{-4}$ Ω.cm < 10 Ω/□	infinite
Ionic conductivity	none	$\sim 10^{-4}$ S/cm
Voltage stability	- 5 V - + 5 V electrochemical stability with respect to the electrodes	- 5 V - + 5 V electrochemical stability with respect to the electrodes
Lifetime	> 20 years	10 - 20 years
Operating temperatures	- 30°C - +80°C	- 30°C - +80°C
Others		adhesiveness to hold two glass panes

Table 2.5 : The optimum performance properties of transparent electronic and ionic conductor materials.

Chapter 3

PROPERTIES OF ELECTROCHROMIC METAL OXIDES

3.1 Introduction

This Chapter presents a review of the chemical and physical properties of transition metal oxides in respect of their electrochromic behaviour. The electrochromism process is the insertion or extraction of ionic species into the lattice, followed simultaneously by the insertion or extraction of electrons into the electronic bands of a material. This Chapter concentrates on the most important factors which influence the electrochromic properties of inorganic transition metal oxides.

The first important factor of electrochromic transition metal oxides is that their crystal structures allow the ionic diffusion process to take place. This Chapter describes the main structural features of these oxides and shows how they are arranged to allow ionic intercalation.

As a consequence of their crystallographic structures, the second important factor is the electronic band structures of transition metal oxide materials. They are characterised by an incomplete filling of the band or bands and those where band overlap occurs. During the ionic intercalation, electrons are inserted into the bands to maintain the overall neutral charge. This Chapter describes how the variation of electronic density in the materials is the key concept for optical modulation of electrochromic materials.

3.2 The crystal structures of transition metal oxides

3.2.1 Static properties of crystals

All inorganic electrochromic materials found to date belong to the transition metal oxide group. They are intermediate crystals between the 3 main types which are described in this section.

At low temperatures, electrostatic forces between electrons and nuclei are responsible for the binding of atoms[1,2]. Attractive Coulomb forces between electrons and nuclei overcome the repulsive Coulomb forces between electrons to hold the structure together. Electrons move independently in well-defined orbits. The orbitals of higher energy which are filled last in accordance with the Pauli principle, are on the outside of the atoms and their energies can be easily modified by neighbouring atoms. The valence electrons are very important in holding solids together. If the atomic orbital of a particular type is completely filled up, more energy is required to break this closed shell. If electrons are extracted or added an ion is formed but the atoms are expected to be particularly stable. If two atoms can form ions by transferring electrons, then they can bind together by mutual Coulomb attraction (*ionic binding*). The second type of crystal is when two atoms share one or several electrons between them (*covalent bonding*). Finally the last type of bonding (*metallic bonding*) is when atoms do not possess a closed electronic shell configuration like the *Van der Waals* crystals. Electrons are weakly bound and tend to be shared by many atoms forming metallic bonds. The main characteristic of metals is their high electrical conductivity due to their large number of relatively free electrons. In the case of covalent crystals, valence electrons are used in bonding, therefore these materials are not good conductors. Nevertheless it is easier to find free electrons in covalent crystals than in Van der Waals or ionic crystals because many are semiconductors. In ionic crystals, binding forces are strong enough to make the materials bad conductors.

However, the ionic type of crystal structure is considered as the dominant type for electrochromic transition metal oxides. This structure is used for instance to model their electronic structures.

3.2.2 Structural features of some electrochromic materials

Transition metal oxides are mainly ionic in their structural features. The close interatomic distances between metal and oxygen provide their stability. This section describes the ways in which metal-oxygen units connect together in electrochromic materials used in this work. These connections have an important influence on electronic properties.

Electrochromic metal oxides and more generally transition metal oxides structures are octahedrally coordinated, although the symmetry is not perfect. Each octahedron can be represented with a metal atom in the centre and oxygen atoms at each of the six corners (MeO_6). The connections between octahedra can be characterised with share corners, edges or faces. These octahedra are arranged so that tunnels or channels with different types of cross section are available for the migration of cations. Most electrochromic metal oxide films are nonstoichiometric polycrystalline or amorphous materials.

The network of corner-sharing octahedra is characteristic of many transition metal oxide bronzes[3]. They are nonstoichiometric compounds in the coloured state formed by inserting atoms into the interstitial sites into the oxide lattice[4,5] and there is one interstitial site per metallic oxide molecule. The guest element (M) inserted into the lattice forms the oxide bronze, originally named by Wöhler[6] in 1823 after HWO_3 which was bronze in colour. Several transition metal oxides with formula M_yMeO_x exhibit similar electrochromic properties. The composition of a bronze can vary from y=0 to y=1. They consist of a $(MeO_x)_n$ covalent network into which yM^+ cations are inserted giving their outer electron to the transition metal array. Best known are the tungsten bronzes M_yWO_3 in which the donor cations occupy tunnels in the crystal structure within the metal oxide network of corner-shared octahedra. This structure is known as the defect *perovskite structure*[7,8] or *rhenium structure*.

Figure 3.1 (a) shows the unit cell for perovskite lattice of tungsten oxide. Figure 3.1 (b) shows an array of octahedra in the perovskite structure. Each octahedron must be imagined with a metal atom in the centre and oxygen atoms at each of the six corners.

The second important crystal structure is the *rutile form*[7,8]. The rutile structure is shown in Figure 3.2 (a). The rutile structure is built of hexagonally packed oxygen lattice with octahedrally coordinated metal ions with 'infinite' edge-sharing chains. The connection of metal-oxygen in the rutile structure is shown in Figure 3.2 (b).

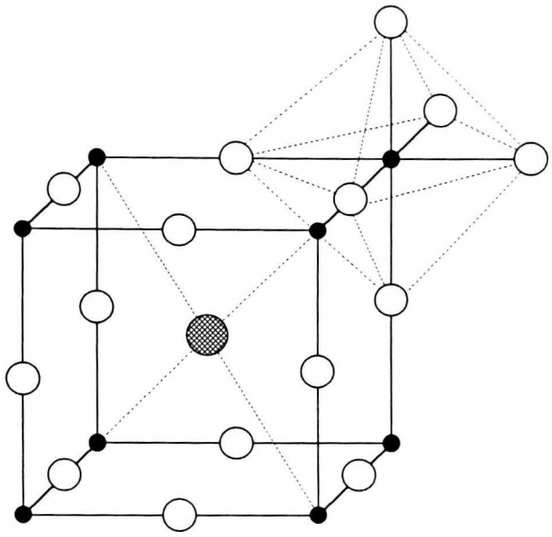

Figure 3.1 (a) : The unit cell for perovskite lattice of WO_3

Legend : ● tungsten, ○ oxygen, ◍ central cation

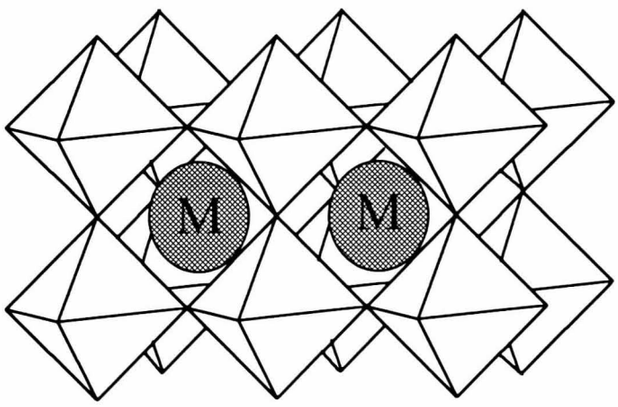

Figure 3.1 (b) : The perovskite structure of octahedra for a M_yMeO_x compound

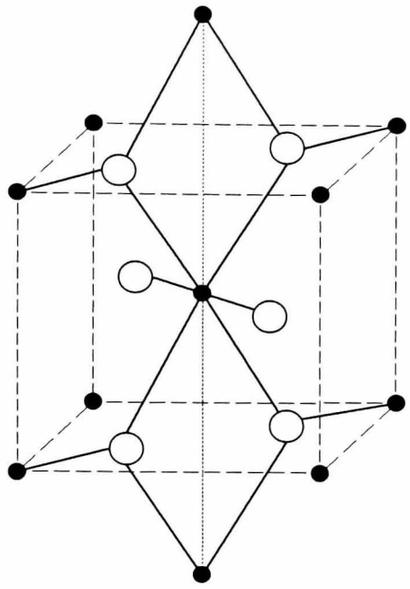

Figure 3.2 (a) : The unit cell for rutile lattice of TiO_2

Legend : ● titanium, ○ oxygen

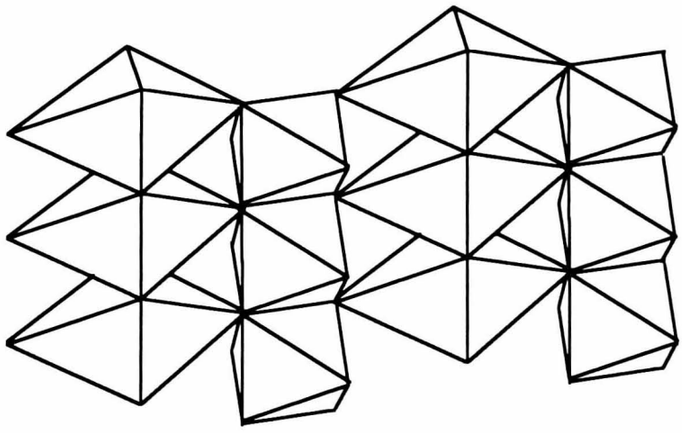

Figure 3.2 (b) : The connection of metal-oxygen octahedra in the rutile structure.

The chains are crosslinked forming vacant channels. Titanium oxide possesses different rutile-like crystal structures. The anatase phase has shown most interest for electrochromic titanium oxide. It consists of a tetragonal structure containing TiO_6 octahedra sharing 2 adjacent edges with two other octahedra forming planar double chains. These chains share corners with other similar chains creating zigzag rows of vacant sites to accommodate ions.

Vanadium dioxide is of tetragonal rutile type structure at temperatures above 68°C, and is of monoclinic configuration at lower temperatures and can still be considered as distorted VO_6 octahedra with a chain configuration characteristic for rutiles.

A number of electrochromic metal oxides present *layered and block structures*[7,8]. Sputtered electrochromic nickel oxide crystals in their as-deposited form are mainly amorphous and non-stoichiometric. Oxygen atoms being larger than nickel atoms, an excess of oxygen in NiO creates a large number of lattice vacancies. They usually present defect versions of the rocksalt structure. Figure 3.3 shows a defect-free rocksalt structure for NiO. Substitution of ions is therefore possible where an alkali metal replaces a missing nickel atom. Such structures, where half the transition metal atoms can be replaced by another atoms, can present alternate layers. Nickel oxide seems to be composed of weakly bound layers made of planes of NiO_6 octahedra sharing edges. The hydrated nickel oxide form has a brucite structure. Empty octahedral and tetrahedral sites contain protons.

3.2.3 Imperfections in crystals

The importance of non-stoichiometry in electrochromic transition metal oxides has been mentioned. The figures shown above describe perfect atomic arrangements that make an ideal crystal. However real crystals have defects and their concentration can be very large. This is of great importance for many physical properties.

At absolute zero temperature, crystals tend to have a perfectly ordered arrangement. When the temperature increases, the amount of thermal vibration of ions in their lattice sites increases as well as their chance to jump out of the lattice: this constitutes a point defect[8,9,10].

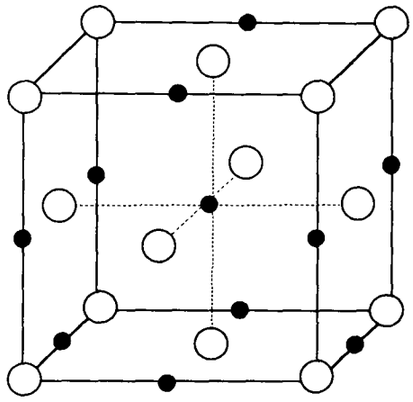

Figure 3.3 : The rocksalt structure of defect free NiO.

Legend : ● nickel, ○ oxygen

The simplest defect is when an atom is absent from a normal lattice site (*lattice defect*). Another is when an atom occupies an irregular site not normally occupied (*interstitial defect*). Ionic compounds can maintain their stoichoimetry in balancing such defects. When a single atom is removed from the lattice, electrical neutrality requires that the missing charge be balanced in some way. It can consist of a pair of "holes" where a missing cation will compensate a missing anion for no net charge. Alternatively the missing ion can be balanced by the presence of an impurity ion of higher charge (*Schottky defect*). Sometimes, electrical neutrality is achieved by not completely removing the ion but by simply moving it to a nearby interstitial site (*Frenkel defect*).

Defects can be eliminated by the formation of crystallographic shear phases. For instance, the alignment of oxygen vacancies in a plane can be shared in such way with another plane that the vacancies are eliminated.

3.2.4 Ionic diffusion in solids

We know that the electrochromic behaviour of transition metal oxides is due to the electronic insertion into its band structure. This intercalation is a consequence of the diffusion of ionic species into the material lattice in order to maintain an overall charge neutrality. Both ionic and electronic conductions are independent, the first being related to the crystal structure and the latter being determined by the electronic bandgap which depends on the individual properties of the constituent ions. A perfectly well ordered crystalline ionic transition metal oxide would in theory not allow any ionic diffusion, therefore electrochromism would not exist. This section presents the main features for ionic diffusion in transition metal oxide materials.

Ionic diffusion is connected to the existence of lattice defects[11] and the most common types of diffusion in crystals are through *vacancies*, through *interstitial sites* and through a combination of both called *interstitialcy mechanism*. In ionic crystals, such motion of ions is created under the influence of an external field.

In a vacancy diffusion[11], ions will move to vacant lattice positions. This is shown in Figure 3.4 (a). The ionic conductivity is high if the number of vacancies is large enough so that an effective number of ions responsible for the diffusion can be present.

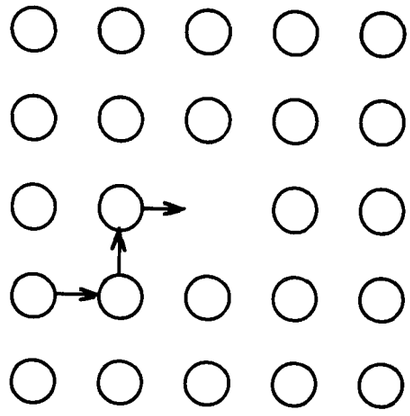

Figure 3.4 (a) : Vacancy diffusion in solids

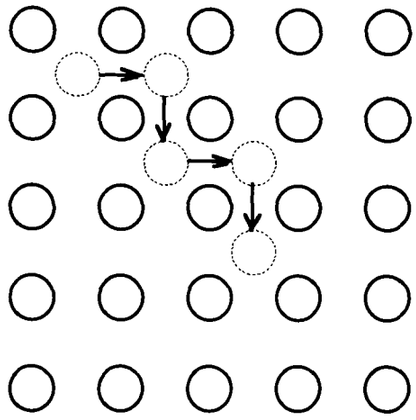

Figure 3.4 (b) : Interstitial diffusion in solids

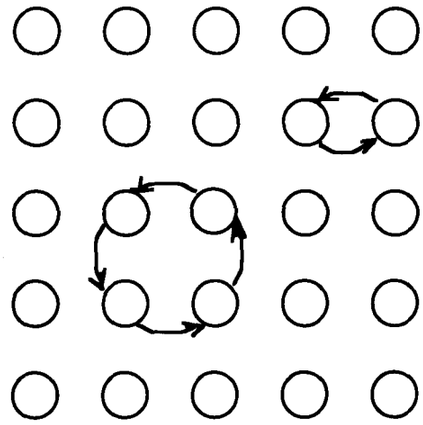

Figure 3.4 (c) : Direct interchange diffusion in solids

If the number of available sites is greater than the number of diffusing ions so that the ions can distribute over all the available sites, a high conductivity can be expected. The characteristics of fast ionic conduction can usually be increased with larger temperatures introducing excitations and structural changes in the lattice. The effect will be the disordering of ions which are constituent units of crystals.

Ionic conduction can also occur in the form of interstitial diffusion[11] where ions will move to normally unoccupied positions like a tetrahedral hole in an octahedral lattice. This is shown in Figure 3.4 (b).

Finally the combination of interstitial and vacancy mechanisms will be the motion of ions into interstitial sites when others will move into the vacancy created. This is shown in Figure 3.4 (c).

In nearly-perfect crystals, the ion diffusion takes place in the form of hopping, and can be described by the random walk theory[11].

However the activation energy is usually very low and it takes a long time to move an ion from one site to another. The probable path which ions would follow between the 2 sites in crystallographic channels and their probable energy will depend on their size. For a favourable size the activation energy of an ion can be low. The ionic motion is also connected to the polarizability of the lattice. An ion will either attract or repel its neighbours from the equilibrium positions. This will create a local polarisation cloud around the central ion, which will be carried with it. The ion motion and the lattice motion are connected.

However, the hopping theory in nearly ordered lattices will only contribute to a very low ionic conduction. Another model based on a vacancy mechanism, where a row of ions moves cooperatively by one interstitial site so that an ion will force an adjacent ion to move out into another adjacent interstitial site.

A disordered lattice where extra interstitial sites are available and where activation energy can be reduced will favour cooperative motions of ions. The major feature of this lattice is that the number of available sites is greater than the number of conduction ions. In disordered systems no clear distinction can be made between the vacancy mechanism and the interstitial or interstitialcy mechanism. Also, preferential sites among available sites as well as the repulsive interactions among ions will contribute positively or negatively to the activation of the diffusion process.

The corner-sharing framework of electrochromic metal oxides can be varied and gives rise to interstices with different sizes. Some of the most common of these structures are based on those of the tungsten bronzes. Depending on the size and concentration, different M cations can be accommodated in the tungsten oxide crystal structure configuration. The cubic structure configuration can accommodate small ions[12] (H^+, Li^+, Na^+), the tetragonal can accommodate ions up to the size of K^+ with the hexagonal configuration for larger ions. The hexagonal tunnel phase of the tungsten bronze is shown in Figure 3.5. The diffusion of cations is most rapid in hexagonal structure[13] where the size of the diffusion channel better matches the size of the mobile ion. Additionally, it is important for the metal oxide to be firstly a single crystal host, secondly to be a small grained polycrystalline thin film (less than 0.5 μm) and finally an amorphous film[5].

The layered and block structures show high ionic diffusion at ambient temperatures. By analogy with the layered β-aluminas, we can assume other layered materials to show high ionic mobility[14].

Finally, the existence of non-stoichiometric compounds makes transition metal oxides more sensitive to preparation conditions.

3.3 The electronic structure of electrochromic transition metal oxides

In the previous section, some basic structural features of transition metal oxides were described. The variation of corner-sharing frameworks, and the presence of defects create channels which can accommodate different cations. As a consequence, the ionic insertion combined with a simultaneous electronic insertion to maintain a charge neutrality inside the crystal is responsible for the alteration of the electronic properties. These properties are essential for transition metal oxide materials to exhibit an electrochromic behaviour. These solids, under normal temperature and pressure, possess a wide range of properties associated with the filling of the *d* orbitals. A particular characteristic of transition metal oxides is their wide range of electronic properties because of the multiplicity of oxidation states.

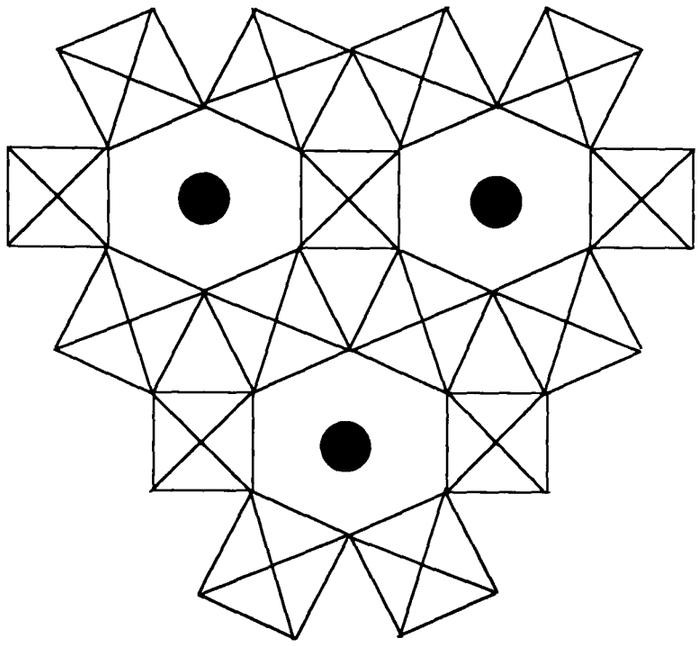

Figure 3.5 : Structure projections of the hexagonal phase of the tungsten bronze M_yWO_3.

In most cases, the crystal structure of electrochromic transition metal oxides is considered based on the ionic type of structure. This can be used to model their electronic structures. Electronic studies are based on quantum mechanical calculation of the total energy. The *ab initio* calculations and *Hartree-Fock* approximations are used to model the electronic structure of well-ordered materials[15,16]. However, defects in materials are much more difficult to treat and require the use of alternative methods[17].
This section presents the electronic band structure of the transitions metal oxides studied in this thesis.

3.3.1 Dynamic properties of crystals

The electron motion is divided into approximately two basic models. In the case of Van der Waals and ionic crystals, electrons are not allowed to move from one constituent to another. The electron orbits are slightly perturbed by the electrical forces of other constituents, but electrons are expected to move in their atomic orbits. In the case of covalent and metallic crystals, the above model is true for the inner electrons, while the outer valence electrons are shared between atoms. Excitations of the crystal occur when electrons are promoted from one state to a higher energy state.
The other type of excitation will be the motion of nuclei which is called vibrational excitation. This excitation has a wave form and is quantised.

3.3.2 The electronic structure of electrochromic materials

It is the energy states of the valence electrons which must be considered in explaining the optical spectra of materials. When atoms are brought together to form a solid, valence electrons start to interact with each other[18]. The electronic levels start to split and at some specific interatomic spacing the system tends to a minimum energy state corresponding to the equilibrium. The discreet energy levels spread into a range of sub-levels called energy bands. The band into which the ground state splits is called the valence band. The lower bands corresponding to inner-lying electronic levels are usually omitted since they have little effect on the main properties of solids. The band just above the valence band is called the conduction band. The energy bands of finite width in a

solid are filled up with electrons according to the Pauli Principle. The Fermi level is the boundary below which all states are filled and above which all states are empty at absolute zero. The basis of optical properties lies in the nature of the electronic energy of bands.

With transition metals, the atomic d orbitals assume crucial importance, due to the different bonding properties associated with these orbitals[18,19]. These complexities include the existence of variable oxidation states. The energy difference between a cation d^n configuration and d^{n+1} or d^{n-1} is rather small, and many transition elements can have several stable oxidation states. This does not exclude phases of intermediate composition, where oxidation states have mixed, or have fractional values. This is associated with the presence of shear planes or Magneli phases and the existence of non-stoichiometry creating a larger number of defects.

The essential concept in understanding the electronic properties of transition metal oxides is the d-symmetry of the principal valence atomic orbitals. The bonding interactions transform the O2p and the metal d orbitals into bonding and anti-bonding orbitals of mixed atomic character. Figure 3.6 shows an energy level diagram of the defect free perovskite lattice of WO_3. On the left side of Figure 3.6 (a) are shown the atomic levels of the metal (W). On right side of Figure 3.6 (e) are shown the O2s and O2p states. These are the valence shells accessible to electrons of the isolated atom. The cation is surrounded by 6 anions, whereas each anion is linearly surrounded by 2 cations (see Figure 3.1). As a result of this arrangement, the 5d levels split up as shown in Figure 3.6 (b). Similarly, the O2p orbitals split into 2 sub-groups as shown in Figure 3.6 (d). Figure 3.6 (c) shows 5 π- and σ-type bonding bands. These are due to the overlaps and interactions in varying degrees of the anions and cations states when they are brought together to form the metal oxide crystal.

The d-electron configuration represents the number of electrons remaining when all the metal oxygen bonding levels are filled. An ionic band structure has a filled valence band composed of combinations of O2p and metal oxide 2s orbitals, while the conduction band is formed from the metal d orbitals. The common geometry in transition metal oxides is octahedral. The d orbitals of transition metals can have five types of degeneracy which give rise to different bonding interactions with nearby atoms: the two e_g orbitals and the three t_{2g} orbitals.

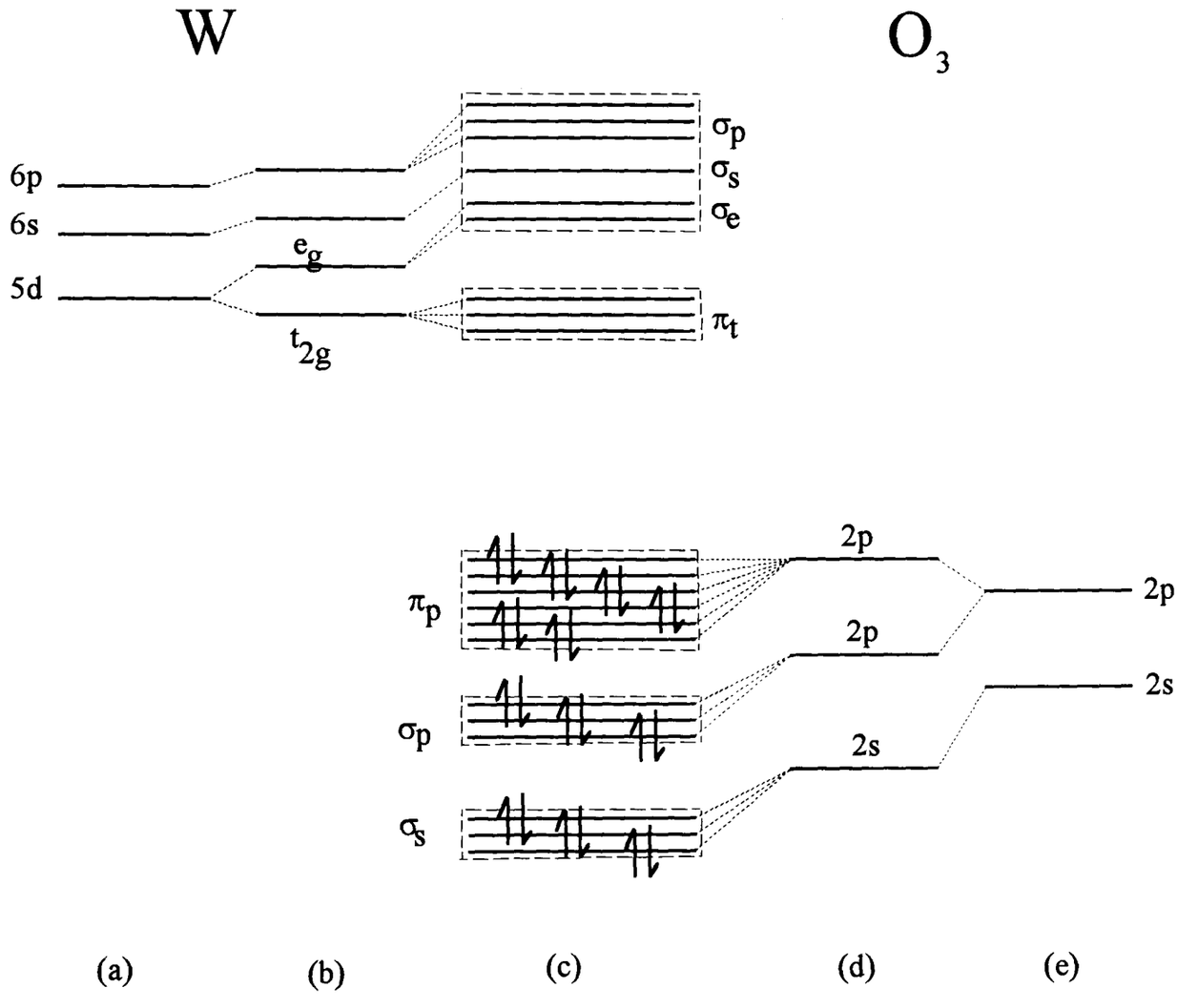

Figure 3.6 : Energy level diagram for the defect-free perovskite lattice of WO_3 [20].

The e_g orbitals point directly at the electronegative oxygen, when the t_{2g} orbitals point away from the nearest ions into empty space. Similarly the O2p orbitals are also split into orbitals pointing to the nearby electropositive Me ion, when others point away into empty space. The optical gap is usually defined as the transition between the highest valence band state into the first maximum of the conduction band state of the band structure. However, defects in materials create one or several intermediate bands inside the band gap. They can allow preferential transitions from the valence band, consequently creating a possible absorption.

In the case of tungsten oxide the conduction band is empty, and the Fermi energy level lies in the gap. The material is an insulator and typical bandgaps are in the range 3-4 eV which render the material transparent. When alkali elements are inserted into the material, electrons are inserted into the lowest part of the t_{2g} band. In fact, the nature of the electronic structure is not a rigid band model. For crystalline or well-ordered tungsten oxide[21], the increase of impurity concentration leads to the formation of an impurity band, split off from the conduction band into the gap. The effect will be the narrowing of the bandgap, making the material less blue and more golden-bronze in appearance. It is after this series that the general class of oxide bronzes was named. At a specific doping level, the impurity band broadens sufficiently that it merges with the conduction band into a single conduction band. The critical concentration for many doped transition metal oxides is found to be at about $x>0.3$ with M_xMeO_3. Finally at high doping levels, the band widens sufficiently that the Fermi level gets extended into the conduction band, and metallic behaviour is reached. The excess electrons in the conduction band can therefore hop from one available site to another by absorbing a photon. The energy required is low, consequently the material appears darker. This is called polaron absorption. Due to the metallic behaviour, materials also exhibit strong reflection below the plasma edge.

For a disordered tungsten oxide, the mean free path for electrons is reduced and becomes more localised. The metallic behaviour disappears as well as the infrared reflectivity. Figure 3.7 shows the bandstructure of defect tungsten oxide materials in the doped and undoped states. When undoped the optical gap Δ is wide, and the material is transparent. The disorder moves the Fermi energy close to the valence band.

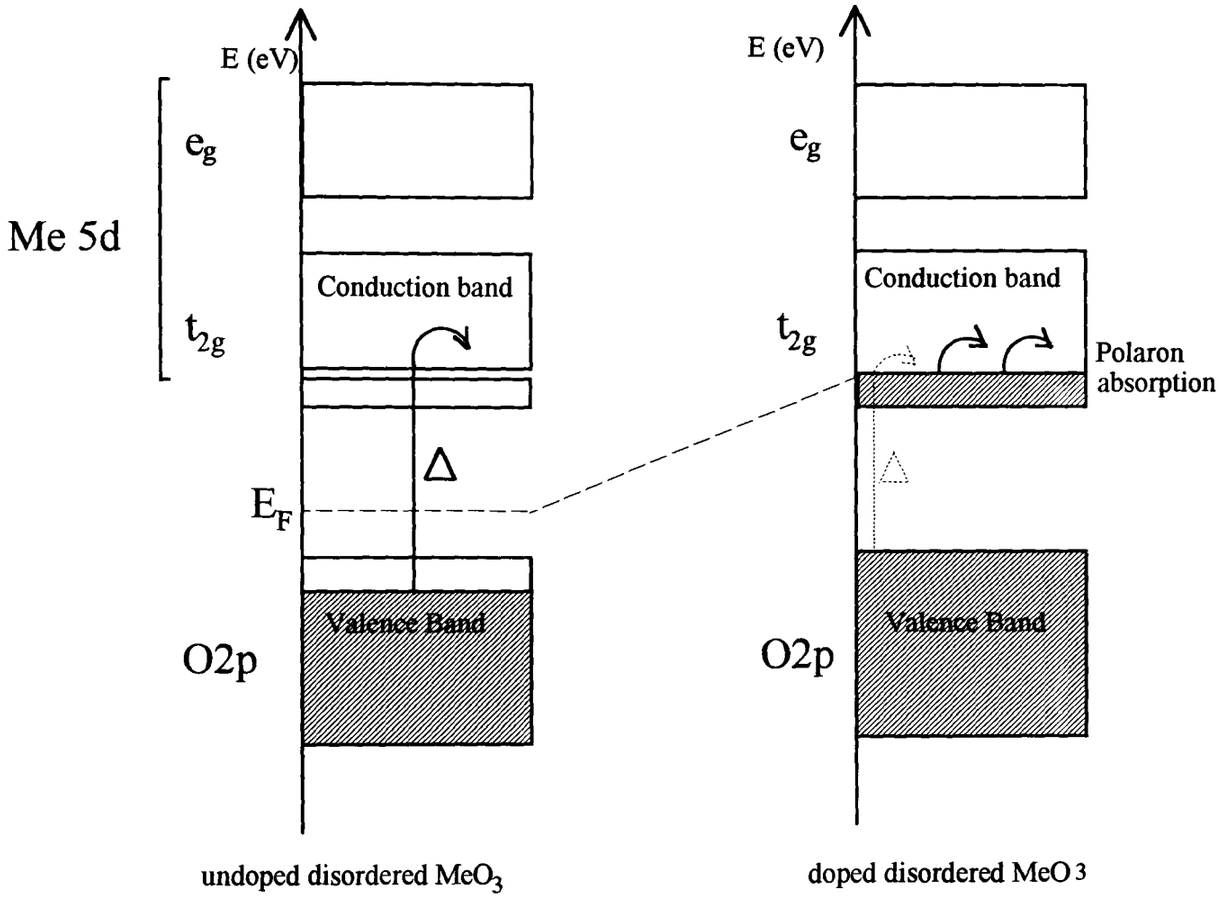

Figure 3.7 : Schematic bandstructure of highly disordered metal oxide in doped and undoped states. This structure is for a perovskite lattice.

When the material is doped the Fermi level moves towards the conduction band, the split-off band is created from the conduction band. The optical gap is smaller, therefore the material becomes blue. When the material is highly doped the split-off band merges with the conduction band and polaron absorption appears.

The metallic behaviour of tungsten oxide does not occur in all transition metal oxides[22] such as $M_xV_2O_5$, even at the highest attainable doping. The optical gap of disordered V_2O_5 is of the order of 2.2 eV. As in ordered tungsten oxide, the electronic structure is not rigid. There is a split-off conduction band when the material is doped, and because transitions between the two 2 bands are not allowed, a widening of the optical gap[23] is created. The material appears bluish. At high doping concentrations, one can expect polaron absorption.

Titanium oxide presents an electronic structure similar to tungsten oxide. Well-ordered TiO_2 would not allow any ionic insertion due to its high compactness, therefore only disordered oxide is considered. If a rigid band model is assumed, the creation of defects into TiO_2 will move the Fermi level away from the valence band so that it eventually comes close to the conduction band. When materials are doped with an alkali element, electrons occupy defect states corresponding to the originally empty conduction band states. The material goes from a non-absorbing state to a darker state due to polaron absorption.

The electronic structure of nickel oxide has gained considerable interest in high temperature superconductors[24] and in electrochromism in particular because in both systems, materials are derived by appropriate doping. Therefore the mechanism of the doping has attracted considerable attention[25]. The creation of nickel defects in NiO produces a charge compensation state of Ni^{3+} centres. The large number of nickel defects introduces states inside the gap and a shift of the Fermi level. Nickel oxide belongs to a group of magnetic insulators. NiO compound is commonly called *Mott* insulator[26] due to the fact that the bandgap excitation is based on electron transfer between 3d orbitals on different ions.

Owing to the band structure of NiO, it is expected to exhibit intraband absorption. However recent work[27] shows that the bandgap excitation for nickel oxide is a transition of charge between oxygen 2p to metal 3d. NiO compounds are then called charge-

transfer insulators. Nevertheless, the presence of the intraband transition is still crucial in nickel oxide and will only be considered in the present case.

Figure 3.8 shows the bandstructure of defect nickel oxide in the undoped and doped states. The onset of strong optical absorption in pure crystalline NiO occurs at 3.5 eV and can be identified as a transition from the top of the valence band to the conduction band minimum[28]. The optical gap of strong absorption occurs at 4.3 eV. In an almost defect-free state, the material is transparent. Non-stoichiometric NiO creates a defect of electrons, therefore decreasing the density of states in the t_{2g} orbital. These nickel defect states seem to behave as colour centres and lead to states just above and below the Fermi energy. This is as if the Fermi level has moved down to the top of the valence band. These states have the particularity to have been produced not near the conduction band but in the middle of the gap instead. Transitions can therefore occur between the maximum of the valence band into the intermediate gap above the Fermi level creating strong absorption of small energy. This makes the as-deposited and non-stoichiometric NiO dark in appearance. When additional electrons are inserted during intercalation, the Fermi level moves away from the valence band, and the optical gap widens. The material becomes transparent.

3.4 Adsorption on transition metal oxides

The interaction[29,30] between metal oxide surfaces and atoms and molecules in the surroundings cannot be ignored. The interaction increases on a macroscopic disordered material, and non-stoichiometric surfaces are usually more active than stoichiometric ones. When defects or vacancies are present on surfaces, the partially occupied d-orbital offers an active site for adsorption of species. These effects could enhance the coloration mechanism of electrochromic materials as well as being responsible for the failure of electrochromic devices. Owing to the fact that transition metal oxides possess different valence states, a wide range of adsorption behaviour can exist. In air, most of the interaction involves CO_2, CO, H_2, O_2 and H_2O principally.

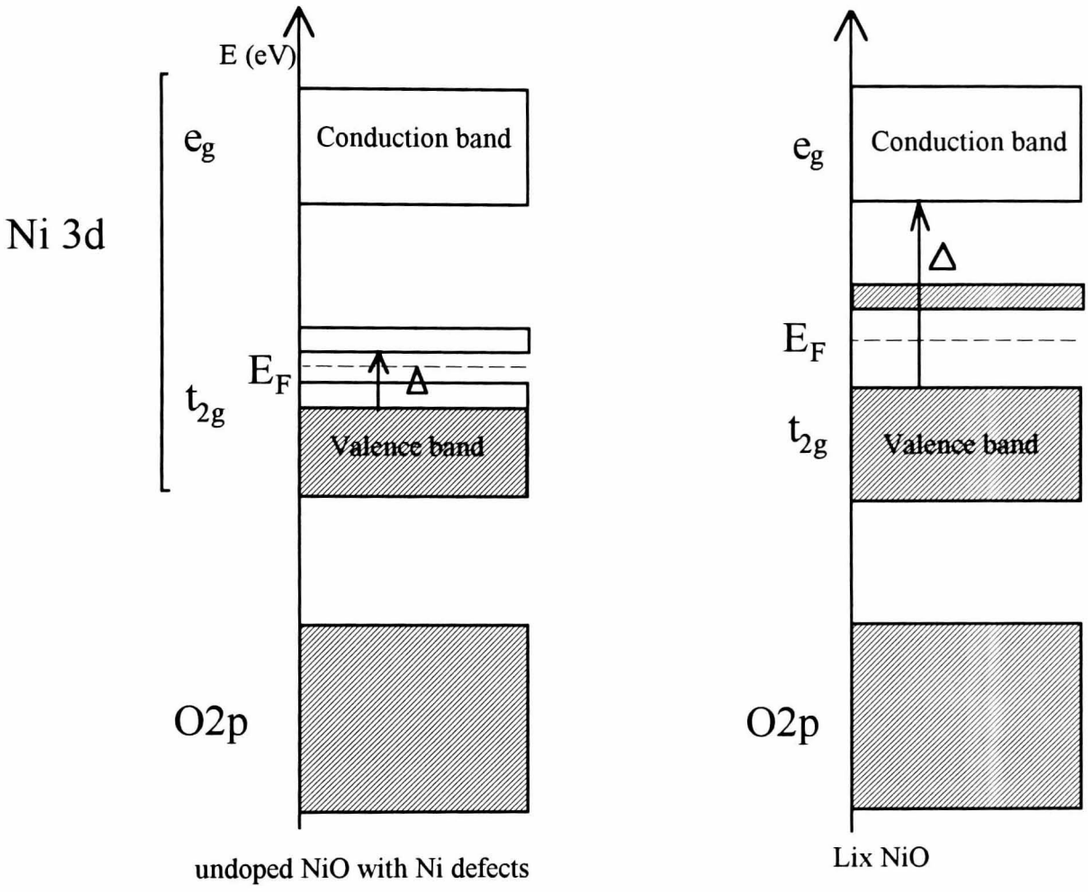

Figure 3.8 : Schematic bandstructure of defect NiO films in a doped and undoped state.

Adsorption can occur in different ways, either during the deposition process, where, for instance, moisture present in the deposition chamber is incorporated into the film, or it could also occur during the handling of the films in air throughout the manufacturing processes of a smart window device.

Chemisorption processes occurring on ionic oxide surfaces are due to donor/acceptor interactions. Electrostatic attraction of sites on materials can interact with molecules or ions and their orbital overlap.

Materials like titanium oxide films possess sufficient compactness to limit chemisorption with species of the surroundings. On the other hand, the different possible oxidation states of vanadium oxide offer different active sites for absorption. However adsorption in this last material has not been studied in great detail. Temperature, non-stoichiometry or disorder enhance the adsorption of water molecules. The most common reaction is the deprotonation of an adsorbate producing hydroxyl groups in polycrystalline oxides like tungsten oxide. Studies[31] showed that water molecules bond to W sites, and can be seen from the presence of W-H_2O stretch modes on sodium-doped tungsten oxide surfaces. Such a result is of importance for the handling and storage of deposited tungsten oxide films.

In the case of transition metal oxides like nickel oxide, which have partially filled d orbitals, d electrons can be easily removed. The oxidation of such materials is similar to defect metal oxide mentioned above and can enhance a wide range of adsorption reactions. Non-stoichiometric NiO containing Ni defects can interact[32] strongly with O, O_2 and H. The presence of adsorbed O will initiate adsorption of H_2O. Water molecules are not adsorbed as such but are dissociated by adsorbed O. Studies[31] have shown the presence of OH^- species in the lattice. However, without adsorbed O, NiO even with defects seems to show little adsorption of water.

Chapter 4

EXPERIMENTAL METHODS AND TECHNIQUES

4.1 Introduction

This chapter describes the main experimental techniques used in the preparation and characterisation of electrochromic thin films and devices in this study. Thin films described in this thesis were mainly prepared by reactive R.F. and/or D.C. magnetron sputtering.

Electrochromic thin films properties have been electrochemically and optically characterised. Spectrophotometers have been used to measure the spectral transmittance and reflectance of the films in the ultraviolet (*UV*), visible (*VIS*), near infrared (*NIR*) and infrared (*IR*) ranges. Instruments used and optical properties calculations are described in this chapter.

Electrochemical properties were simultaneously measured with optical transmittance using a spectro-electrochemical cell purposely designed for in-situ characterisation. This last technique is reviewed together with the electrophysical characterisation techniques used in this work.

4.2 Sputtering deposition techniques

4.2.1 The process

Spray pyrolysis and sputter deposition are the two principal techniques used in industry for preparing thin films on the scale of square metres. A brief description of sputtering technology, and the operating principles used in this work are given in this chapter.

The properties of thin film coating are directly related to its chemical and physical nature and are then dependent on the preparation technique employed.

Electrochromic films are directly dependent on the degree of crystallinity, crystal structure and level of impurities in the film. The main advantage of sputtering over other thin film deposition techniques is the good adhesion of the coating. A good control of the film stoichiometry and of the deposition rate can be achieved. Sputtering is also notable for its versatility and the possibilities of process control, but on the other hand is a costly investment.

The sputtering process is the bombardment of a target material by the ions of a glow discharge. The discharge is created by applying an electric field across a low-pressure gas. Figure 4.1 shows the basis of a sputtering system cross-section[1]. The process takes place in a chamber where unwanted impurities are removed by pumping down to a high vacuum (5×10^{-6} Torr). Then an inert gas such as argon is introduced into the chamber. A negative voltage is applied to the target so causing it to attract positive ions (argon ions) present in the plasma. The argon ions collide with the target surface and the target material is knocked out by a process of momentum transfer and condenses onto the substrate material. Secondary electrons emitted from the target surface generate more ionisation.

More than one ion is required to release most materials in a given area. As more power is applied, the bombarded area increases until the whole target area is covered. When the number of electrons produced is sufficient to give ions that can create the same number of electrons, the discharge is called[2] "normal discharge" and the gas starts to glow. If the power is increased further, both voltage and current density are increased in the discharge. This mode[2] is known as the "abnormal glow" and is the condition under which most sputtering is carried out. The atoms leaving the target are able to travel to the substrate when the number of gas molecules is suitably low. At high pressures, when the chamber contains a lot of gas molecules, most of the atoms will collide with the molecules and return to the target and the sputtering rate drops. The bombardment of the target causes the production of secondary electrons as well as other particles (desorbed gases) and radiations (photons and X-rays). These affect the properties of the growing film.

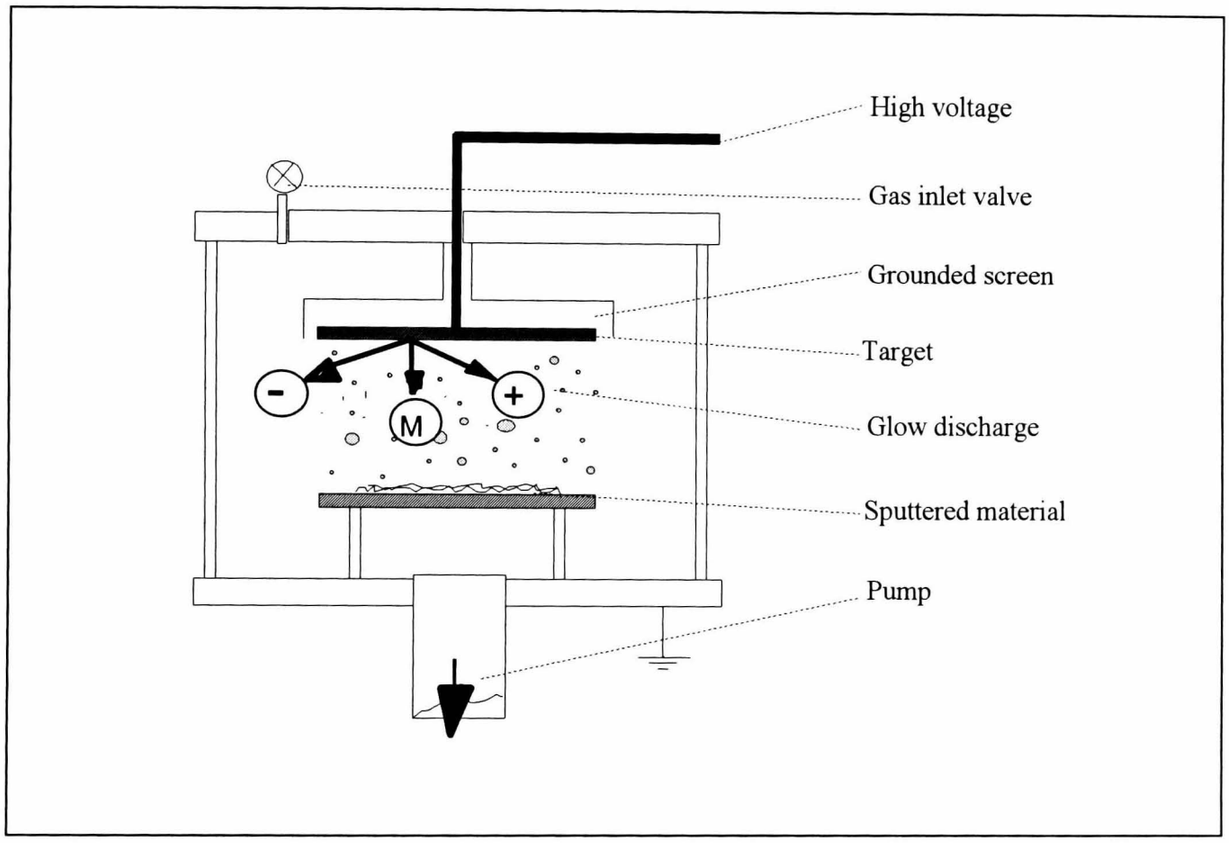

Figure 4.1 : Cross-section of a simplified sputtering system.

Many other factors can affect the sputtering process such as substrate temperature, target to substrate spacing, sputter gas purity, working pressure, target voltage, and whether the substrate is electrically grounded or biased.

Non-conductive materials can also be sputtered by the use of a Radio Frequency (R.F.) power supply. In this case, the target surface is coupled to the power supply through a resistance-capacitance (RC) network. In order not to cause a complete (D.C.) discharge on each half of the cycle, the frequencies used are greater than 50 kHz. Both cathode and anode would be sputtered otherwise.

The electrons oscillate in the glow space, and can gain sufficient energy to create more ionisation. The discharge is less dependent on the secondary electron emission. The discharge in both D.C. and R.F. sputtering processes can be supported by a magnetic field. Magnets placed behind the target create a flux which gives rise to a magnetic field almost parallel to the target surface. The combined effect of the electric and magnetic field lines causes the electrons in the plasma to follow helical paths perpendicular to both electric and magnetic fields. As electrons are confined close to the target region, ionising collisions are increased. Then the rate of ion bombardment at the target will increase as well as the deposition rate. Figure 4.2 illustrates how the magnetic field lines are arranged. The electrons move continuously in a closed loop which is called "the racetrack". This high ionisation region causes an erosion pattern on the target and gives a non-uniform thickness of the deposited film.

4.2.2 The Nordiko R.F./D.C. magnetron sputtering system

A Nordiko NS-3750 series magnetron sputtering system was used to prepare electrochromic films. A 1.25 kW R.F. generator and a 6 kW D.C. generator supply two water cooled 4" x 12" vertical electrodes. A rotary substrate carrier mounted inside the chamber can be indexed from the control rack of the instrument[3] to permit static or co-sputtering deposition. A power splitter allows the substrate to be R.F. sputter etch-cleaned and also R.F. bias sputtering to be carried out. The pumping system includes a two-stage high capacity rotary pump (640 l/mn) coupled with a 3500 l/s water-cooled diffusion pump. A liquid nitrogen cold trap is used for the removal of condensables. The pumping system is automatically controlled from the control rack of the machine.

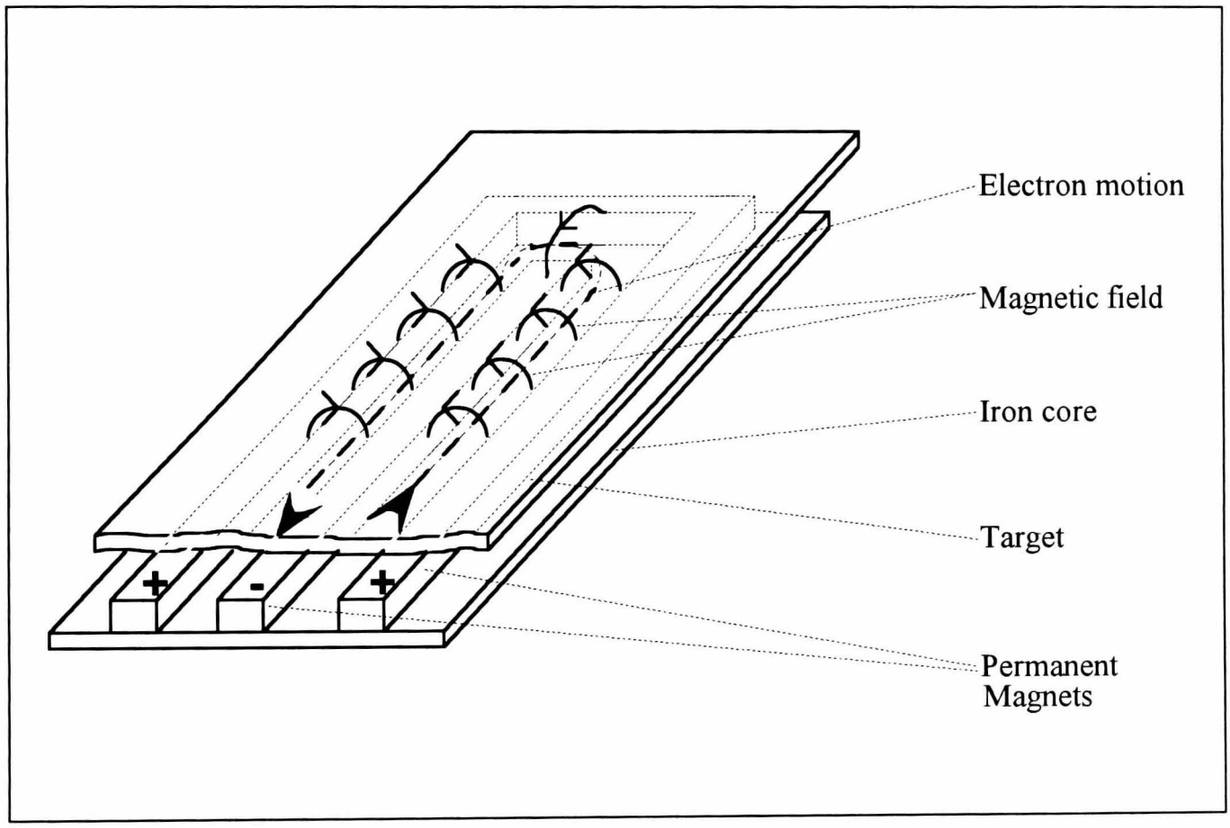

Figure 4.2 : Schematic of the magnetic field configuration onto the electrode.

A manually-driven shutter is provided to permit sputter cleaning of the targets. Control of three process gases is provided using a 3 channel mass flow control system.

Figures 4.3 and 4.4 present a schematic diagram and a photograph respectively of the Nordiko sputter coater.

A typical sequence for normal operation of the CVC LCS-100 magnetron sputter coater is as follows.

Glass and ITO substrates were held vertically on a carousel positioned at 10 cm from the target. The carousel holds 3 different sets of substrates, and each of them can be indexed to the appropriate target. Substrates were held in place with heat-resistant tape. The chamber was sealed and an automatic pump-down started. The chamber pressure was first reduced to 0.1 Torr with a rotary pump. This usually took 3 minutes from atmospheric pressure. The roughing valve was then closed and the foreline valve opened. The diffusion pump valve was opened ensuring that the foreline pressure did not exceed 0.1 Torr. This prevented the diffusion pump from stalling. After a further period of 30 minutes, the pressure of the chamber reached a vacuum below 5×10^{-6} Torr. A shutter was indexed between the target and the carousel to carry out presputtering. The required flow rates were set on a controller unit. Presputtering was performed to reach steady-state conditions before the actual film was deposited. After a required time, the shutter was removed and deposition onto the substrate initiated. When the deposition was completed, the generators were switched off, and the gas flows turned off. Samples were then left for 20 minutes to cool down before venting the chamber with nitrogen gas. This prevented water condensation build-up on the inside of the chamber walls which could increase the next pump-down time. New substrates were fitted onto the cooled platform, and the pump-down cycle recommenced.

4.2.3 The CVC R.F. / D.C. magnetron sputtering system

The LCS-100 CVC is a 4 cathode (6" diameter) upward-sputtering magnetron system. Three electrodes are supplied by a 1 kW R.F. generator power. An adjustable R.F. power splitter allows the substrates to be sputter-etched and also bias sputtering to be carried out. A R.F. matching unit is provided and can be adjusted with controls on the control panel. The fourth electrode is powered by a 4.5 kW D.C. power supply.

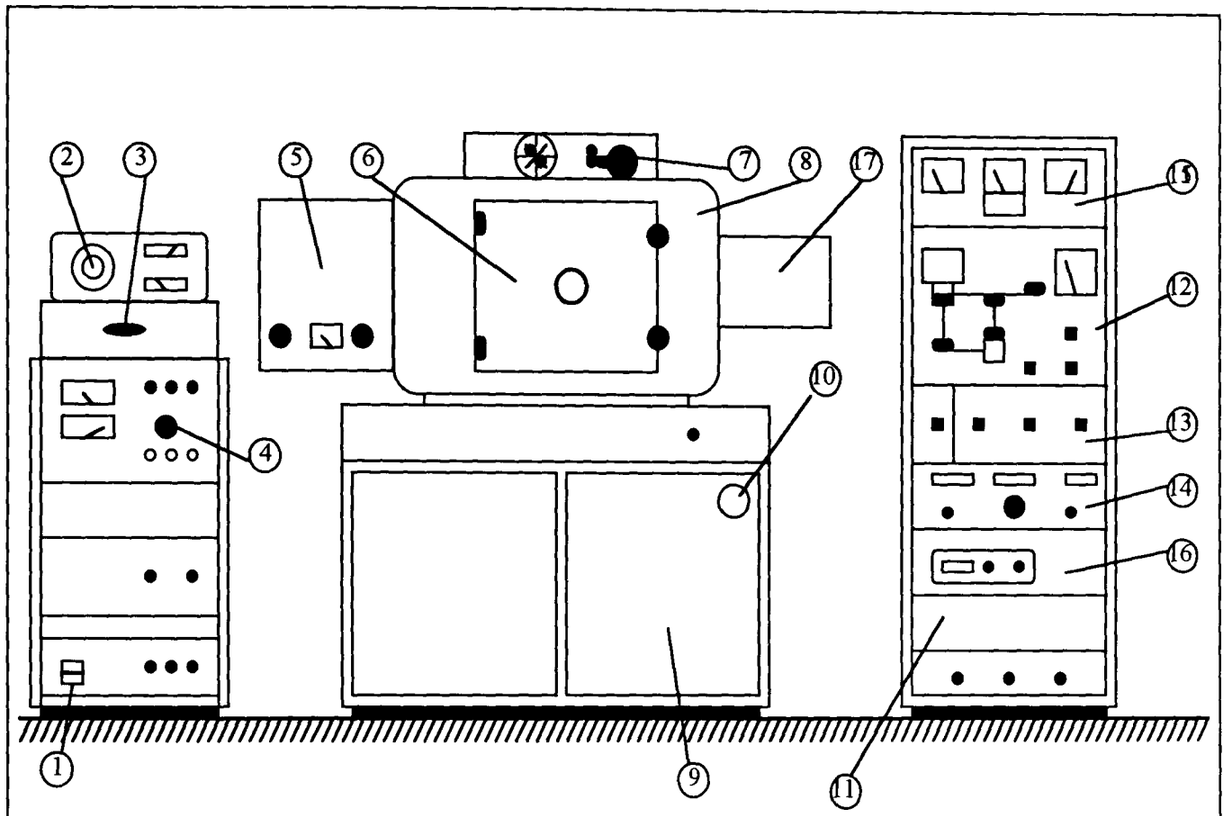

Legend

1	R.F. Generator /Power supply	10	Liquid nitrogen filler
2	Power splitter	11	Main control rack
3	R.F. mode switch	12	Pumping system
4	R.F. power supply control	13	Gas inlet system
5	R.F. electrode matching unit	14	D.C. generator/power supply
6	Front opening door of chamber	15	Gauges control unit
7	Manual shutter drive	16	Gas inlet control unit chamber
8	Non-magnetic stainless steel vacuum	17	D.C. electrode unit
9	Pumping station		

Figure 4.3 : Schematic of the Nordiko NS-3750 sputter coater.

(18) A. W. Czanderna, C. M. Lampert, " *Evaluation Criteria and Test Methods for Electrochromic Windows*", Report for the U.S. Department of Energy under contract No. DE-AC02-83CH10093, July 1990.

Chapter 9

(1) S. Tanemura, " *Energy Benefit of Smart Windows and the State-of-the-Art of their R & D in Japan*", Proc. of the 5th Intl. Sym. on New Glass, p. 37, October 1995.

(2) I.D. Brotherston, Z. Cao, G. Thomas, P. Weglicki, J. R. Owen, " *Counterelectrode Films for Electrochromic Windows*", Solar Energy Materials and Solar Cells, Vol. 39, p. 257, 1995.

(3) A. M. Andersson, " *Electrochromic Materials: Optical, Electrophysical and Structural Properties*", PhD Thesis, Department of Physics, University of Göteborg, 1992.

(4) S. Passerini, B. Scrosati, A. Gorenstein, " *The Intercalation of Lithium in Nickel Oxide and its Electrochromic Properties*", Journal of the Electrochemical Society, Vol. 137, No. 10, p. 3297, October 1990.